

SYNTHESIS AND CHARACTERIZATION OF NOVEL
POLYVINYLEETHER POLYMERS PRODUCED USING CARBOCATIONIC
POLYMERIZATION

A Dissertation
Submitted to the Graduate Faculty
of the
North Dakota State University
of Agriculture and Applied Science

By

Samim Alam

In Partial Fulfillment of the Requirements
for the Degree of
DOCTOR OF PHILOSOPHY

Major Department:
Coatings and Polymeric Materials

October 2011

Fargo, North Dakota

North Dakota State University

Graduate School

Title

Synthesis and characterization of novel polyvinylether polymers

produced using carbocationic polymerization

By

Samim Alam

The Supervisory Committee certifies that this *disquisition* complies with North Dakota State University's regulations and meets the accepted standards for the degree of

DOCTOR OF PHILOSOPHY

North Dakota State University Libraries Addendum

To protect the privacy of individuals associated with the document, signatures have been removed from the digital version of this document.

ABSTRACT

Alam, Samim, Ph.D., Department of Coatings and Polymeric Materials, College of Science and Mathematics, North Dakota State University, October 2011. Synthesis and Characterization of Novel Polyvinylether Polymers Produced Using Carbocationic Polymerization. Major Professor: Dr. Bret Chisholm.

Using carbocationic polymerization, a series of novel polyvinylether polymers and copolymers were synthesized and characterized. A series of polysiloxane copolymers containing polymer grafts possessing Triclosan moieties (PTVE) were synthesized using living carbocationic polymerization followed by hydrosilylation and investigated for potential application as environmental friendly coatings to control biofouling on marine vessels and biomedical devices. Copolymers possessing a relatively low molecular weight polysiloxane backbone and relatively high PTVE content exhibited very high reductions in biofilm retention for *S. epidermidis* and moderate reductions for *C. lytica* and *C. albicans*. In the second example, a novel monoallyl-functional initiator that was capable of producing very fast initiation of the living carbocationic polymerization of chloroethyl vinyl ether was synthesized and characterized. The monoallyl-functional polymers were used to produce a series of block copolymers containing blocks of polyquaternary ammonium compounds and polydimethylsiloxane (PDMS-*b*-PCVE-*b*-PQ) using hydrosilylation followed by quaternization with an n-alkyldimethyl amine. The PDMS-*b*-PCVE-*b*-PQ copolymers in solution showed very high antimicrobial activity toward *E. coli* and *S. aureus* when the n-alkyl chains attached to the nitrogens of the quaternary ammonium compounds are consisted of 12 - 14 carbons and 14 – 16 carbons, respectively. In the third example, a novel, highly brominated polymer was synthesized from

pentabromo-6-ethoxybenzene vinyl ether (BrVE) using cationic polymerization. The thermal and rheological properties of the polyBrVE (PBrVE) were compared to a commercially available oligomeric brominated flame retardant, poly(pentabromobenzyl acrylate) (PBrBA). In addition, polymer blends based on polybutylene terephthalate (PBT) were prepared with the two brominated polymers and the thermal stability, mechanical, and rheological properties compared. The use of PBrVE resulted in lower melt viscosity and better compatibility in blends with PBT which would be expected to provide enhanced processability with regard to creating injection molded parts with relatively thin walls, such as those encountered in the electronics industry. Finally, a process was developed to obtain vinyl ether-functional monomers containing fatty acid pendent groups directly from soybean oil (SBO) using base-catalyzed transesterification. Moreover, a carbocationic polymerization process was developed for the vinyl ether monomers that allowed for high molecular weight polymers to be produced. Compared to SBO, which possesses on average 4.5 vinyl groups per molecule, the polyvinylethers based on the soybean oil-derived vinyl ether monomers (polyVESFA) can possess tens to hundreds of vinyl groups per molecule depending on the polymer molecular weight produced. As a result of this difference, coatings based on polyVESFA were shown to possess much higher crosslink density at a given degree of functional group conversion compared to analogs based on conventional SBO. In addition, the dramatically higher number of functional groups per molecule associated with polyVESFA results in gel-points being reached at much lower functional group conversion, which was shown to dramatically reduce cure-time compared to SBO-based analogs.

ACKNOWLEDGEMENTS

It is my immense pleasure to thank my advisor, Dr. Bret J. Chisholm, for his constant support, guidance, and uncountable hours devoted towards the completion of this research work. There is absolutely no way I would have made it without support from a great mentor like him. I am grateful to my advisory committee members, Dr. Dean Webster, Dr. Wenfang Sun, and Dr. Achintya Bezbaruah for their constant guidance during my study in NDSU.

I also want to thank Dr. Chisholm's present and past group members for all the help and fun over the years. My special thanks go to Undergraduate Research Assistants John Jepperson and Anurad Jayasooriya for their sincere help in this research. I would like to thank Shane, Justin, and Lyndsi for their effort in evaluating the antimicrobial characteristics of coatings and polymers synthesized in this research. I would like to thank Venkata Chevali and Mike Fuqua for their wonderful help in extrusion molding, injection molding and mechanical testing. Over the years, many people have helped me at the CNSE and CPM to conduct this research smoothly. Persons who stand out are Christy, Dave, Jim, Liz, Heidi, and Jared – thank you for sharing your expertise in instrument handling.

Finally, I would like to thank my family members for their support throughout my graduate work, especially my parents and my wife. Their encouragement and enduring support was vital my completion of this goal.

The financial supports for this work from the Office of Naval Research, North Dakota Soybean Council, and Bioactive Coatings Systems are gratefully acknowledged.

DEDICATION

To my parents Abdur Rahim, Mukaruman Nisa; to my wife Tania Tazeen.

TABLE OF CONTENTS

ABSTRACT.....	iii
ACKNOWLEDGEMENTS.....	v
DEDICATION.....	vi
LIST OF TABLES	xvi
LIST OF FIGURES	xx
CHAPTER 1. GENERAL INTRODUCTION: CARBOCATIONIC POLYMERIZATION OF VINYL ETHERS – A COMPREHENSIVE LITERATURE REVIEW	1
1.1. ABSTRACT	1
1.2. INTRODUCTION.....	1
1.2.1. Components of cationic polymerization.....	3
1.3. LIVING CARBOCATIONIC POLYMERIZATION	7
1.3.1. Factors influencing the living carbocationic polymerization	8
1.4. LIVING CATIONIC POLYMERIZATION OF VINYL ETHER.....	8
1.4.1. Stabilization of the carbocation by counter ion	9
1.4.2. Stabilization of carbocation by added base.....	9
1.5. VINYL ETHER MONOMER DERIVED FROM RENEWABLE RESOURCES	14
1.6. END-FUNCTIONAL POLYVINYLEETHER POLYMERS	15

1.6.1. End-capping by functional initiator	16
1.6.2. End-capping by functional terminators.....	17
1.7. COPOLYMERIZATION OF VINYL ETHER	18
1.7.1. Poly(vinylether)- <i>b</i> -poly(vinylether) copolymers.....	19
1.8. SUMMARY.....	21

CHAPTER 2. SYNTHESIS, CHARACTERIZATION, AND ANTIMICROBIAL
ACTIVITY OF POLY[(DIMETHYL-*CO*-TRIMETHYL(PROPYL)
SILYLMETHYL)SILOXANE]-*g*-POLY[2,4-DICHLORO-1-(4-CHLORO-2-(2-
(VINILOXY)ETHOXY)PHENOXY)BENZENE] PRODUCED USING

LIVING CARBOCATIONIC POLYMERIZATION AND HYDROSILYLATION.....	22
2.1. ABSTRACT	22
2.2. INTRODUCTION	23
2.3. EXPERIMENTAL.....	29
2.3.1. Materials	29
2.3.2. Synthesis of TVE, PTVE, and PDMS- <i>g</i> -PTVE.....	31
2.3.3. Instrumentation and measurements	40
2.3.4. Coating surface characterization.....	42
2.3.5. Deposition of coatings for antimicrobial characterization.....	43
2.3.6. Characterization of antimicrobial properties	44
2.4. RESULTS	48
2.4.1. Characterization of TVE, PTVE, and PDMS- <i>g</i> -PTVE.....	48

2.4.2. Antimicrobial properties of tethered Triclosan coatings	65
2.5. DISCUSSION.....	77
2.5.1. Reduction in biofilm viability.....	77
2.5.2. Reduction in biofilm retention.....	78
2.5.3. Reduction in biofilm retraction.....	84
2.6. CONCLUSION.....	85

CHAPTER 3. SYNTHESIS AND CHARACTERIZATION OF A NOVEL INITIATOR, 1-(2-(4-ALLYL-2-METHOXYPHENOXY)ETHOXY)ETHYL ACETATE, AND ANTIMICROBIAL ACTIVITY OF POLY(DIMETHYL SILOXANE)- <i>b</i> -POLY[CHLOROETHYL VINYLETHER)- <i>b</i> -POLY(N,N,N- ALKYLDIMETHYL-2-(VINILOXY) ETHANAMINIUM CHLORIDE] PRODUCED USING LIVING CARBOCATIONIC POLYMERIZATION, HYDROSILYLATION, AND QUATERNIZATION	88
3.1. ABSTRACT	88
3.2. INTRODUCTION	89
3.3. EXPERIMENTAL.....	95
3.3.1. Materials	95
3.3.2. Synthesis of the initiator, 1-(2-(4-allyl-2- methoxyphenoxy)ethoxy)ethyl acetate (AMEA).....	96
3.3.3. Synthesis of the monoallyl-functional PCVE using the AMEA initiator	98

3.3.4. Synthesis of the block copolymer of PCVE and PDMS (PDMS- <i>b</i> -PCVE).....	100
3.3.5. Synthesis of the quaternized block copolymer of PCVE and PDMS (PDMS- <i>b</i> -PCVE- <i>b</i> -PQ)	101
3.3.6. Instrumentation and measurements	104
3.3.7. Antimicrobial activity of PDMS- <i>b</i> -PCVE- <i>b</i> -PQs (polyquats)	105
3.4. RESULTS AND DISCUSSION.....	107
3.4.1. Characterization of AMB and AMEA.....	107
3.4.2. Polymerization using the AMEA/Et _{1,5} AlCl _{1,5} initiating system.....	111
3.4.3. Synthesis and characterization of PDMS- <i>b</i> -PCVE.....	115
3.4.4. Synthesis and characterization of PDMS- <i>b</i> -PCVE- <i>b</i> -PQ.....	120
3.5. CONCLUSION.....	127

CHAPTER 4. SYNTHESIS AND CHARACTERIZATION OF A NOVEL, HIGHLY BROMINATED, FLAME RETARDANT POLYMER PRODUCED USING CARBOCATIONIC POLYMERIZATION.....	129
4.1. ABSTRACT	129
4.2. INTRODUCTION	129
4.3. EXPERIMENTAL.....	134
4.3.1. Materials	134

4.3.2. Synthesis of 1,2,3,4,5-pentabromo-6-(2-(vinylloxy)ethoxy) benzene (BrVE)	135
4.3.3. Synthesis of the polymer of BrVE.....	138
4.3.4. Determination of the solution viscosity of PBrVE	142
4.3.5. Determination of the Specific gravity of PBrVE.....	143
4.3.6. Instrumentation and procedures.....	144
4.4. RESULTS AND DISCUSSION.....	146
4.4.1. Characterization of BrVE	146
4.4.2. Polymerization kinetics studies	149
4.4.3. Characterization of PBrVE using NMR and FTIR.....	154
4.4.4. Comparison of the solution viscosities of PBrVE to PBrBA	155
4.4.5. Comparison of the glass transition temperature (T_g) of PBrVE to PBrBA.....	156
4.4.6. Determination of thermal decomposition kinetics of PBrVE and PBrBA.....	157
4.4.7. Film formation and refractive index	163
4.4.8. Comparison of the rheological properties of PBrVE to PBrBA.....	165
4.5. CONCLUSION.....	166

CHAPTER 5. CHARACTERIZATION OF BLENDS OF POLYBUTYLENE TEREPHTHALATE AND POLY(PENTABROMO-6-(2-(VINYL OXY) ETHOXY)BENZENE)	168
5.1. ABSTRACT	168
5.2. INTRODUCTION	168
5.3. EXPERIMENTAL.....	173
5.3.1. Materials	173
5.3.2. Polymer blend preparation.....	173
5.3.3. Instrumentation and procedures.....	175
5.4. RESULTS AND DISCUSSION.....	178
5.4.1. Measurement of thermal properties of PBT and PBT/BFRs blends	180
5.4.2. Thermogravimetric analysis of PBT, PBT/PBrVE, and PBT/PBrBA	181
5.4.3. Tensile testing of PBT/BFRs and PBT/BFRs/Sb ₂ O ₃ blends	183
5.4.4. Flexural testing of PBT/Sb ₂ O ₃ /BFR blends.....	185
5.4.5. Izod impact testing of PBT/Sb ₂ O ₃ and PBT/Sb ₂ O ₃ /BFR blends	187
5.4.6. Comparison of the rheological properties of a PBT/PBrVE blend to a PBT/PBrBA blend.....	187
5.4.7. Comparison of the morphology of a PBT/PBrVE blend to a PBT/PBrBA blend	188

5.4.8. Flame retardancy testing for PBT/Sb ₂ O ₃ , PBT/Sb ₂ O ₃ /PBrVE, and PBT/Sb ₂ O ₃ /PBrBA blends using a vertical burn test	189
5.5. CONCLUSION.....	191
 CHAPTER 6. COATINGS DERIVED FROM NOVEL, SOYBEAN OIL- BASED POLYMERS PRODUCED USING LIVING CARBOCATIONIC POLYMERIZATION	
	192
6.1. ABSTRACT	192
6.2. INTRODUCTION	193
6.3. EXPERIMENTAL.....	198
6.3.1. Materials	198
6.3.2. Synthesis of the vinyl ether of SBO fatty acids (VESFA) and polymer of VESFA (polyVESFA).....	199
6.3.3. Synthesis of polyethylene glycol-functional monovinylether monomer (VEPEG) and the polymer of VEPEG (polyVEPEG	203
6.3.4. Comparison of polyVESFA with SBO.....	206
6.3.5. Instrumentation and procedures.....	207
6.4. RESULTS AND DISCUSSION.....	209
6.4.1. VESFA and polyVESFA synthesis and characterization	209
6.4.2. Characterization of polyVEPEG and polyVESFA- <i>r</i> -VEPEG	221
6.4.3. Property comparison of polyVESFA with SBO	224

6.4.4. Coatings cured using autoxidation.....	227
6.4.5. Coatings cured using sulfur vulcanization.....	229
6.5. CONCLUSION.....	231

CHAPTER 7. SYNTHESIS, CHARACTERIZATION, AND APPLICATION
OF A NOVEL EPOXY-FUNCTIONAL POLYMER OF VESFA

(E-POLYVESFA) AND DERIVATIVES OF E-POLYVESFA.....	233
7.1. ABSTRACT	233
7.2. INTRODUCTION	234
7.3. EXPERIMENTAL.....	241
7.3.1. Materials	241
7.3.2. Synthesis of E-polyVESFA	242
7.3.3. Synthesis of acrylated polyVESFA (A-polyVESFA) and acrylated soybean oil (A-SBO).....	242
7.3.4. Synthesis of alcohol-functional polyVESFA (OH-polyVESFA) and soybean oil (OH-SBO)	244
7.3.5. Coating preparation to compare the difference between E-polyVESFA and E-SBO in epoxy-amine cure systems	246
7.3.6. Coating preparation to compare the difference between E-polyVESFA and E-SBO in cationic photocure systems	246
7.3.7. Coating preparation to compare the difference between A- polyVESFA and A-SBO in free-radical photocure systems.....	248

7.3.8. Coating preparation to compare the difference between OH-polyVESFA and OH-SBO in polyurethane coating systems.....	249
7.3.9. Instrumentation and procedures.....	250
7.4. RESULTS AND DISCUSSION.....	253
7.4.1. Characterization and property comparison of E-polyVESFA with E-SBO (ESO).....	253
7.4.2. Characterization of coatings to compare the difference between E-polyVESFA and E-SBO in epoxy-amine cure systems.....	258
7.4.3. Characterization of coatings to compare the difference between E-polyVESFA and E-SBO in cationic photocure systems.....	260
7.4.4. Characterization of A-polyVESFA and A-SBO.....	273
7.4.5. Characterization of coatings to compare the difference between A-polyVESFA and A-SBO in free-radical photocure cure systems.....	276
7.4.6. Characterization of OH-polyVESFA and OH-SBO	282
7.4.7. Characterization of coatings to compare the difference between OH-polyVESFA and OH-SBO in polyurethane coating systems	284
7.5. CONCLUSION.....	285
CHAPTER 8. GENERAL CONCLUSION.....	288
LITERATURE CITED	293

LIST OF TABLES

<u>Table</u>	<u>Page</u>
2.1. Chemicals used.	30
2.2. Compositions of PDMS- <i>g</i> -PTVE/H and PDMS- <i>g</i> -PTVE/P copolymers based on weight of A-PTVE and molecular weight of poly(dimethyl-co-methylhydrosiloxane).	39
2.3. Surface roughness of coatings produced from PDMS- <i>g</i> -PTVE/P coatings with PDMS-63K and PDMS-6K.	65
2.4. MIC data for both biomedically-relevant and marine-relevant microorganisms.	74
3.1. Chemicals used.	95
3.2. Formulation table for the synthesis of PDMS- <i>b</i> -PCVE.....	101
3.3. Formulation table for the quaternization of PDMS- <i>b</i> -PCVE synthesized from PDMS/H-1.05K.....	103
3.4. Formulation table for the quaternization of PDMS- <i>b</i> -PCVE synthesized from PDMS/H-17.2K.....	103
3.5. Theoretical and GPC number average molecular weight obtained for PCVE, PDMS/H, and PDMS- <i>b</i> -PCVE.	118
3.6. T_{onset} and T_0 data obtained for PCVE, PDMS/H, and PDMS- <i>b</i> -PCVE.	120
3.7. Actual quaternization (mole percentage) calculated using ^1H NMR spectra of PDMS- <i>b</i> -PCVE- <i>b</i> -PQs.	122
4.1. The chemical structure of some commercially available monomeric brominated flame retardants.	133
4.2. The chemical structure of some commercially available polymeric brominated flame retardants.	134
4.3. Chemicals used.	135

4.4.	Formulation of BrVE polymerizations.	141
4.5.	BrVE conversion and PBrVE intrinsic viscosity obtained for polymerizations described in Table 4.4.	154
4.6.	Viscometric parameters for PBrVE and PBrBA.	156
4.7.	Values of T_{onset} , T_0 , and ash content for BFRs.....	160
4.8.	Activation energies at different percentage of decomposition for PBrVE and PBrBA using Flynn–Wall method.....	162
4.9.	Activation energies of decomposition for PBrVE and PBrBA determined using Kissinger method.	163
4.10.	Results obtained from AFM experiment.	164
4.11.	Shear Viscosity values for PBrVE and PBrBA at different temperatures.	166
5.1.	Chemicals used.	173
5.2.	Compositions of PBT-based blends produced from PBrVE and PBrBA.	174
5.3.	Parameters of melt extrusion process used to produce PBT-based blends.	174
5.4.	Parameters for injection molding process.	175
5.5.	Data obtained from DSC thermograms of PBT, PBT/PBrVE, and PBT/PBrBA.	181
5.6.	Values of the T_{onset} , T_0 , and ash content for pure PBT, PBT/PBrVE, and PBT/PBrBA.	182
5.7.	Data obtained from tensile test for PBT, PBT/PBrVE, and PBT/PBrBA samples with and without Sb_2O_3	185
5.8.	Data obtained from flexural test for PBT/ Sb_2O_3 , PBT/ Sb_2O_3 /PBrVE, and PBT/ Sb_2O_3 /PBrBA.	186
5.9.	Izod impact strength data for PBT/ Sb_2O_3 , PBT/ Sb_2O_3 /PBrVE, and PBT/ Sb_2O_3 /PBrBA.	187
5.10.	Results obtained from vertical burn flame retardant test for PBT/ Sb_2O_3 and PBT/ Sb_2O_3 /BFR blend.	190

6.1.	A list of the starting materials used for the investigation.	198
6.2.	Compositions used to compare the effect of a Lewis acid ($\text{Et}_{1.5}\text{AlCl}_{1.5}$) and MCAc to the polymerization of VESFA.	202
6.3.	Compositions used to determine the VESFA polymerization kinetic in the absence of an external base.	203
6.4.	Compositions used to compare the difference between polyVESFA and SBO in autoxidation-curable systems.	206
6.5.	Compositions used to compare the difference between polyVESFA and SBO in a sulfur vulcanization system.	207
6.6.	Theoretical and experimental integration values of proton obtained for VESFA.	210
6.7.	Theoretical and experimental integration values of proton obtained for polyVESFA.	214
6.8.	GPC number average molecular weight and PDI.	216
6.9.	Data obtained from TGA thermograms of VESFA, polyVESFA, and SBO.	226
6.10.	Cure characteristics obtained for coatings based on polyVESFA and SBO and cured using autoxidation. The composition of the coatings is described in Table 6.4.	228
7.1.	A list of the starting materials used for the investigation.	241
7.2.	Compositions used to compare the difference between E-polyVESFA and E-SBO in epoxy-amine cure systems.	246
7.3.	Compositions used to compare the difference between E-polyVESFA and E-SBO in cationic photocure systems.	247
7.4.	Compositions used to compare the difference between A-polyVESFA and A-SBO in free-radical photocure systems.	249
7.5.	Compositions used to compare the difference between OH-polyVESFA and OH-SBO in polyurethane coating systems.	250
7.6.	Data obtained from photo-DSC experiments on the coatings described in Table 7.3.	264

7.7.	Properties of coatings produced from E-polyVESFA and E-SBO in cationic photocure systems cured at a belt speed of 24 ft/min with 1 pass.	266
7.8.	Storage modulus, crosslink densities, and Tg of free films produced from E-polyVESFA and E-SBO in cationic photocure systems using one and two passes under the UVA lamp.	271
7.9.	Data obtains from DMA experiments for E-polyVESFA and E-SBO based coatings in cationic photocure systems using one pass under the UVA lamp.	273
7.10.	Real time FTIR data obtained for A-polyVESFA/HDDA and A-SBO/HDDA curing.	279
7.11.	Induction time and time to peak max values of Photo-DSC results for the acrylate-based coatings.	281
7.12.	Storage modulus and Tg obtained for free films produced from OH-polyVESFA and OH-SBO in a polyurethane coating system.	285

LIST OF FIGURES

<u>Figure</u>	<u>Page</u>
1.1. Mechanism of carbocationic polymerization.	2
1.2. Chain transfer to monomer and spontaneous termination for polymerization of isobutylene.	3
1.3. Chain transfer by backbiting for polymerization of styrene.	3
1.4. Resonance stabilized carbocation produced from vinyl ether.	4
1.5. Resonance stabilized carbocation produced from styrene.	4
1.6. Monomers used in cationic polymerization.	4
1.7. Initiation process in the presence of aluminum chloride and t-butyl chloride.....	5
1.8. Interaction of propagating carbocation, counterion and solvent; (I) Covalent species, (II) contact ion pair, (III) solvent separated ion-pair, and (IV) highly solvated ion-pair.	6
1.9. Cationic polymerization of vinyl ether initiated by HI/I ₂ and HI/ZnI ₂	10
1.10. Cationic polymerization of isobutyl vinyl ether initiated by Cationogen /EtAlCl ₂ in the absence and presence of an ester-functional base.	11
1.11. Vinyl ether monomer containing pendent functional moieties.	13
1.12. Vinyl ether monomers derived from renewable resources.	15
1.13. Functional-initiators used in combination with I ₂ or, ZnI ₂ to produce end-functional poly(vinyl ether).	16
1.14. Functional-terminators used to produce end-functional poly(vinyl ether).....	18
1.15. Synthesis of carboxylic acid end-functional polymer of vinyl ether	18
1.16. Synthesis of poly(TCDVE)-block-poly(NBVE)-block-poly(TCDVE).	20
1.17. Synthesis of poly(BMSiVE)-block-poly(IBVE).....	20

2.1.	The synthetic scheme used to produce 2-iodoethyl vinyl ether.	31
2.2.	The synthetic scheme used to produce TVE.	32
2.3.	The synthetic scheme used to produce IBEA.	33
2.4.	The synthetic scheme used to produce PTVE.	34
2.5.	The synthetic scheme used to produce A-PTVE.	37
2.6.	The synthetic scheme used to produce PDMS-g-PTVE/H.	38
2.7.	The synthetic scheme used to produce PDMS-g-PTVE/P.	39
2.8.	The synthetic scheme used to produce PDMS-g-PTVE/S.	40
2.9.	¹ H NMR spectrum obtained for 2-iodoethyl vinyl ether.	49
2.10.	¹ H NMR spectrum obtained for TVE.	49
2.11.	(a) DEPT-135, (b) ¹³ C NMR, and (c) HETCOR spectra obtained for TVE.	51
2.12.	FTIR spectrum obtained for TVE.	51
2.13.	¹ H NMR spectrum obtained for polymerization initiator, IBEA.	52
2.14.	TVE polymerization reaction spectra were taken using ReactIR before the addition of co-initiator and after the completion of polymerization ([TVE] ₀ : [IBEA] ₀ : [MCAC] ₀ : [Et _{1.5} AlCl _{1.5}] ₀ = 200:1:250:5).	53
2.15.	(A) Conversion % as a function of reaction time and (B) ln([M] ₀ /[M] _t) as function of reaction time for the carbocationic polymerization of TVE (With Base represents an initial composition of [TVE] ₀ : [IBEA] ₀ : [MCAC] ₀ : [Et _{1.5} AlCl _{1.5}] ₀ = 200:1:250:5 and No Base represents an initial composition of [TVE] ₀ : [IBEA] ₀ : [Et _{1.5} AlCl _{1.5}] ₀ = 200:1:5).	54
2.16.	GPC Mn as a function of conversion for the carbocationic polymerization of TVE ([TVE] ₀ : [IBEA] ₀ : [MCAC] ₀ : [Et _{1.5} AlCl _{1.5}] ₀ = 200:1:250:5).	54
2.17.	¹ H NMR spectrum obtained for monoallyl-functional PTVE. The integration values of total protons at different peak regions are mentioned here.	56
2.18.	¹³ C NMR spectrum obtained for monoallyl-functional PTVE.	56

2.19.	FTIR spectrum obtained for monoallyl-functional PTVE.	57
2.20.	¹ H NMR spectrum obtained for PDMS-g-PTVE/H.	58
2.21.	¹ H NMR spectrum obtained for PDMS-g-PTVE/P.	58
2.22.	FTIR spectrum obtained for PDMS-g-PTVE/P.	59
2.23.	DSC thermograms for PDMS-g-PTVE/P copolymers with PDMS-63K.	60
2.24.	DSC thermograms for PDMS-g-PTVE/P copolymers with PDMS-6K.	61
2.25.	TEM images of PDMS-g-PTVE/P copolymers with PDMS-63K and PDMS-6K.....	62
2.26.	AFM images (phase) of PDMS-g-PTVE/P coatings with PDMS-63K and PDMS-6K.	64
2.27.	AFM image (phase) of PDMS-g-PTVE/S coating with 52 wt. % PTVE.	64
2.28.	Surface energy and contact angle hysteresis of coatings produced from PDMS-g-PTVE/P copolymers with PDMS-63K and PDMS-6K. Each surface energy data was reported as the mean value of three replicate coatings. Error bars represent the standard deviation of the surface energy.	65
2.29.	Toxicity evaluation of PDMS-g-PTVE/P coating leachates against (A) <i>C. albicans</i> , (B) <i>E. coli</i> , and (C) <i>S. epidermidis</i> . Each data point represents the percentage of reduction in biofilm growth compared to a control coating. Error bars represent standard deviations from the mean value of three replicate measurements.....	68
2.30.	Toxicity evaluation of PDMS-g-PTVE/P coating leachates against (A) <i>N. incerta</i> and (B) <i>C. lytica</i> . Each data point represents the percentage of reduction in biofilm growth compared to a control coating. Error bars represent standard deviations from the mean value of three replicate measurements.	68
2.31.	Evaluation of <i>C. Lytica</i> biofilm (A) retention and (B) viability for coatings surfaces produced from PDMS-g-PTVE/P copolymers with PDMS-63K and PDMS-6K. Percent reduction values are reported after comparing to a silicone elastomeric control coating, DC 3140. Error bars represent standard deviations from the mean value of three replicate measurements.....	70

- 2.32. (A) Evaluation of *C. Lytica* biofilm retraction for coatings surfaces produced from PDMS-g-PTVE/P copolymers with PDMS-6K. Pictures in right side represent images of coating array plates after crystal violet staining for (B) PDMS-63K and (C) PDMS-6K with 29%, 42%, 52%, and 100% PTVE. Percent reduction values are reported after comparing to a silicone elastomeric control coating, DC 3140. Error bars represent standard deviations from the mean value of three replicate measurements.....71
- 2.33. Evaluation of *N. Incerta* biofilm growth for coatings surfaces produced from PDMS-g-PTVE/P copolymers with PDMS-63K and PDMS-6K. Percent reduction values are reported after comparing to a silicone elastomeric control coating, DC 3140. Error bars represent standard deviations from the mean value of three replicate measurements.71
- 2.34. Evaluation of *S. epidermidis* biofilm (A) retraction and (B) viability for coatings surfaces produced from PDMS-g-PTVE/P copolymers with PDMS-63K and PDMS-6K. (C) Pictures in right side represent images of coating array plates after crystal violet staining for PDMS-6K with 29%, 42%, 52%, and 100% PTVE. Percent reduction values are reported after comparing to a silicone elastomeric control coating, DC 3140. Error bars represent standard deviations from the mean value of three replicate measurements.72
- 2.35. Evaluation of *E. coli* biofilm (A) retention and (B) viability for coatings surfaces produced from PDMS-g-PTVE/P copolymers with PDMS-63K and PDMS-6K. Percent reduction values are reported after comparing to a silicone elastomeric control coating, DC 3140. Error bars represent standard deviations from the mean value of three replicate measurements.....72
- 2.36. (A) Evaluation of *E. coli* biofilm retraction for coatings surfaces produced from PDMS-g-PTVE/P copolymers with PDMS-63K and PDMS-6K. Pictures in right side represent images of coating array plates after crystal violet staining for (B) PDMS-63K and (C) PDMS-6K with 29%, 42%, 52%, and 100% PTVE. Percent reduction values are reported after comparing to a silicone elastomeric control coating, DC 3140. Error bars represent standard deviations from the mean value of three replicate measurements.73

2.37.	Evaluation of <i>C. albicans</i> biofilm (A) retention and (B) viability for coatings surfaces produced from PDMS-g-PTVE/P copolymers with PDMS-63K and PDMS-6K. Pictures in right side represent images of coating array plates after crystal violet staining for (C) PDMS-63K and (D) PDMS-6K with 29%, 42%, 52%, and 100% PTVE. Percent reduction values are reported after comparing to a silicone elastomeric control coating, DC 3140. Error bars represent standard deviations from the mean value of three replicate measurements.	73
2.38.	Toxicity evaluation of PDMS-g-PTVE/S coating leachates against <i>C. lytica</i> , <i>N. incerta</i> , <i>S. aureus</i> , <i>C. albicans</i> , and <i>E. coli</i> . Each data point represents the percentage of reduction in biofilm growth compared to a control coating. Error bars represent standard deviations from the mean value of three replicate measurements.	75
2.39.	Evaluation of <i>C. Lytica</i> , <i>S. aureus</i> , <i>C. albicans</i> , and <i>E. coli</i> biofilm retention for coating surface produced from PDMS-g-PTVE/S containing 52 wt. % PTVE. Percent reduction values are reported after comparing to a silicone elastomeric control coating, DC 3140. Error bars represent standard deviations from the mean value of three replicate measurements.	75
2.40.	Images of the PDMS-g-PTVE/S (52 wt. % PTVE) coating array plates after crystal violet staining for <i>C. lytica</i> , <i>S. aureus</i> , <i>E. coli</i> , and <i>C. albicans</i> in biofilm retention experiment.	76
2.41.	(A) Evaluation of <i>N. incerta</i> biofilm growth and (B) <i>S. aureus</i> and <i>E. coli</i> biofilm viability for coating surface produced from PDMS-g-PTVE/S containing 52 wt. % PTVE. Percent reduction values are reported after comparing to a silicone elastomeric control coating, DC 3140. Error bars represent standard deviations from the mean value of three replicate measurements.	76
3.1.	Chemical structure of initiator (A - F) used in combination with I ₂ or, ZnI ₂ ; and Et ₃ Al ₂ Cl ₃ (G - H).	90
3.2.	(A) Possible chemical structure of a novel initiator and (B) synthesis scheme of a monoallyl-functional polymer-1 using the initiator.	91
3.3.	Synthesis of monoallyl-functional copolymer (random and block) using the initiator.	91
3.4.	Synthesis of block and graft copolymers using the monoallyl-functional polymer-1.	92

3.5.	Derivatization of monoallyl-functional polymer-1 and crosslinking to produce cured coatings.	92
3.6.	Derivatization of monoallyl-functional polymer-1 to produce functional polymers.	92
3.7.	Preparation of surface monolayer of polymer-1 over a treated glass.	93
3.8.	Structure of the novel initiator, 1-(2-(4-allyl-2-methoxyphenoxy)ethoxy)ethyl acetate (AMEA).	94
3.9.	The synthetic scheme used to produce 2-iodoethylvinylether.	96
3.10.	The synthetic scheme used to produce AMB.	97
3.11.	The synthetic scheme used to produce AMEA.	98
3.12.	The synthetic scheme used to produce PCVE.	99
3.13.	The synthetic scheme used to produce PDMS- <i>b</i> -PCVE.	101
3.14.	The synthetic scheme used to produce PDMS- <i>b</i> -PCVE- <i>b</i> -PQ.	102
3.15.	¹ H NMR spectrum obtained for AMB.	108
3.16.	¹ H NMR spectrum obtained for AMEA.	109
3.17.	DEPT-135 and ¹³ C NMR spectra obtained for AMEA.	109
3.18.	HETCOR spectrum obtained for AMEA.	110
3.19.	FTIR spectrum obtained for AMEA.	110
3.20.	Mechanism of initiation process of vinyl ether polymerization in the presence of a AMEA/Et _{1.5} AlCl _{1.5} initiating system.	111
3.21.	Mechanism of initiation process of vinyl ether polymerization in the presence of AMEA/Et _{1.5} AlCl _{1.5} initiating system and an added base, for example, methyl chloroacetate.	112
3.22.	Plot of (A) GPC number average molecular weight as a function of % of conversion and (B) ln{[M] ₀ /[M] _t } as a function of polymerization time for CVE initiated by AMEA/Et _{1.5} AlCl _{1.5} in the presence of MCAC as an added base. [CVE] ₀ : [AMEA] ₀ : [MCAC] ₀ : [Et _{1.5} AlCl _{1.5}] ₀ = 200:1:250:5.	113

3.23.	¹ H NMR spectrum obtained for monoallyl-functional PCVE.....	114
3.24.	¹ H NMR spectrum obtained for PDMS- <i>b</i> -PCVE copolymer.	116
3.25.	FTIR spectrum obtained for PDMS- <i>b</i> -PCVE copolymer.	117
3.26.	GPC chromatograms obtained for PCVE, PDMS/H, and PDMS- <i>b</i> -PCVE.	117
3.27.	TGA thermograms obtained for PCVE, PDMS/H, and PDMS- <i>b</i> -PCVE.	119
3.28.	DTG thermograms obtained for PCVE, PDMS/H, and PDMS- <i>b</i> -PCVE.....	120
3.29.	¹ H NMR spectrum obtained for PDMS- <i>b</i> -PCVE- <i>b</i> -PQ.	121
3.30.	FTIR spectrum obtained for PDMS- <i>b</i> -PCVE- <i>b</i> -PQ.	122
3.31.	Images of array plates illustrate representative results obtained combinatorial high throughput screening of antimicrobial activity in aqueous solution. Dilutions were presented in each row of the plates. Three replicate wells used per dilution were shown in columns.	124
3.32.	Variation of log reduction with the number of n-alkyl carbons attached to the nitrogen atom in PDMS- <i>b</i> -PCVE- <i>b</i> -PQ for (A) 10 mole %, (B) 30 mole %, and 50 mole % quaternization when tested against <i>S. aureus</i>	125
3.33.	Variation of log reduction with the number of n-alkyl carbons attached to the nitrogen atom in PDMS- <i>b</i> -PCVE- <i>b</i> -PQ for (A) 10 mole %, (B) 30 mole %, and 50 mole % quaternization when tested against <i>E. coli</i>	125
4.1.	The synthetic scheme used to produce 2-iodoethylvinylether.	136
4.2.	The synthetic scheme used to produce BrVE.	137
4.3.	The synthetic scheme used to produce IBEA.	139
4.4.	The synthetic scheme used to produce PBrVE.	140
4.5.	The synthetic scheme used to produce PBrVE in the absence of the IBEA and MCAc.....	141
4.6.	¹ H NMR spectra of (A) IVE and (B) BrVE.	147
4.7.	¹³ C NMR and DEPT-135 spectra of BrVE.	148
4.8.	HETCOR spectrum of BrVE.	148

4.9.	FTIR spectrum of BrVE.....	149
4.10.	Plot of (A) reduced viscosity and (B) inherent viscosity as a function of monomer conversion for BrVE polymerization at 0 °C ($[M]_0:[IBEA]_0:[MCAc]_0:[Et_{1.5}AlCl_{1.5}]_0 = 200:1:250:5$).	150
4.11.	BrVE polymerization spectra before the addition of $Et_{1.5}AlCl_{1.5}$ and after 2 hours of reaction at a reaction temperature of 22 °C ($[BrVE]_0:[IBEA]_0:[MCAc]_0:[Et_{1.5}AlCl_{1.5}]_0 = 200:1:250:5$).	151
4.12.	Plot of % of conversion vs. reaction time at three different reaction temperatures of 0 °C, 22 °C, and 50 °C. ($[M]_0:[IBEA]_0:[MCAc]_0:[Et_{1.5}AlCl_{1.5}]_0 = 200:1:250:5$).	151
4.13.	Plot of $\ln([M]_0/[M]_t)$ vs. reaction time at three different reaction temperatures of 0 °C, 22 °C, and 50 °C. ($[M]_0:[IBEA]_0:[MCAc]_0:[Et_{1.5}AlCl_{1.5}]_0 = 200:1:250:5$).....	152
4.14.	1H NMR spectrum for PBrVE.	155
4.15.	FTIR spectrum for PBrVE.	155
4.16.	Plot of η_{sp}/c as a function of c and $(\ln \eta_r)/c$ as a function of c for (A) PBrVE and (B) PBrBA.	156
4.17.	DSC thermograms for PBrVE and PBrBA.	157
4.18.	Plot of weight % as a function of temperature and (B) derivative of weight % as function of temperature for PBrVE and PBrBA when a heating rate of 20 °C/minute was used.	159
4.19.	Plot of weight % as a function of temperature for PBrVE and PBrBA when five different heating rates were used.	159
4.20.	Plot of $-\log\beta$ as a function of $1/T$ for PBrVE.	161
4.21.	Plot of $-\log\beta$ as a function of $1/T$ for PBrBA.	161
4.22.	AFM images of PBrVE and PBrBA films.	163
4.23.	Refractive index as a function of wavelength for PBrVE and PBrBA.	164
4.24.	Shear viscosity as a function of frequency at 230 °C.	165
4.25.	Shear viscosity as a function of temperature.	166

5.1.	Schematic representation of flame test set up.	178
5.2.	DSC thermograms obtained from (A) second heating and (B) first cooling for PBT, PBT/PBrVE, and PBT/PBrBA.	180
5.3.	TGA thermograms obtained for pure PBT, PBT/PBrVE, and PBT/PBrBA in an air atmosphere.	182
5.4.	Plot of tensile stress as a function of tensile strain for (A) PBT, PBT/PBrVE, and PBT/PBrBA; and (B) PBT/Sb ₂ O ₃ , PBT/Sb ₂ O ₃ /PBrVE, and PBT/Sb ₂ O ₃ /PBrBA.	184
5.5.	Plot of flexural stress as a function of flexural strain for PBT/Sb ₂ O ₃ , PBT/Sb ₂ O ₃ /PBrVE, and PBT/Sb ₂ O ₃ /PBrBA.	186
5.6.	Shear viscosity as a function of frequency for PBT, PBT/PBrVE, and PBT/PBrBA at (A) 230 °C and (B) 255 °C.	188
5.7.	TEM micrographs of the PBT/PBrVE and PBT/PBrBA blends.	189
6.1.	A schematic illustrating the difference in molecular architecture between a plant oil triglyceride and a synthetic polymer containing a fatty acid pendent group in the repeat	197
6.2.	The relationship between theoretical gel-point (i.e. degree of conversion that results in the production of a crosslinked network) and DP of polymers possessing a fatty acid pendent group in the repeat unit. To generate this plot, equation (I) was modified by substituting $DP\gamma$ for f where γ is the average number of functional groups per fatty acid pendent group.	197
6.3.	The synthetic scheme used to produce VESFA.	199
6.4.	The synthetic scheme used to produce polyVESFA.	201
6.5.	The synthetic scheme used to produce VEPEG.	204
6.6.	The synthetic scheme used to produce polymer of VEPEG.	204
6.7.	The synthetic scheme used to produce copolymer of VESFA and VEPEG.	205
6.8.	¹ H NMR spectrum obtained for VESFA.	210
6.9.	¹³ C NMR and DEPT-135 spectra obtained for VESFA.	211
6.10.	FTIR spectrum obtained for VESFA.	212

6.11.	¹ H NMR spectrum obtained for polyVESFA.	213
6.12.	¹³ C NMR spectrum obtained for polyVESFA.	214
6.13.	FTIR spectrum obtained for polyVESFA.	215
6.14.	Plot of normalized peak intensity as a function of retention time for GPC chromatograms of SBO, VESFA, and polyVESFA.	215
6.15.	Plot of % of conversion as a function of Lewis acid amount after 17 hours of polymerization when carried out both in the presence ([VESFA] ₀ : [MCAC] ₀ = 200:250) and absence ([VESFA] ₀ : [MCAC] ₀ = 200:0) of an external base (MCAC). The X-axis indicates the value of the ratio [Et _{1.5} AlCl _{1.5}] ₀ : [VESFA] ₀ , when [VESFA] ₀ was selected as 200.	217
6.16.	Plot of (A) GPC number average molecular weight and (B) PDI as a function of Lewis acid amount after 17 hours of polymerization when carried out both in the presence ([VESFA] ₀ : [MCAC] ₀ = 200:250) and absence ([VESFA] ₀ : [MCAC] ₀ = 200:0) of an external base (MCAC). The X-axis indicates the value of the ratio [Et _{1.5} AlCl _{1.5}] ₀ : [VESFA] ₀ , when [VESFA] ₀ was selected as 200.	217
6.17.	Stabilization of carbocation in the presence of ester group of VESFA.	218
6.18.	Plot of (A) ln{[M] ₀ /[M] _t } and (B) monomer concentration as a function of polymerization time. The symbols MCAC/LA-0/5, MCAC/LA-0/10, and MCAC/LA-0/18 represent the condition of polymerizations in the absence of an external base when the LA was used at three different molar concentrations of 5, 10, and 18, respectively.....	220
6.19.	Plot of GPC number average molecular weight and PDI as a function of % of conversion for the polymerization of VESFA. ([VESFA] ₀ : [IBEA] ₀ : [Et _{1.5} AlCl _{1.5}] ₀ was used as 200:1:18).	221
6.20.	¹ H NMR spectrum obtained for VEPEG.	222
6.21.	FTIR spectrum obtained for VEPEG.....	222
6.22.	¹ H NMR spectrum obtained for polyVEPEG.	223
6.23.	¹ H NMR spectrum obtained for polyVESFA- <i>r</i> -polyVEPEG.	224
6.24.	(A) DSC thermograms for polyVESFA, SBO, and (B) VESFA.	226
6.25.	TGA thermograms for VESFA, polyVESFA, and SBO.	226

6.26.	Plot of viscosity as a function of shear rate for polyVESFA and SBO.	227
6.27.	Shear storage modulus and shear viscosity as a function of vulcanization time at 140 °C for SBO/S and polyVESFA/S cure systems.	230
7.1.	World production of oil seven major crops.	234
7.2.	Schematic representation of cationic photopolymerization in presence of alcohols.	237
7.3.	Chemical structure of (A) diazonium salt, (B) iodonium salt, (C) sulfonium salt, and (D) iron-arene salt.	238
7.4.	Photolysis of sulfonium salt and generation of protons in the (a) presence and (b) absence of proton donor.	238
7.5.	Free radical photoinitiator: Cleavage type (I and II), Bimolecular type (III).	239
7.6.	The synthetic scheme used to produce E-polyVESFA.	242
7.7.	The synthetic scheme used to produce A-polyVESFA.	243
7.8.	The synthetic scheme used to produce OH-polyVESFA.	245
7.9.	The synthetic scheme used to produce polyurethane coating.	250
7.10.	¹ H NMR spectrum obtained for E-polyVESFA.	253
7.11.	¹³ C NMR spectrum obtained for E-polyVESFA.	254
7.12.	FTIR spectrum obtained for E-polyVESFA.	255
7.13.	¹ H NMR spectrum obtained for E-SBO.	255
7.14.	(A) DSC thermograms for E-polyVESFA and E-SBO. (B) TGA thermograms for E-polyVESFA and E-SBO.	257
7.15.	Plot of viscosity as a function of shear rate for E-polyVESFA and E-SBO.	257
7.16.	Shear modulus as a function time at 120 °C for a blend of E-polyVESFA and TETA as well as E-SBO and TETA. A 1/1 stoichiometry between the epoxy groups and NH groups was used.	259

7.17.	Results obtained from RT-FTIR experiments on the coatings described in Table 7.3.	261
7.18.	Results obtained from photo-DSC experiments on the coatings described in Table 7.3.	263
7.19.	Results obtained from thermal cure that was applied immediately after photo-DSC experiments on the coatings described in Table 7.3.	263
7.20.	Viscoelastic properties obtained for free films produced from E-polyVESFA and E-SBO in cationic photocure systems using (A) one and (B) two passes under the UVA lamp.	271
7.21.	Viscoelastic properties obtained for free films produced from E-polyVESFA and E-SBO in cationic photocure systems using one pass under the UVA lamp.	272
7.22.	Viscoelastic properties obtained for free films produced from E-polyVESFA and E-SBO in cationic photocure systems using one pass under the UVA lamp.	272
7.23.	¹ H NMR spectrum obtained for A-polyVESFA.	274
7.24.	FTIR spectrum obtained for A-polyVESFA.	275
7.25.	¹ H NMR spectrum obtained for A-SBO.	275
7.26.	% of conversion as a function of UV exposure time for a free-radical photo curable system in air.	278
7.27.	Real time FTIR results for the acrylate-based coatings described in Table 7.4.	278
7.28.	Photo-DSC results for the acrylate-based coatings described in Table 7.4.	281
7.29.	¹ H NMR spectrum obtained for OH-polyVESFA.	283
7.30.	FTIR spectrum obtained for OH-polyVESFA.	283
7.31.	¹ H NMR spectrum obtained for OH-SBO.	284
7.32.	Viscoelastic properties obtained for free films produced from OH-polyVESFA and OH-SBO in a polyurethane coating system.	285

CHAPTER 1. GENERAL INTRODUCTION: CARBOCATIONIC POLYMERIZATION OF VINYL ETHERS – A COMPREHENSIVE LITERATURE REVIEW

1.1. ABSTRACT

Polymerization of the carbon-carbon double bond by cationic initiator has been at the forefront of research in polymer science and engineering for last couple of decades. In general, the components of cationic polymerization are monomer, cationic initiator, co-initiator (Lewis acid), solvent, and additive such as Lewis base. In a living carbocationic polymerization, the propagating species do not take part in side reactions, such as chain termination and chain transfer. In living carbocationic polymerization, a well defined polymer can be produced with narrow molecular weight distribution. The major advantage of living carbocationic polymerization is the synthesis of new polymeric structure, for example, hyperbranched polymers, star-branched polymers, graft, and block copolymers. In this review, the concept, design, and synthesis of poly(vinylether) using cationic polymerization are discussed.

1.2. INTRODUCTION

Cationic polymerization has a long history, and initially it was thought that polymerizations of styrene and dienes with controlled molecular weight are very difficult. The first cationic polymerization reported was in the late 18th century. Since then, cationic polymerization were conducted on numerous monomers. In the early 20th century the first kinetic study was reported.¹ Since then a considerable amount of research was carried out

to control the reactivity of the carbocation. However, until 1960 it was postulated that due to the high reactivity of the carbocation, living carbocationic polymerization could not be possible.²

The general mechanism of carbocationic polymerization can be described according to Figure 1.1. Unlike free-radical polymerization, termination of cationic polymerization never involves the bimolecular reaction between two propagating species of similar charge. In a non-living polymerization, the highly reactive carbocation undergoes a variety of side reactions, such as β -proton abstraction, chain transfer to monomer, and backbiting which cause unexpected termination of the carbocation (Figure 1.2 – 1.3).³ Living polymerization is one of the most important techniques used in polymer science. The term ‘living’ was first introduced by Szwarc to differentiate polymerizations in which chain-breaking processes, such as chain termination and chain transfer were absent.⁴

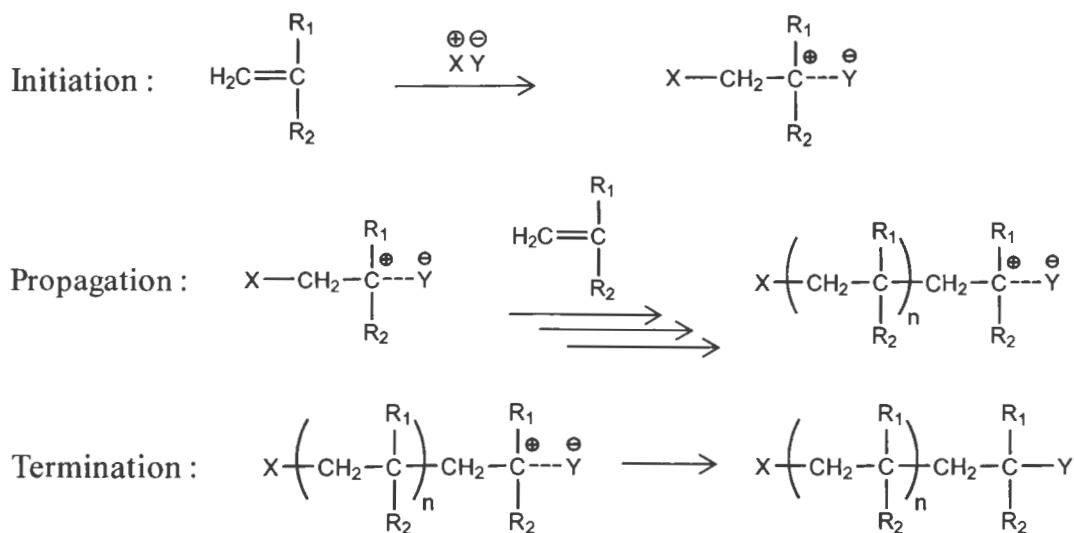


Figure 1.1. Mechanism of carbocationic polymerization.

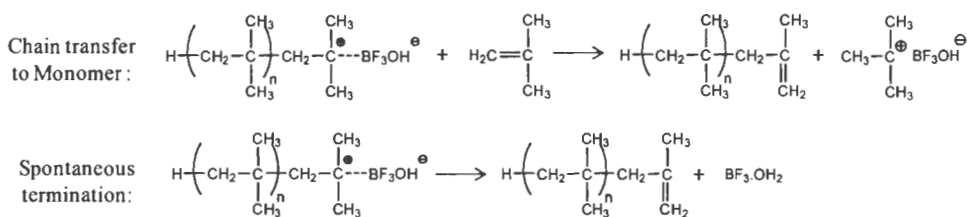


Figure 1.2. Chain transfer to monomer and spontaneous termination for polymerization of isobutylene.

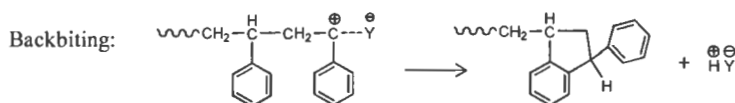


Figure 1.3. Chain transfer by backbiting for polymerization of styrene.

1.2.1. Components of cationic polymerization

1.2.1.1. Monomer

Monomers capable of producing stable carbocations should be able to undergo carbocationic polymerization. Carbocations generated by vinyl ether and styrene are quite stable due to resonance stabilization by delocalization of the positive charge (Figure 1.4 and 1.5). A series of monomers capable of producing polymers using carbocationic polymerization are listed in the Figure 1.6. The negative inductive effect of oxygen atom in vinyl ether is superseded by the conjugation of π bond with the lone pair of oxygen which reduces the reactivity of the carbocation. For styrene, the π bonds of olefin and aromatic ring can overlap; and the benzylic carbocation formed by the addition proton to the olefinic unsaturation is stabilized by resonance. In addition to the resonance and inductive effects, the hyperconjugation effect (σ - π) also provides stability of the carbocation generated by substituted olefins such as isobutylene.

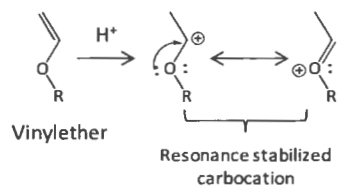


Figure 1.4. Resonance stabilized carbocation produced from vinyl ether.

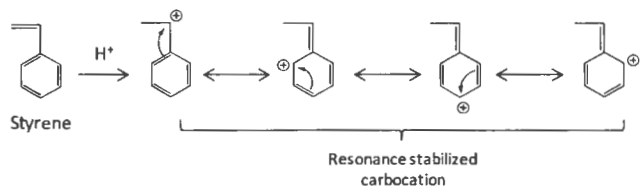


Figure 1.5. Resonance stabilized carbocation produced from styrene.

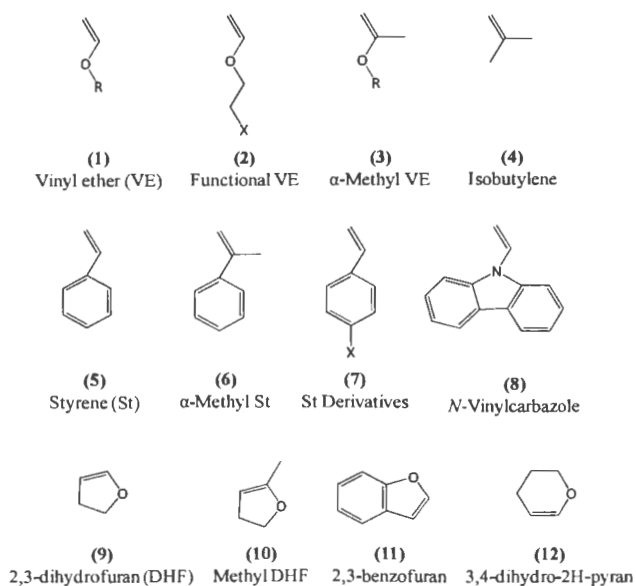


Figure 1.6. Monomers used in cationic polymerization.

1.2.1.2. Initiator

Various initiators producing cationic species with the reaction of Lewis acids can be used to polymerize monomers with electron releasing substituent.^{2, 5} The primary

requirement for the counter-ion not to be highly nucleophilic normally limits the use of strong acids as cationic initiators. Hydrogen iodide, cationogen (adduct of vinyl ether with a protonic acid) are commonly used as initiator for living carbocationic polymerization of vinyl ether.⁶⁻¹⁰

1.2.1.3. Co-initiator (Lewis Acid)

A wide variety of Lewis acids are used in cationic polymerization to initiate polymerization usually at low temperature. Typical examples are metal halides^{3, 11-13} (such as ZnCl₂, TiCl₄, PCl₅, SbCl₅, SnCl₄, BF₃, and AlCl₃), oxyhalides¹⁴⁻¹⁶ (such as VOCl₃, SOCl₂, CrO₂Cl, POCl₃), and organometallic compounds¹⁷⁻¹⁸ (such as R₃Al, R₂AlCl, RAlCl₂, R₃Al₂Cl₃). The generation of initiator-coinitiator complex can be described by the reaction between aluminum chloride and t-butyl chloride (Figure 1.7).

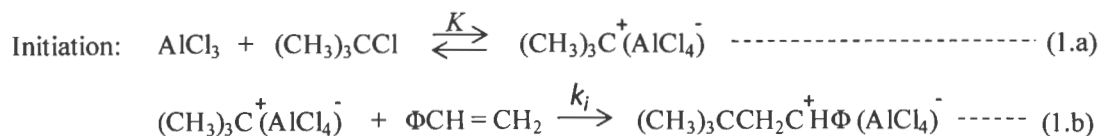
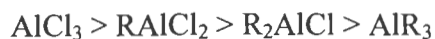


Figure 1.7. Initiation process in the presence of aluminum chloride and t-butyl chloride.³

The efficiency of the initiation process depends on the rate of formation of the initiator-coinitiator complex (i.e. the value of K in the equation 1.a) and its rate of addition to monomer (i.e. the value of k_i in equation 1.b).³ Generally the activity of initiator-coinitiator complex increases with the increase in Lewis acidity.¹⁸⁻²⁰



1.2.1.4. Solvent

The reaction medium (solvent) plays an important role in carbocationic polymerization. The solvent can alter the rate of polymerization by changing the relative concentration of free-ion, ion pair and gegenion.³ As the solvating power of solvent increases, the rate and degree of polymerization generally increases.^{11-13, 16} As shown in Figure 1.8, for cationic polymerization the propagating carbocation can be imagined to range from one extreme of a completely covalent species (I) to the other of a completely free (highly solvated) ion (IV). With the increase in solvating power, the free-ion concentration increases and hence, the rate of polymerization. Additionally, with the increase in solvating power of the medium, the nature of the ion-pair changes from intimate ion-pair to solvent separated ion-pair.³

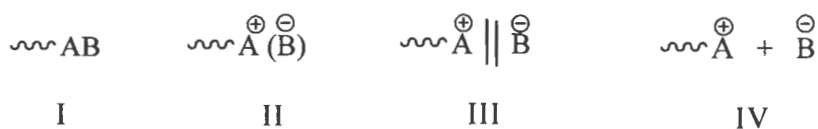


Figure 1.8. Interaction of propagating carbocation, counterion and solvent; (I) Covalent species, (II) contact ion pair, (III) solvent separated ion-pair, and (IV) highly solvated ion-pair.³

However, with the increase in solvating power of solvent the rate constant somewhat decreases. In the transition state, the free ion and ion-pair dispose some charges. Thus, the solvent with higher polarity stabilizes the ground state configuration than the transition state configuration. In addition to the influence on the rate of propagation, the solvent polarity (dielectric constant) has the effect on the order of polymerization. With the

use of the poorly solvating medium, the order of polymerization may increase depending upon the solvation of the ion-pairs generated by monomer, initiator, and coinitiator. For example, polymerization of styrene in the presence of SnCl_4 was found to depend on $[\text{M}]^2$ in benzene solution and $[\text{M}]^3$ in carbon tetrachloride solution. Carbon tetrachloride being a poor solvating agent compared to benzene, styrene is taking part in the solvation of the propagating species and the gegenion.²¹

1.3. LIVING CARBOCATIONIC POLYMERIZATION

The key to living carbocationic polymerization is the development of a reaction condition where the propagating carbocation is temporarily deactivated in a reversible way to participate in side reactions. This temporary deactivation reduces the overall (apparent) rate of polymerization with respect to rate of initiation. This allows all of the carbocations generated from the initiator to propagate uniformly to produce polymer with narrow molecular weight distribution.²² The term living is used for polymerizations that produce well defined polymer with narrow molecular weight distribution as result of quantitative and fast initiation, and termination-free propagation. The rate of reaction for living carbocationic polymerization with fast initiation can be described as follows:²³

$$\text{Rate of polymerization, } R_p = -\frac{d[\text{M}]}{dt} = k_p[\text{R}^+][\text{M}] = k_{app}[\text{M}]$$

$$\frac{d[\text{M}]}{[\text{M}]} = -k_{app} dt$$

$$\text{Integrating: } \ln([\text{M}]_0/[\text{M}]_t) = k_{app} t$$

where, R_p , k_p , $[M^+]$, and k_{app} are the rate of polymerization, rate constant for propagation, concentration of actively growing carbocation, and apparent rate constant for propagation, respectively. The plot of $\ln([M]_0/[M]_t)$ as a function of polymerization time (t) yields a straight line passing through the origin. From the slope of the straight line the apparent rate constant for propagation can be easily determined. The living nature of carbocationic polymerization is demonstrated by the linear relationship between GPC number average molecular weight and monomer conversion.

1.3.1. Factors influencing the living carbocationic polymerization

To achieve a living carbocationic polymerization, controlled initiation and propagation are necessary. In order to suppress the transfer and termination reactions, the choice of counter ion, solvent, and Lewis acid is very important. For example, in styrene polymerization linear and cyclic dimers are accompanied by polymers. In polar solvent, the dimer yield is greatly reduced.²⁴⁻²⁶ In non-polar solvent, the strong interaction between the carbocation and counter-ion inhibited the propagation. The effect of an added base in the living carbocationic polymerization of vinyl ether initiated by Cationogen (adduct of acetic acid and IBVE)/EtAlCl₂ was demonstrated by Kishimoto et al.²⁷ In this review the recent development in the living carbocationic polymerization of vinyl ether is listed.

1.4. LIVING CATIONIC POLYMERIZATION OF VINYL ETHER

Typical initiating systems for vinyl ether polymerization are HI/I₂,⁶ HI/ZnI₂,²⁸⁻³² CH₃COOH/Zn(CH₃COO)₂,³³⁻³⁴ and protonic acids (Cationogen)/Lewis acid.²⁷ Living polymerization of vinyl ether monomers with strong Lewis acids can be accomplished by

the use of Lewis bases (nucleophiles) such as esters³⁵⁻³⁶ and ethers.³⁶⁻³⁷ The living carbocationic polymerization using Lewis acids/Cationogen in combination with an ester functional base is generally referred as ‘stabilization of carbocation by added base’. However, another class of initiating system consisting of either HI/I₂ or HI/ZnX₂ induces living polymerization which is referred as ‘stabilization of the carbocation by counter ion’.

1.4.1. Stabilization of the carbocation by counter ion

A mixture of hydrogen iodide (HI) and iodine (I₂) effectively initiate polymerization of vinyl ether to produce polymers of controlled molecular weight and molecular weight distribution.^{24, 38-42} Hydrogen iodide quantitatively forms a 1:1 adduct after addition to vinyl ether. The adduct is too stable to further initiate vinyl ether polymerization. Lewis acids (electron acceptor) such as iodine and zinc iodide²⁸ are used to activate the carbon-iodine bond electrophilically which allows the incoming monomer to add the activated terminal linkage. Repetition of the activation and addition process leads to the living polymer bearing CH-I terminal that can be activated by Lewis acid and continue propagation (Figure 1.9). The advantage of using HI/ZnI₂ in the place of HI/I₂ is that, it enables the well-defined living polymerization of vinyl ether even above room temperature.²⁸

1.4.2. Stabilization of carbocation by added base

Living carbocationic polymerization can be achieved by the use of external bases to reduce the reactivity of Lewis acid.³⁵ Strong Lewis acids such as EtAlCl₂ induce very-fast and uncontrolled (non-living) cationic polymerization. The advantage of the concept

'stabilization of carbocation by added base' is the formation of living polymers at room temperature which is much higher than the cryogenic temperature (-100 °C) commonly used for HI/I₂ initiated living polymerization.

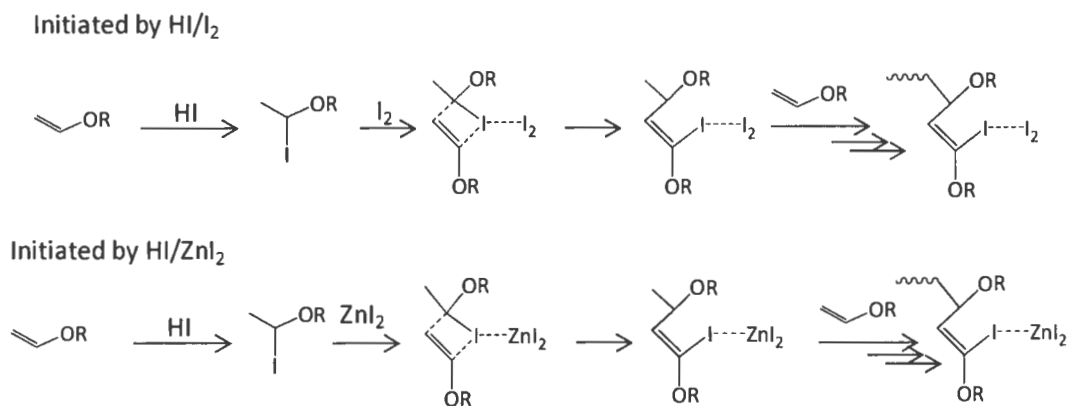


Figure 1.9. Cationic polymerization of vinyl ether initiated by HI/I₂ and HI/ZnI₂.

Additionally, skilled and cumbersome techniques are required to handle HI and maintain low polymerization temperature to prevent side reaction. However, a large excess of ester-functional base is necessary (e.g. 25 to 250 fold molar excess of base) over EtAlCl₂ to produce living cationic polymerization.³⁶

As shown in Figure 1.10, the polymerization of isobutyl vinyl ether initiated by Cationogen/EtAlCl₂ is very fast and non-living. The EtAlCl₂ based propagating species (I) is very unstable due to the poorly nucleophilic and non-interacting counter-ion. However, an added ester interacts with the propagating species forming a living carbocationic site (II and III) which is free from chain transfer and other side reactions. The interaction of the ester group with the cationic propagating site is strong and involves the nucleophilic carbonyl groups.

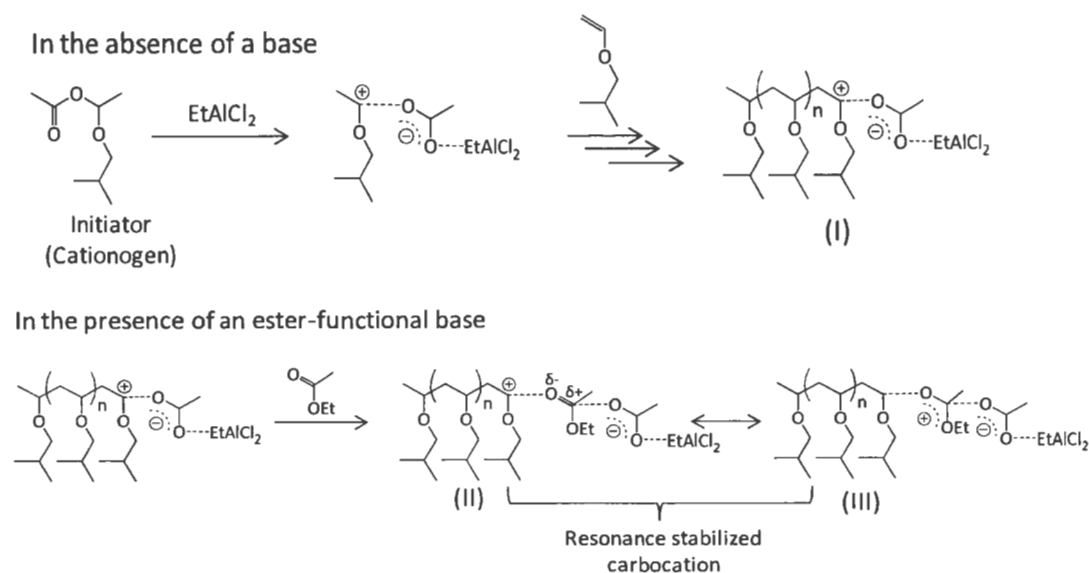


Figure 1.10. Cationic polymerization of isobutyl vinyl ether initiated by Cationogen/ EtAlCl_2 in the absence and presence of an ester-functional base.

Thermosensitive homopolymers and copolymers containing pendent hydroxyl groups can be synthesized by the living carbocationic polymerization of silicon containing vinyl ethers (**13**, **14**, and **15**). The polymerization was carried out in the presence of cationogen (IBVE and acetic acid adduct)/ $\text{Et}_3\text{Al}_2\text{Cl}_3$ initiating system in the presence of an added base.⁴³ Subsequent desilylation produced well-defined both water-soluble and water-insoluble polymers containing pendent hydroxyl groups. Amphiphilic diblock copolymers were synthesized using living carbocationic polymerization of 2-phenoxyethyl vinyl ether (**16**) and 2-methoxyethyl vinyl ether (**17**) in the presence of ethyl acetate and $\text{Et}_3\text{Al}_2\text{Cl}_3$ in toluene at 0 °C. Physical gelation of the copolymer was observed in appropriate solvents, such as water-acetone.⁴⁴ Living carbocationic polymerizations of urethane functional vinyl ether (**18**) and cyclic acetal functional vinyl ether (**19**) were demonstrated by Namikoshi T. et al.⁷ Although both the monomers are acid sensitive, living carbocationic polymerization

was successfully carried out after judicious choice of substituent attached to the nitrogen atom. The polymerization was initiated in the presence of HCl/ZnCl₂ at a temperature of -30 °C. For the cyclic acetal functional vinyl ether, various systems were employed starting from HCl/ZnCl₂, CH₃CH(OiBu)OCOCH₃/(Et₃Al₂Cl₃)/CH₃COOC₂H₅, and CH₃CH(OiBu)OCOCH₃/SnBr₄/di-tert-butylpyridine.⁹ This acetal functional moiety could be used as a protecting group under the living carbocationic polymerization condition. Fluorine containing polymers have unique properties of low surface energy. Fluorine containing water soluble block copolymer was synthesized using living carbocationic polymerization of an ester functional vinyl ether (**20**) and a fluorine containing vinyl ether (**21**) followed by the hydrolysis of ester group.¹⁰ This non-ionic polymeric surfactant was able to reduce the surface tension of water to 30 mN/m at a polymer concentration of 1 × 10⁻⁴ mole/liter.

In general poly(vinylether) polymers containing linear alkyl chains are sticky polymer with low glass transition temperature (T_g). In order to increase the T_g, a series of vinyl ethers containing aliphatic polycyclic units (**22**, **23**, and **24**) were polymerized and the thermal properties were evaluated. Living carbocationic polymerization of vinyl ether containing cyclohexyl (**22**),⁴⁵ tricyclodecane (**23**),⁸ and 2-adamantyl (**24**)⁴⁶ were carried out in the presence of VE-Cl/ZnCl₂/*n*Bu₄NI/CH₂Cl₂ at -30 °C, CH₃CH(OiBu)OCOCH₃/Et₃Al₂Cl₃/CH₃COOEt/ toluene at 0 °C, and HCl/ZnCl₂/toluene at -30 °C, respectively. The linear relationship between number average molecular weights and percentage of conversions demonstrated the living nature of carbocationic polymerization. The T_g's of

polymers obtained from monomers **(22)**, **(23)**, and **(24)** were 50 °C, 95 °C, and 178 °C, respectively.

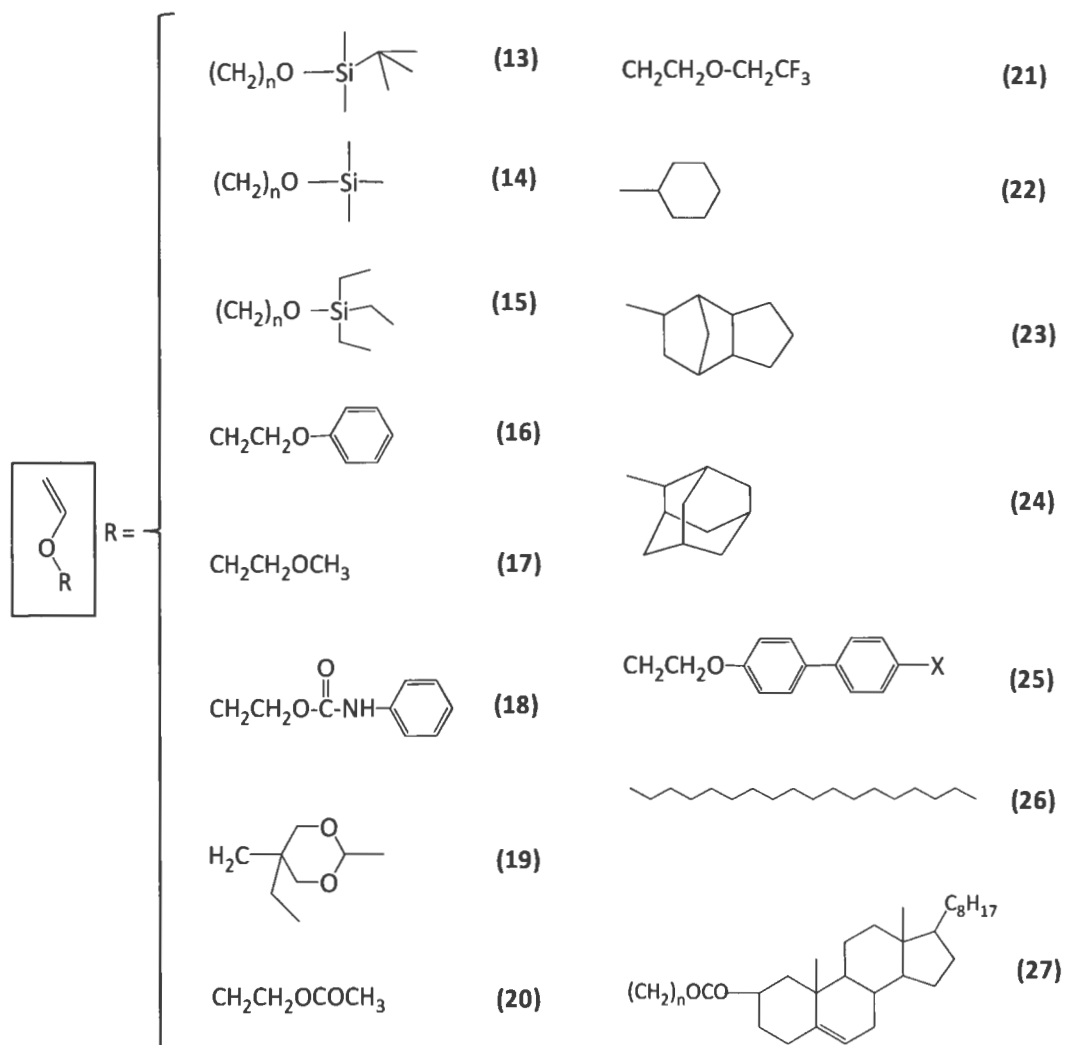


Figure 1.11. Vinyl ether monomer containing pendent functional moieties.

Vinyl ether monomer containing mesogenic groups **(25)**, such as cyanobiphenyl,⁶ 4-methoxy-4'-hydroxybiphenyl⁴⁷ were polymerized and copolymerized using HI/I₂, HI/ZnI₂, or EtAlCl₂ in CH₂Cl₂ initiating system.⁴⁸ The living carbocationic polymerization of

octadecyl vinyl ether (**26**) and copolymerization with 2-methoxyethyl vinyl ether (**17**) were carried out using $\text{H}_3\text{CH}(\text{O}i\text{Bu})\text{OCOCH}_3/\text{EtAlCl}_2$ initiating system in hexane in the presence of an added Lewis base at 30 °C. Aqueous solution of amphiphilic block and random copolymers with crystallizable substituents of (**26**) and (**17**) yielded physical gelation upon cooling due to the crystallization of C-18 chains, regardless of the copolymer structure.⁴⁹⁻⁵⁰ Copolymerization using crystallizable vinyl ethers containing long alkyl chain (**26**) and liquid crystalline mesogenic structure (**27**) in the presence of EtAlCl_2 /ethyl acetate/hexane was carried out at a temperature of 30 °C.⁵¹ The copolymer in various organic solvents was found to be highly sensitive to UCST-type phase separation.

1.5. VINYL ETHER MONOMER DERIVED FROM RENEWABLE RESOURCES

Currently, there has been increasing interest to synthesize vinyl ether monomers from bio-based materials. Vinyl ether monomers derived from bio-based materials are listed in Figure 1.12. Various glycopolymers containing pendant sugar moieties which act as specific biological functional groups were synthesized using living cationic polymerization of their corresponding vinyl ethers.⁵²⁻⁵⁶ Glycopolymers referred to synthetic polymers containing sugar moieties similar to those naturally occurring glycolconjugates. The sugar portions of the glycopolymers are expected to play an important role as recognition sites between cells. Living carbocationic polymerization of vinyl ether of acyl-protected glucose (**28**) was successfully demonstrated using $\text{CF}_3\text{COOH}/\text{EtAlCl}_2$ in the presence of 1,4-dioxane as an added base at 0 °C. Vinyl ether of isopropylidene-protected glucose (**29**) was polymerized at - 15 °C using HCl/ZnI_2 initiating system.⁵⁵ D-

Glucosamine-bearing glycopolymer with narrow molecular weight distribution ($M_w/M_n \sim 1.1$) was synthesized using living carbocationic polymerization of vinyl ether containing acyl and phthaloyl-protected glucose (**31**).⁵⁶ Living polymerization was initiated by Cationogen ($\text{CF}_3\text{COOH/IBVE adduct}$)/ EtAlCl_2 in the presence of 1,4-dioxane in toluene. Quantitative deprotection with hydrazine monohydrate yielded water soluble polymer containing pendent D-glucosamine moiety which exhibited unique characteristic in biological and pharmaceutical sciences.

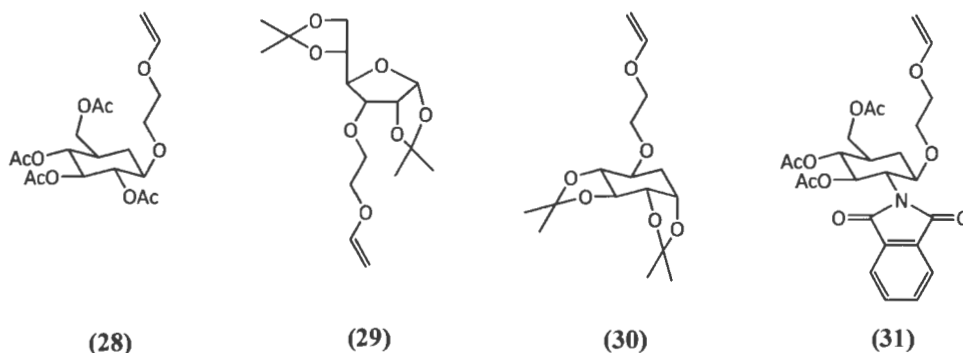


Figure 1.12. Vinyl ether monomers derived from renewable resources.

1.6. END-FUNCTIONAL POLYVINYLEETHER POLYMERS

End-functional polymers and macromers are of great interest due to their possibility of further reaction associated with the end functional groups. In the living polymerization, end-functionalization can be achieved by the following three steps: (1) initiation from functionalized initiator, (2) Termination from functionalized terminator, (3) combination of (1) and (2). Essentially, the combined approach produces a telechelic polymer.

1.6.1. End-capping by functional initiator

Figure 1.13 describes the functional-initiators used in combination with I_2 or ZnI_2 to produce end-functional poly(vinylether). The synthesis of functional initiators (**32**, **33**) those were used in living carbocationic polymerization of vinyl ether was first demonstrated by the reaction of HI and a vinyl ether possessing a pendent functional moiety.⁵⁷⁻⁵⁸ These initiators, prepared by the reaction of equimolar HI and vinyl ether, were able to produce living carbocationic polymerization of vinyl ether in the presence of either I_2 or ZnI_2 as a Lewis acid.^{57, 59} Methacrylate (**34**), allyl (**35**), and epoxy functional polymers (chemical modification of allyl group) of vinyl ether were synthesized and characterized elsewhere.⁵⁹⁻⁶⁰ The acrylate moiety in the initiator is not reactive under the living cationic polymerization condition. The initiator was synthesized by the reaction between 2-vinyloxyethyl methacrylate and HI.⁶⁰

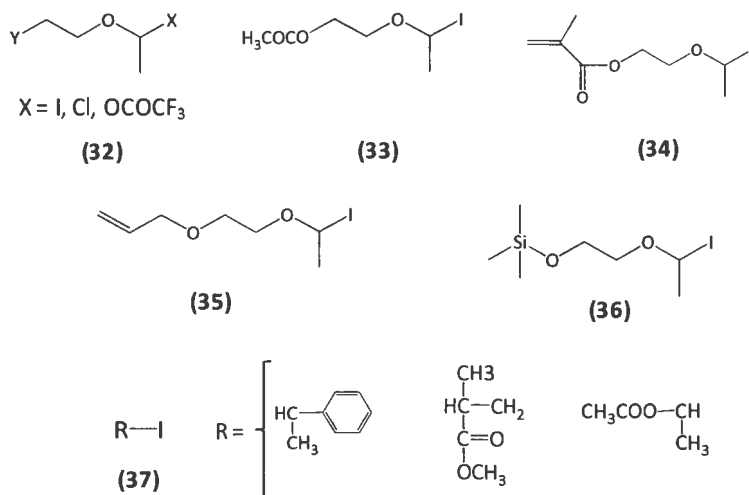


Figure 1.13. Functional-initiators used in combination with I_2 or, ZnI_2 to produce end-functional poly(vinylether).

Other initiators, such as trimethylsilyl iodide⁶¹⁻⁶² (**36**) and HI adducts of various monomers (vinyl acetate, styrene, methyl methacrylate)⁶³ (**37**) were able to produce living polymerization of vinyl ether in the presence of Lewis acid. By using these initiators various end-functional such as hydroxyl and ester end-functional polyvinylethers were synthesized.⁵⁹

1.6.2. End-capping by functional terminators

In this technique, living carbocations of polyvinylethers are quenched with functional terminator. The end-capping reaction involves the nucleophilic addition of terminating agent to the living carbocationic end where the unexpected side reaction and termination do not involve during the propagation of carbocation. Figure 1.14 describes the functional-terminators used to produce end-functional poly(vinylether). Examples of such process involve the end-capping of living carbocation chain ends with malonate anions,⁶⁴ amines (**40**),⁴² alcohols,⁶⁵ anilines,⁶⁶ silyl enol ether,⁶⁷ and silyl ketene acetals⁶⁸ to produce various end-functional polymers. For example, sodium salt of malonate carboanions quantitatively reacts with living carbocationic chain end of polyvinylether initiated by HI/I₂ to produce stable C-C bond (Figure 1.15). Malonic ester terminated polymer was further converted to carboxylic acid by base catalyzed hydrolysis followed by decarboxylation (**38**).⁶⁴ Methacrylate-end functional (**41**) poly(isobutyl vinyl ether) and poly(ethyl vinylether) were synthesized after terminating the living propagating species, initiated by CF₃SO₃H in CH₂Cl₂ at -30 °C in the presence of thiolane as an added base, with 2-hydroxy ethyl methacrylate (HEMA).⁶⁹ Poly(vinyl alcohol) graft copolymers were synthesized

using living carbocationic polymerization of 2-methoxyethyl vinyl ether followed by termination with partially hydrolyzed polyvinylether acetate.⁷⁰ A monoallyl-functional (42) polymer of Triclosanvinylether (TVE) was synthesized after quantitative nucleophilic addition of 2-allyloxyethanol to the living carbocationic propagating species of TVE initiated by Cationogen (adduct of acetic acid and IBVE)/Et₃Al₂Cl₃.⁷¹

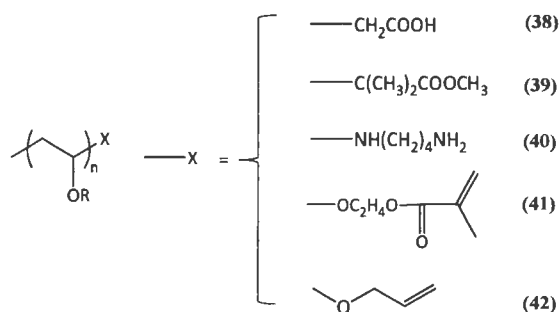


Figure 1.14. Functional-terminators used to produce end-functional poly(vinylether).

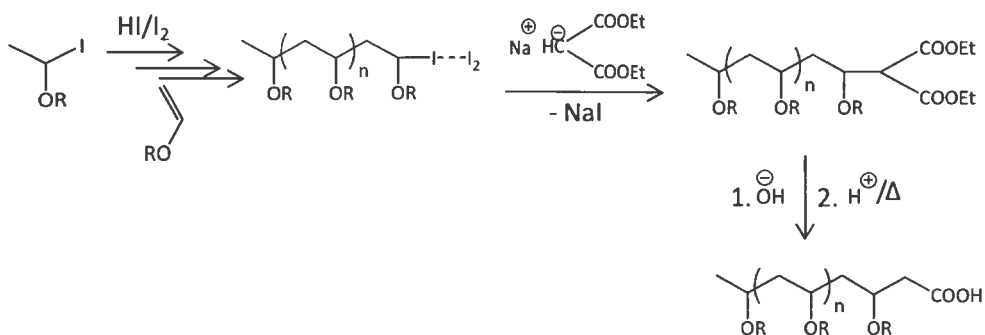


Figure 1.15. Synthesis of carboxylic acid end-functional polymer of vinyl ether.⁶⁴

1.7. COPOLYMERIZATION OF VINYL ETHER

The major advantage of living carbocationic polymerization is the synthesis of new polymeric structures, for example, hyperbranched polymers, star-branched polymers, graft,

and block copolymers. In this review the recent developments in the block copolymers synthesized from vinyl ether monomers are described.

1.7.1. Poly(vinylether)-*b*-poly(vinylether) copolymers

A wide variety of poly(vinylether) block copolymers can be synthesized by sequential addition of vinyl ether monomers. Amphiphilic block copolymers of vinyl ether consisting of water soluble polyalcohol segment and hydrophobic poly(alkylvinylether) segment were produced by living carbocationic copolymerization of ester-functional vinyl ether and alkylvinylether followed by the hydrolysis of the ester groups. This copolymer surprisingly lowered the surface tension of its aqueous solution and the interfacial tension of water/toluene interface.⁵⁷ A thermoplastic elastomer consisting of *A-B-A* type triblock copolymer consisting of poly(TCDVE) (hard segment) and poly(NBVE) (soft segment) was produced using living carbocationic polymerization of corresponding vinyl ethers in toluene at -30 °C (Figure 1.16).⁷² Water soluble block copolymer of poly(hydroxyethyl vinyl ether) and poly(isobutyl vinyl ether) was synthesized using living carbocationic polymerization from *tert*-butyldimethylsilyl protected hydroxyethyl vinyl ether (BMSiVE) and isobutylene vinyl ether in toluene at 0 °C (Figure 1.17).⁷³ The polymerization was initiated by Cationogen (IBVE and acetic acid adduct)/Et₃Al₂Cl₃ and the living nature of the carbocationic propagating species was maintained using methyl chloroacetate as an added base.

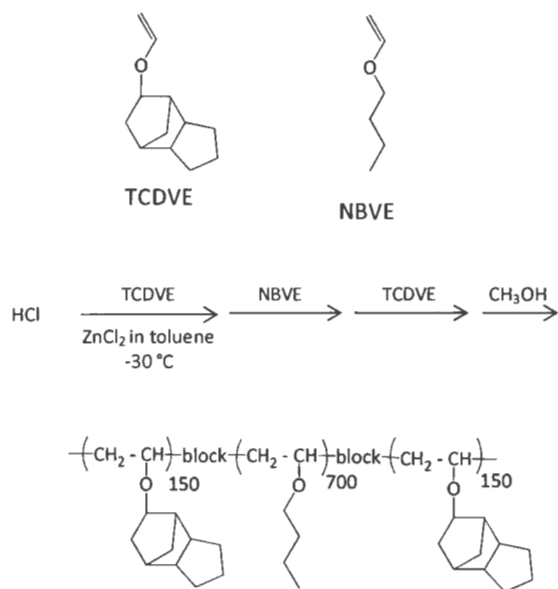


Figure 1.16. Synthesis of poly(TCDVE)-*block*-poly(NBVE)-*block*-poly(TCDVE).⁷²

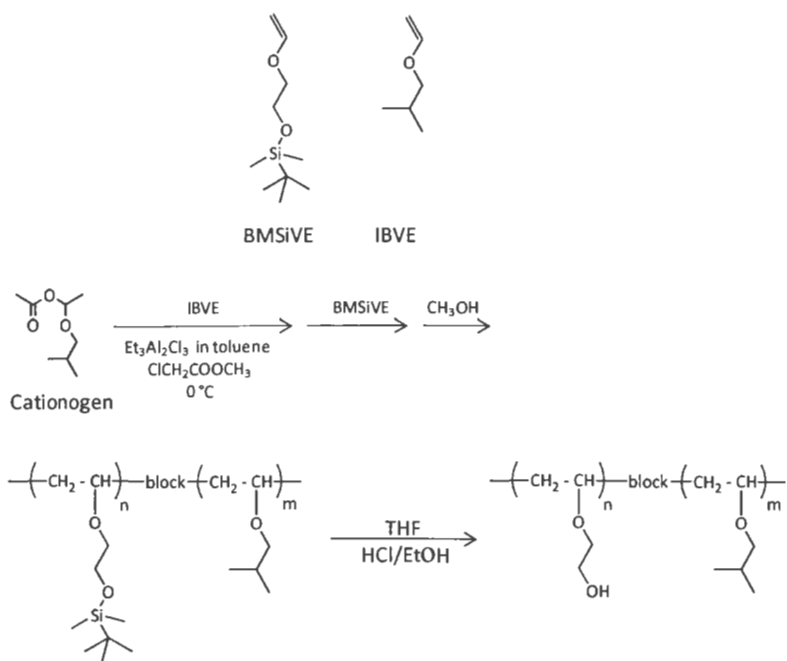


Figure 1.17. Synthesis of poly(BMSiVE)-*block*-poly(IBVE).⁷³

1.8. SUMMARY

Carbocationic polymerization, especially living carbocationic polymerization, is one of the important techniques used in polymer science to develop various polymeric building blocks. In this review, the most recent developments of monomer, initiator, and Lewis acid related to the living carbocationic polymerization of vinyl ether are discussed. Many innovative breakthroughs have been seen and the future of this field is very promising. A lot of very interesting research is happening in the field of living carbocationic polymerization of styrene and isobutylene, cationic ring opening polymerization of heterocyclic compounds, and photo-induced cationic polymerization which are not included here as this dissertation is mainly focused on the carbocationic polymerization of vinyl ether.

**CHAPTER 2. SYNTHESIS, CHARACTERIZATION, AND
ANTIMICROBIAL ACTIVITY OF POLY[(DIMETHYL-*co*-
TRIMETHYL(PROPYL)SILYLMETHYL)SILOXANE]-*g*-POLY[2,4-
DICHLORO-1-(4-CHLORO-2-(2-
(VINILOXY)ETHOXY)PHENOXY)BENZENE] PRODUCED USING
LIVING CARBOCATIONIC POLYMERIZATION AND
HYDROSILYLATION**

2.1. ABSTRACT

Polysiloxane coatings containing chemically attached (tethered) Triclosan moieties were investigated to find potential application as environmental friendly coatings to control biofouling on marine vessels and biomedical devices. A polysiloxane graft copolymer containing biocide-functional grafts was produced using a two-step synthetic process. First, a monoallyl-functional polymer (PTVE) containing Triclosan as a biocide moiety in the repeat unit was synthesized using living carbocationic polymerization. Next, the monoallyl-functional PTVE was grafted to a polysiloxane copolymer by hydrosilylation. The biocide-functional monomer (TVE) was a vinyl ether derived from the reaction of 2-iodoethyl vinyl ether with the biocide, Triclosan. The living carbocationic polymerization of TVE was accomplished in toluene at 0 °C using $\text{CH}_3\text{CH}(\text{O}i\text{Bu})\text{OCOCH}_3$, ethylaluminum sesquichloride, and methyl chloroacetate as the initiator, coiniciator, and electron donor, respectively. A series of thermoplastic polysiloxane graft copolymers containing grafts derived from the living carbocationic polymerization of TVE were synthesized and the morphology and antimicrobial properties determined. Antimicrobial properties were

determined using both marine microorganisms and biomedically-relevant microorganisms. An array of graft copolymers was produced that varied with respect to the polysiloxane backbone molecular weight and the concentration of PTVE grafts. Characterization of polymer films using thermal analysis, transmission electron microscopy, and atomic force microscopy showed that the copolymers were two-phase materials and morphology was dependent on both polysiloxane backbone molecular weight and the concentration of PTVE grafts. With regard to antimicrobial properties, the results indicated that graft copolymers possessing a relatively low polysiloxane backbone molecular weight exhibited higher antimicrobial activity than graft copolymers derived from a relatively high molecular weight polysiloxane backbone. Graft copolymers possessing a relatively low molecular weight polysiloxane backbone and relatively high PTVE content exhibited very high reductions in biofilm retention for *S. epidermidis*, moderate reductions for *C. lytica* and *C. albicans*, and no reduction for *E. coli* or *N. incerta*. Interestingly, major reductions in biofilm viability were not observed for any of the microorganisms suggesting that the tethered Triclosan moieties inhibit biofilm growth and retention without extensive cell death. Additionally, significant biofilm retraction was observed for *C. lytica* and *E. coli* biofilm over the coatings surfaces synthesized from the thermoplastic graft copolymer.

2.2. INTRODUCTION

An antimicrobial compound is described as a compound that effectively prevents or eliminates the colonization and growth of unwanted microorganisms. Microbial infection due to contamination by microorganisms is a serious problem in biomedical and hospital

equipment,⁷⁴ agriculture,⁷⁵ water purification system,⁷⁶ architecture,⁷⁷ personal care,⁷⁸ marine applications,⁷⁹⁻⁸¹ food and packaging industry.⁸² Thus, the development of antimicrobial coatings has been the motivation of research for years to inhibit the formation of biofilm and to kill microorganisms over the surface of interest.

Infection and failure of an implant due to microbial attack is a major issue in the health care industry. The health care industry has estimated that approximately 2,000,000 infection-related incidents occur in US health care industry per year causing the death of approximately 60,000 – 90,000 and a cost of \$17-29 billion dollars.⁸³ It was found that out of a total of 98,987 health care associated infection deaths, 30,665 deaths were directly from blood stream infections (BSIs), 13,088 from urinary tract infections (UTIs), and 8,205 from surgical infection.⁸⁴ Among surgical infections, the most common cases are the infection due to orthopedic device implantation. A large number of patients suffer from medical device related infection due to biofilm formation over the device.

Upon insertion of a biomedical device inside the body, bacterial cells and fungal cells adhere to the implant surface forming thick layers of extracellular matrix called biofilm. These biofilms possess higher resistance towards antibiotics compared to free flowing cells.⁸⁵⁻⁸⁷ The possible mechanism for the increased drug resistance of biofilm is the incomplete or slow penetration of antibiotics through thick layers of biofilm. Moreover, the dead microorganisms create a barrier to the diffusion of antibiotics. The growth rates of biofilms are different at lower layers where the nutrients and oxygen are limited as compared to the surface layer. These cause localized slow growth or starvation at the bulk of the biofilm.⁸⁸⁻⁸⁹ Many antibiotics are known to be non-reactive towards slow/non-

growing stationary cells than fast growing bacterial cells.⁹⁰ Moreover, microbial waste products can be toxic.⁹¹

The related issue with biofilm-based infection is that biofilms are polymicrobial communities which are produced by both bacteria and fungi. *Candida* species is the fourth most common cause of fungal infection in North America.⁹² It was found that *Candida* species can form polymicrobial biofilms in conjunction with *Staphylococcus aureus*.⁹³⁻⁹⁴ Other common microorganisms primarily responsible for causing bacterial biofilm related infections are *Staphylococcus epidermidis* and *Escherichia coli*. *S. epidermidis* extracellular matrix is known to resist the penetration of the antibiotics, fluconazole. However, *C. albicans* is found to protect *S. epidermidis* against vancomycin, an antibiotic used to treat infection caused by Gram-positive bacteria⁹⁵.

Various approaches have been developed to find a long-term solution for these problems, for example, biocide release and contact active antimicrobial coatings.⁹⁶ The common way to combat these problems is the mixing of antimicrobial agents, for example, halogen,⁹⁷ silver-ion,⁹⁸ antibiotics,⁹⁹ into bulk materials¹⁰⁰ or coatings¹⁰¹ and slow release into the environment to prevent the growth of microorganisms. It has been shown that silicone catheters and shunts coated with various antibiotics effectively reduce *S. epidermidis* biofilm formation.¹⁰²⁻¹⁰⁴ The major disadvantage of these approaches is the limited life time of the active ingredient. Polymeric or inorganic nanoparticles can be properly targeted at a specific area to release the necessary drug.¹⁰⁵⁻¹⁰⁶ Another approach is the generation of either super hydrophobic surfaces¹⁰⁷⁻¹⁰⁹ (contact angle > 150°) or

hydrogel forming non-charged coatings.¹¹⁰ In both cases, the adhesion between microorganisms and surfaces is greatly reduced, but not zero.

Marine biofouling is defined as the unwanted accumulation of marine plants, animals, and microorganisms over manmade surfaces partially or fully immersed in sea water. Particularly, biological fouling of a ship hull drastically increases overall roughness, hydrodynamic drag, and weight of the ship hull. US Navy has estimated that soft fouling can increase fuel consumption up to 15% while heavy fouling can increase fuel consumption up to 45%. In 1989, the marine coatings industry estimated an increase of approximately \$3 billion dollars in fuel costs due to biofouling of naval vessels.¹¹¹ Moreover, biofouling causes an increase in the frequency of dry docking and initiates corrosion. Additionally, transportation of microorganisms by biofouled ship hulls from one harbor to another changes the ecosystem of marine environments as ships travel around the world. Until now, the most effective way to prevent the settlement of microorganisms over the ship hull is to incorporate biocidal compounds (tributyltin or copper) into coatings that slowly release toxic biocides into the marine environment.¹¹²⁻¹¹⁷ Very effective antifouling coatings have been synthesized consisting of a copolymer of tributyltin methacrylate (TBTM) and methyl methacrylate (MMA).¹¹⁸⁻¹²⁰ The coatings deter the settlement of microorganisms by release of toxic tributyltin after the hydrolysis of tributyltin ester linkage in sea water.

There are more than 4000 marine organisms identified as biofoulers. The fouling process occurs in different stages.¹²¹ At the beginning, organic polysaccharides and proteins are accumulated over the fresh surfaces that support the attachment of single cell

microfouling organisms such as diatoms and bacteria forming a bacterial biofilm. Next, the biofilms produced by microfoulers facilitate the attachment and growth of more complex organisms called macrofoulers.¹²² The mode of action for every biofouler is different, so there is a technical challenge to develop a coating surface that combats biofouling by the entire array of organisms.

In order to fulfill the demands of a non-toxic alternative to biocide-releasing coatings, extensive research is going on to develop foul-release (FR) and antifouling (AF) coatings. FR coatings do not necessarily deter the settlement of organisms but facilitate the removal from surface under the application of shear. The most effective non-biocidal FR coatings available in the market are based on polydimethylsiloxane (PDMS). FR coatings work by reducing the adhesion of the marine macrofoulers such as tubeworms, barnacles, and macroalgae and facilitate release of them from ship hull under cruising velocity. There are varieties of factors influencing the performance of such coatings, for example, coatings modulus,¹²³ surface energy,¹²⁴⁻¹²⁶ thickness,^{123, 127} and frictional slippage.¹²⁸⁻¹²⁹ However, silicone-based coatings suffer from poor durability and adhesion to the substrate.

Commercial AF coatings containing copper or tin are toxic and efforts have been taken to eradicate these coatings from market. In order to get rid of problems associated with leaching of toxic biocides to the environment, extensive research work is going on to develop environmental friendly, non-toxic bioactive coatings. One approach is to tether biocides such as Triclosan,^{74, 130-132} organic quaternary ammonium compounds^{80, 133} to a polymer backbone through hydrolytically stable chemical linkages. These antimicrobial coatings either inhibit the settlement of microorganisms or kill them via a contact-active

mechanism. It has been assumed that the antimicrobial coatings will prevent the formation of bacterial biofilms, which in turn reduce the settlement of macrofoulers. Majumdar et al.^{80, 133} synthesized organic quaternary ammonium compounds tethered to a crosslinked PDMS elastomer and antifouling characteristics were evaluated against *C. lytica* and *N. incerta*. These non-leaching coatings were found to reduce greater than 80% *C. lytica* biofilm retention and 90% *N. incerta* biofilm growth.

Thomas et al.⁷⁹ synthesized silicone copolymers containing pendant Triclosan as a biocide moiety. Antifouling characteristics of crosslinked coatings were evaluated by static immersion tests in the India River Lagoon at the Florida Institute of Technology for 30 days. It was concluded that in order to be an effective antifouling coating against macrofoulers, coatings modulus needed be less than 10 MPa. In case of a high modulus coating, it was thought that the biocide may be trapped inside the highly crosslinked polymer matrix. The influence of tethered Triclosan to deter settlement of microorganism over a series of leachate non-toxic, antimicrobial PDMS coating surfaces was previously reported by Chisholm et al.^{131-132, 134} The authors had tethered Triclosan moieties to a crosslinked PDMS backbone through a hydrolytically stable ether linkage. It is found that a significantly high concentration of Triclosan moieties (>30%) was necessary to reduce the *C. lytica* biofilm retention.

Kugel et al.⁷⁴ synthesized an environmental friendly, antimicrobial polyurethane coating containing tethered Triclosan moieties. The antifouling characteristics of coating surfaces were evaluated against *S. epidermidis*, *E. coli*, *C. lytica*, and *N. incerta*. It was found that the coating surfaces showed excellent antimicrobial activity against *S.*

epidermidis (>90% reduction in biofilm retention) without leaching free Triclosan from the coatings and the level of bioactivity was found to increase with the increase in Triclosan moieties. Chen et al.¹³⁰ synthesized cationic UV curable coatings containing tethered Triclosan as a biocide moiety. The Triclosan was chemically attached to a PDMS backbone using hydrolytically stable ether linkages. A substantial reduction (>97%) in *S. epidermidis* biofilm retention and a moderate reduction (20-35%) in *E. coli* biofilm retention was observed on these coating surfaces.

The objective of the research was to investigate the antimicrobial activity of novel, amphiphilic PDMS coatings containing non-leaching, tethered biocide moieties derived from the ubiquitous biocide, Triclosan. Triclosan was chosen as the biocide because it is registered with the EPA, non-toxic to mammals, cheap, used in many common consumer products, and readily tetherable. PDMS was used as a backbone polymer as it was found to be effective for easy removal of marine organisms. Moreover, it is biocompatible and is a good choice to use as a coating over implantable devices. Four bacteria responsible for failure and infection in medical devices, *E. coli*, *S. epidermidis*, *C. albicans*, *S. aureus*, and two marine fouling microorganisms, *N. incerta*, and *C. lytica* were employed to determine the broad-spectrum antimicrobial activity of the experimental coating surfaces.

2.3. EXPERIMENTAL

2.3.1. Materials

Table 2.1 describes the starting materials used for the investigation. Unless specified otherwise, all materials were used as received.

Table 2.1. Chemicals used.

Chemicals	Description	Supplier
CIVE	2-chloroethyl vinyl ether, 99%	Sigma-Aldrich
NaI	Sodium Iodide, $\geq 99\%$	Sigma-Aldrich
K ₂ CO ₃	Potassium carbonate, $\geq 99\%$	Sigma-Aldrich
Triclosan	5-Chloro-2-(2,4-dichlorophenoxy)phenol, 99%	Alfa Aesar
MCAc	Methyl chloroacetate, $\geq 99\%$, Distilled over calcium hydride	Sigma-Aldrich
Ethylaluminum sesquichloride	25 wt. % in toluene	Sigma-Aldrich
Toluene	ACS grade, 99.5%	EMD Chemicals
n-hexane	ACS grade, 98.5%	VWR
Magnesium sulfate	Anhydrous, ReagentPlus®, $\geq 99.5\%$	Sigma-Aldrich
MeOH	Methanol, $\geq 99.8\%$	Sigma-Aldrich
CDCl ₃	Deuterated chloroform	Sigma-Aldrich
AcOH	Acetic acid, glacial	
IBVE	Isobutyl vinyl ether, 99%	Sigma-Aldrich
2-allyloxyethanol	98%	Sigma-Aldrich
PDMS-63K (PDMS/H)	HMS-064, Trimethylsiloxy terminated methylhydrosilane-dimethylsilane copolymer, Mn = 60K-65K, hydride equivalent weight of 1240 g/mole	Gelest
PDMS-6K (PDMS/H)	HMS-082, Trimethylsiloxy terminated methylhydrosilane-dimethylsilane copolymer, Mn = 5.5K-6.5K, hydride equivalent weight of 925 g/mole	Gelest
ATMS	Allyltrimethyl Silane, $\geq 99\%$	Alfa Aesar
Karstedt's catalyst	Platinum(0)-1,3-divinyl-1,1,3,3-tetramethyldisiloxane complex solution (Pt ~2 % in xylene)	Sigma-Aldrich
SIT7900.0	1,3,5,7-tetravinyl-1,3,5,7-tetramethylcyclotetrasiloxane Molecular weight 344.66 g/mole	Gelest
DMS-V05	Vinyl terminated polydimethylsiloxane, Molecular weight 800 g/mole, vinyl equivalent weight of 377.4 g/mole	Gelest

2.3.2. Synthesis of TVE, PTVE, and PDMS-g-PTVE

2.3.2.1. Synthesis of 2-iodoethyl vinyl ether (IVE)

IVE was synthesized using the synthetic scheme shown in Figure 2.1. A detailed procedure is as follows: 100.65 g of 2-chloroethyl vinyl ether, 200.16 g of sodium iodide, and 730 g of acetone were combined in a 2-liter, 3-neck round bottom flask and heated to 60 °C for 72 hours. Next, the reaction mixture was cooled down to room temperature and diluted with 600 ml of diethyl ether. The organic layer was washed thrice with deionized water (DI) and dried with anhydrous magnesium sulfate. The product was recovered by rotary evaporation of diethyl ether and excess 2-chloroethyl vinyl ether at a temperature of 50 °C and a pressure of 60 mmHg for 1 hour. Proton NMR was used to confirm the production of 2-iodoethyl vinyl ether: ^1H NMR (CDCl_3) δ 6.44 ppm (q, 1H, $\text{OCH}=\text{C}$), 4.19, 4.05 ppm (dd, 2H, $\text{CH}_2=\text{C}$), 3.95 ppm (t, 2H, OCH_2), 3.3 ppm (t, 2H, CH_2I).

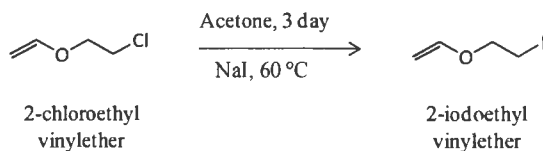


Figure 2.1. The synthetic scheme used to produce 2-iodoethyl vinyl ether.

2.3.2.2. Synthesis of 2,4-dichloro-1-(4-chloro-2-(2-(vinylloxy)ethoxy)phenoxy)benzene (TVE)

TVE was synthesized using the synthetic scheme shown in Figure 2.2. A detailed procedure is as follows: 102.69 g of 2-iodoethyl vinyl ether, 116.75 g of Triclosan, 71.72 g of potassium carbonate, and 531 g of DMF were combined in a 2-liter, 3-neck round

bottom flask and heated at a temperature of 80 °C for 24 hours. Next, the reaction mixture was cooled down to room temperature and diluted with 500 ml of diethyl ether. The organic layer was washed thrice with deionized water (DI) and dried with anhydrous magnesium sulfate. The crude product was recovered by rotary evaporation of volatiles. The monomer was purified by repeated crystallization from n-hexane and dried under vacuum overnight. Proton NMR, carbon NMR, DEPT-135, HETCOR, and FTIR were used to confirm the structure of TVE: ^1H NMR (CDCl_3) δ 6.34 ppm (q, 1H, $\text{OCH}=\text{C}$), 3.85-3.88 (t, 2H, $\text{OCH}_2\text{-C}$), 4.15 – 4.17 ppm (m, 2H, $\text{C-CH}_2\text{-O}$), 3.97, 4.12 ppm (m, 2H, $\text{CH}_2=\text{C}$), 6.65 - 7.4 ppm (m, 6H, Ar-H); ^{13}C NMR (CDCl_3) δ 151.5 ppm ($\text{OCH}=\text{C}$), 87.02 ppm ($\text{C}=\text{CH}_2$), 65.85 ppm ($\text{OCH}_2\text{-C}$), 68.1 ppm ($\text{C-CH}_2\text{O}$), 152.4, 150.4, 130.26, 128.13, 124.59, 122.07, 118.46, and 115.7 ppm (12 Ar-C); IR (KBr) 2960-2830 (CH_2), 3000-3100 (Ar. =C-H), 942, 980 (vinyl =C-H), 1640 (vinyl ether C=C), 1595, 1471 (Ar. C=C) cm^{-1} .

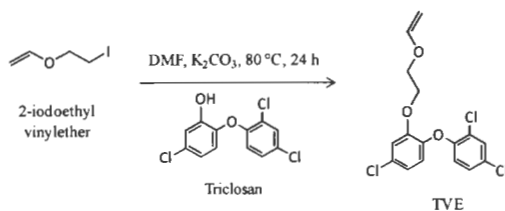


Figure 2.2. The synthetic scheme used to produce TVE.

The purity of TVE monomer was determined using an Agilent 1100 Series High Performance Liquid Chromatography (HPLC) fitted with an Agilent 1100 auto-sampler and a diode array detector. Sample solutions were prepared at 1 mg/ml in methanol and injected at a volume of 20 microliters through a Zorbax Eclipse XDB-C18 HPLC column. The mobile phase was a mixture of water and acetonitrile (30/70 vol. %) and the column

was maintained at a constant temperature of 40 °C. Free Triclosan showed a strong peak at a retention time of 3.9 minutes when a detector signal of 280 nm was used. The absence of any peak at a retention time of 3.9 minutes had confirmed that the TVE was totally free from Triclosan.

2.3.2.3. Synthesis of 1-isobutoxyethyl acetate (IBEA)

The polymerization initiator, IBEA was prepared using the procedure of Aoshima and Higashimura.³⁶ A detailed description is as follows (Figure 2.3): 18 g of glacial acetic acid and 45 g of isobutyl vinyl ether were combined in a 250 ml, 2-neck round bottom flask fitted with a reflux condenser and heated at 60 °C for 3 hours. Next, the reaction mixture was cooled down to room temperature and diluted with 200 ml of diethyl ether. The organic layer was washed thrice with deionized water (DI) and dried with anhydrous magnesium sulfate. The crude product was recovered by rotary evaporation of diethyl ether and unreacted isobutyl vinyl ether under a temperature of 25 °C and a pressure of 20 millibar. The purified IBEA was collected after one time distillation over calcium hydride. Proton NMR was used to confirm the production of IBEA: ¹H NMR (CDCl₃) δ 5.87 ppm (q, 1H, O-CH-O), 3.19, 3.4 (m, 2H, O-CH₂-C), 2.05 ppm (s, 3H, O=C-CH₃), 1.8 ppm (m, 1H, C-CH-C), 1.36 ppm (d, 3H, O-C-CH₃), 0.86 ppm (dd, 6H, C-C-CH₃).

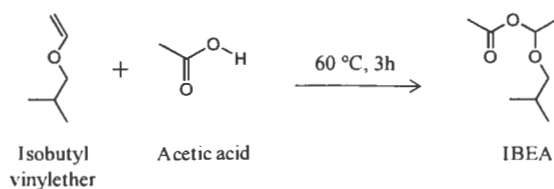


Figure 2.3. The synthetic scheme used to produce IBEA.

2.3.2.4. Synthesis of PTVE

The PTVE was prepared using living cationic polymerization as shown in Figure 2.4. A detailed procedure is as follows: Prior to use, TVE was dried under vacuum overnight at a temperature of 50 °C. 19.64 g of TVE, 43.6 mg of IBEA, 7.41 g of methyl chlosroacetate, and 35.73 g of toluene were combined together in a dry 250 ml round bottom flask inside a glove box. The polymerization of TVE was carried out at 0 °C inside the glove box in a series of dry test tubes partially immersed in a heptane bath. In each test tube, 3.5 g of reaction mixture was added and cooled to 0 °C. Each polymerization reaction was started by the addition of 46 microliters of supplied ethyl aluminum sesquichloride solution. Each polymerization was carried out at molar ratio of $[TVE]_0:[IBEA]_0:[MCAc]_0:[Et_{1.5}AlCl_{1.5}]_0 = 200:1:250:5$. After predetermined time intervals, the polymerization reactions were terminated with 10 ml of chilled methanol which precipitated the polymer. Each polymer was purified by dissolving it in toluene and re-precipitating into methanol to remove initiator and co-initiator fragments. Polymer yield was determined gravimetrically after drying the purified polymer at 40 °C under vacuum overnight.

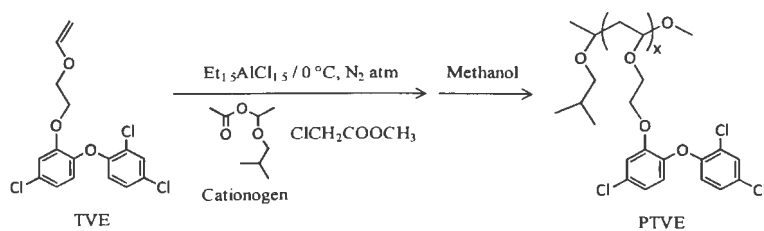


Figure 2.4. The synthetic scheme used to produce PTVE.

Polymer molecular weight was characterized using a high-throughput Symyx Rapid Gel Permeation Chromatography (GPC) equipped with an evaporative light scattering detector (PL-ELS 1000) and polystyrene standards. The progress of polymerization was monitored using Real-Time FTIR (ReactIR™ iC10 from Mettler Toledo) fitted with a diamond tip K6 conduit probe inside the glove box. At first, a dry 100 ml 3-neck round bottom flask was fixed with the probe and the initial background spectrum was collected. Next, 4 g of TVE, 8.9 mg of IBEA, 1.51 g of MCAc, and 7.43 g of toluene were combined together in the round bottom flask. The solution was cooled to 0 °C and the polymerization was started by the addition of 0.154 ml of supplied ethyl aluminum sesquichloride solution. The rate of consumption of TVE monomer was directly determined by integrating the peak area of reaction spectra in between 1611 cm⁻¹ and 1651 cm⁻¹. FTIR spectra were taken at a resolution of 8 cm⁻¹ and a Mercury Cadmium Telluride detector was used to analyze the signal.

The effect of an added base on the polymerization kinetics of TVE was demonstrated by the following experiment. 6 g of TVE, 13.2 mg of IBEA, and 11.1 g of toluene were combined together in a dry 100 ml round bottom flask inside a glove box. The polymerization of TVE was carried out at 0 °C inside the glove box in a series of dry test tubes partially immersed in a heptane bath. In each test tube, 1.5 g of such solution was added and cooled to 0 °C. Each polymerization reaction was started by the addition of 20 microliters of supplied ethyl aluminum sesquichloride solution. The polymerization was carried out at a molar ratio of $[M]_0:[IBEA]_0:[Et_{1.5}AlCl_{1.5}]_0 = 200:1:5$. After predetermined time intervals, polymerization reactions were terminated by the addition of 10 ml of chilled

methanol which precipitated the polymer. Each polymer was purified by dissolving it in toluene and re-precipitation into methanol to remove initiator and co-initiator fragments. Polymer yield was determined gravimetrically after drying the purified polymer at 40 °C under vacuum overnight.

2.3.2.5. Synthesis of monoallyl-functional polymer of TVE

A monoallyl-functional PTVE polymer (A-PTVE) was synthesized by terminating the polymerization reaction (Figure 2.5) with chilled 2-allyloxyethanol. A detailed procedure is as follows: 10 g of TVE, 0.178 g of IBEA, 6.04 g of MCAc, and 20 g of toluene were combined in a large dry test tube and cooled to 0 °C. The polymerization reaction was started by the addition of 0.61 ml of ethylaluminum sesquichloride solution. The polymerization was carried out at a molar ratio of $[\text{TVE}]_0:[\text{IBEA}]_0:[\text{MCAc}]_0:[\text{Et}_{1.5}\text{AlCl}_{1.5}]_0 = 125:5:250:5$. After 10 minutes, the reaction was terminated by the addition of 20 ml chilled 2-allyloxyethanol. The polymer was isolated by precipitation into methanol and vacuum filtration. The polymer was purified by dissolving it in toluene and re-precipitation into methanol. Polymer yield, which was determined gravimetrically after drying the purified polymer at 40 °C under vacuum overnight, was found to be 58%. Proton NMR, carbon NMR and FTIR were used to confirm the production of A-PTVE: ^1H NMR (CDCl_3) δ 3.50 – 3.90 ppm (m, $\text{OCH}_2\text{CH}_2\text{O-Ar}$, backbone CH), 1.47 – 1.65 ppm (m, backbone CH_2), 6.63 – 7.3 ppm (m, Ar-H); ^{13}C NMR (CDCl_3) δ 152.4 ($\text{OCH}=\text{C}$), 87.2 ($\text{C}=\text{CH}_2$), 66.3 (OCH_2), 68.1 (CH_2O), 115.7, 118.5, 121.8, 122.1, 124.8, 127.8, 128.1, 130.3, 130.5, 143.7, 150.6, 151.5 (12 Ar-C); IR (KBr) 2960-2830 ($\text{sp}^3 \text{CH}_2$), 3000-3100 ($\text{Ar.}=\text{C-H}$), 1595, 1471 ($\text{Ar. C}=\text{C}$) cm^{-1} .

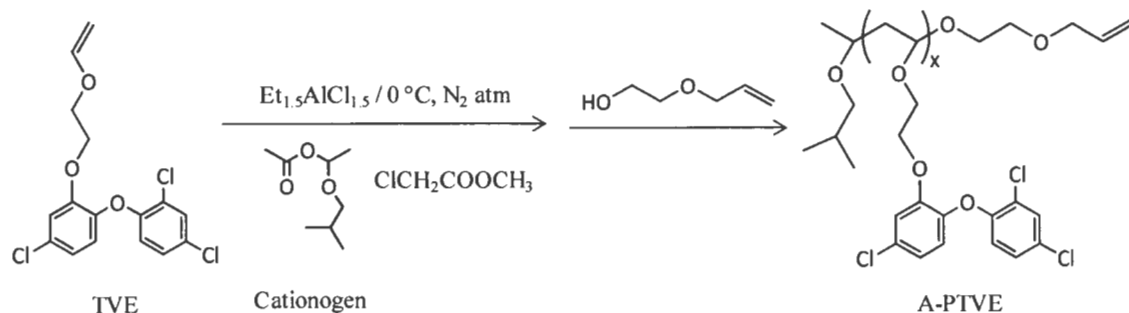


Figure 2.5. The synthetic scheme used to produce A-PTVE.

2.3.2.6. Synthesis of poly[(dimethyl-*co*-methylhydro)siloxane]-*g*-poly [2,4-dichloro-1-(4-chloro-2-(2-(vinylloxy)ethoxy)phenoxy)benzene] graft copolymer (PDMS-*g*-PTVE/H)

The PDMS-*g*-PTVE/H was synthesized (Figure 2.6) using hydrosilylation between A-PTVE and a trimethylsiloxy-terminated poly(dimethyl-*co*-methylhydrosiloxane) (PDMS/H). Different weight ratios of A-PTVE and PDMS/H copolymers (either HMS 064 or HMS 082) described in Table 2.2 were combined together in a series of dry 40 ml vials inside a glove box. The reactants were dissolved in toluene (15 wt. % solids) with constant stirring at 30 °C. The reaction was started by the addition of 70 microliters of Karstedt's catalyst and raising the temperature to 90 °C. The reaction was continued for 48 hours until the total disappearance of proton absorptions associated with the allyl group at 5.2 and 5.9 ppm were observed in the ^1H NMR spectrum. Proton NMR was used to confirm the production of PDMS-*g*-PTVE/H copolymer: ^1H NMR (CDCl_3) δ 4.69 ppm (Si-H), 0.06 ppm (Si- CH_3), 0.57 ppm (Si- CH_2).

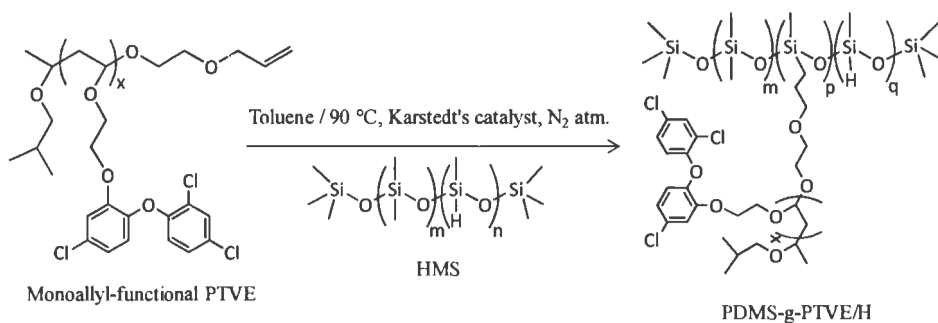


Figure 2.6. The synthetic scheme used to produce PDMS-g-PTVE/H.

2.3.2.7. Synthesis of poly[(dimethyl-*co*-trimethyl(propyl)silylmethyl)siloxane]-g-poly[2,4-dichloro-1-(4-chloro-2-(2-(vinylloxy)ethoxy)phenoxy)benzene] graft copolymer (PDMS-g-PTVE/P)

PDMS-g-PTVE/P graft copolymer was synthesized (Figure 2.7) by reacting the excess Si-H groups in PDMS-g-PTVE/H with allyltrimethyl silane (ATMS). A detailed procedure is as follows: To the solution of PDMS-g-PTVE/H copolymer (Table 2.2) in toluene, 2 g of ATMS and 70 microliters of Karstedt's catalyst were added. The reaction mixture was heated at a temperature of 90 °C under nitrogen atmosphere for 3 days until the total disappearance of the proton absorption associated with the Si-H groups at 4.69 ppm was observed in the ¹H NMR spectrum. Polymers were isolated by precipitation into methanol. Each PDMS-g-PTVE/P copolymer was purified by dissolving it in toluene, reprecipitating into methanol, and drying under vacuum overnight. Proton NMR and FTIR were used to confirm the production of PDMS-g-PTVE/P copolymer: ¹H NMR (CDCl₃) δ 0.06 ppm (Si-CH₃), 0.57 ppm (Si-CH₂), 6.63 – 7.3 ppm (m, Ar-H); IR (KBr) 2960 (sp³ C-H), 1093, 1018 (Si-O-Si), 1260 (Si-CH₃), 1405 (Si-CH₂), 1594, 1494 (Ar C=C) cm⁻¹.

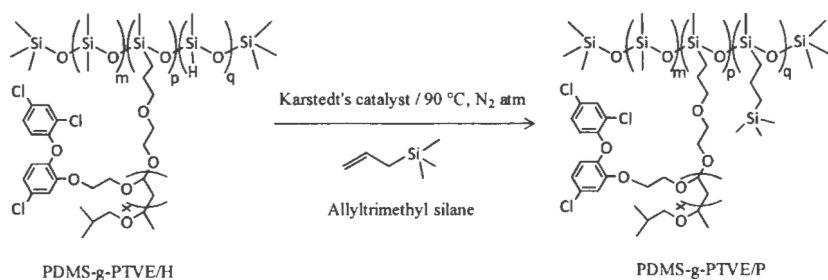


Figure 2.7. The synthetic scheme used to produce PDMS-g-PTVE/P.

Table 2.2. Compositions of PDMS-g-PTVE/H and PDMS-g-PTVE/P copolymers based on weight of A-PTVE and molecular weight of poly(dimethyl-co-methylhydrosiloxane).

Formulation	PDMS-g-PTVE/P				[PTVE] _c : [HMS] _o : [ATMS] _o
	PDMS-g-PTVE/H			ATMS (g)	
	PTVE (g)	HMS 064 (g)	HMS 082 (g)		
PDMS-63K-29	3.52	7.83	—	0.64	1 : 9.3 : 8.3
PDMS-63K-42	5.06	6.45	—	0.48	1 : 5.3 : 4.3
PDMS-63K-52	6.33	5.32	—	0.35	1 : 3.5 : 2.5
PDMS-63K-63	7.62	4.16	—	0.22	1 : 2.3 : 1.3
PDMS-6K-29	3.46	—	7.67	0.87	1 : 12.5 : 11.5
PDMS-6K-42	4.99	—	6.34	0.67	1 : 7.1 : 6.1
PDMS-6K-52	6.24	—	5.24	0.51	1 : 4.7 : 3.7
PDMS-6K-63	7.55	—	4.1	0.34	1 : 3.1 : 2.1

2.3.2.8. Synthesis of poly[(dimethyl-co-trimethyl(propyl)silylmethyl)siloxane]-g-poly[2,4-dichloro-1-(4-chloro-2-(2-(vinylxy)ethoxy)phenoxy)benzene] coatings using addition cure (PDMS-g-PTVE/S)

The PDMS-g-PTVE/S coatings were produced (Figure 2.8) by reacting the excess hydride groups of PDMS-g-PTVE/H with a divinyl-terminated PDMS, DMS V05 (3

equivalents of Si-H/1 equivalent of double bonds) in the presence of a moderator (SIT7900.0) and Karstedt's catalyst. A detailed description is as follows: PDMS-g-PTVE/H copolymer containing 52 wt. % PTVE was synthesized from HMS-064 using the synthesis scheme as described in Figure 2.6. 3.62 g of PDMS-g-PTVE/H, 80.8 mg of DMS V05, 14 mg of SIT7900.0, and 30 microliters of Karstedt's catalyst were dissolved in 8.47 g of toluene to make a homogeneous solution. The solution was cast over a desired substrate and cured at 40 °C in air oven overnight.

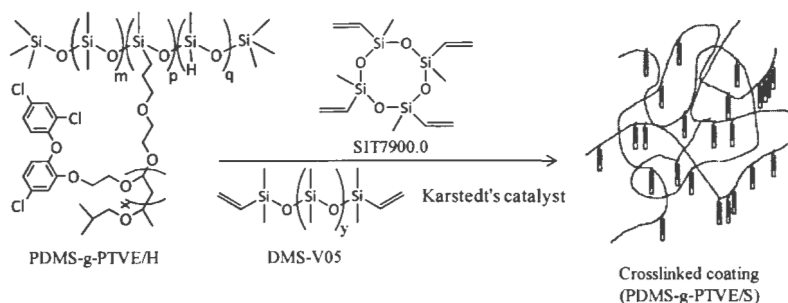


Figure 2.8. The synthetic scheme used to produce PDMS-g-PTVE/S.

2.3.3. Instrumentation and measurements

An MBraun glove box system equipped with a cold well and a chiller from FTSTM Systems was used for the cationic polymerization of TVE. Normal heptane was used as the cooling medium.

2.3.3.1. Gel Permeation Chromatography (GPC)

A high-throughput Symyx Rapid GPC equipped with an evaporative light scattering detector (PL-ELS 1000) and 2xPLgel Mixed-B columns of 10 μm particle size was used to determine the molecular weight and molecular weight distribution of polymer. Polymer

solutions of 3 mg/ml were prepared in THF and the temperature of the column was maintained at 45 °C. Molecular weight data was reported relative to polystyrene standards.

2.3.3.2. Nuclear Magnetic Resonance (NMR) spectroscopy

¹H and ¹³C NMR measurements were carried out with a JEOL-ECA 400 (400MHz) NMR spectrometer equipped with an autosampler. CDCl₃ was used as the lock solvent. Data acquisition was completed using 16 scans for proton NMR and 1000 scans for carbon NMR at a temperature of 23 °C. A Delta software was used to process the data. Heteronuclear Chemical Shift Correlation (HETCOR) and Distortionless Enhancement by Polarization Transfer (DEPT) experiments were used to assign the ¹³C peaks.

2.3.3.3. Fourier Transform Infrared (FTIR) spectroscopy

A Nicolet Magna-850 FTIR instrument was employed to measure FTIR spectra. Samples were coated on dry potassium bromide disc, and the measurements were carried out in the range of wavenumbers from 600 cm⁻¹ to 3900 cm⁻¹ using 64 scans with a data spacing of 0.964 cm⁻¹.

2.3.3.4. Differential Scanning Calorimetry (DSC)

A DSC Q1000 from TA Instruments equipped with an autosampler accessory was used to determine the glass transition temperature (T_g) of polymers. All polymers were first heated from -120 °C to 120 °C at a heating rate of 10 °C/minute (1st heat), cooled from 120 °C to -120 °C at a cooling rate of 10 °C/minute (cooling), and reheated from -120 °C to 120 °C at a heating rate 10 °C/minute (2nd heat). The T_g reported was obtained from the 2nd heat.

2.3.3.5. Transmission Electron Microscopy (TEM)

10-20 microliters of PDMS-*g*-PTVE/P copolymer solutions in toluene (1 wt. % solid) were deposited over a copper grid and dried overnight at room temperature. Images of the thin films over the copper grid were analyzed using a JEOL JEM-100 CX II electron microscope.

2.3.4. Coating surface characterization

PDMS-*g*-PTVE/P copolymers described in Table 2.2 were dissolved in THF at 42 weight percent solids and deposited over circular, primed aluminum discs and dried at 40 °C overnight. Addition-curable coatings were coated over prime aluminum discs at a concentration of 30 weight percentage solids in toluene and cured at 40 °C overnight. AFM and contact angle measurements were carried out over these surfaces.

2.3.4.1. Atomic Force Microscopy (AFM)

The coatings surfaces were characterized using an AFM consisting of a Dimension 3100® microscope coupled with a Nano-scope IIIa controller manufactured by Veeco Incorporated. Measurements were carried out in tapping mode using a silicon probe with a spring constant of 0.1 to 0.4 Nm⁻¹ and a resonance frequency of 17-24 kHz.

2.3.4.2. Surface Energy (SE) and water Contact Angle hysteresis (CA hysteresis)

An automated surface energy measurement unit manufactured by Symyx Discovery Tools, Incorporated was used to measure surface energy (SE), water contact angle, and water contact angle hysteresis (CA hysteresis) of the coatings.¹³⁵ Water contact angle was calculated by dispensing 10 µl of deionized water on the coating surface, capturing the

image of the water drop using a charged coupled device (CCD) camera, and analyzing images using an image analysis software. The surface energy was calculated by measuring contact angle for both water and methylene iodide and in putting the values in the Owens–Wendt equation.¹³⁶ Each data point was reported as the mean surface energy value of three replicate coatings. Error bars represent the standard deviation of the surface energy. In addition to static measurements, a dynamic contact angle experiment was carried out to calculate the CA hysteresis. A detailed description is as follows: 10 μl of deionized water was dispensed robotically with a constant rate of 0.1 $\mu\text{l/s}^{-1}$ for a total time period of 1 minute and images were taken at 10 second intervals. After 1 minute, water was removed at the same rate and contact angle determined every 10 second. The advancing contact angle (θ_A) and receding contact angle (θ_R) were reported after averaging the first three and last three contact angle values, respectively. The CA hysteresis was reported by subtracting θ_R from θ_A .

2.3.5. Deposition of coatings for antimicrobial characterization

A series of solutions were prepared by dissolving PDMS-*g*-PTVE/P copolymers (Table 2.2) in THF at 42 weight percentage solids. Solutions of PDMS-*g*-PTVE/H, DMS V05, SIT7900.0, and Karstedt's catalyst in toluene were prepared to produce thermoset PDMS-*g*-PTVE/S coatings according to Figure 2.8. The solutions were deposited into 24-well polystyrene plates modified with primed aluminum discs at the bottom. The volume of polymer solution deposited into each well was 175 microliters. Polymers were dried in an air-oven overnight at a temperature of 40 °C.

2.3.6. Characterization of antimicrobial properties

The antimicrobial properties of the solution-cast films deposited into 24-well polystyrene plates were evaluated using a novel combinatorial workflow as described by Stafslein et al.^{81, 133, 137-138} Coatings deposited into 24-well polystyrene plates were preconditioned in a circulating deionized water bath for 1 day. Antifouling performance of each coating was evaluated using biofilm retention, viability, and growth assays. The procedure for determining leachate toxicity (LT assay) was as follows: Preconditioned coatings were incubated in 1.0 ml of a biofilm growth medium, BGM (0.5 g of peptone and 0.1 g of yeast extract/1.0 L of artificial sea water) for 18 hours and the coatings leachates collected. Coatings leachates were analyzed for toxicity against two marine microorganisms (*C. lytica* and *N. incerta*) and three medically-relevant microorganisms (*S. epidermidis*, *E. coli*, and *C. albicans*). A 50 µl suspension of a microorganism in BGM was added to each 1 ml of leachate at a concentration of $\sim 10^7$ cells/ml. 0.2 ml of each leachate containing microorganism was transferred in triplicate to a 96-well polystyrene plate and incubated for 18 hours. Plates were rinsed thrice with deionized water and strained with crystal violet dye. 0.5 ml of glacial acetic acid was added to each well to extract the crystal violet and the absorbance was measured at 600 nm using a multi-well plate reader. A significant reduction in the amount of biofilm growth compared to a control coating was considered to be the consequence of toxic coating components leaching from the coating.

2.3.6.1. Bacterial biofilm retention assay

A 1.0 ml suspension of microorganism at a concentration of $\sim 10^7$ cells/ml of a BGM was added to each well of the 24 well coating plates. The plates were then incubated statically at a temperature of 28 °C for 18 hours to facilitate bacterial attachment and subsequent colonization. Next, the plates were rinsed with 1.0 ml of deionized water three times to remove any loosely attached biofilm and dried for 1 hour to fix the retained biofilm to the surface of the substrate without adding fixatives.¹³⁹ Upon drying, 0.5 ml of crystal violet solution (0.3% alcohol solution) was added to each well to stain the biomass. Excess stain was removed by rinsing with 1.0 ml of deionized water three times. After drying, the crystal violet dye was extracted by the addition of 0.5 ml of glacial acetic acid. The resulting elute was measured for absorbance at 600 nm. The absorbance values were directly proportion to the amount of biofilm retained over the surface of the coatings. Each data point was reported as the mean absorbance value of three replicate coating wells and as a ratio to the reference silicone coating. Error bars represent one standard deviation of the absorption ratio.

2.3.6.2. Algal biofilm growth assay

Algal biofilm growth was measured using the procedure previously described by Casse et al.¹⁴⁰ A detailed description is as follows: Coatings cast into the 24 well plates were inoculated with a suspension of the marine diatom, *N. incerta*, in artificial sea water and placed in an illuminated growth chamber at a temperature of 18 °C for 48 hours. Plates were then removed from the growth chamber and 1.0 ml of dimethyl sulfoxide was added to each well to extract the chlorophyll from the algal biomass attached to the coating

surfaces. 0.2 ml of such extract was transferred in triplicate to a 96-well plate and the fluorescence was measured (excitation wavelength of 360 nm and emission wavelength at 670 nm). Fluorescence, recorded as Relative Fluorescence Units (RFU), was reported as the mean value of three replicate coating wells and as a ratio to the reference silicone coating. Error bars represent one standard deviation of the RFU ratio.

2.3.6.3. Bacterial biofilm retraction assay

The biofilm retraction assay provides a measure of the adhesion strength of biofilms to coating surfaces. A detailed description of the procedure is as follows: 1.0 ml suspension of microorganism at a concentration of $\sim 10^7$ cells/ml of a BGM was added to each well of the 24 well coating plates. The plates were then incubated statically at a temperature of 28 °C for 18 hours to facilitate bacterial attachment and subsequent colonization. Next, the plates were rinsed with deionized (DI) water three times to remove any loosely attached biofilm. A solution of the biomass staining indicator, crystal violet, was added immediately after rinsing the plates with DI water. Digital images of stained biofilms were taken for each sample. Each image was converted to grayscale shading in AdobePhotoshop. The grayscale images were opened with PhotoGrid 1.0 software to analyze the percentage of bacterial biofilm surface coverage. The percentage of surface coverage was determined after evaluating the ratio of dark pixels (CV-stained biofilm) to light pixels (non-covered coating surface). Each data point was reported as the mean value of three replicate coating wells. Error bars represent one standard deviation.

2.3.6.4. Bacterial biofilm viability assay

For the evaluation of biofilm viability, the coating plates were rinsed with phosphate buffered saline (PBS) solution thrice. Then, 0.5 mL of 200 mg/L XTT (2,3-bis(2-methoxy-4-nitro-5-sulfophenyl)-5-phenylamino)carbonyl]-2H-tetrazoliumhydroxide) and 20 mg/L phenazine methosulphate in PBS were added to each well and incubated for 3 hours at a temperature of 37 °C. 0.1 mL from each well was then transferred to a 96-well plate and the absorbance measured at a wavelength of 490 nm using a multiwell plate spectrophotometer. Each data point was reported as the mean absorbance value of three replicate coating wells and as a ratio to the reference silicone coating. Error bars represent one standard deviation of the absorption ratio.

2.3.6.5. Determination of Minimum Inhibitory Concentration (MIC)

A detailed description for the determination of minimum inhibitory concentration (MIC) of antimicrobial polymers in solution was described by Shane Stafslie et al.⁸¹ Triclosan was serially diluted (2-fold) in marine broth (MB) and the MIC experiment was carried out for *C. lytica*, *N. incerta*, *S. epidermidis*, *E. coli*, and *C. albicans*. PDMS-g-PTVE/P copolymers synthesized from PDMS-6K was dissolved in THF at a concentration of 10 mg ml⁻¹ and serially diluted with MB. The concentration range of antimicrobial agents was 0.2 µg ml⁻¹ to 100 µg ml⁻¹. Pure MB without any antimicrobial agent was used as a positive control. 0.2 ml aliquots were dispensed into a 96-well plate. Plates were then incubated statically for 18 hours at a temperature of 28 °C and the absorbance at 600 nm measured. MIC data was reported as the minimum concentration of an antimicrobial agent to completely inhibit the growth compared to a control MB.

2.4. RESULTS

2.4.1. Characterization of TVE, PTVE, and PDMS-g-PTVE

2.4.1.1. Characterization of TVE and PTVE

The approach for producing nontoxic antimicrobial coatings involved the synthesis of a novel biocide-functional polymer, PTVE tethered to PDMS. The approach consisted of the preparation of a monoallyl-functional PTVE using living carbocationic polymerization (Figure 2.5) followed by hydrosilylation of monoallyl-functional PTVE to poly(methylhydrosiloxane-dimethylsiloxane) copolymers to produce PDMS-g-PTVE/H copolymers (Figure 2.6) possessing residual hydride functionality. The residual hydride groups in PDMS-g-PTVE/H copolymer were reacted with a large excess of allyltrimethyl silane to synthesize the PDMS-g-PTVE/P copolymers (Figure 2.7). For crosslinked systems, the residual hydride groups in PDMS-g-PTVE/H copolymers were crosslinked with a divinyl crosslinker to produce addition-cured PDMS-g-PTVE/S coatings (Figure 2.8).

As shown in Figure 2.5, the monoallyl-functional PTVE was synthesized using living carbocationic polymerization of TVE monomer followed by termination with 2-allyloxy ethanol. TVE monomer, a solid crystalline material with a melting point of 53 °C, was synthesized directly from Triclosan by the reaction with 2-iodoethyl vinyl ether in the presence of potassium carbonate in DMF (Figure 2.2). 2-iodoethyl vinyl ether was produced from 2-chloroethyl vinyl ether by the reaction with sodium iodide in acetone for 3 days (Figure 2.1).

The synthesis of 2-iodoethyl vinyl ether (IVE) was demonstrated using proton NMR experiment. As shown in Figure 2.9, one methine and two methylene protons in the vinyl double bond of IVE appeared at 6.4, 4.1, and 4.2 ppm, respectively. Successful synthesis of TVE monomer was confirmed by ^1H NMR, ^{13}C NMR, DEPT-135, HETCOR, and FTIR (Figures 2.10 – 2.12) spectra. According to Figure 2.10, the absorption associated with one methine and two methylene protons of the vinyl double bond in TVE were at 6.34, 4.0, and 4.15 ppm, respectively.

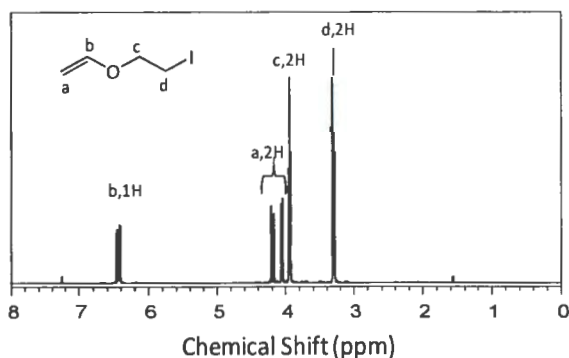


Figure 2.9. ^1H NMR spectrum obtained for 2-iodoethyl vinyl ether.

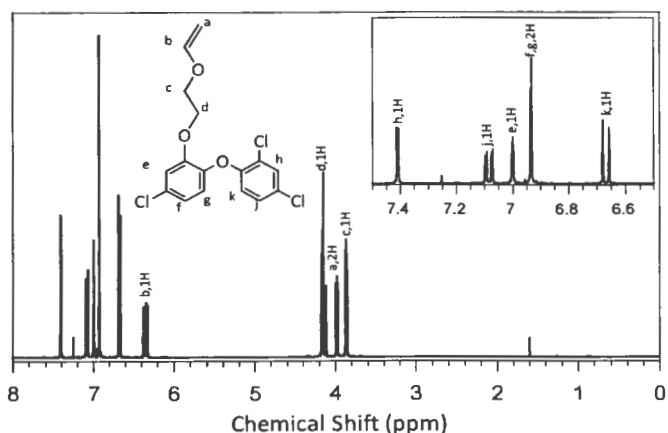


Figure 2.10. ^1H NMR spectrum obtained for TVE.

The Distortionless Enhancement by Polarization Transfer (DEPT) method is useful for determining the number of hydrogen atoms attached to a given carbon atom. In a DEPT-135 spectrum, methyl and methine carbons appear as positive peaks, while the methylene carbons appear as negative peaks. As shown in Figure 2.11.a, The methylene carbon (number 1) and methine carbon (number 2) in the vinyl double bond can be seen as a negative peak at 87.4 ppm and as a positive peak at 151.5 ppm, respectively. All methine carbons in aromatic rings at the position numbers of 7, 8, 10, 13, 15, and 16 produce positive peaks at 122.1, 122.1, 115.7, 130.5, 128.1, and 118.5 ppm, respectively. Two methylene carbons in the ethyl spacer in between the vinyl ether and the aromatic ring produce negative peaks at 66.3 and 67.7 ppm. Quaternary carbons in aromatic rings at position numbers 5, 6, 9, 11, 12, and 14 do not appear in the DEPT-135 spectrum because it has no attached hydrogen atoms.

The positions of protons were assigned using a HETCOR experiment (Figure 2.11.c). One carbon at 87.4 ppm and two proton doublets of doublet at 4.0 and 4.1 ppm correspond to methylene group (1); one carbon at 151.5 ppm and one proton quartet at 6.3 ppm correspond to methine group (2); one carbon at 66.3 ppm and two proton triplet at 3.9 ppm correspond to methylene group (3); one carbon at 67.7 ppm and two protons triplet at 4.2 ppm correspond to methylene group (4), one carbon at 115.8 ppm and one proton at 7.0 ppm correspond to aromatic methine group (10), and two carbons at 121.8 ppm, 122.1 ppm and two protons at 6.9 ppm correspond to two aromatic methine group (7, 8). FTIR spectrum of TVE (Figure 2.12) confirmed the presence of the vinyl ether double bond between 1611 cm^{-1} and 1651 cm^{-1} .

Successful synthesis of the polymerization initiator, IBEA, was confirmed using ^1H NMR (Figure 2.13) by integrating and comparing the ratio of proton absorptions at 0.87 ppm associated with 6 protons in two methyl groups in the isobutyl vinyl ether fragment to the proton absorptions at 2.1 ppm associated with 3 protons in methyl group in the acetic acid fragment.

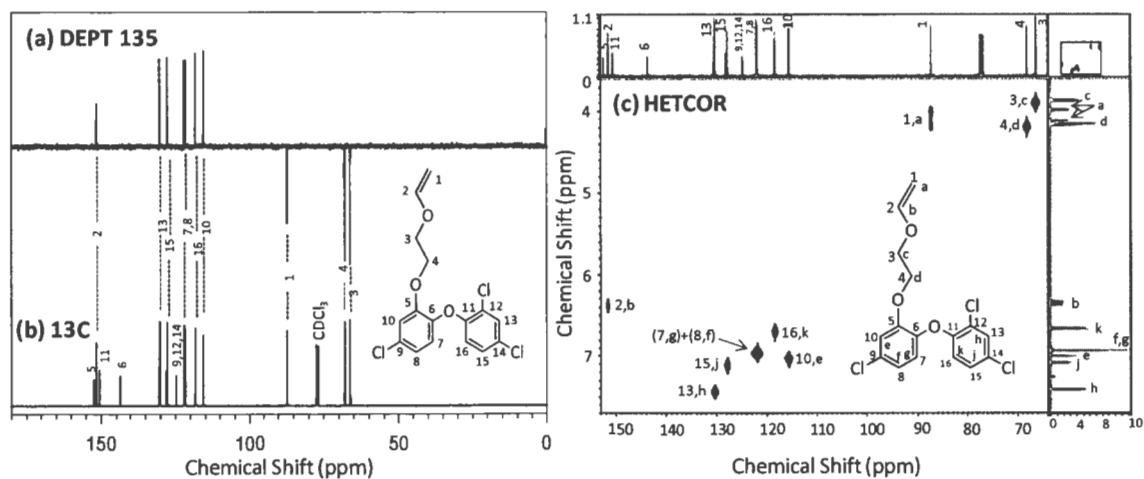


Figure 2.11. (a) DEPT-135, (b) ^{13}C NMR, and (c) HETCOR spectra obtained for TVE.

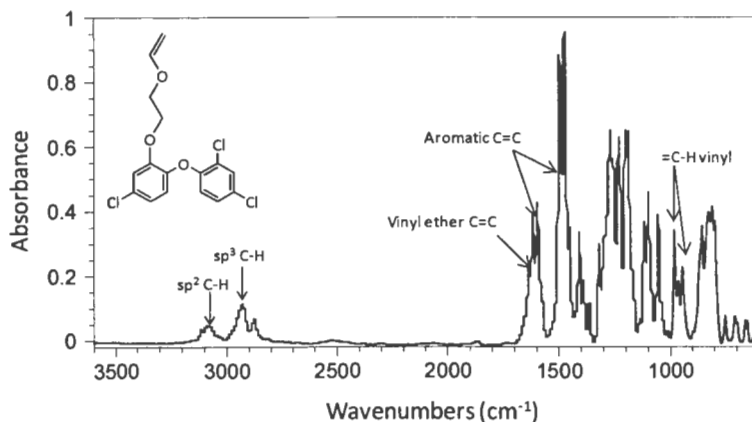


Figure 2.12. FTIR spectrum obtained for TVE.

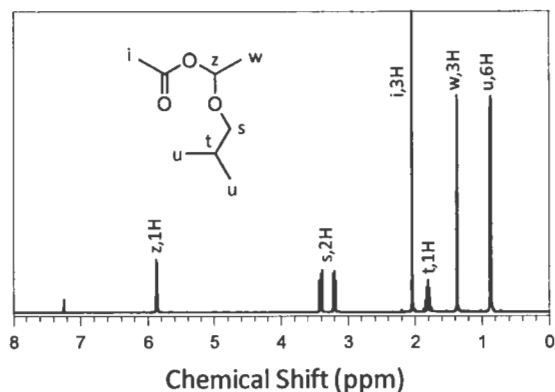


Figure 2.13. ^1H NMR spectrum obtained for polymerization initiator, IBEA.

2.4.1.2. Polymerization kinetics of TVE

TVE was polymerized using living carbocationic polymerization in the presence of IBEA, $\text{Et}_{1.5}\text{AlCl}_{1.5}$, and MCAc in toluene at $0\text{ }^\circ\text{C}$ under nitrogen atmosphere. When the polymerization reaction was terminated with 2-allyloxy ethanol, a monoallyl-functional PTVE was produced (Figure 2.5). The progress of polymerization was monitored using both Real Time FTIR and gravimetric analysis. Figure 2.14 represents reaction spectra taken before the addition of the co-initiator ($\text{Et}_{1.5}\text{AlCl}_{1.5}$) and after the completion of reaction. As shown in Figure 2.14, the progress of polymerization was directly monitored after integrating the peak area of vinyl ether double bond between 1611 cm^{-1} and 1651 cm^{-1} with reaction time. From the raw data of reaction trend graph, monomer concentrations at different reaction times were calculated and plotted to produce percentage of conversion versus reaction time (Figure 2.15.A) and $\ln([M]_0/[M]_t)$ versus reaction time (Figure 2.15.B) graphs. As shown in Figure 2.15.B, TVE polymerization follows the first order reaction kinetics in the presence of MCAc as an added base. In the absence of MCAc the

polymerization of TVE monomer initiated by IBEA/ $\text{Et}_{1.5}\text{AlCl}_{1.5}$ was rapid, non-living, and 98% polymerization was observed after 30 seconds of reaction resulting in a polymer possessing a GPC number average molecular weight of 28,700 and a molecular weight distribution value of 1.43. Large excess of carboxylate esters complexes with growing carbocations to control the unwanted termination and transfer reactions in the propagating step by reducing the Lewis acidity of organo-aluminum compound.³⁶

Living nature of TVE polymerization in the presence of MCAc was demonstrated by monitoring molecular weight as a function of monomer conversion. The linearity of GPC number-average molecular weight with monomer conversion, shown in Figure 2.16, indicated the obtainment of a living polymerization in the presence of an added base. In addition, the molecular weight distribution was determined to be 1.2 which also indicated living polymerization as well as a relatively fast initiation process.

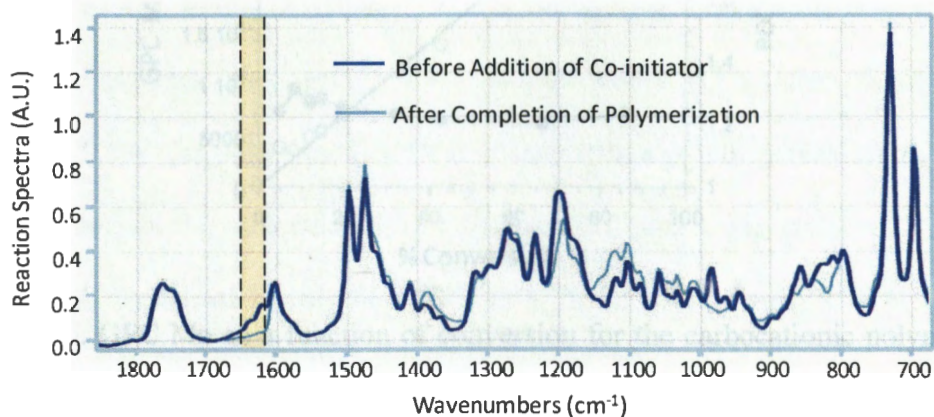


Figure 2.14. TVE polymerization reaction spectra were taken using ReactIR before the addition of co-initiator and after the completion of polymerization ($[\text{TVE}]_0:[\text{IBEA}]_0:[\text{MCAc}]_0:[\text{Et}_{1.5}\text{AlCl}_{1.5}]_0 = 200:1:250:5$).

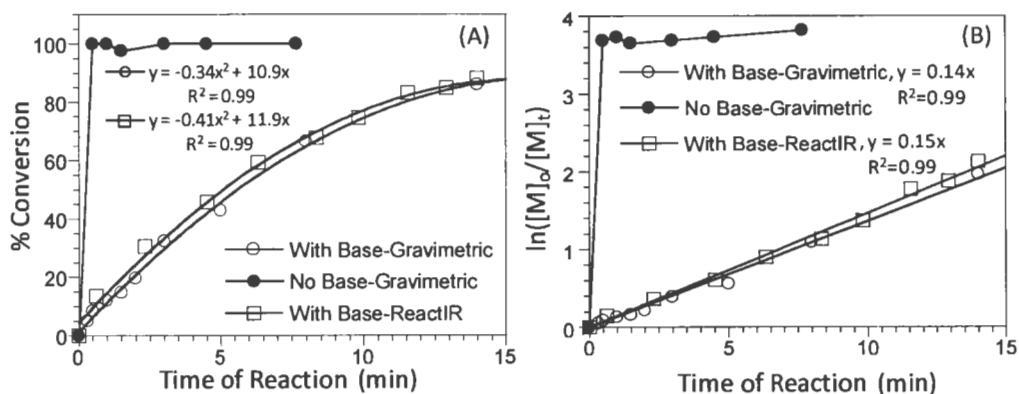


Figure 2.15. (A) Conversion % as a function of reaction time and (B) $\ln([M]_0/[M]_t)$ as function of reaction time for the carbocationic polymerization of TVE (With Base represents an initial composition of $[TVE]_0:[IBEA]_0:[MCAc]_0:[Et_{1.5}AlCl_{1.5}]_0 = 200:1:250:5$ and No Base represents an initial composition of $[TVE]_0:[IBEA]_0:[Et_{1.5}AlCl_{1.5}]_0 = 200:1:5$).

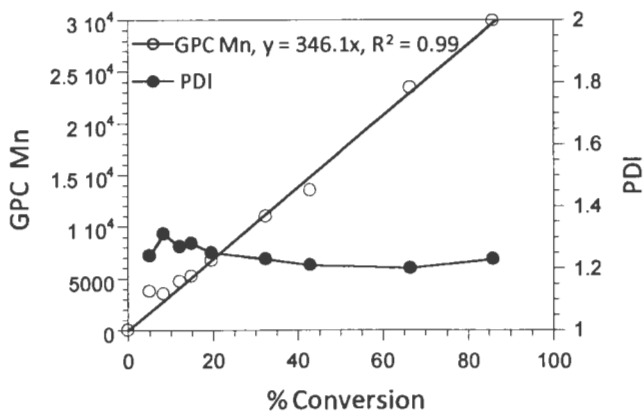


Figure 2.16. GPC Mn as a function of conversion for the carbocationic polymerization of TVE ($[TVE]_0:[IBEA]_0:[MCAc]_0:[Et_{1.5}AlCl_{1.5}]_0 = 200:1:250:5$).

Essentially, the incorporation of monoallyl functionality in PTVE enabled the formation of graft copolymer comprised of PDMS backbone. As shown in the 1H NMR spectrum (Figure 2.17) of PTVE, the quantitative fictionalization was characterized after

integrating and comparing the peak areas under the proton absorption at 0.87 ppm associated with two methyl groups in the initiator fragment to the proton absorption at 5.2 ppm associated with the terminal vinyl group in PTVE. The synthesis of end functional polymer obtained after terminating living anionic polymerization with functional terminating agent was described elsewhere.¹⁴¹⁻¹⁴³

The degree of polymerization (DP) calculated after integrating and comparing the peak areas under the proton absorption in the backbone methylene groups of repeating unit at 1.17 – 1.78 ppm to the proton absorption in the two methyl groups of initiator fragment at 0.87 ppm was 16.5. The percentage of conversion calculated using gravimetric analysis was 58%. The DP calculated from the initial concentration of monomer and initiator, and the percentage of conversion was 14.5. The close match of DP values obtained from both the gravimetric analysis and the NMR experiment suggested a fast initiation process. The PTVE molecular weight calculated was 5200 g/mole considering the percentage of conversion obtained using gravimetric analysis. The GPC number average molecular weight of PTVE was determined as 4400 g/mole with a polydispersity index value of 1.2. The difference in the molecular weight values calculated using gravimetric analysis and GPC can be explained by the fact that the GPC molecular weight is determined with respect to polystyrene internal standard.

The presence of a monoallyl end group in PTVE was also confirmed using ¹³C NMR and FTIR. As shown in ¹³C NMR spectrum (Figure 2.18), the methylene and methine carbons in the terminal vinyl group in PTVE appeared at 135 ppm and 117 ppm respectively. The FTIR absorption peak for the terminal vinyl group in PTVE at 1600 cm⁻¹

overlapped with the unsaturation in aromatic ring (Figure 2.19). However, after polymerization the vinyl ether double bond peak in TVE monomer (1611 cm^{-1} to 1651 cm^{-1}) was totally absent in PTVE.

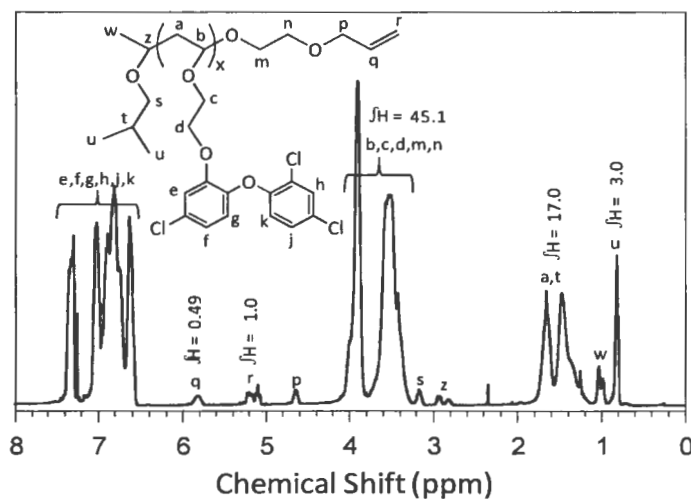


Figure 2.17. ^1H NMR spectrum obtained for monoallyl-functional PTVE. The integration values of total protons at different peak regions are mentioned here.

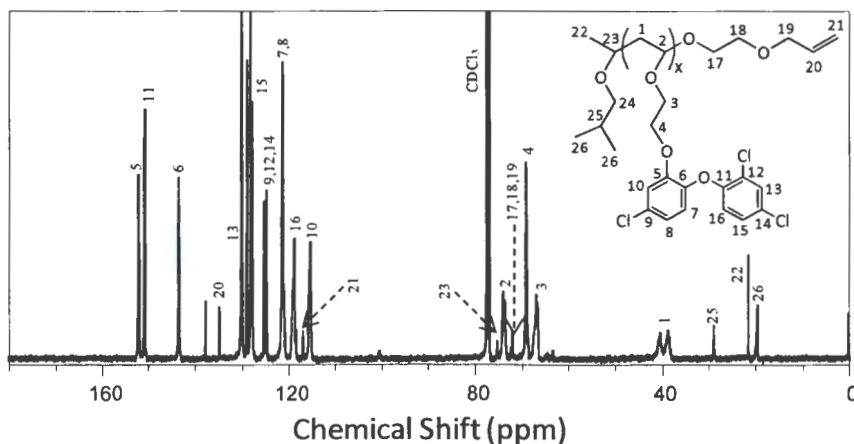


Figure 2.18. ^{13}C NMR spectrum obtained for monoallyl-functional PTVE.

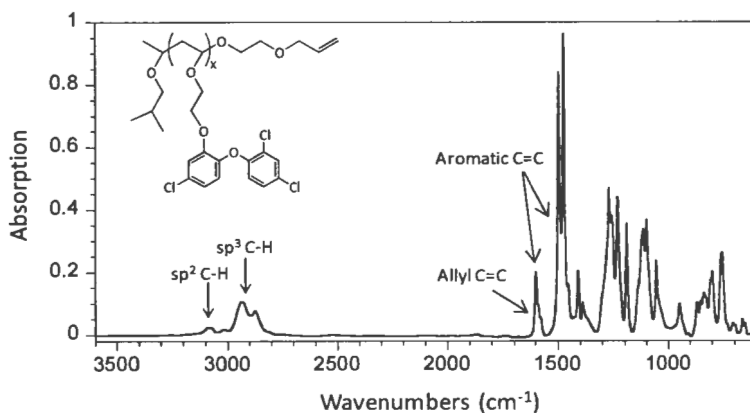


Figure 2.19. FTIR spectrum obtained for monoallyl-functional PTVE.

2.4.1.3. Characterization of PDMS-g-PTVE

The biocide moiety (PTVE) was grafted to PDMS backbone using hydrosilylation reaction as mentioned in Figure 2.6. Successful grafting was confirmed by the complete disappearance of methylene protons of monoallyl-functionality in PTVE (δ 5.8 ppm and δ 5.1 – 5.2 ppm) and the generation of a new peak corresponding to methylene protons next to silicon atom at 0.45 ppm in ^1H NMR spectrum (Figure 2.20). The synthesis of PDMS-g-PTVE/P copolymer was confirmed by the complete disappearance of hydride (Si-H) peak at δ 4.7 ppm in ^1H NMR spectra (Figure 2.21). The absence of trace amount of hydride in PDMS-g-PTVE/P copolymer was confirmed by the complete disappearance of the Si-H absorption peak at 2145 cm^{-1} and the appearance of a new Si-CH₂ peak at 1405 cm^{-1} in FTIR spectrum (Figure 2.22).

In another example, the residual hydride group in PDMS-g-PTVE/H copolymer was crosslinked with a divinyl crosslinker to produce addition-cured PDMS-g-PTVE/S coating (Figure 2.8). The advantage of the addition curing system is that no by-product is

generated. As shown in Figure 2.8, the curing reaction was conducted in the presence of a divinyl crosslinked (DMS-V05) and a moderator, 1,3,5,7-tetravinyl-1,3,5,7-tetramethyl cyclotetrasiloxane (SIT7900.0). Moderator was used to slow the hydrosilylation reaction and to increase the application time.

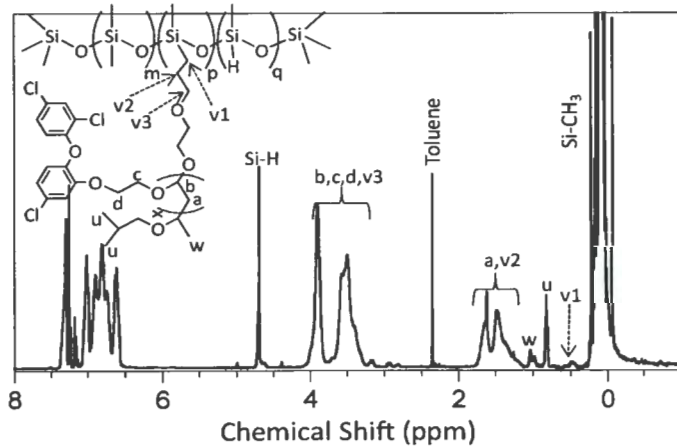


Figure 2.20. ^1H NMR spectrum obtained for PDMS-g-PTVE/H.

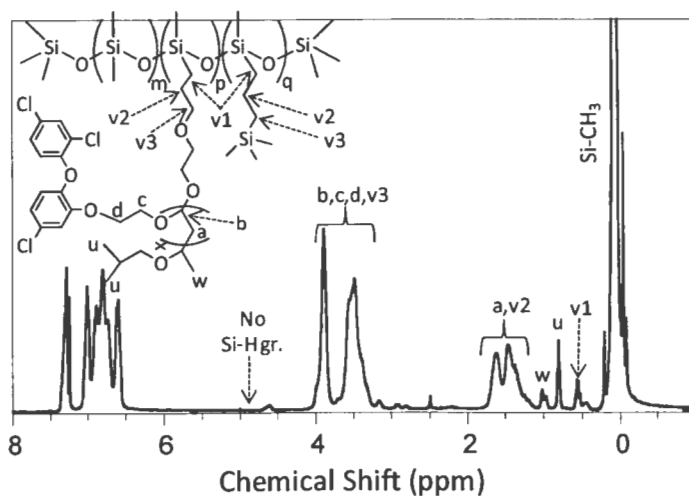


Figure 2.21. ^1H NMR spectrum obtained for PDMS-g-PTVE/P.

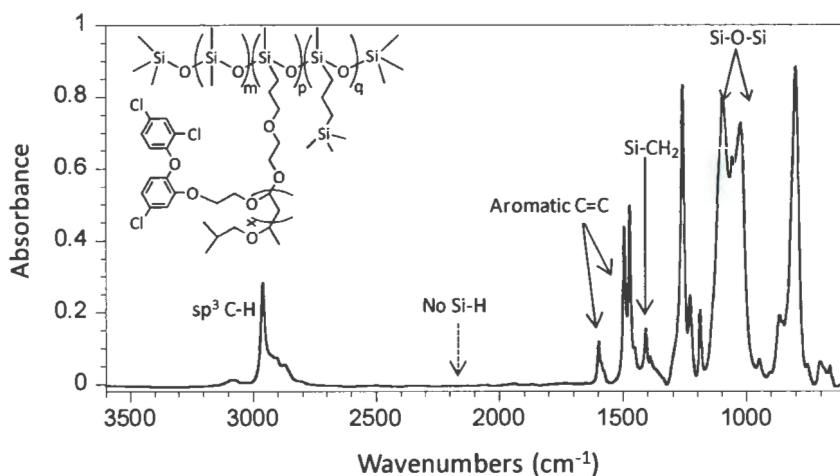


Figure 2.22. FTIR spectrum obtained for PDMS-g-PTVE/P.

In general, the PDMS-g-PTVE/P copolymers were rubbery material at room temperature. Thermal analysis (Figures 2.23 and 2.24) revealed that PDMS-g-PTVE/P copolymers had two phase morphology. Glass transition temperature (T_g) measured for PTVE was 34 °C. DSC thermograms obtained for PDMS-g-PTVE/P copolymers indicated two glass transition temperatures (Figures 2.23 and 2.24). One T_g below -120 °C was characteristic of PDMS, and the other T_g above 15 °C was characteristic of PTVE.

As shown in Figure 2.23, pure PDMS-63K has a T_g of -125.7 °C. As the temperature was increased from -125 °C, PDMS-63K showed a melting exotherm at a peak maximum temperature of -87.7 °C ($\Delta H_m = 7.5$ J/g) followed by a crystallization endotherm at a peak minimum temperature of -57.8 °C ($\Delta H_c = 9.7$ J/g). As the amount of PTVE graft was increased from 29 wt. % to 42 wt. %, the PDMS-g-PTVE-P copolymers showed a significant reduction in both ΔH_m and ΔH_c of PDMS segments. The reduction of both the melting and crystalline region with the increase in PTVE loading suggested the partial

miscibility of PTVE and PDMS phases. Interestingly, with PTVE loading beyond 42 wt. % no crystallization and melting region were observed indicating the increase in miscibility of hard and soft segments. Moreover, with the increase in miscibility of PDMS and PTVE phases in PDMS-63K-52 and PDMS-63K-63 copolymers, glass transition temperatures correspond to soft and hard segments shifted towards relatively lower temperatures.

As shown in Figure 2.24, pure PDMS-6K has a T_g of $-127.5\text{ }^\circ\text{C}$. Similar to the analogous graft copolymers synthesized from PDMS-63K, the glass transition temperatures of soft (PDMS) and hard (PTVE) segments in PDMS-6K-52 and PDMS-6K-63 copolymers shifted towards relatively lower temperatures. This indicates the extent of miscibility of PDMS and PTVE phases is higher with the PTVE content greater than 42 weight percentage. However, the crosslinked PDMS-g-PTVE/S coating itself is glassy at room temperature with a T_g of $27.5\text{ }^\circ\text{C}$.

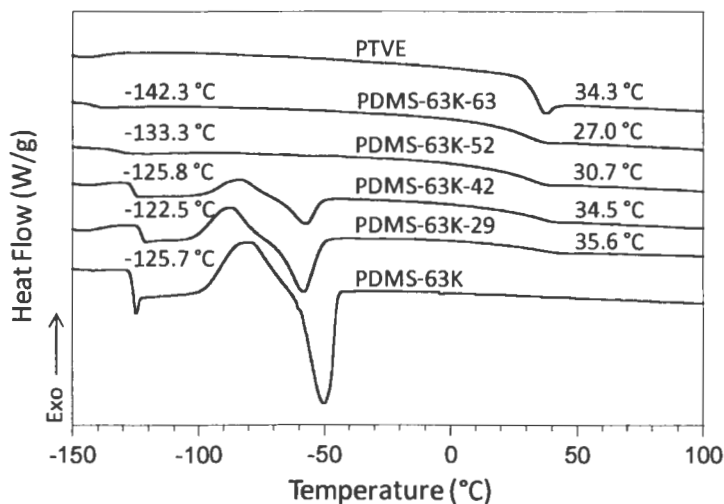


Figure 2.23. DSC thermograms for PDMS-g-PTVE/P copolymers with PDMS-63K.

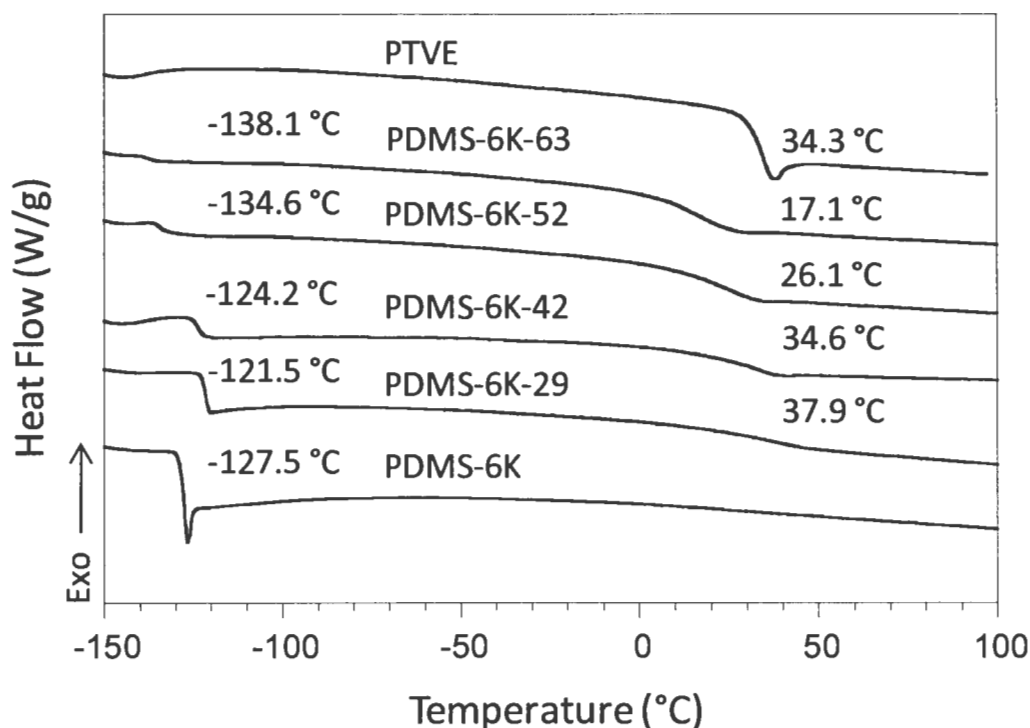


Figure 2.24. DSC thermograms for PDMS-g-PTVE/P copolymers with PDMS-6K.

The two phase morphology of PDMS-g-PTVE/P copolymers based on both PDMS-63K and PDMS-6K was illustrated by TEM images (Figure 2.25). In case of PDMS-63K-29 and PDMS-63K-42, the PTVE and PDMS were the continuous and dispersed phase respectively. As the PTVE content increased beyond 42 weight percentage, the opposite trend was observed. However, for PDMS-63K-63 copolymer both the PDMS and PTVE phases existed as bi-continuous phase. For copolymers based on PDMS-6K with entire range of PTVE loading, the PTVE was the dispersed phase and PDMS was the continuous phase. However, in the case of PDMS-6K-52 and PDMS-6K-63, both the PDMS and PTVE existed as bi-continuous phases.

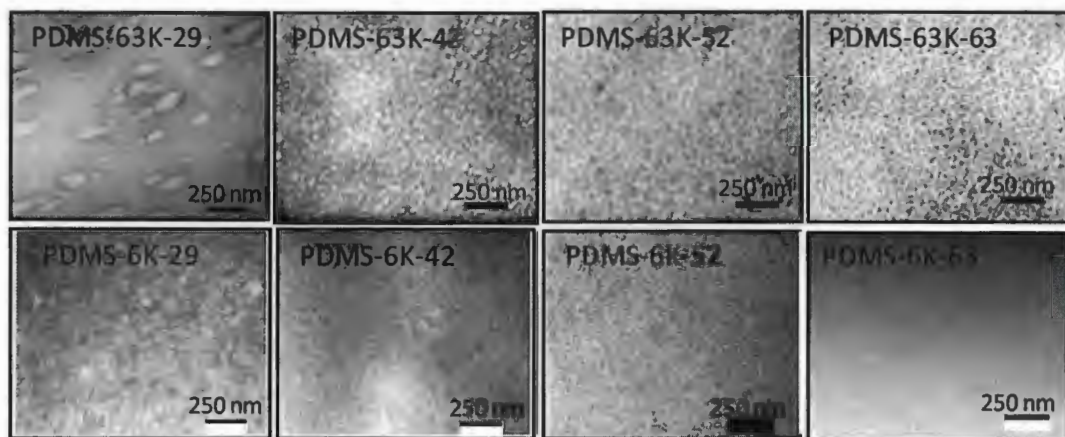


Figure 2.25. TEM images of PDMS-g-PTVE/P copolymers with PDMS-63K and PDMS-6K.

In order to correlate the antimicrobial activities with phase separation morphology of coatings surfaces, the antimicrobial characterization, AFM and contact angle analysis experiments were conducted over the coatings surface prepared under the same condition. The surface morphology of Triclosan tethered PDMS containing hard domains (PTVE) and soft domains (PDMS) were characterized using an AFM in tapping mode. AFM images (Figure 2.26) of PDMS-g-PTVE/P coatings based on both PDMS-63K and PDMS-6K backbone showed two phase morphology with an average RMS roughness from 8 nm to 1 nm.

Table 2.3 describes the variation of average RMS roughness of three replicate surfaces as a function of PTVE content and PDMS molecular weight. In general, for PDMS-g-PTVE/P coatings synthesized from PDMS-6K showed a finer phase morphology than that of PDMS-63K analog. However, in both cases the surface RMS roughness reduced monotonically with the increase in PTVE content. PDMS-g-PTVE/P coatings

synthesized from both PDMS-63K and PDMS-6K showed a significant reduction in RMS roughness beyond 42 weight percentage of PTVE demonstrating the increase in partial miscibility of PTVE and PDMS domains. However, no phase separation morphology was observed in the case of coatings surfaces synthesized using addition cure (Figure 2.27).

Figure 2.28 shows the variation in surface energy (SE) and water contact angle hysteresis with PTVE weight percentage and PDMS molecular weight for PDMS-g-PTVE/P coatings. The surface of pure PTVE was essentially hydrophilic and had a surface energy value of 40.5 mN/m. On the other hand a moisture curable PDMS reference coating, DC 3140, is hydrophobic possessing a surface energy value of 18.38 mN/m. Data obtained from Figure 2.28 suggested that coating surfaces based on PDMS-6K were more hydrophilic and allowed more triclosan moieties on the surface than the PDMS-63K analog. The surface energy for coatings produced from PDMS-6K increased constantly with the increase in PTVE content. However, for coatings produced from PDMS-63K, the surface energy remained constant up to 42 wt % of PTVE and reduced for 52 and 63 wt. % of PTVE. The surface obtained from thermoset PDMS-g-PTVE/S coating was hydrophobic possessing a surface energy value of 19.5 mN/m.

As shown in Figure 2.28, the water contact angle hysteresis values of PDMS-g-PTVE/P coatings synthesized from PDMS-6K were relatively constant indicating chemical homogeneity of the surfaces towards polar and dispersive interaction. For surfaces synthesized from PDMS-63K, the water contact angle hysteresis value was the highest with 29 wt.% PTVE and then reduced drastically beyond 42 wt.% PTVE. This reduction

represented an increase in surface homogeneity due to the formation of fine phase separation morphology.

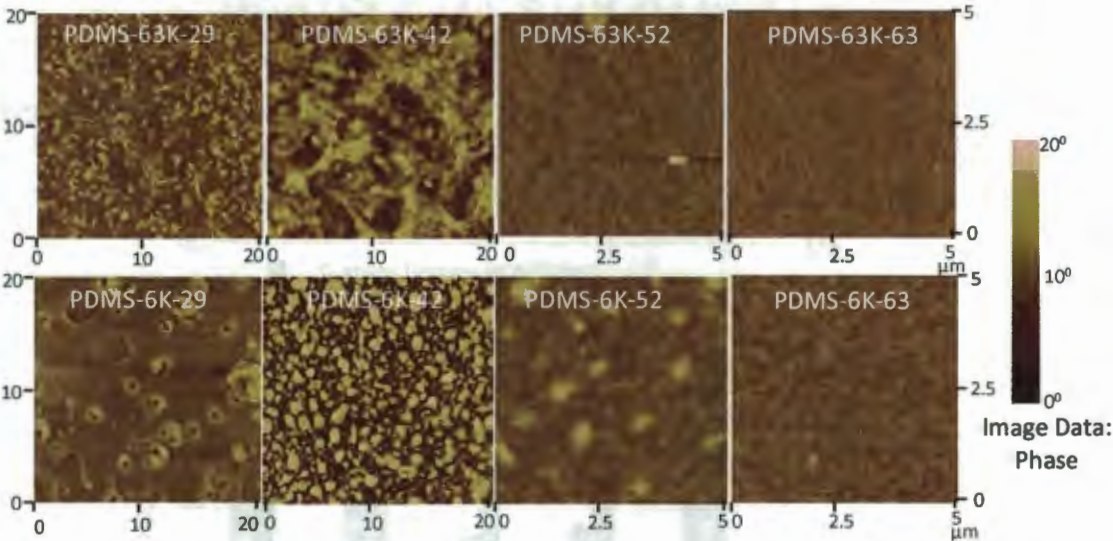


Figure 2.26. AFM images (phase) of PDMS-g-PTVE/P coatings with PDMS-63K and PDMS-6K.

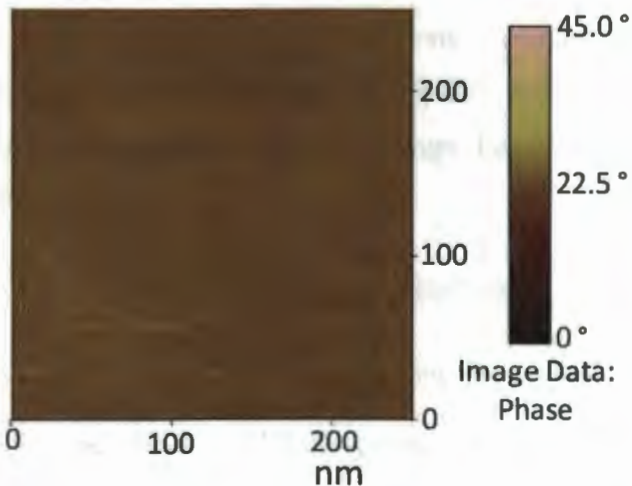


Figure 2.27. AFM image (phase) of PDMS-g-PTVE/S coating with 52 wt. % PTVE.

Table 2.3. Surface roughness of coatings produced from PDMS-g-PTVE/P coatings with PDMS-63K and PDMS-6K.

Coatings	PDMS-63K-29	PDMS-63K-42	PDMS-63K-52	PDMS-63K-63	PDMS-6K-29	PDMS-6K-42	PDMS-6K-52	PDMS-6K-63
RMS roughness \pm SD (nm)	8.46 \pm 0.74	5.61 \pm 1.35	1.90 \pm 0.37	1.87 \pm 0.50	3.28 \pm 0.38	3.46 \pm 1.25	1.22 \pm 0.11	1.01 \pm 0.14

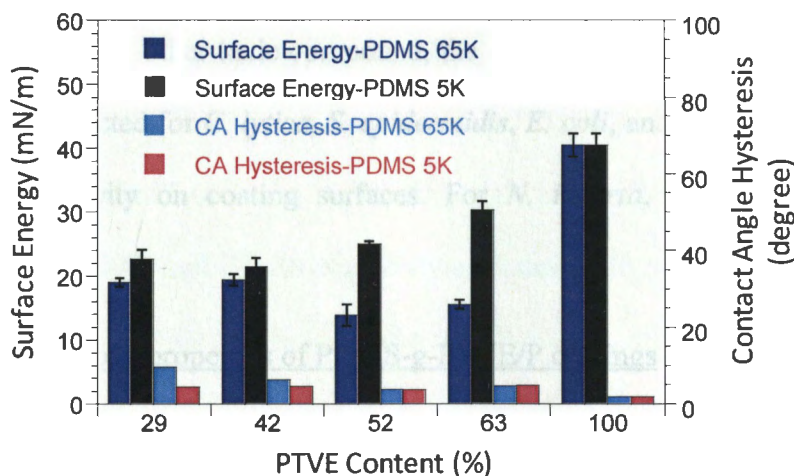


Figure 2.28. Surface energy and contact angle hysteresis of coatings produced from PDMS-g-PTVE/P copolymers with PDMS-63K and PDMS-6K. Each surface energy data was reported as the mean value of three replicate coatings. Error bars represent the standard deviation of the surface energy.

2.4.2. Antimicrobial properties of tethered Triclosan coatings

The objectives of the research were to evaluate the antimicrobial properties of the environmental friendly and non-toxic PTVE grafted PDMS coatings. High-throughput screening methods were employed to analyze the bioactivity of the coatings quickly and efficiently. Both the PDMS-g-PTVE/P and PDMS-g-PTVE/S coatings surfaces were tested

against three biomedically relevant microorganisms and two marine-relevant microorganisms. Since these coatings exhibit antimicrobial activity through a contact-active mechanism, prior to examine the antimicrobial properties, leachate toxicity tests were conducted. This process was necessary to ensure that any antimicrobial activity observed was due to surface associated phenomenon of coatings and not due to leaching of Triclosan or toxic components. After confirming that the coatings were not leaching lethal levels of Triclosan or other toxic compound, the biofilm retention, retraction, and viability assays were conducted for *C. lytica*, *S. epidermidis*, *E. coli*, and *C. albicans* to evaluate the antimicrobial activity on coating surfaces. For *N. incerta*, biofilm growth tests were performed.

2.4.2.1. Antimicrobial properties of PDMS-g-PTVE/P coatings

The leachate toxicity data of coating surfaces produced from PDMS-g-PTVE/P coatings according to the formulation in Table 2.2 were shown in Figures 2.29 and 2.30. The results showed that none of the coating leachates were substantially toxic (~25% reduction in biofilm retention) when tested against microorganisms employed in this experiment. However, coatings produced from PDMS-6K-63 required 3 weeks of pre-leaching before leachate toxicity analysis when tested against *S. epidermidis*. In addition to leachate toxicity, HPLC was used to detect the free Triclosan in TVE monomer. The detection limit of Triclosan in HPLC was 100 nanograms/ml. No detectable free Triclosan in TVE monomer was observed in HPLC. This result is consistent with the leachate toxicity test which indicated that PTVE leachate was not contaminated with any toxic

components or free Triclosan. Thus, the leachate toxicity test of surfaces produced from PDMS-g-PTVE/P coatings showed that any subsequent observation in antimicrobial characteristics would be purely coating surfaces associated phenomenon and not due to leaching of toxic components.

Figure 2.31 shows the reduction in *C. lytica* biofilm retention and viability of the coatings surfaces produced according to the formulation described in Table 2.2. Figure 2.32.A shows the biofilm retraction during the drying process. Figures 2.32.B and 2.32.C display the images of well plates with stained biomass over the coatings surfaces synthesized from PDMS-63K and PDMS-6K respectively. With regards to the amount of biofilm, PDMS-6K-42 and PDMS-6K-52 showed moderate reduction in biofilm retention with a value of 50% and 45% respectively. However, the XTT cell viability assay demonstrated that the maximum reduction (32%) in biofilm viability was observed for PDMS-6K-42. Coatings surfaces produced from PDMS-63K were not able to reduce either biofilm retention or viability significantly. From the images of coatings array plates (Figures 2.32.B and 2.32.C), it was observed that coating surfaces produced from the PDMS-6K-42 and PDMS-6K-52 underwent a significant amount of biofilm retraction (99% and 77% respectively) which was not observed for PDMS-6K-29 and PDMS-6K-63. Visually, it was observed from the image in Figure 2.32.C that none of the coating surfaces synthesized from PDMS-63K showed significant reduction in biofilm retraction.

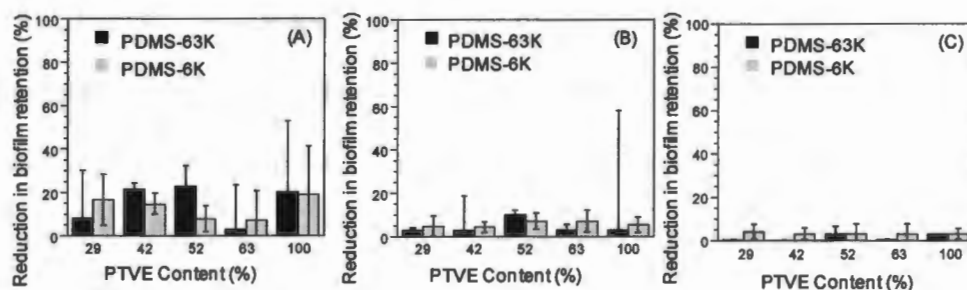


Figure 2.29. Toxicity evaluation of PDMS-g-PTVE/P coating leachates against (A) *C. albicans*, (B) *E. coli*, and (C) *S. epidermidis*. Each data point represents the percentage of reduction in biofilm growth compared to a control coating. Error bars represent standard deviations from the mean value of three replicate measurements.

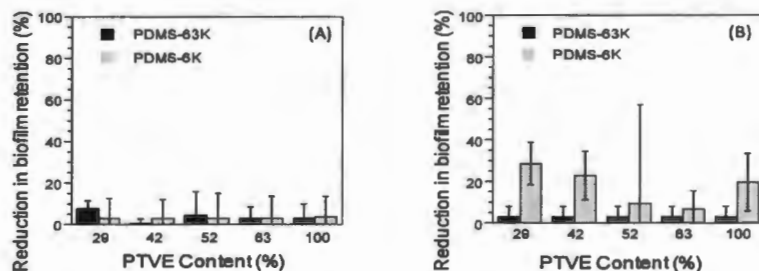


Figure 2.30. Toxicity evaluation of PDMS-g-PTVE/P coating leachates against (A) *N. incerta* and (B) *C. lytica*. Each data point represents the percentage of reduction in biofilm growth compared to a control coating. Error bars represent standard deviations from the mean value of three replicate measurements.

Figure 2.33 shows the reduction in *N. incerta* biofilm growth of the coating surfaces produced according to the formulation described in Table 2.2. With regards to the amount of biofilm growth, none of the coating surfaces were effective against *N. incerta* irrespective of the tethered PTVE content and PDMS molecular weight.

Figures 2.34.A and 2.34.B show the reduction in *S. epidermidis* biofilm retention and viability of the coatings surfaces produced according to the formulation described in

Table 2.2. Figure 2.34.C display the images of well plates with stained biomass over the coating surfaces synthesized from PDMS-6K. With regards to the amount of biofilm, PDMS-6K-52 and PDMS-6K-63 showed significant reduction in biofilm retention values of 79% and 98% respectively. However, the XTT cell viability assay demonstrated that none of the coatings surfaces were able to kill the bacterial cell significantly. The maximum percentage of reduction (36%) in biofilm viability was observed with the coating PDMS-63K-63 containing 63 wt % of tethered PTVE. Coating surfaces produced from 63K PDMS were not able to reduce the biofilm retention effectively. From the images of 6K PDMS coatings array plate (Figure 2.34.C), no significant amount of biofilm retraction was visually observed for PDMS-6K-29 and PDMS-6K-42.

Figure 2.35 shows the reduction in *E. coli* biofilm retention and viability of the coatings surfaces produced according to the formulation described in Table 2.2. Figure 2.36.A shows the biofilm retraction during the drying process. Figures 2.36.B and 2.36.C display the images of well plates with stained biomass over the coating surfaces synthesized from PDMS-63K and PDMS-6K. Data obtained from Figure 2.35 demonstrated that none of these coatings surfaces were able to reduce the *E. coli* biofilm retention or viability. From the images of coatings array plates (Figure 2.36.C), it was observed that coating surfaces produced from the PDMS-6K-42 underwent a significant amount of biofilm retraction (88%) which was not observed for coatings containing 29, 52, and 63 wt. % of tethered PTVE. However, the coatings surfaced produced from the PDMS-63K-42 and PDMS-63K-52 underwent moderate amount of biofilm retraction (37% and 59% respectively).

Figures 2.37.A and 2.37.B show the reduction in *C. albicans* biofilm retention and viability of the coating surfaces produced according to the formulation described in Table 2.2. Figures 2.37.C and 2.37.D display the images of well plates with stained biomass over the coatings surfaces synthesized from PDMS-63K and PDMS-6K. With regards to amount of biofilm, PDMS-6K-42 and PDMS-6K-52 showed moderate reduction in biofilm retention with a value of 42% and 57% respectively. However, the XTT cell viability assay demonstrated that none of the coating surfaces were able to kill the microorganism. From the images of coatings array plates (Figures 2.37.C and 2.37.D), it was observed that none of the coatings surfaces produced from the PDMS-63K and PDMS-6K were able to retract the biofilm. Table 2.4 showed the MIC data for both biomedically-relevant and marine-relevant microorganisms.

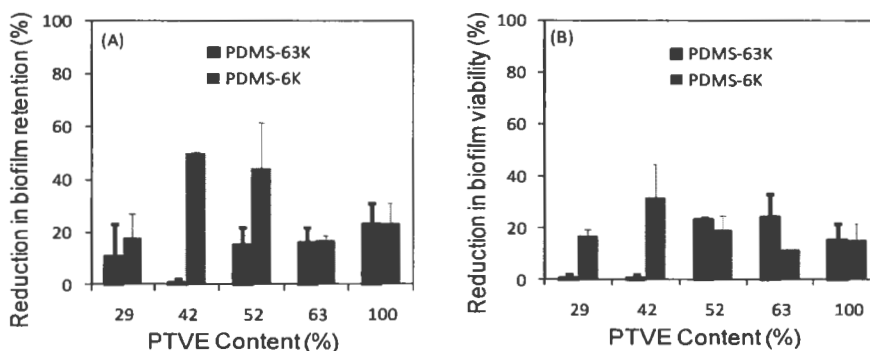


Figure 2.31. Evaluation of *C. Lytica* biofilm (A) retention and (B) viability for coatings surfaces produced from PDMS-g-PTVE/P copolymers with PDMS-63K and PDMS-6K. Percent reduction values are reported after comparing to a silicone elastomeric control coating, DC 3140. Error bars represent standard deviations from the mean value of three replicate measurements.

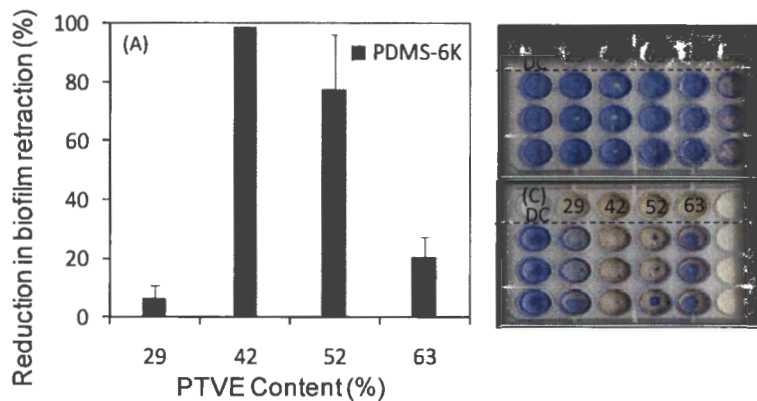


Figure 2.32. (A) Evaluation of *C. Lytica* biofilm retraction for coatings surfaces produced from PDMS-*g*-PTVE/P copolymers with PDMS-6K. Pictures in right side represent images of coating array plates after crystal violet staining for (B) PDMS-63K and (C) PDMS-6K with 29%, 42%, 52%, and 100% PTVE. Percent reduction values are reported after comparing to a silicone elastomeric control coating, DC 3140. Error bars represent standard deviations from the mean value of three replicate measurements.

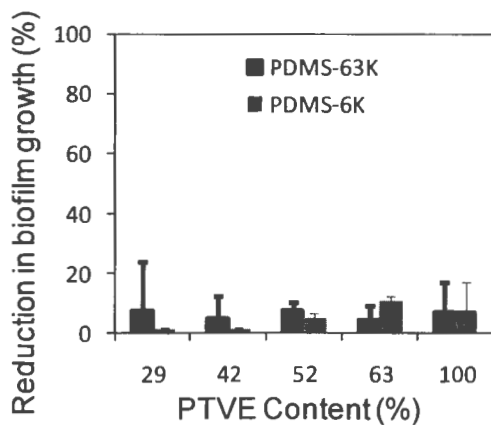


Figure 2.33. Evaluation of *N. Incerta* biofilm growth for coatings surfaces produced from PDMS-*g*-PTVE/P copolymers with PDMS-63K and PDMS-6K. Percent reduction values are reported after comparing to a silicone elastomeric control coating, DC 3140. Error bars represent standard deviations from the mean value of three replicate measurements.

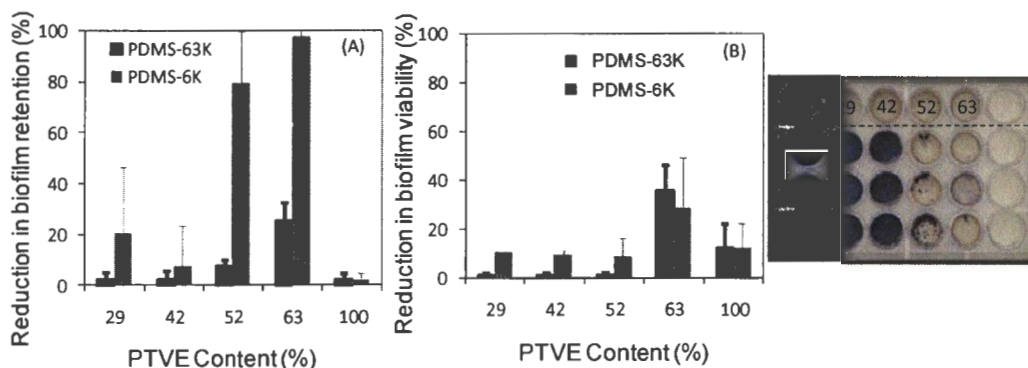


Figure 2.34. Evaluation of *S. epidermidis* biofilm (A) retraction and (B) viability for coatings surfaces produced from PDMS-g-PTVE/P copolymers with PDMS-63K and PDMS-6K. (C) Pictures in right side represent images of coating array plates after crystal violet staining for PDMS-6K with 29%, 42%, 52%, and 100% PTVE. Percent reduction values are reported after comparing to a silicone elastomeric control coating, DC 3140. Error bars represent standard deviations from the mean value of three replicate measurements.

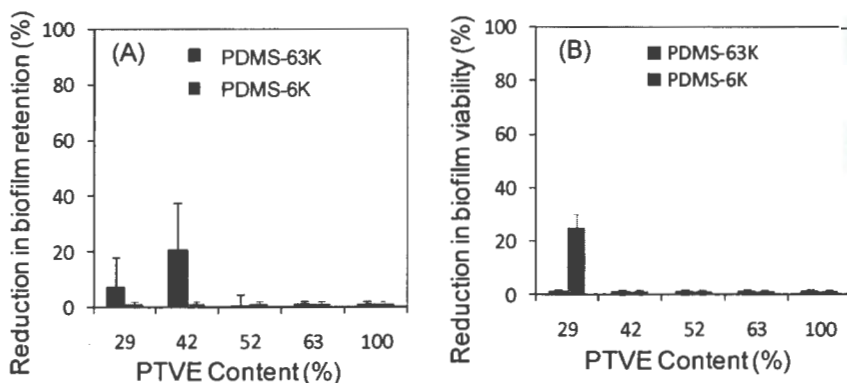


Figure 2.35. Evaluation of *E. coli* biofilm (A) retention and (B) viability for coatings surfaces produced from PDMS-g-PTVE/P copolymers with PDMS-63K and PDMS-6K. Percent reduction values are reported after comparing to a silicone elastomeric control coating, DC 3140. Error bars represent standard deviations from the mean value of three replicate measurements.

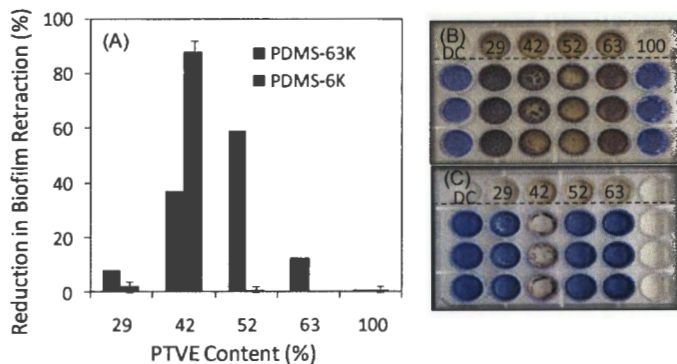


Figure 2.36. (A) Evaluation of *E. coli* biofilm retraction for coatings surfaces produced from PDMS-g-PTVE/P copolymers with PDMS-63K and PDMS-6K. Pictures in right side represent images of coating array plates after crystal violet staining for (B) PDMS-63K and (C) PDMS-6K with 29%, 42%, 52%, and 100% PTVE. Percent reduction values are reported after comparing to a silicone elastomeric control coating, DC 3140. Error bars represent standard deviations from the mean value of three replicate measurements.

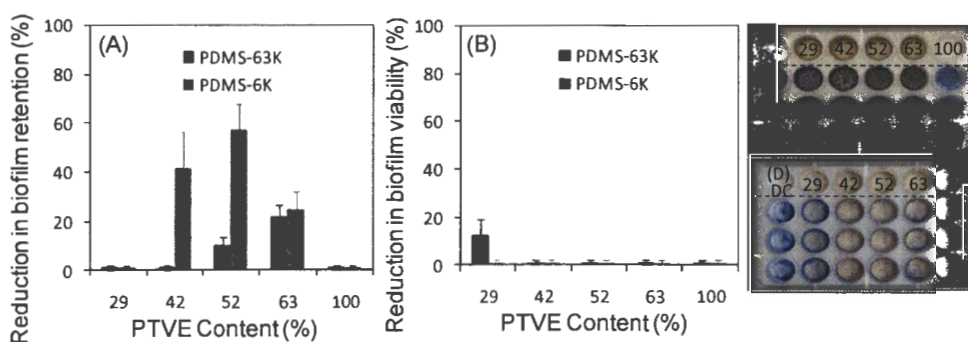


Figure 2.37. Evaluation of *C. albicans* biofilm (A) retention and (B) viability for coatings surfaces produced from PDMS-g-PTVE/P copolymers with PDMS-63K and PDMS-6K. Pictures in right side represent images of coating array plates after crystal violet staining for (C) PDMS-63K and (D) PDMS-6K with 29%, 42%, 52%, and 100% PTVE. Percent reduction values are reported after comparing to a silicone elastomeric control coating, DC 3140. Error bars represent standard deviations from the mean value of three replicate measurements.

Table 2.4. MIC data for both biomedically-relevant and marine-relevant microorganisms.

	Triclosan μg/ml	THF μg/ml	PDMS- 6K-29 μg/ml	PDMS- 6K-42 (μg/ml)	PDMS- 6K-52 (μg/ml)	PDMS- 6K-65 (μg/ml)	PTVE μg/ml
<i>C. lytica</i>	12.5	> 100	> 100	> 100	> 100	> 100	> 100
<i>N. incerta</i>	6.25	> 100	> 100	> 100	> 100	> 100	> 100
<i>E. coli</i>	0.8	> 100	> 100	> 100	> 100	> 100	> 100
<i>S. epidermidis</i>	< 0.2	> 100	> 100	> 100	> 100	> 100	> 100
<i>C. albicans</i>	> 100	> 100	> 100	> 100	> 100	> 100	> 100

2.4.2.2. Antimicrobial properties of thermoset PDMS-g-PTVE/S coatings

The coating surfaces produced from PDMS-g-PTVE/S containing 52 wt. % PTVE were found to contain no substantial amount of leachate toxic compounds (~20% reduction in biofilm retention/growth) when tested against five microorganisms used for this study (Figure 2.38). Figure 2.39 shows the reduction in biofilm retention data for *C. lytica*, *S. aureus*, *C. albicans*, and *E. coli*. Figures 2.41.A and 2.41.B demonstrated both the reduction in biofilm growth data for *N. incerta* and biofilm viability data for *S. aureus* and *E. coli*, respectively.

Data obtained from Figures 2.39 and 2.41 demonstrated that the coating surface was not able to reduce the biofilm retention, growth, and viability for none of these microorganisms. Figure 2.40 displays the images of well plates with stained biomass over the coatings surfaces produced from PDMS-g-PTVE/S. From the images of coatings array plates, it was observed that coatings surfaced produced from the PDMS-g-PTVE/S underwent no significant amount of biofilm retraction.

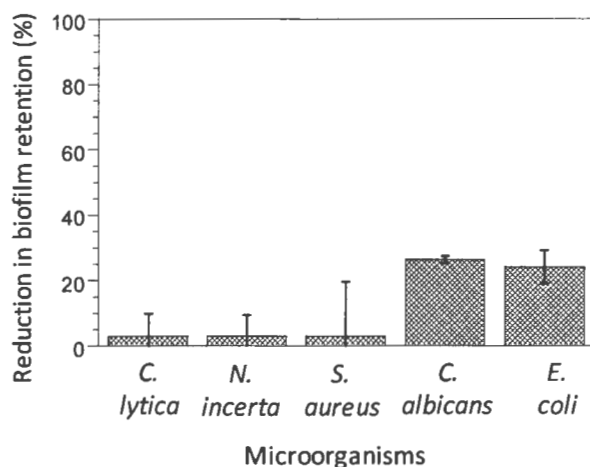


Figure 2.38. Toxicity evaluation of PDMS-g-PTVE/S coating leachates against *C. lytica*, *N. incerta*, *S. aureus*, *C. albicans*, and *E. coli*. Each data point represents the percentage of reduction in biofilm growth compared to a control coating. Error bars represent standard deviations from the mean value of three replicate measurements.

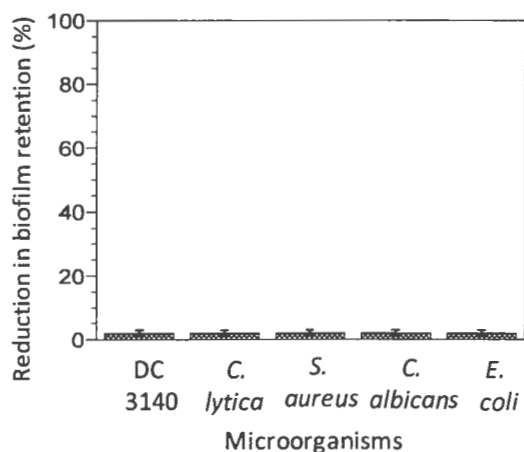


Figure 2.39. Evaluation of *C. Lytica*, *S. aureus*, *C. albicans*, and *E. coli* biofilm retention for coating surface produced from PDMS-g-PTVE/S containing 52 wt. % PTVE. Percent reduction values are reported after comparing to a silicone elastomeric control coating, DC 3140. Error bars represent standard deviations from the mean value of three replicate measurements.

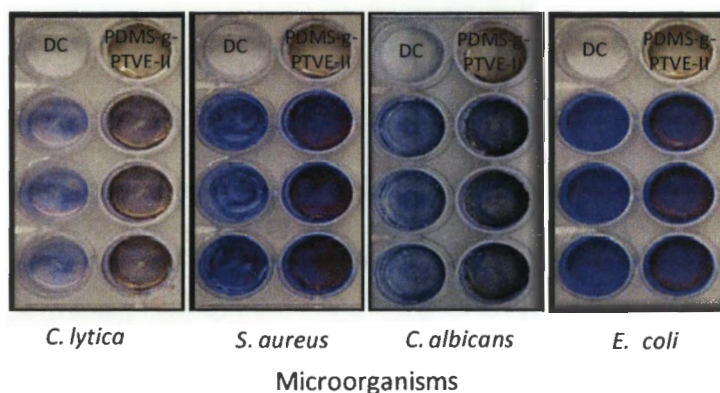


Figure 2.40. Images of the PDMS-g-PTVE/S (52 wt. % PTVE) coating array plates after crystal violet staining for *C. lytica*, *S. aureus*, *E. coli*, and *C. albicans* in biofilm retention experiment.

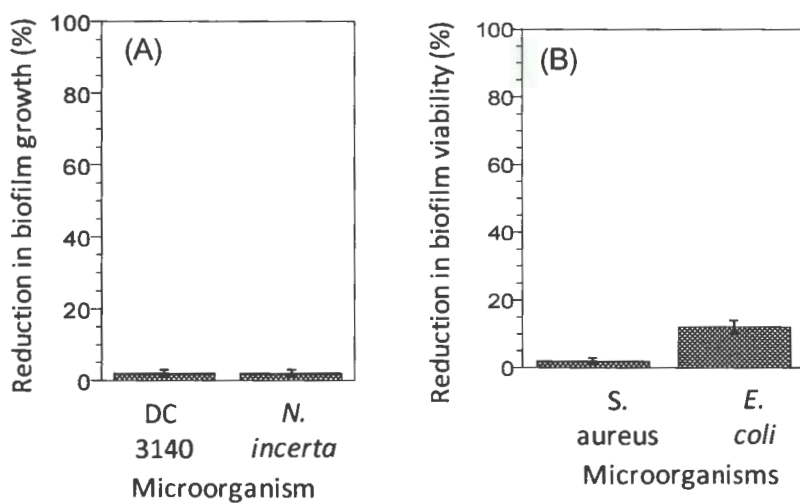


Figure 2.41. (A) Evaluation of *N. incerta* biofilm growth and (B) *S. aureus* and *E. coli* biofilm viability for coating surface produced from PDMS-g-PTVE/S containing 52 wt. % PTVE. Percent reduction values are reported after comparing to a silicone elastomeric control coating, DC 3140. Error bars represent standard deviations from the mean value of three replicate measurements.

2.5. DISCUSSION

The objective of the research was to investigate the feasibility of synthesizing a novel, environmental friendly antimicrobial coating containing tethered biocide moiety that could exhibit antimicrobial activity through a contact active mechanism without leaching the biocide. PTVE was used as a biocide and grafted to PDMS backbone. The bioactivity of coating surfaces produced from the phase separated thermoplastic coatings and single phase thermoset coating were tested against both the biomedical-relevant and marine-relevant organisms.

2.5.1. Reduction in biofilm viability

The antimicrobial testing results clearly demonstrated that the bioactivities of these coatings were highly microorganism specific. Generally, the reduction in biofilm viabilities data demonstrated that none of the PDMS-g-PTVE/P and PDMS-g-PTVE/S coatings surfaces could kill the microorganisms significantly. Only moderate reduction in *C. lytica* (32 %) and *S. epidermidis* (36%) biofilm viabilities were observed for thermoplastic PDMS-6K-42 and PDMS-63K-63 coatings respectively as compared to a PDMS control coating (DC 3140). These results are also supported by the leachate toxicity data of coatings which eliminated the presence of any free Triclosan or toxic leachates. Additionally, MIC data in Table 2.4 showed that chemically bonded Triclosan in PTVE is not lethal to any of the microorganisms tested in this experiment.

2.5.2. Reduction in biofilm retention

PTVE grafted PDMS is a class of environmentally friendly, non-toxic antimicrobial coatings that reduces biofilm formation by a contact active mechanism without killing microorganisms. The ability of the tethered Triclosan to deter the settlement of biofilm over coatings surfaces largely depends upon the phase separation morphology, weight percentages of PTVE, and PDMS molecular weight. PDMS-g-PTVE/S coating surface was not able to reduce the biofilm retention even at a PTVE concentration of 52 weight percent. In contrast to thermoplastic coatings, the PDMS-g-PTVE/S coating was not able to phase separate as shown in AFM images (Figure 2.27). The coating itself was glassy at room temperature ($T_g = 27.5\text{ }^\circ\text{C}$). The initial water contact angle (110°) and surface energy (19.5 mN/m) values illustrated that the coating surface was more likely to be hydrophobic. The biocide moiety, PTVE was possibly impinged into the PDMS matrix and the concentration of tethered Triclosan moieties at the water/coating interface might not be sufficient to prevent the retention and/or growth of biofilm produced by microorganisms tested.

The influence of tethered Triclosan to deter settlement of microorganisms over a series of leachate non-toxic, antimicrobial PDMS coating surfaces was previously reported by Chisholm et al.^{131-132, 134} The authors had tethered the Triclosan moiety to a moisture cured PDMS backbone through a hydrolytically stable ether linkage.¹³¹ It was found that a significantly high concentration of Triclosan moiety (>30%) was necessary to reduce the *C. lytica* biofilm retention. In another example, Chisholm et al.¹³² tethered Triclosan moiety to an addition-cured PDMS backbone through a hydrolytically stable ether linkage and found that a high level of tethered Triclosan (25%) was effective to reduce *C. lytica* biomass

retention. A similar result was reported by Chisholm et al.¹³⁴ for *C. lytica* biomass retention over an antimicrobial PDMS surface. Triclosan was attached to a PDMS backbone using a hydrolytically stable ether linkage and the epoxy-modified PDMS was crosslinked according to a procedure used by Thomas et al.⁷⁹ It was found that moderate reduction (37%) in *C. lytica* biofilm retention was observed for the PDMS coating containing 25% tethered Triclosan. Chen et al.¹³⁰ synthesized cationic UV curable coatings containing tethered Triclosan as a biocide moiety. The Triclosan was chemically attached to PDMS backbone using a hydrolytically stable ether linkage. These coatings were reported to be non-toxic to leachate toxicity experiment. A substantial reduction (>97%) in *S. epidermidis* biofilm retention and a moderate reduction (20-35%) in *E. coli* biofilm retention was observed on these coating surfaces. Interestingly, these leachate non-toxic, biocidal coatings can kill greater than 97% *S. epidermidis* even with a relatively low amount (6.4%) of tethered Triclosan moiety.

Kugel et al.⁷⁴ synthesized an antimicrobial polyurethane coating containing tethered Triclosan acrylate moiety. The tethered Triclosan was attached to a PDMS backbone in a polyurethane coating through an ester linkage. The authors had found a significant reduction in *S. epidermidis* biofilm retention and a moderate reduction in *C. lytica* biofilm retention with the coatings surface of interest. However, no reduction of biofilm retention and growth was observed for *E. coli* and *N. incerta* respectively. It was reported that the coatings surfaces could reduce the *S. epidermidis* biofilm retention at high concentration of Triclosan acrylate. According to the authors, one potential explanation of the organism specific antimicrobial activities towards *S. epidermidis* was the accumulation of free

Triclosan at the water/coating interface resulting from hydrolysis or enzymatic cleavage of the ester tether linking Triclosan to the coating matrix.

However, the mechanism of antimicrobial activity of PDMS based coatings investigated in this research is different than that described by Kugel et al.⁷⁴ but relatively similar to that described by Chisholm et al.^{131-132, 134} The polymer of tethered Triclosan (PTVE) was chemically grafted to a PDMS backbone through an ether linkage which is not known to be easily cleavable by hydrolytic or enzymatic process.¹⁴⁴ The detailed mechanisms of antimicrobial activity of Triclosan are not fully developed.¹⁴⁵ As mentioned by Escalada et al.¹⁴⁶ a multiple mechanism may exist depending upon the concentration of Triclosan. The mechanism of antimicrobial activity of Triclosan is mainly contributed to the inhibition of bacterial fatty acid synthesis.¹⁴⁷ It was reported that at low concentration, free Triclosan specifically blocks the activity of the enoyl-acyl carrier protein reductase (FabI) enzyme which is mainly responsible for bacterial fatty acid biosynthesis.^{145, 148} Some researchers also reported that at higher concentration, Triclosan may damage the bacterial extra cellular process involving the maintenance of membrane integrity and activity¹⁴⁶ which may occur by a contact mechanism as opposed to ingestion by bacteria.¹⁴⁹

The Triclosan moiety in this experiment is covalently bound to a polymer backbone through a hydrolytically stable ether linkage. Thus, it is highly unlikely that the bioactivity of tethered biocide polymer is due to the inhibition of reductase (FabI) enzyme or other metabolic process that occur within the cell. On the contrary, the bioactivity is likely due to tethering the effectiveness towards microorganism may change. Stewart et al.¹⁵⁰ reported that the 2-hydroxyl substitution on Triclosan is necessary to inhibit the activity of enoyl-

acyl carrier protein FabI enzyme. According to the minimum inhibitory concentration (MIC) data in Table 2.4, the bioactivity of tethered Triclosan in PTVE polymer was greatly reduced as compared to free Triclosan. This suggests that the microbial activity observed in PDMS-g-PTVE/P coatings is not due to the inhibition of bacterial fatty acid synthesis. However, it is possible that the bioactivity mechanism of this tethered Triclosan is attributed to the interaction of Triclosan moiety with the activity and maintenance of the bacterial cell membrane process. This mechanism is also supported by the fact that the bioactivity of PDMS-g-PTVE copolymer is organism specific depending upon the cell structure of microorganisms employed in this research.

The PDMS-g-PTVE/P copolymers synthesized from PDMS-6K were found to be more bioactive than the PDMS-63K analog. However, the reductions in biofilm retention were largely dependent on the nature of the cell wall of the microorganisms used for the evaluation. Considering the results obtained from the antimicrobial test, the PDMS-g-PTVE/P coatings from PDMS-6K were able to reduce the retention of biofilm significantly (80 - 97%) formed by a Gram-positive bacterium *S. epidermidis*. Biofilm retention was moderate for a Gram-negative marine bacterium *C. lytica* (45 – 50%), and a yeast *C. albicans* (42 – 58%). However, no biofilm retention and growth were observed for a Gram-negative bacterium *E. coli* and a marine diatom *N. incerta*. The bioactivity difference in between *S. epidermidis* (Gram-positive) and *E. coli* (Gram-negative) can be explained by the cell wall structure of these microorganisms. The multiwall cell of *E. coli* is composed of a thin, inner wall (2-3 nm) containing 10-20% peptidoglycan followed by an outer lipid bilayer (7 nm) containing phospholipids and lipopolysaccharides. On the other hand, the

cell wall of *S. epidermidis* is a thick (20-80 nm), single wall membrane containing 60 to 90% peptidoglycan. Due to the absence of phospholipids in the cell wall, *S. epidermidis* is found to be more vulnerable towards free Triclosan than *E. coli* as shown in the MIC data (Table 2.4). The cell wall of a marine diatom *N. incerta* is composed of a hard and porous layer of silica, called a frustule. The *C. albicans* cell wall consisted of almost inert cellular structure that protects the protoplast against osmotic offence. The major components of the cell wall are hydrophobic polysaccharides, such as chitin, glucan, and mannoproteins which provide the structural rigidity. Additionally, cell wall proteins increase the adhesion with substrates.¹⁵¹⁻¹⁵² For PDMS-g-PTVE/P coatings produced from PDMS-6K, the concentrations of tethered Triclosan at the coatings/water interface are sufficient enough to reduce the *E. epidermidis* biofilm significantly but not high enough to affect *E. coli* and *N. incerta*.

Data obtained from the reduction in biofilm retention and viability showed that the surface of pure PTVE polymer containing the maximum amount (80.3%) of Triclosan moiety was not able to either reduce the biomass settlement or kill any bacteria utilized in this experiment. Moreover, pure PTVE polymer surface is not able to retract the biomass formed by any of the organisms during dehydration of the coating surface. The data obtained from initial water contact angle and surface energy demonstrates that the PTVE surface is hydrophilic (surface energy 40.5 mN/m) due to the presence of the maximum amount of polar Triclosan moieties. On the other hand, a hydrophobic moisture curable control PDMS (DC 3140) surface (surface energy 18.38 mN/m) was not able to reduce the biofilm retention, viability, and retraction when tested against any of these microorganisms.

Thus, it is easily understandable that in order to interact with the cell wall of microorganisms effectively, Triclosan tethered PDMS surfaces should be amphiphilic in nature.

In general, coating surfaces based on lower molecular weight polysiloxane backbone possess greater antimicrobial activity than the copolymer based on higher molecular weight polysiloxane backbone. The coating surfaces synthesized from PDMS-*g*-PTVE/P copolymers are more likely amphiphilic possessing surface energy between 21 mN/m and 30 mN/m. However, AFM images demonstrating more finer two phase morphology was observed for PDMS-*g*-PTVE/P coatings synthesized from PDMS-6K than the PDMS-63K analog. Moreover, surface energy data demonstrates that PDMS-*g*-PTVE/P coatings produced from PDMS-6K are more hydrophilic than those with PDMS-63K analog. The surface energy increased with the increase in the concentration of PTVE moiety. According to Table 2.3, the phase sizes of PDMS-63K-52 and PDMS-63K-52 are comparable to those synthesized from PDMS-6K analog, but they still are not bioactive which could be due to increase in hydrophobicity. Thus, it is conceivable that PDMS-*g*-PTVE/P coatings from PDMS-6K offering finer phase separation and amphiphilic surface allow more Triclosan moieties at the water/coating interface and interact with the amphiphilic bacterial cell wall more effectively.

S. epidermidis is a widely recognized microorganism causing infection and failure in orthopedic implants, urinary catheters, and heart valves. Once the biomedical device is implanted inside the body, *S. epidermidis* attached over the surface and form thick slick layers of biofilm consisting of polymeric extra cellular matrix. These extra cellular

matrixes effectively shield the bacteria from adverse environment created inside the body in the presence of antibiotics and the host immune response. This is one of the well recognized causes of the implant failure requiring retrieval of the device. The result described in this research shows that Triclosan tethered PDMS coatings can effectively reduce (>97%) the biofilm formed by *S. epidermidis* without leaching any Triclosan in the environment. This class of compound is environmental friendly as it is not releasing any toxic compound. As a result the coating can be used on biomedical devices for long term protection against *S. epidermidis*.

2.5.3. Reduction in biofilm retraction

The biofilm retraction experiment shows a clear difference between biofilm surface coverage before drying and after drying of coatings. This phenomenon was not observed over either pure PDMS (DC 3140) or PTVE. The biofilm retraction process can be considered to be a slow de-wetting over PDMS in the presence of PTVE moiety. Significant biofilm retraction was observed for *C. lytica* and *E. coli* biofilm over the coatings surfaces synthesized from PDMS-g-PTVE/P copolymers. The maximum amount reduction in biofilm retraction was observed for thermoplastic coatings containing 42% and 52% PTVE. Chisholm et al.¹³¹⁻¹³² reported that the tethered Triclosan over a PDMS surface reduced the *C. lytica* biofilm adhesion. The authors concluded that the tethered Triclosan moiety at the surface may cause stress to the bacterial cells resulting in a reduction in biofilm adhesion over the surface without killing them. It was also found that a high

amount of tethered Triclosan (30 - 40%) was needed to get a significant reduction (>90%) in surface coverage.

As the coating surfaces dehydrated, the capillary forces acting due to the presence of high content of Triclosan moiety is enough to cause detachment of some portion of biofilm causing reduction in surface coverage.¹³² For *C. albicans* no significant biofilm retraction was observed that could be due to the cell wall proteins increasing adhesion with substrate.¹⁵¹⁻¹⁵² The crosslinked, PTVE tethered PDMS (PDMS-g-PTVE/S) surface was unable to reduce the biofilm retraction which could be due to the absence of high tethered Triclosan content at the coating/microorganism interface.

For long term antimicrobial activity of Triclosan tethered PDMS, the coatings surfaces should have a good foul release property. The antimicrobial surface covered by layers of retained biofilm may shield the activity of Triclosan moiety. In combination with antifouling and foul release properties the Triclosan tethered PDMS could be a good candidate against reducing *C. lytica* biofilm. However, in case of *E. coli*, no reduction of biofilm retention was observed but a significant amount of biofilm retraction (> 85%) was observed for 42 wt. % tethered PTVE.

2.6. CONCLUSION

A novel TVE monomer containing Triclosan as a biocide moiety was synthesized and polymerized using living carbocationic polymerization initiated by IBEA/Et_{1.5}AlCl_{1.5}. In the presence of methyl chloroacetate, a well-defined and living polymerization was successfully achieved. The monoallyl-functional PTVE was achieved by terminating the

living polymerization with 2-allyloxyethanol. Quantitative functionalization was confirmed using ^1H NMR. The incorporation of monoallyl-functionality in PTVE enabled the formation of Triclosan tethered polydimethylsiloxane graft copolymer possessing excess Si-H groups. The excess hydride was used to synthesize both PDMS-*g*-PTVE/P and PDMS-*g*-PTVE/S copolymers. The PDMS-*g*-PTVE/P copolymers were transparent rubbery materials. Both morphology and antimicrobial properties were found to depend on the molecular weight of PDMS and PTVE content. Thermal analysis of the PDMS-*g*-PTVE/P copolymers revealed that the graft copolymers were two phase materials. Copolymers possessing two glass transition temperatures (below $-120\text{ }^\circ\text{C}$ and above $15\text{ }^\circ\text{C}$) indicated the co-existence of PDMS and PTVE phases. Moreover, two phase morphology of PDMS-*g*-PTVE/P copolymers was also confirmed using AFM and TEM images. However, the surface energy analysis showed that the copolymers synthesized from PDMS-6K allow more Triclosan moiety at the surface of coatings than PDMS-63K analog. The PDMS-*g*-PTVE/P coatings based on the PDMS-6K exhibited higher antimicrobial activity than analogous coatings based on PDMS-63K. Antimicrobial activity of these leachate non-toxic coatings revealed that the surfaces produced from PDMS-6K provided excellent reduction in *S. epidermidis* biofilm retention (80% – 97%) and moderate reduction in both *C. albicans* (42% – 58%) and *C. lytica* (45% - 50%) biofilm retention. The PDMS-*g*-PTVE/P coating surfaces produced from PDMS-6K provided enough PTVE concentration at the coating/water interface, so that PTVE can effectively interacts with the microorganism cell wall to damage the bacterial extra cellular process. However, no bioactivity was observed for PDMS-*g*-PTVE/P coating surfaces when tested against *N.*

incerta and *E. coli*. Reduction in biofilm viability data showed that none of these coatings surfaces were capable of killing the microorganisms. However, significant biofilm retraction was observed for *C. lytica* and *E. coli* biofilm over the coatings surfaces produced from PDMS-g-PTVE/P. The maximum amount reduction in biofilm retraction was observed for PDMS-g-PTVE/P coatings containing 42% and 52% PTVE. On the other hand, coating surfaces synthesized from PDMS-g-PTVE/S were not able to reduce biofilm retention, viability, and retraction. The surfaces generated from PDMS-g-PTVE/S coatings were single phase and hydrophobic in nature. Water contact angle analysis demonstrated that the surface composition of PDMS-g-PTVE/S is very similar to that of crosslinked PDMS coatings. Due to crosslinking, the PDMS-g-PTVE/S coating surfaces were unable to provide enough concentration of the PTVE moiety at the coating/water interface which is necessary to damage the bacterial extra cellular process effectively. Thus, the results obtained from Triclosan tethered thermoplastic copolymers containing PDMS-6K provide an excellent antimicrobial activity against a Gram-positive bacterium *S. epidermidis*. Additionally, these classes of coatings are considered as environmental friendly coatings due to the absence of any leachate toxic components. *S. epidermidis* is considered as one of the major organism responsible for biomedical failure due to infection, so these coatings can be a used in implantable devices as long-term antimicrobial coatings towards *S. epidermidis*.

CHAPTER 3. SYNTHESIS AND CHARACTERIZATION OF A NOVEL INITIATOR, 1-(2-(4-ALLYL-2-METHOXYPHENOXY)ETHOXY)ETHYL ACETATE, AND ANTIMICROBIAL ACTIVITY OF POLY(DIMETHYLSILOXANE)-*b*-POLY[CHLOROETHYL VINYLETHYR)-*b*-POLY(N,N,N-ALKYLDIMETHYL-2-(VINILOXY) ETHANAMINIUM CHLORIDE] PRODUCED USING LIVING CARBOCATIONIC POLYMERIZATION, HYDROSILYLATION, AND QUATERNIZATION

3.1. ABSTRACT

A novel initiator, 1-(2-(4-allyl-2-methoxyphenoxy)ethoxy)ethyl acetate, (AMEA) containing a monoallyl-functional moiety was synthesized to use in the cationic polymerization of vinyl ethers. Using AMEA, a monoallyl-functional polymer of chloroethyl vinyl ether (PCVE) was synthesized. The attachment of allyl-functionality to one end of PCVE was successfully achieved by the dissociation of AMEA to produce an initiating species containing an allyl group and acetate as counter-ion. The narrow molecular weight distribution of the polymer (PCVE) measured using a gel permeation chromatography (GPC) indicated a relatively fast and efficient initiation process associated with the use of AMEA. The quantitative incorporation of allyl-functional moiety to PCVE was confirmed using ^1H NMR. The incorporation of allyl-functional moiety into PCVE enabled the formation of block copolymer (PDMS-*b*-PCVE) comprised of polydimethylsiloxane (PDMS) blocks using hydrosilylation with a hydride terminated PDMS (PDMS/H). The chlorine atoms of the PDMS-*b*-PCVE were replaced with a series of n-alkyldimethyl amines after varying the n-alkyl chain lengths (from 12 carbons to 18

carbons) and percentage of quaternization. The resulting copolymers containing blocks of quaternary ammonium chloride (PDMS-*b*-PCVE-*b*-PQs) were evaluated for antimicrobial activity in solution against a Gram-positive bacterium *S. aureus* and a Gram-negative bacterium *E. coli*.

3.2. INTRODUCTION

End functional polymers and macromers are of great interest due to their potential application in numerous important areas. The end functional polymers and macromers can be synthesized using living/controlled polymerization by three routes as described below: (a) initiation of polymerization with functional initiator, (b) termination of polymerization with functional terminator (end-capping), and (c) combination of the both. Essentially, the combination of approaches (a) and (b) will produce a telechelic polymer. Figures 3.1(A-F) show examples of such functional initiators used in living carbocationic polymerization of vinyl ether. These initiators are adducts of HI and vinyl ether containing a pendant functional group. The use of these initiators for the synthesis of functional polymer in the presence of a Lewis acid (I_2 or ZnI_2) is described elsewhere.^{57-62, 153-155} However, skilled and cumbersome techniques are required to handle HI and maintain low polymerization temperature (- 40 °C) to prevent side reactions. An easy-to-use initiator system consisted of an alkylaluminum halide as a co-initiator and an added base that provides living polymerization of vinyl ether even at 0 °C.⁴³ The commonly used initiators for such systems are shown in Figures 3.1(G and H). Using the initiator shown in Figure 3.1.G, no telechelic polymer can be synthesized. With the use of initiator as described in

Figure 3.1.H, the methacrylate group constitutes the counter-ion. However, a broad molecular weight distribution (PDI = 2.6 – 2.96) was observed as a result of strong nucleophilicity of the counter-ion.^{34, 156}

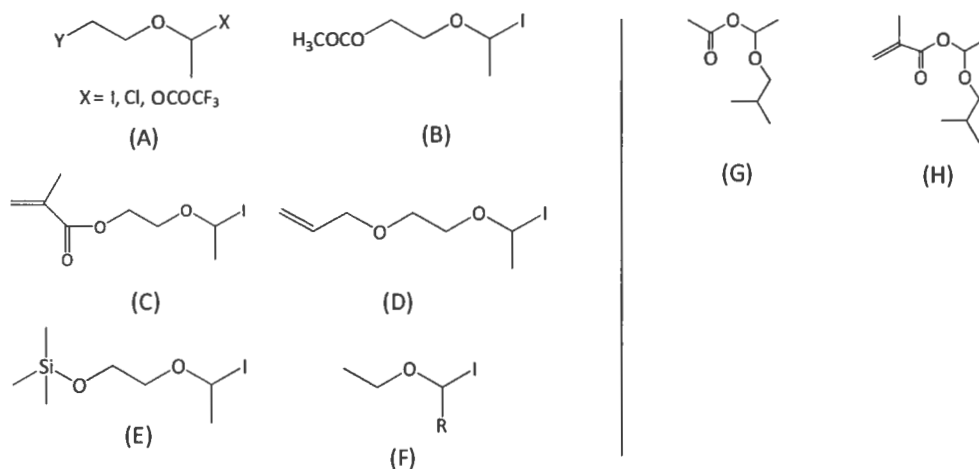


Figure 3.1. Chemical structure of initiator (A - F) used in combination with I_2 or, ZnI_2 ; and $Et_3Al_2Cl_3$ (G - H).

Thus, it is necessary to develop a novel initiator (Figure 3.2.A) containing an allyl-functional moiety that can provide fast initiation in the presence of ethyl aluminum sesquichloride to polymerize vinyl ether at relatively higher temperature. Figure 3.2.B shows the polymerization scheme with the use of the novel initiator. Monoallyl-functional random and block copolymers can be synthesized according to the scheme shown in Figure 3.3. Essentially, the use of the initiator produces a monoallyl-functional polymer that can further be used to produce copolymers with controllable block lengths (Figure 3.4). Additionally, the monoallyl-functional group of the polymer can be derivatized to enable other mechanisms of crosslinking (Figure 3.5). The monoallyl-functional polymer can be

converted to halogen and alcohol end-functional polymer according to the synthesis scheme in Figure 3.6. Trichlorosilyl end-functional polymer that enables the formation of polymer monolayer over a treated glass substrate can be synthesis by the hydrosilylation of monoallyl-functional polymer with trichlorosilane (Figure 3.7).

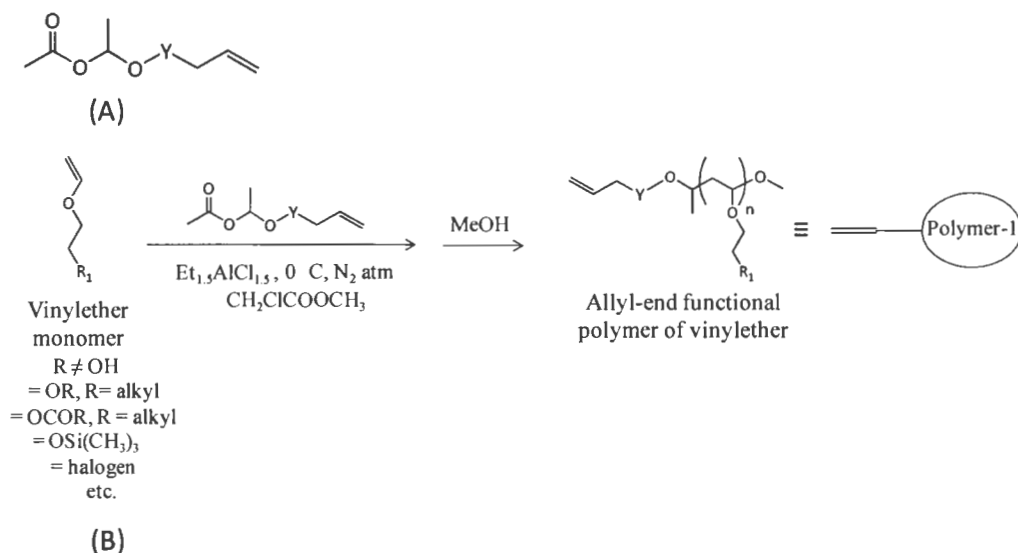


Figure 3.2. (A) Possible chemical structure of a novel initiator and (B) synthesis scheme of a monoallyl-functional polymer-1 using the initiator.

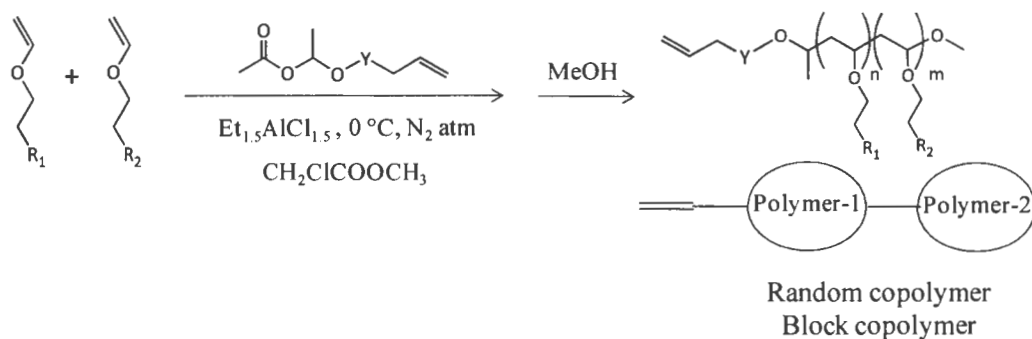


Figure 3.3. Synthesis of monoallyl-functional copolymer (random and block) using the initiator.

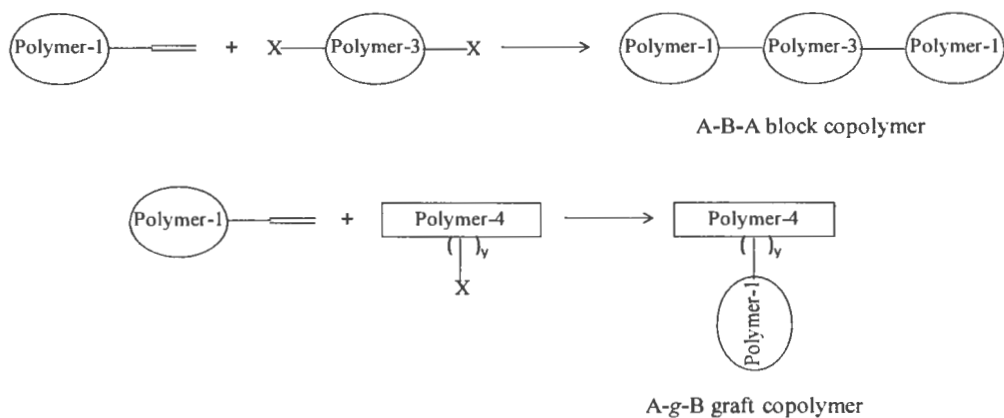


Figure 3.4. Synthesis of block and graft copolymers using the monoallyl-functional polymer-1.

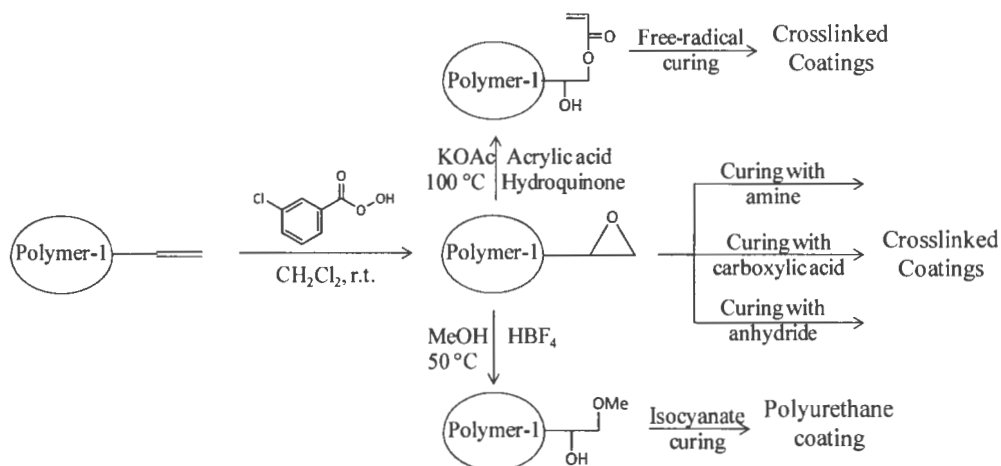


Figure 3.5. Derivatization of monoallyl-functional polymer-1 and crosslinking to produce cured coatings.

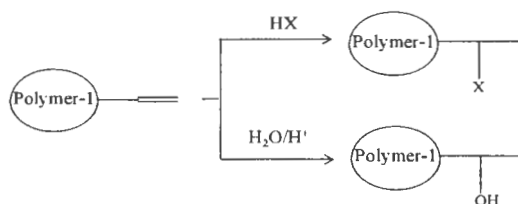


Figure 3.6. Derivatization of monoallyl-functional polymer-1 to produce functional polymers.

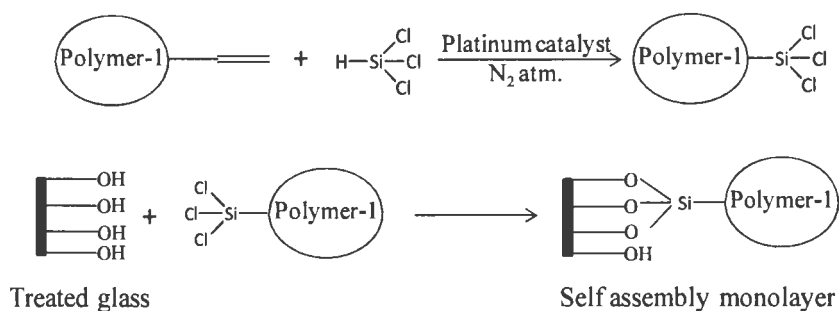


Figure 3.7. Preparation of surface monolayer of polymer-1 over a treated glass.

Quaternary ammonium compounds (QACs) have been used for more than half century as disinfectants for a variety of applications, for example, implants, biomedical devices, water cooling systems, fiber treatment, hair rinses, and wood preservation.¹⁵⁷⁻¹⁶³ It is well known that QACs provide the bioactivity by interacting with microbial cell wall that leads to cell death. The mechanism by which the QACs interact with bacterial cell wall consists of a multistep process.¹⁶⁴⁻¹⁶⁶ The first step is the absorption of the QAC to the microbial cell through electrostatic interaction between the positively charged QAC and negatively charged bacterial cell wall. After absorption onto the surface the QAC diffuses through the cell wall and disrupt the cytoplasmic membrane releasing potassium and other constituents causing the cell death. The chemical composition (charge density, amphiphilicity), molecular size, and mobility of the QACs have a strong influence over the absorption and diffusion processes onto the cell wall and hence the antimicrobial activity.¹⁶⁷⁻¹⁷⁰ Since the cell wall structure and chemical composition vary from one microorganism to another, the effectiveness of QACs vary from one microorganism to other.^{161, 171} Commercial products possessing one or two quaternary ammonium groups have been using as an antimicrobial agent. However, compounds containing multiple

quaternary groups per molecule possess much higher charge densities and thus, effectively interact with negatively charged microbial cell wall.¹⁷² Until today, much attention has been given to develop quaternary ammonium salt functional polymers which are capable of providing larger charge density. QACs containing high molecular weight and high charge densities causes extensive inter and intra molecular interactions and hence reduce diffusion through cell membranes. In order to increase the charge density of a QAC, Chen et al.¹⁷³ synthesized a poly(propylene imine) dendrimer containing 16 quaternary ammonium salt groups per molecule and found the twice much antimicrobial activity than a monofunctional counterpart. Majumdar et al.¹⁷⁴ synthesized quaternary ammonium functionalized POSS (Q-POSS) and found that Q-POSS possessing a relatively low extent of quaternization and longer n-alkyl chains provided the highest antimicrobial activity.

This document describes the synthesis and characterization of a novel initiator possessing an allyl double bond in the ester fragment of the initiator (Figure 3.8). Using this initiator, a monoallyl-functional PCVE was synthesized and characterized. To demonstrate the application of such end-functional polymer, PCVE was hydrosilylated with PDMS/H to produce a block copolymer. The chlorine groups of this block copolymer were then replaced with tertiary amines to synthesize polymers of quaternary ammonium salts and bioactivities of such polymers were evaluated.

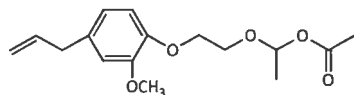


Figure 3.8. Structure of the novel initiator, 1-(2-(4-allyl-2-methoxyphenoxy)ethoxy)ethyl acetate (AMEA).

3.3. EXPERIMENTAL

3.3.1. Materials

Table 3.1 describes the starting materials used for the investigation. Unless specified otherwise, all materials were used as received.

Table 3.1. Chemicals used.

Chemical name	Description	Source
CVE	2-chloroethyl vinyl ether, 99 %	Sigma-Aldrich
NaI	Sodium iodide, $\geq 99\%$	Sigma-Aldrich
Acetone	ACS Grade, 99.5%	VWR Chemicals
Diethyl ether	ACS Grade, 99%	VWR Chemicals
KOH	Potassium hydroxide, 90 %	Sigma-Aldrich
Eugenol	2-Methoxy-4-(2-propenyl)phenol, 99%	Sigma-Aldrich
Acetic acid	Glacial, 99.7 %	EMD Chemicals
Magnesium sulfate	Anhydrous, ReagentPlus®, $\geq 99.5\%$	Sigma-Aldrich
MCAc	Methyl chloroacetate, 99%, a Lewis base used in cationic polymerization, distilled over calcium hydride	Sigma-Aldrich
$\text{Et}_{1.5}\text{AlCl}_{1.5}$	Ethylaluminum sesquichloride (25 wt. % in toluene)	Sigma-Aldrich
MeOH	Methanol, $\geq 99.8\%$	Sigma-Aldrich
CDCl_3	Deuterated chloroform	Sigma-Aldrich
DMS-H11 (PDMS/H-1.05K)	Hydride Terminated PolyDimethylsiloxanes, Molecular Weight = 1000-1100 g/mole, Equivalent Weight = 550 g/eq	Gelest
DMS-H25 (PDMS/H-17.2K)	Hydride Terminated PolyDimethylsiloxanes, Molecular Weight = 17,200 g/mole, Equivalent Weight = 8,600 g/eq	Gelest
PtO_2 (Pt Catalyst)	Pt, 81-83%	Sigma-Aldrich
Toluene	ACS grade, 99.5%	EMD Chemicals
C-12 amine	N,N-dimethyldodecylamine, $\geq 97\%$	Sigma-Aldrich
C-14 amine	N,N-dimethyltetradecylamine, $\geq 95\%$	Sigma-Aldrich
C-16 amine	N,N-dimethylhexadecylamine, $\geq 95\%$	Sigma-Aldrich
C-18 amine	N,N-dimethyloctadecylamine, $\geq 85\%$	TCI America

3.3.2. Synthesis of the initiator, 1-(2-(4-allyl-2-methoxyphenoxy)ethoxy)ethyl acetate (AMEA)

Synthesis of the initiator, AMEA consisted of the preparation of the 4-allyl-2-methoxy-1-(2-(vinylloxy)ethoxy)benzene (AMB) followed by the reaction with acetic acid at 60 °C. Synthesis of AMB consisted of the preparation of 2-iodoethyl vinyl ether followed by the reaction with Eugenol in the presence of potassium hydroxide in methanol.

3.3.2.1. Synthesis of 2-iodoethyl vinyl ether

2-iodoethyl vinyl ether was synthesized using the synthetic scheme shown in Figure 3.9. A detailed procedure is as follows: 100.65 g of 2-chloroethyl vinyl ether, 200.16 g of sodium iodide and 730 g of acetone were combined in a 2-liter, 3-neck round bottom flask and heated at a temperature of 60 °C for 72 hours. Next, the reaction mixture was cooled to room temperature and diluted with 600 ml of diethyl ether. The organic layer was washed thrice with deionized water and dried with anhydrous magnesium sulfate. The product was recovered by rotary evaporation of diethyl ether and excess 2-chloroethyl vinyl ether at a temperature of 50 °C and a pressure of 60 mmHg for 1 hour. Proton NMR was used to confirm the production of 2-iodoethyl vinyl ether: ^1H NMR (CDCl_3) δ 6.44 ppm (q, 1H, $\text{OCH}=\text{C}$), 4.19, 4.05 ppm (dd, 2H, $\text{CH}_2=\text{C}$), 3.95 ppm (t, 2H, OCH_2), 3.3 ppm (t, 2H, CH_2I).

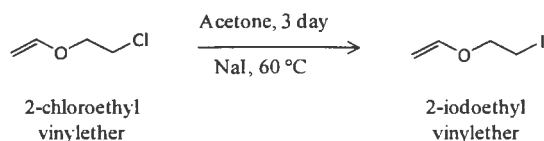


Figure 3.9. The synthetic scheme used to produce 2-iodoethyl vinyl ether.

3.3.2.2. Synthesis of 4-allyl-2-methoxy-1-(2-(vinylloxy)ethoxy)benzene (AMB)

AMB was synthesized using the synthetic scheme shown in Figure 3.10. A detailed procedure is as follows: 146.9 g of 2-iodoethyl vinyl ether, 87.4 g of Eugenol, 42.7 g of potassium hydroxide, and 500 ml of methanol were combined in a 1000 ml, round bottom flask fitted with a reflux condenser and stirred at a temperature of 62 °C. After 40 hours of reaction, the reaction mixture was cooled to room temperature and diluted with diethyl ether. The organic layer was washed with deionized water thrice and dried with anhydrous magnesium sulfate. The crude product was collected after rotary evaporation of all volatiles at 30 °C for 3 hours. The product, AMB was crystallized from methanol at a temperature of – 30 °C and dried under vacuum overnight. Proton NMR was used to confirm the production of AMB: ^1H NMR (CDCl_3) δ 6.5 ppm (q, 1H, $\text{OCH}=\text{C}$), 4.22 ppm – 4.25 ppm (m, 2H, $\text{CH}_2=\text{C}-\text{O}$), 4.0 ppm – 4.2 ppm (m, 4H, CH_2-CH_2), 3.3 ppm (d, 2H, $\text{C}=\text{C}-\text{CH}_2$), 5.9 ppm (m, 1H, $\text{C}=\text{CH}-\text{C}$), 5.1 (m, 2H, $\text{CH}_2=\text{C}-\text{C}$), 3.8 ppm (s, 3H, CH_3), 6.7 ppm, 6.9 ppm (m, 3H, Ar-H).

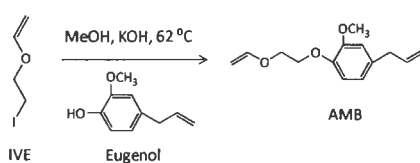


Figure 3.10. The synthetic scheme used to produce AMB.

3.3.2.3. Synthesis of the initiator, 1-(2-(4-allyl-2-methoxyphenoxy)ethoxy)ethyl acetate (AMEA)

AMEA was synthesized using the synthetic scheme shown in Figure 3.11. A detailed procedure is as follows: 39.3 g of AMB and 12.2 g of glacial acetic acid were

combined in a 250 ml, round bottom flask fitted with a reflux condenser and stirred at a temperature of 60 °C for 18 hours. The reaction mixture was cooled to room temperature and diluted with diethyl ether. The organic layer was washed with deionized water and dried with anhydrous magnesium sulfate. The crude product was recovered after rotary evaporation of diethyl ether under a reduced pressure at 30 °C. The product initiator (AMEA) was separated from the unreacted AMB by passing the crude product through a column packed with silica gel possessing a pore size of 60 Å. The mobile phase was selected as a combination of ethyl acetate and n-hexane (10:90 vol/vol). The pure initiator was collected after rotary evaporation of all volatiles and dried with anhydrous magnesium sulfate before use. Proton NMR, carbon NMR and FTIR were used to confirm the production of AMEA: ¹H NMR (CDCl₃) δ 5.9 ppm (m, 2H, O-CH₂-O, C=CH-C), 1.3 ppm (d, 3H, H₃C-C-O), 4.03 ppm (t, 2H, CH₂-CH₂), 3.8 ppm (m, 2H, CH₂-CH₂), 3.3 ppm (d, 2H, C=C-CH₂), 3.7 ppm (s, 3H, H₃C-O), 6.7 ppm, 6.9 ppm (m, 3H, Ar-H), 1.9 ppm (s, 3H, CH₃-C=O).

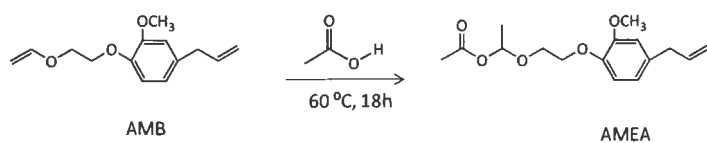


Figure 3.11. The synthetic scheme used to produce AMEA.

3.3.3. Synthesis of the monoallyl-functional PCVE using the AMEA initiator

The synthesis of monoallyl-functional PCVE was shown in Figure 3.12. A living carbocationic polymerization technique was employed to polymerize the chloroethyl vinyl ether (CVE). The CVE and toluene were distilled over calcium hydride before use.

3.3.3.1. Polymerization kinetic study using gravimetric analysis

The polymerization kinetic study was conducted by the procedure as follows: Polymerizations were carried out in a series of dry test tubes partially immersed into a heptane bath at 0 °C inside a glove box. In each test tube, 30.4 mg of AMEA, 2.2 g of CVE ([CVE]₀:[AMEA]₀ = 200:1), and 2.8 g of MCAc ([CVE]₀:[MCAc]₀ = 200:250) were dissolved in 6.36 g of dry toluene and chilled to 0 °C. Each polymerization was initiated by the addition of 256 mg of supplied ethylaluminum sesquichloride solution ([CVE]₀:[Et_{1.5}AlCl_{1.5}]₀ = 200:5). Each reaction was terminated after predetermined interval times by the addition of 15 ml of chilled methanol which caused the polymer to precipitate. The polymer was isolated and washed multiple times with methanol using centrifugation. The purified polymer was collected as a viscous liquid after centrifugation at 4500 rpm at a temperature of 21 °C for 10 minutes and drying under vacuum overnight. The percentage of conversion of each polymer was calculated gravimetrically and the number average molecular weight was measured using a gel permeation chromatography.

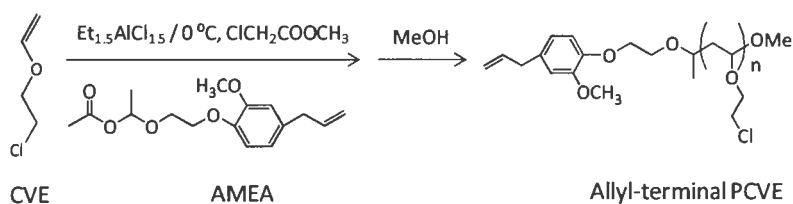


Figure 3.12. The synthetic scheme used to produce PCVE.

3.3.3.2. Synthesis of PCVE possessing a theoretical degree of polymerization of 50

53.35 g of CVE, 2.95 g of AMEA, 65.8 ml of MCAc ([CVE]₀:[AMEA]₀:[MCAc]₀ = 50:1:75) were dissolved in 154 g of dry toluene and taken in a 500 ml round bottom

flask. The solution was cooled to 0 °C and the reaction was started by the addition of 9.9 g of supplied ethylaluminum sesquichloride solution ($[\text{CVE}]_0:[\text{Et}_{1.5}\text{AlCl}_{1.5}]_0 = 50:2$). After 32 minutes of reaction the reaction mixture was terminated by the addition of 350 ml of chilled methanol which caused the polymer to precipitate. The polymer was isolated and washed multiple times with methanol using centrifugation. The purified polymer was collected as a viscous liquid after centrifugation at 4500 rpm at a temperature of 21 °C for 10 minutes and drying under vacuum overnight. The percentage of conversion was calculated gravimetrically and the number average molecular weight was measured using gel permeation chromatography.

3.3.4. Synthesis of the block copolymer of PCVE and PDMS (PDMS-*b*-PCVE)

The synthesis procedure of PDMS-*b*-PCVE is consisted of the hydrosilylation between monoallyl-functional PCVE and PDMS/H in the presence of a platinum catalyst under nitrogen atmosphere. Figure 3.13 demonstrates the synthesis of PDMS-*b*-PCVE. A detailed procedure is as follows: PCVE and PDMS/H were combined together in a dry one liter round bottom flask inside a glove box according to the formulation in Table 3.2. Polymers were dissolved by the addition of toluene and the final concentration of the reaction mixture was maintained as 16 weight percent solid. The reaction was started by the addition of 270 mg of platinum oxide and heating at a temperature of 90 °C. The completion of hydrosilylation was monitored using proton NMR and FTIR spectra. The reaction was continued for 4 days until the Si-H protons at 4.7 ppm and allyl protons at 5.1 ppm were totally disappeared in a proton NMR spectrum of PDMS-*b*-PCVE. The reaction

was then cooled to room temperature and the platinum oxide was vacuum filtered through a silica bed. The PDMS-*b*-PCVE was precipitated into methanol and dried under vacuum overnight.

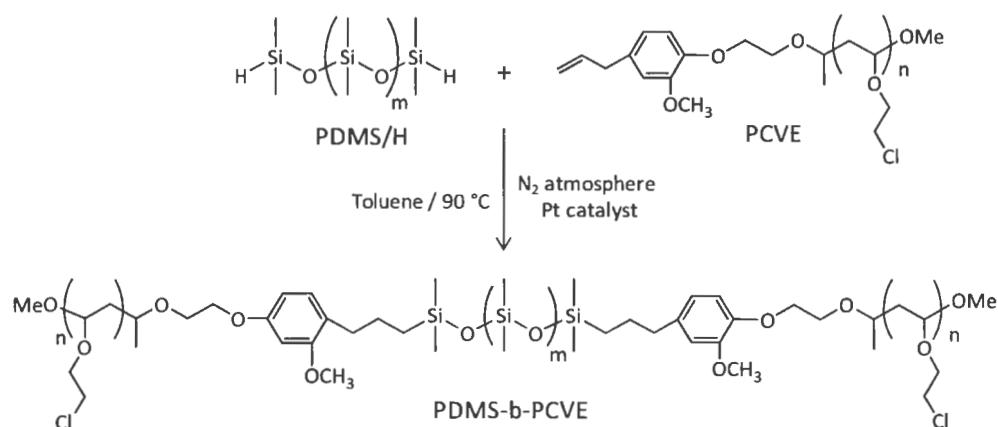


Figure 3.13. The synthetic scheme used to produce PDMS-*b*-PCVE.

Table 3.2. Formulation table for the synthesis of PDMS-*b*-PCVE.

PDMS- <i>b</i> -PCVE	Wt of PCVE, (g)	Wt. of PDMS/H-1.05K (DMS-H11), (g)	Wt. of PDMS/H-17.2K (DMS-H25), (g)	Ratio of PCVE:PDMS (Wt. %)
PDMS-1.05K	40	4.17	--	90.6 : 9.4
PDMS-17.2K	40	--	65.22	38 : 62

3.3.5. Synthesis of the quaternized block copolymer of PCVE and PDMS (PDMS-*b*-PCVE-*b*-PQ)

The synthesis of the PDMS-*b*-PCVE-*b*-PQ consisted of the quaternization of PDMS-*b*-PCVE in the presence of a *n*-alkyldimethyl amine at a temperature of 100 °C for 8 days (Figure 3.14). The detailed procedure is as follows: PDMS-*b*-PCVE and a tertiary

amine were combined in a 40 ml vial and dissolved with toluene at a concentration of 5 weight percent solid. A series of such solutions was produced by varying the n-alkyl chain lengths and concentration of tertiary amine. Four different tertiary amines, for example, N,N-dimethyldodecylamine (C-12), N,N-dimethyltetradecylamine (C-14), N,N-dimethylhexadecylamine (C-16), and N,N-dimethyloctadecylamine (C-18) were used. For each amine, three different concentrations were used to replace the chlorine by 10 mole %, 30 mole %, and 50 mole %. Thus, a total 12 polymer solutions were produced from each PDMS-*b*-PCVE. The detailed formulation is described in Tables 3.3 and 3.4.

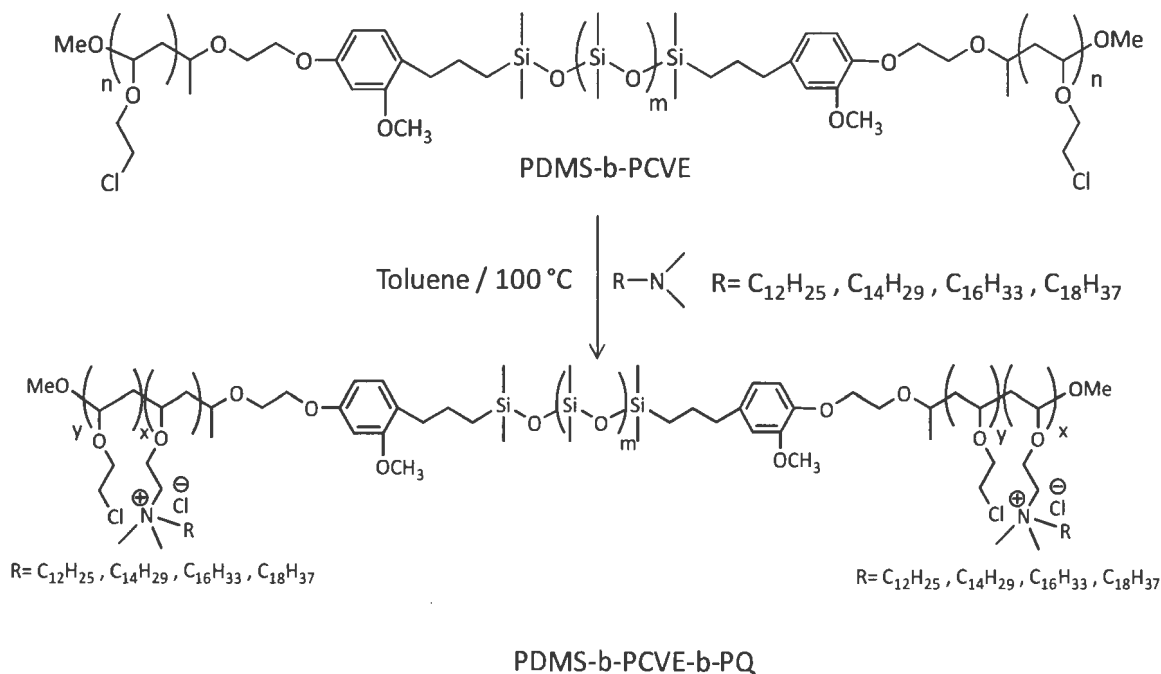


Figure 3.14. The synthetic scheme used to produce PDMS-*b*-PCVE-*b*-PQ.

Table 3.3. Formulation table for the quaternization of PDMS-*b*-PCVE synthesized from PDMS/H-1.05K.

PDMS- <i>b</i> -PCVE- <i>b</i> -PQ	Wt. of PDMS-1.05K (g)	Wt. of C-12 amine (g)	Wt. of C-14 amine (g)	Wt. of C-16 amine (g)	Wt. of C-18 amine (g)
PDMS-1.05K-C12-10%	1.5	0.281	--	--	--
PDMS-1.05K-C12-30%	1.5	0.842	--	--	--
PDMS-1.05K-C12-50%	1.5	1.403	--	--	--
PDMS-1.05K-C14-10%	1.5	--	0.324	--	--
PDMS-1.05K-C14-30%	1.5	--	0.973	--	--
PDMS-1.05K-C14-50%	1.5	--	1.621	--	--
PDMS-1.05K-C16-10%	1.5	--	--	0.362	--
PDMS-1.05K-C16-30%	1.5	--	--	1.086	--
PDMS-1.05K-C16-50%	1.5	--	--	1.809	--
PDMS-1.05K-C18-10%	1.5	--	--	--	0.447
PDMS-1.05K-C18-30%	1.5	--	--	--	1.34
PDMS-1.05K-C18-50%	1.5	--	--	--	2.23

Table 3.4. Formulation table for the quaternization of PDMS-*b*-PCVE synthesized from PDMS/H-17.2K.

PDMS- <i>b</i> -PCVE- <i>b</i> -PQ	Wt. of PDMS-17.2K (g)	Wt. of C-12 (g)	Wt. of C-14 (g)	Wt. of C-16 (g)	Wt. of C-18 (g)
PDMS-17.2K-C12-10%	1.5	0.119	--	--	--
PDMS-17.2K-C12-30%	1.5	0.357	--	--	--
PDMS-17.2K-C12-50%	1.5	0.596	--	--	--
PDMS-17.2K-C14-10%	1.5	--	0.138	--	--
PDMS-17.2K-C14-30%	1.5	--	0.413	--	--
PDMS-17.2K-C14-50%	1.5	--	0.688	--	--
PDMS-17.2K-C16-10%	1.5	--	--	0.154	--
PDMS-17.2K-C16-30%	1.5	--	--	0.461	--
PDMS-17.2K-C16-50%	1.5	--	--	0.768	--
PDMS-17.2K-C18-10%	1.5	--	--	--	0.189
PDMS-17.2K-C18-30%	1.5	--	--	--	0.568
PDMS-17.2K-C18-50%	1.5	--	--	--	0.947

3.3.6. Instrumentation and measurements

An MBraun glove box system equipped with a cold well and a chiller from FTSTM Systems was used for the cationic polymerization of TVE. Normal heptane was used as cooling medium.

3.3.6.1. Gel Permeation Chromatography (GPC)

A high-throughput Symyx Rapid GPC equipped with an evaporative light scattering detector (PL-ELS 1000) and 2xPLgel Mixed-B columns of 10 μm particle size was used to determine the molecular weight and molecular weight distribution of polymer. Polymer solutions of 3 mg/ml were prepared in THF and the temperature of the column was maintained at 45 $^{\circ}\text{C}$. Molecular weight data was reported relative to polystyrene standards.

3.3.6.2. Nuclear Magnetic Resonance (NMR) spectroscopy

^1H NMR and ^{13}C NMR measurements were carried out with a JEOL-ECA 400 (400MHz) NMR spectrometer equipped with an autosampler. CDCl_3 was used as the lock solvent. Data acquisition was completed using 16 scans for proton NMR and 1000 scans for carbon NMR at a temperature of 23 $^{\circ}\text{C}$. A Delta software was used to process the data. Heteronuclear Chemical Shift Correlation (HETCOR) and Distortionless Enhancement by Polarization Transfer (DEPT) experiments were used to assign the ^{13}C NMR peaks.

3.3.6.3. Fourier Transform Infrared (FTIR) spectroscopy

A Nicolet Manga-850 FTIR instrument was employed to measure FTIR spectra. Samples were coated on dry potassium bromide disc, and the measurements were carried out in the range of wavelengths from 600 cm^{-1} to 3900 cm^{-1} using 64 scans with a data spacing of 0.964 cm^{-1} .

3.3.6.4. Differential Scanning Calorimetry (DSC)

A DSC Q1000 from TA Instruments equipped with an autosampler accessory was used to determine the glass transition temperature (T_g) of polymers. All polymers were first heated from 30 °C to 50 °C at a heating rate of 10 °C/minute (1st heat), cooled from 50 °C to -140 °C at a cooling rate of 10 °C/minute (cooling), and reheated from -140 °C to 70 °C at a heating rate 10 °C/minute (2nd heat). The T_g reported was obtained from the 2nd heat.

3.3.6.5. Thermogravimetric Analysis (TGA)

TGA was carried out using a Q500 from TA Instruments. Samples sizes were 10 mg to 15 mg. In a ramp heating mode samples were heated from 30 °C to 800 °C at a heating rates of 20 °C/minute in air.

3.3.7. Antimicrobial activity of PDMS-*b*-PCVE-*b*-PQs (polyquats)

The PDMS-*b*-PCVE-*b*-PQs synthesized from PDMS-17.2K and PDMS-1.05K were dissolved at a concentration of 2% (w/v) solution in DMSO and isopropanol, respectively. The antimicrobial activities of the PDMS-*b*-PCVE-*b*-PQs in solution were determined by the procedure as described previously.¹⁷⁴⁻¹⁷⁷ The detailed description is as follows: Stocks of *S. aureus* ATCC 25923 and *E. coli* ATCC 12435 were maintained weekly at a temperature of 4 °C on TSB and LBA respectively. Broth culture of *S. aureus* and *E. coli* were prepared by inoculating one colony into 10 ml of broth and incubating at a temperature of 37 °C with shaking. Overnight culture were pelleted by using centrifugation at 4500 rpm for 10 minutes, washed twice in 0.9% NaCl solution, and resuspended to a 0.5 McFarland turbidity standard ($\sim 10^8$ cells ml⁻¹). 100 microliters of 2% (w/v) solution of

PDMS-*b*-PCVE-*b*-PQs in either DMSO or isopropanol was added to 1 ml of bacterial suspension previously dispensed into a sterile 24-well plate polystyrene plate. The plates were then placed on a orbital shaker and allowed to incubate for 15 minutes at room temperature. 0.1 ml of each PDMS-*b*-PCVE-*b*-PQ/bacterial suspension was immediately transferred to 0.9 ml of Dey/Engley (D/E) neutralization medium in a 1.5 ml centrifuge tube, and serially diluted (1:10) in D/E medium. Then 0.2 ml of each dilution was transferred in triplicate to a 96-well plate and incubated statically at a temperature of 37 °C. After 24 hours of incubation, the plated were removed from the incubator and photographed with a digital camera to quantify the bacterial growth in solution. Bacterial log reduction was reported as the average of three replicate samples. The bacterial suspension in 0.9 wt % NaCl (without PDMS-*b*-PCVE-*b*-PQ) served as the positive growth control, while the blank D/E medium served as a negative growth control. DMSO and isopropanol were also evaluated for antimicrobial activity as these were used to solubilize the PDMS-*b*-PCVE-*b*-PQs.

D/E neutralization medium contains a pH indicator, bromo cressol purple that is converted to yellow color as a consequence of bacterial growth (i.e., utilization of dextrose). This allows for the rapid determination of bacterial log reduction by visual evaluation of growth. D/E neutralization medium was employed in this study to inactivate the antimicrobial activity of PDMS-*b*-PCVE-*b*-PQs solution after the 15 minutes of exposure to the bacterial suspensions.¹⁷⁷ D/E neutralization medium is generally used to neutralize a variety of disinfectant chemicals and antiseptics including iodine, chlorine

compounds, phenolics, quaternary ammonium compounds, glutaraldehydes, and formaldehydes.¹⁷⁵

3.4. RESULTS AND DISCUSSION

3.4.1. Characterization of AMB and AMEA

The successful synthesis of AMB was demonstrated using proton NMR. As shown in Figure 3.15, one methine and two methylene protons in the vinyl ether double bond appeared at 6.5, 4.22, and 4.2 ppm, respectively. Successful synthesis of AMEA initiator was confirmed by ¹H NMR, ¹³C NMR, DEPT-135, HETCOR, and FTIR (Figures 3.16 – 3.19). As shown in Figure 3.16, the successful synthesis of AMEA was demonstrated by integrating and comparing the peak areas associated with the 3 protons of methyl group in acetic acid fragment at 1.9 ppm to the 3 protons of methoxy group in Eugenol fragment at 3.7 ppm. The protons in the allyl unsaturation were at 4.9 ppm and 5.8 ppm.

The Distortionless Enhancement by Polarization Transfer (DEPT) method is useful for determining the number of hydrogen atoms attached to a given carbon atom. In a DEPT-135 spectrum, methyl and methine carbons appeared as positive peaks, while the methylene carbons appear as negative peaks. As shown in Figure 3.17, the methylene carbon (number 16) and methine carbon (number 15) in the allyl double bond can be seen as a negative peak at 115.3 ppm and as a positive peak at 137 ppm, respectively. All methine carbons in aromatic ring at the position numbers of 9, 10, and 12 produced positive peaks at 114.3, 120.5, and 112.4 ppm, respectively. Three methyl carbons at the position numbers of 3, 1, and 7 came out as positive peaks at 20.5, 20.7 and 55.8 ppm,

respectively. Two methylene protons in the ethyl spacer in between acetate and aromatic ring produced negative peaks at 67 and 68 ppm. Four quaternary carbons at position numbers of 2, 8, 11, and 13 did not appear in DEPT-135 spectrum.

The positions of protons in AMEA were assigned using a HETCOR experiment (Figure 3.18). One carbon at 137 ppm and one proton at 5.9 ppm correspond to methine group (15); one carbon at 115.3 ppm and two protons multiplet at 5.0 ppm correspond to methylene group (16); one carbon at 20.7 ppm and three protons singlet at 1.9 ppm correspond to methyl group (1); one carbon at 20.5 ppm and three protons doublet at 1.3 ppm correspond to methyl group (3), one carbon at 114.3 ppm and one proton at 6.7 ppm correspond to aromatic methine group (9), and two carbons at 120.5 ppm, 112.4 ppm and two protons at 6.6 ppm correspond to two aromatic methine group (10, 12). FTIR spectrum of AMEA (Figure 3.19) confirmed the presence of vinyl ether double bond between 1620 cm^{-1} and 1645 cm^{-1} with a peak maximum at 1635 cm^{-1} .

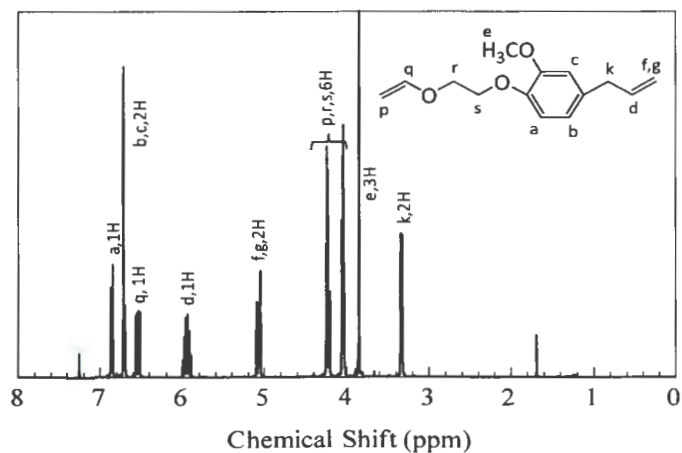


Figure 3.15. ^1H NMR spectrum obtained for AMB.

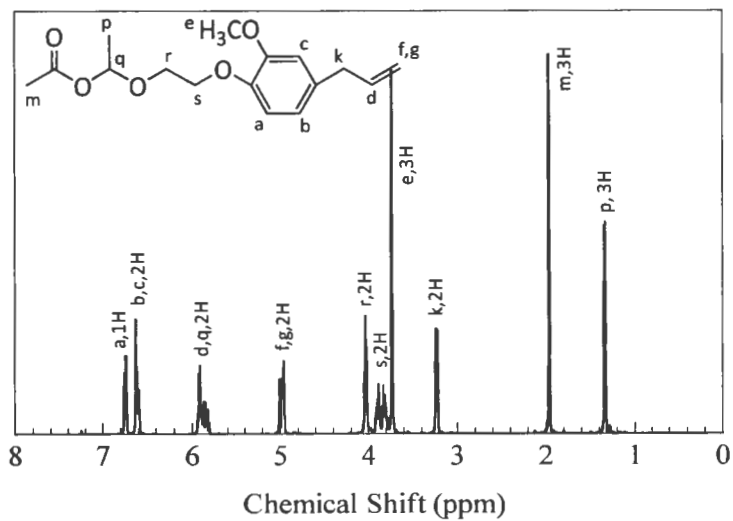


Figure 3.16. ¹H NMR spectrum obtained for AMEA.

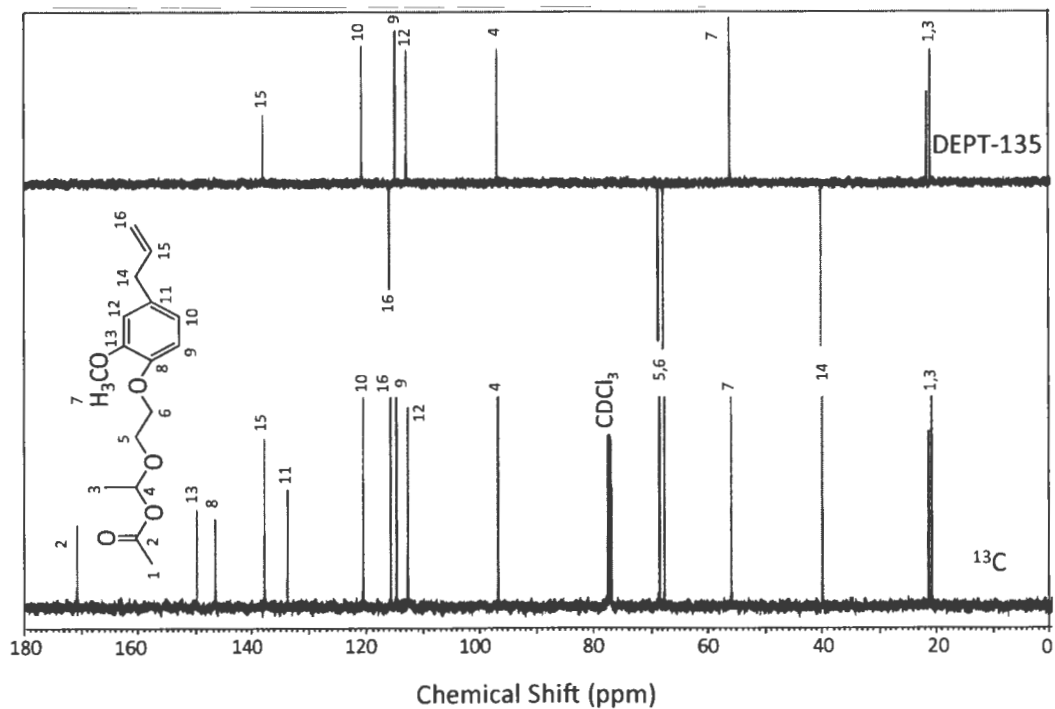


Figure 3.17. DEPT-135 and ¹³C NMR spectra obtained for AMEA.

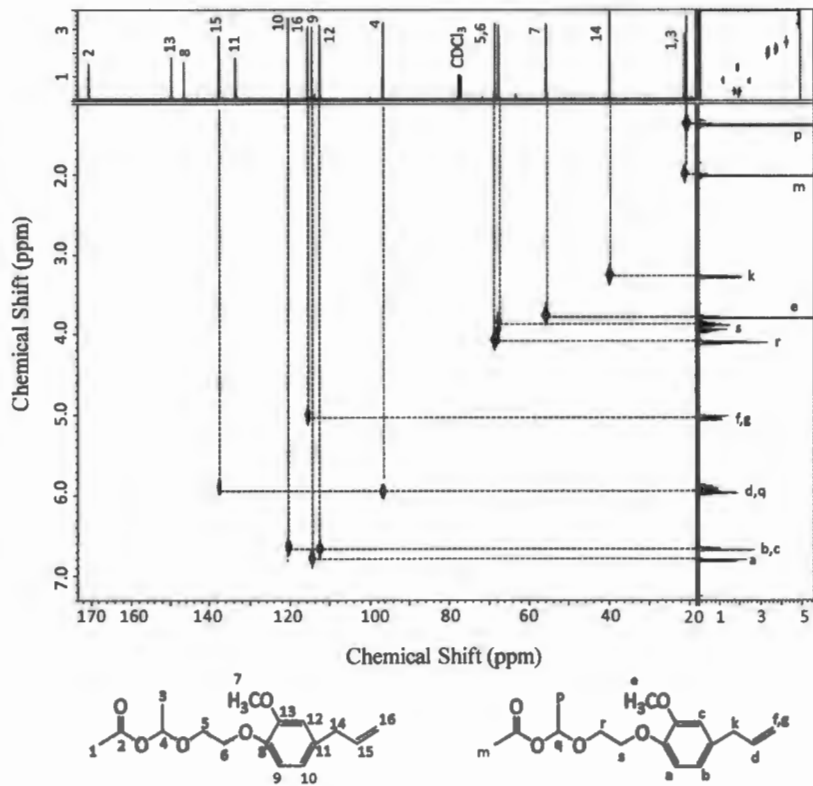


Figure 3.18. HETCOR spectrum obtained for AMEA.

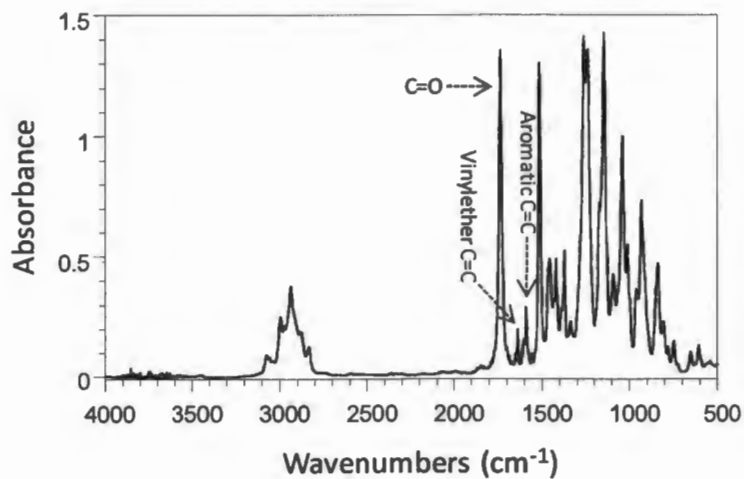


Figure 3.19. FTIR spectrum obtained for AMEA.

3.4.2. Polymerization using the AMEA/ $\text{Et}_{1.5}\text{AlCl}_{1.5}$ initiating system

The proposed mechanism for the initiation process of a vinyl ether polymerization in the presence of AMEA/ $\text{Et}_{1.5}\text{AlCl}_{1.5}$ can be described in Figures 3.20 and 3.21. As shown in Figure 3.20, the carbocation generated after the dissociation of AMEA in the initiation process is highly reactive. An added base possessing an ester group delocalizes the carbocation via resonance stabilization (Figure 3.21) and provides added stability to the propagating species.³⁶ Example of such ester functional bases are: (1) methyl chloroacetate, $\text{H}_2\text{C}(\text{Cl})\text{COOCH}_3$, (2) ethyl acetate, $\text{H}_3\text{CCOOC}_2\text{H}_5$, and (3) methyl dichloroacetate $\text{HC}(\text{Cl})_2\text{COOCH}_3$. The order of basicity depends on the electronegativity of the functional group(s) attached to the alpha-carbon to carbonyl carbon. The order of basicity for the above mentioned bases are:

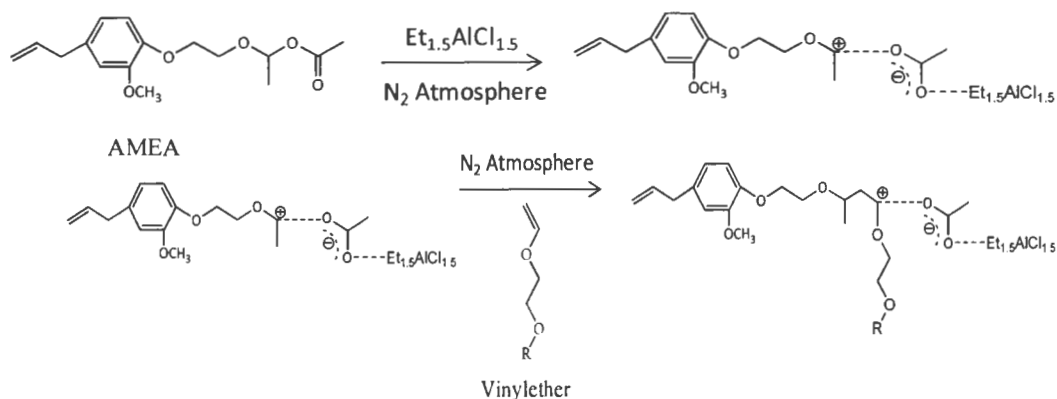
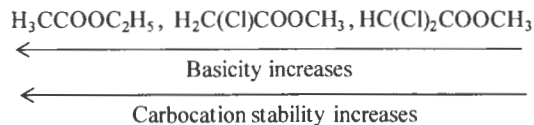


Figure 3.20. Mechanism of initiation process of vinyl ether polymerization in the presence of a AMEA/ $\text{Et}_{1.5}\text{AlCl}_{1.5}$ initiating system.

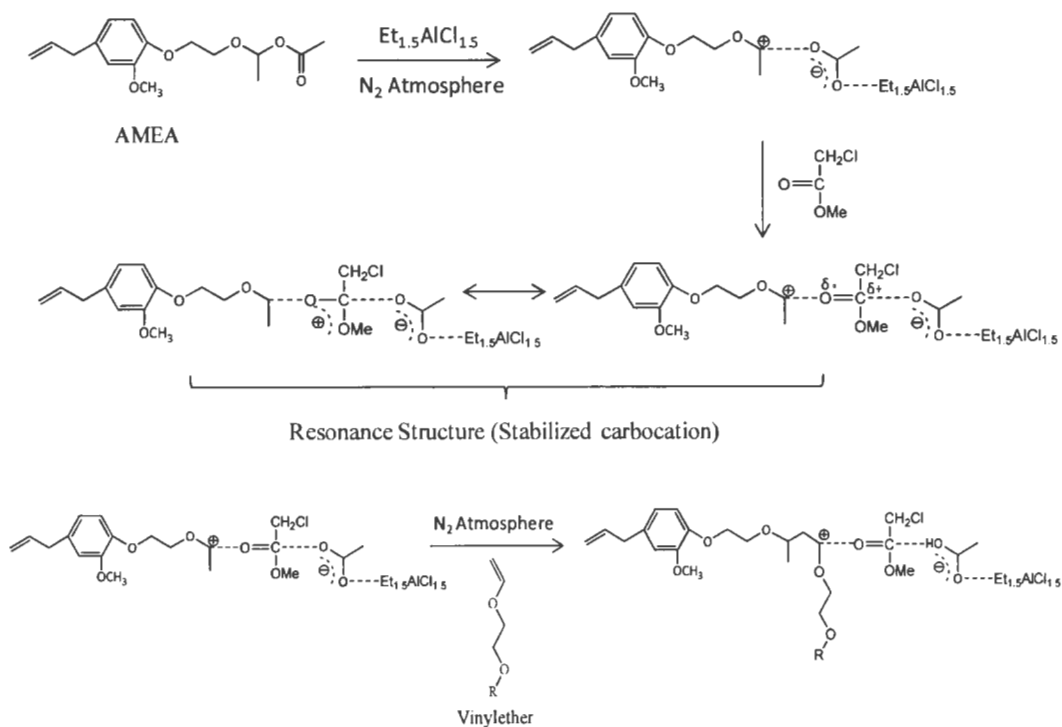


Figure 3.21. Mechanism of initiation process of vinyl ether polymerization in the presence of AMEA/ $\text{Et}_{1.5}\text{AlCl}_{1.5}$ initiating system and an added base, for example, MCAC.

The utility of the AMEA as a novel initiator in a living carbocationic polymerization was demonstrated by the polymerization of CVE. The living nature of CVE polymerization initiated by AMEA/ $\text{Et}_{1.5}\text{AlCl}_{1.5}$ in the presence of MCAC was demonstrated by plotting the GPC number average molecular weight (M_n) as a function of CVE conversion. The linearity of GPC M_n with monomer conversion, shown in Figure 3.22.A, indicated the obtainment of a living polymerization in the presence of MCAC. Though the relationship between the GPC M_n and percent of conversion is linear, it is somewhat surprising that the straight line did not pass through the origin (0,0). The possible reason could be the way of molecular weight measurement. The GPC, fitted with an evaporative

light scattering detector determines the weight average molecular weight with respect to polystyrene as an internal standard. Thus, the number average molecular weight molecular weight obtained from the instrument is relative to the molecular weight of polystyrene. The molecular weight distribution was determined as less than 1.2 which indicated the obtainment of living polymerization as well as relatively fast and efficient initiation process when AMEA was used to initiate the polymerization. From the percentage of conversion value, $\ln([M]_0/[M]_t)$ was plotted as a function of polymerization time. The linear relation between $\ln([M]_0/[M]_t)$ and reaction time demonstrated the first order nature of the polymerization (Figure 22.B) with a rate constant value of 0.23 min^{-1} .

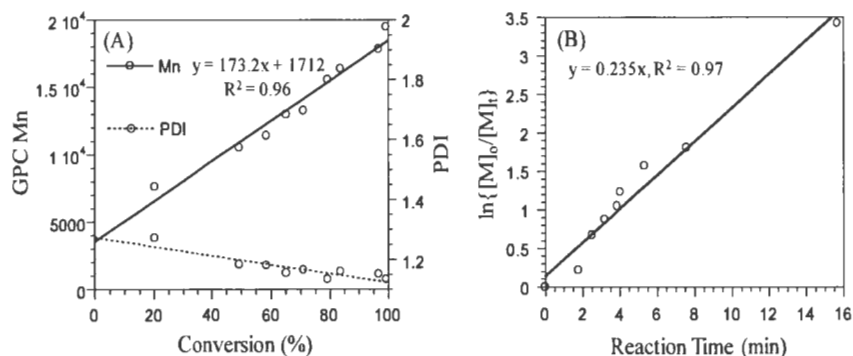


Figure 3.22. Plot of (A) GPC number average molecular weight as a function of % of conversion and (B) $\ln\{[M]_0/[M]_t\}$ as a function of polymerization time for CVE initiated by AMEA/ $\text{Et}_{1.5}\text{AlCl}_{1.5}$ in the presence of MCAc as an added base. $[\text{CVE}]_0:[\text{AMEA}]_0:[\text{MCAc}]_0:[\text{Et}_{1.5}\text{AlCl}_{1.5}]_0 = 200:1:250:5$.

3.4.2.1. Characterization of monoallyl-functional PCVE

The successful synthesis of monoallyl-functional PCVE was characterized using proton NMR. Figure 3.23 shows the proton NMR spectrum of PCVE possessing a

theoretical degree of polymerization of 50. As shown in Figure 3.23, the three aromatic protons from the initiator fragment at the position numbers of a, b, c were at 6.8 ppm, 6.63, and 6.65 ppm, respectively. The two methylene and one methine protons in the monoallyl-functional group appeared at 5.0 ppm and 5.9 ppm respectively. The degree of polymerization (DP) calculated after integrating and comparing the peak areas under the proton absorption in the backbone methylene groups of repeating unit at 1.4 – 1.8 ppm to the proton absorption in the one aromatic methine proton (a) of initiator fragment at 6.8 ppm was 55. The percentage of conversion calculated using gravimetric analysis was 99%.

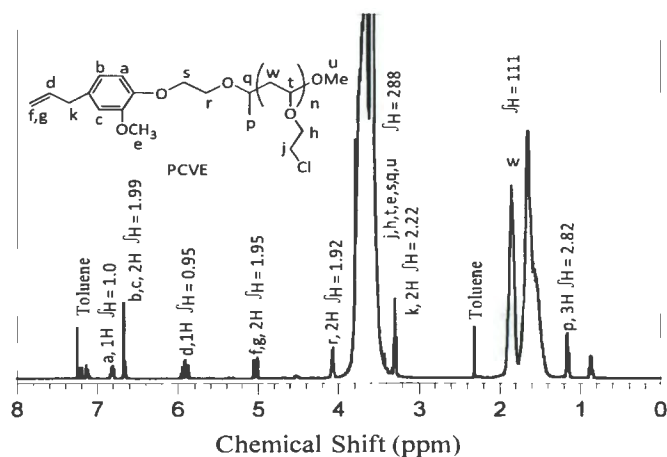


Figure 3.23. ^1H NMR spectrum obtained for monoallyl-functional PCVE.

The DP calculated from the initial concentration of monomer and initiator combined with gravimetric analysis was 49. The close match of DP values obtained from both the gravimetric analysis and the NMR experiment suggested a fast initiation process. The theoretical molecular weight of PCVE calculated using the percentage of conversion from gravimetric analysis was 5487 g/mole. The GPC number average molecular weight of

PTVE was determined as 8153 g/mole with a polydispersity index of 1.2. The difference in the molecular weight calculated using gravimetric analysis and GPC can be explained by the fact that the GPC molecular weight is determined with respect to a polystyrene internal standard.

3.4.3. Synthesis and characterization of PDMS-*b*-PCVE

3.4.3.1. Synthesis of PDMS-*b*-PCVE

The synthesis of monoallyl-functional polymer has tremendous potential in various application areas as shown in Figures 3.4 – 3.7 in the *Introduction*. The monoallyl-functional polymer can be used to synthesize various block and graft copolymers. This document describes the synthesis and characterization of a block copolymer, PDMS-*b*-PCVE, by utilizing the monoallyl-end functionality in PCVE. The synthesis of PDMS-*b*-PCVE consisted of the hydrosilylation of monoallyl-functional PCVE and PDMS/H (Figure 3.13) in the presence of a platinum catalyst. The successful synthesis of block copolymer was confirmed by the complete disappearance of methylene protons of terminal allyl-group in PCVE (δ 5.9 ppm and δ 5.0 ppm) and the generation of two new peaks corresponding to methylene protons attached to the α (f,g) and γ (k) position to silicon atom at 0.45 ppm and 2.5 ppm respectively (Figure 3.24). Additionally, the complete disappearance of hydride (Si-H) peak at δ 4.7 ppm in ^1H NMR spectrum confirmed that the PDMS/H was totally consumed by the hydrosilylation. The absence of a trace amount of hydride in PDMS-*b*-PCVE copolymer was confirmed by the complete disappearance of the Si-H absorption peak at 2145 cm^{-1} in a FTIR spectrum (Figure 3.25). The GPC analysis of

PCVE, PDMS/Hs and PDMS-*b*-PCVEs was carried out and shown in Figure 3.26. As shown in the chromatogram, the copolymer had a mono-modal molecular weight distribution which is a characteristic of block copolymer. Table 3.5 shows the comparison between the theoretical molecular weight and GPC number average molecular weight (polystyrene as internal standard). The low molecular weight distribution and close match between the theoretical and experimental molecular weight demonstrate the successful synthesis of PDMS-*b*-PCVEs.

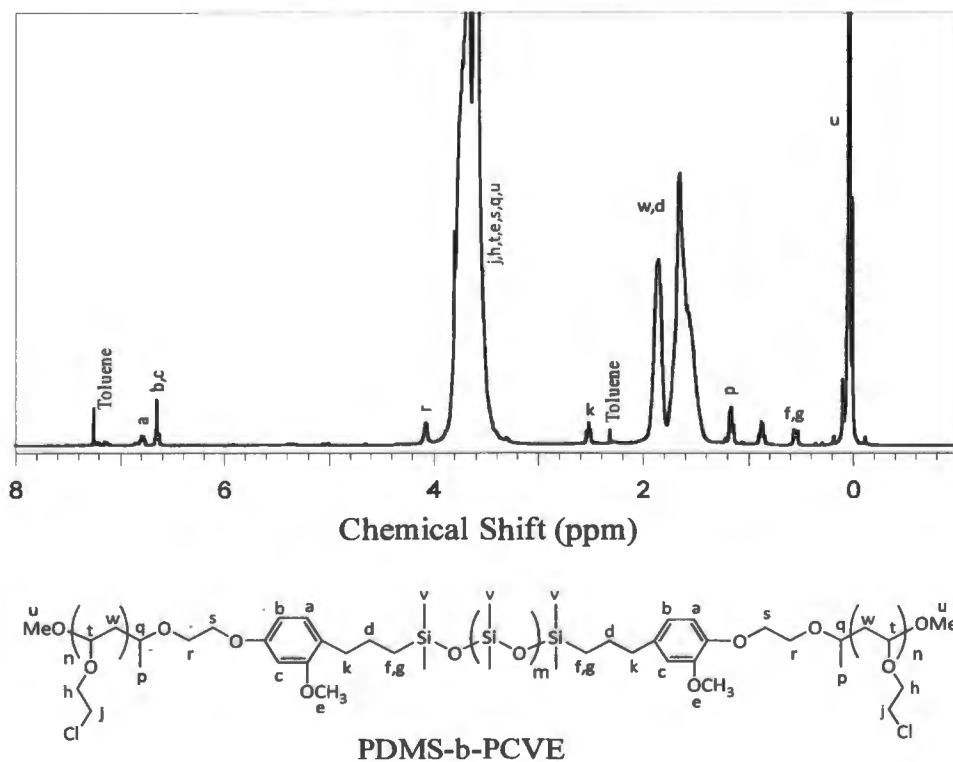


Figure 3.24. ^1H NMR spectrum obtained for PDMS-*b*-PCVE copolymer.

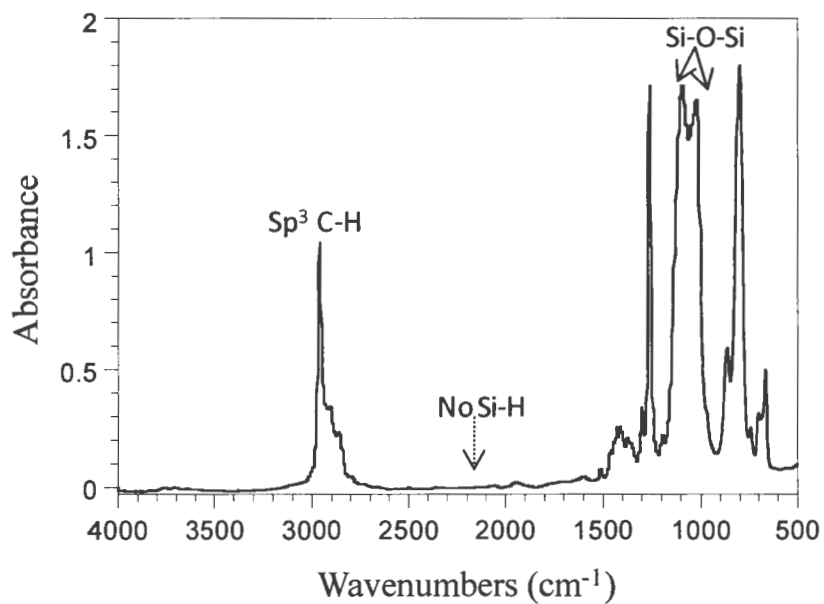


Figure 3.25. FTIR spectrum obtained for PDMS-*b*-PCVE copolymer.

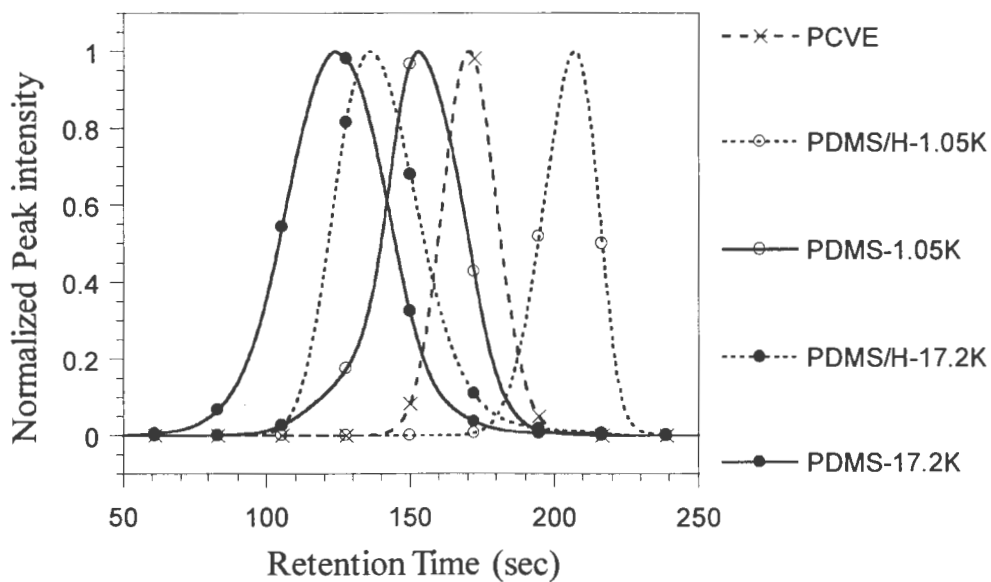


Figure 3.26. GPC chromatograms obtained for PCVE, PDMS/H, and PDMS-*b*-PCVE.

Table 3.5. Theoretical and GPC number average molecular weight obtained for PCVE, PDMS/H, and PDMS-*b*-PCVE.

Sample	PCVE	PDMS/H-1.05K (DMS-H11)	PDMS- 1.05K	PDMS/H-17.2K (DMS-H25)	PDMS- 17.2K
Mn (g/mole) (Theoretical)	5,487	1,050	12,024	17,200	28,174
Mn (g/mole) (GPC)	8153	2033	15,238	23,247	45,174
PDI (GPC)	1.2	1.2	1.5	1.6	1.8

3.4.3.2. Characterization of PDMS-*b*-PCVE

The TGA was performed in an air-oxidative environment with a constant increase in temperature. TGA thermograms of PCVE, PDMS/Hs, and PDMS-*b*-PCVEs were shown in Figure 3.27. Corresponding DTG graphs were shown in Figure 3.28. From the thermograms, two important parameters, for example, the decomposition temperature (T_0) and onset temperature (T_{onset}) are listed in Table 3.6. The T_0 can be defined as the temperature of maximum weight loss rate (dm/dt_{max}). The T_{onset} can be considered as the point when decomposition just begins. TGA/DTG graphs of PCVE shows one main degradation step with a peak maximum (T_0) of 316.7 °C and two small degradation steps with T_{0s} of 437.3 °C and 610.2 °C respectively. The DTG graph of PDMS/H-1.05K showed one main degradation step and two small degradation steps with peak maximum values of 218.9 °C, 383.3 °C, and 536.8 °C, respectively. However, the block copolymer, PDMS-1.05K showed one major and one minor degradation steps with T_{0s} of 339.2 °C and 458.5 °C respectively. Due to the addition of relatively higher molecular weight PCVE to

PDMS/H-1.05K, the onset decomposition temperature (T_{onset}) of the resulting block copolymer was increased. Moreover, the decomposition peak of PDMS/H-1.05K with T_0 of 218.9 °C cannot be seen in the block copolymer. The DTG graph of PDMS/H-17.2K showed one broad degradation step with T_0 value of 548.9 °C. However, the block copolymer, PDMS-17.2K showed two major degradation steps with T_0 s of 347.3 °C and 544.3 °C respectively. Due to the addition of relatively higher molecular weight PDMS/H-17.2K, the onset decomposition temperature (T_{onset}) of resulting block copolymer was increased compared to PCVE. Two major degradation steps in the block copolymer correspond to the degradation steps of PCVE and PDMS/H-17.2K.

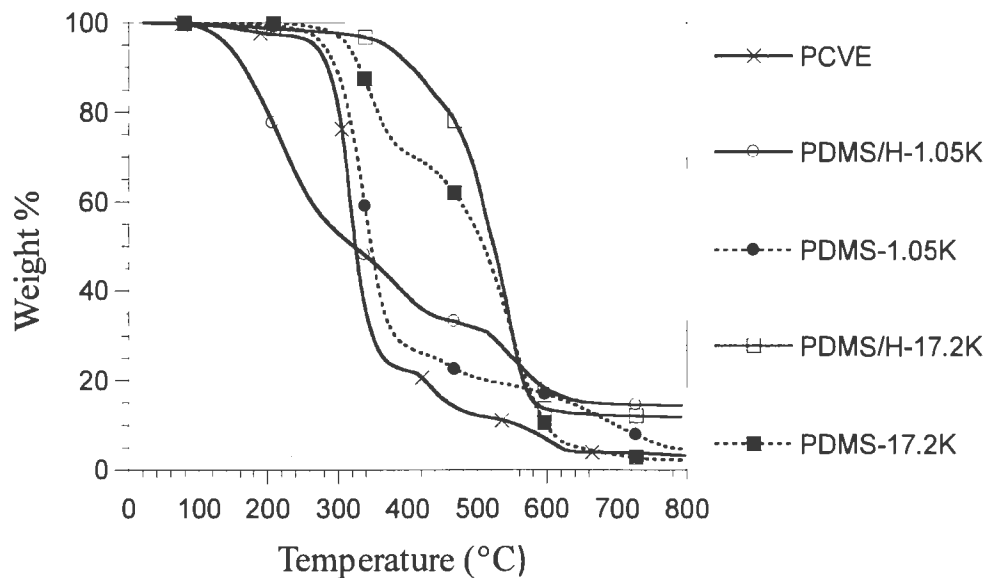


Figure 3.27. TGA thermograms obtained for PCVE, PDMS/H, and PDMS-*b*-PCVE.

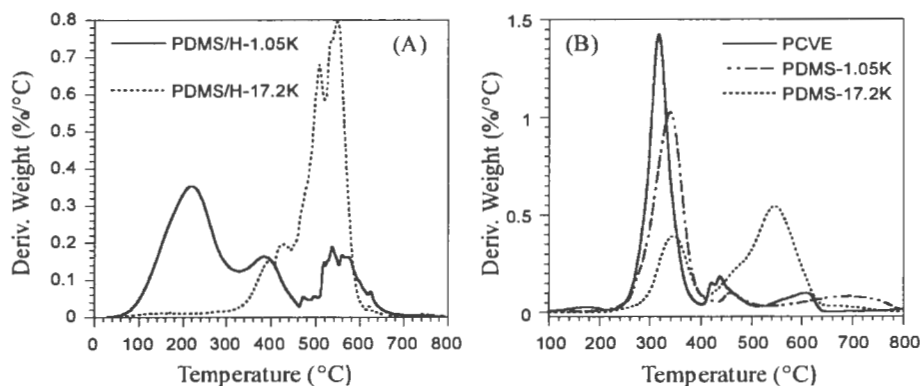


Figure 3.28. DTG thermograms obtained for PCVE, PDMS/H, and PDMS-*b*-PCVE.

Table 3.6. T_{onset} and T_0 data obtained for PCVE, PDMS/H, and PDMS-*b*-PCVE.

Sample	T_{onset} (°C)	T_0 (°C)		
		Step-1	Step-2	Step-3
PCVE	292.1	316.7	437.3	610.2
PDMS/H-1.05K	148.6	218.9	383.3	536.8
PDMS-1.05K	300.2	339.2	458.5	--
PDMS/H-17.2K	465.3	548.9	--	--
PDMS-17.2K	310.5	347.3	544.3	--

3.4.4. Synthesis and characterization of PDMS-*b*-PCVE-*b*-PQ

3.4.4.1. Synthesis of PDMS-*b*-PCVE-*b*-PQs

The synthesis of PDMS-*b*-PCVE-*b*-PQs (polyquats) consisted of the quaternization of PDMS-*b*-PCVE in the presence of *n*-alkyldimethyl amines at a temperature a 100 °C in toluene. The process involves the replacement of chlorine in PDMS-*b*-PCVE with tertiary amines to produce quaternary ammonium cation with chloride as a counter-ion (Figure 3.14). A series of such polyquats were produced by varying the *n*-alkyl chain lengths (12

carbons to 18 carbons) of tertiary amines and the extent of quaternization. For each amine, three different concentrations were used to replace the chlorine by 10 mole %, 30 mole %, and 50 mole %. However, the complete quaternization was not observed after heating at 8 days. Thus, the PDMS-*b*-PCVE-*b*-PQs are consisted of the unreacted tertiary amine. The unreacted tertiary amine concentration was calculated using a ^1H NMR spectrum of crude polyquat. The percentage of quaternization was calculated after integrating and comparing the initial and final concentrations of 8 protons directly attached to the nitrogen of a tertiary amine (Figure 3.29). Protons at 0.84 ppm were used to normalize the peak. Table 3.7 lists the actual quaternization (mole %) calculated using proton NMR spectra. In the FTIR spectrum, the quaternary ammonium groups can be seen as a broad absorption peak centered at 3370 cm^{-1} (Figure 3.30).

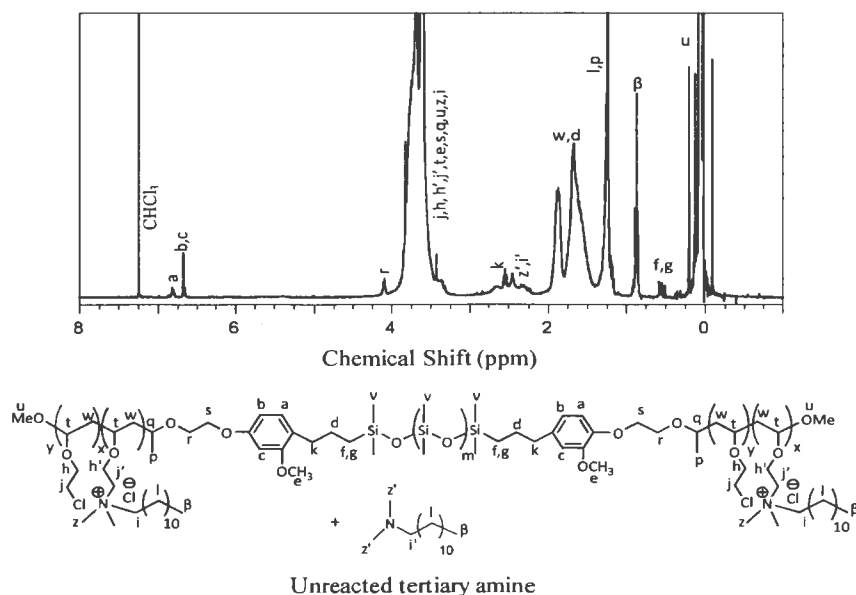


Figure 3.29. ^1H NMR spectrum obtained for PDMS-*b*-PCVE-*b*-PQ.

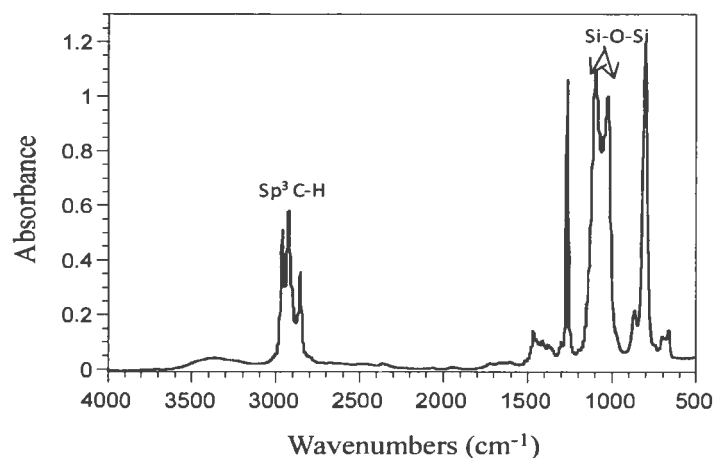


Figure 3.30. FTIR spectrum obtained for PDMS-*b*-PCVE-*b*-PQ.

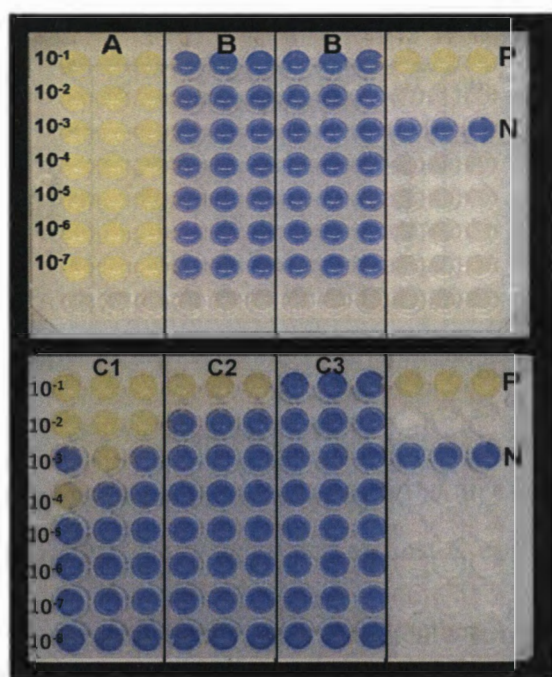
Table 3.7. Actual quaternization (mole percentage) calculated using ¹H NMR spectra of PDMS-*b*-PCVE-*b*-PQs.

PQs synthesized from 1.05K PDMS		PQs synthesized from 17.2K PDMS	
PDMS- <i>b</i> -PCVE- <i>b</i> -PQ	Actual value (mole %)	PDMS- <i>b</i> -PCVE- <i>b</i> -PQ	Actual value (mole %)
PDMS-1.05K-C12-10%	8.5	PDMS-17.2K-C12-10%	8.5
PDMS-1.05K-C12-30%	24	PDMS-17.2K-C12-30%	28.2
PDMS-1.05K-C12-50%	48	PDMS-17.2K-C12-50%	39
PDMS-1.05K-C14-10%	8.5	PDMS-17.2K-C14-10%	8.5
PDMS-1.05K-C14-30%	24	PDMS-17.2K-C14-30%	24
PDMS-1.05K-C14-50%	33.5	PDMS-17.2K-C14-50%	33
PDMS-1.05K-C16-10%	8.5	PDMS-17.2K-C16-10%	8.5
PDMS-1.05K-C16-30%	22.3	PDMS-17.2K-C16-30%	24
PDMS-1.05K-C16-50%	33	PDMS-17.2K-C16-50%	33
PDMS-1.05K-C18-10%	8.5	PDMS-17.2K-C18-10%	8.5
PDMS-1.05K-C18-30%	22.8	PDMS-17.2K-C18-30%	24
PDMS-1.05K-C18-50%	33	PDMS-17.2K-C18-50%	46

3.4.4.2. Characterization of PDMS-*b*-PCVE-*b*-PQ

The antimicrobial activities of PDMS-*b*-PCVE-*b*-PQs in solution were evaluated against the Gram-positive bacterium, *S. aureus* and the Gram-negative bacterium, *E. coli*. Figure 3.31 shows the image of array plates that is a representative result obtained from combinatorial high throughput screening of antimicrobial activity in aqueous solution. Figures 3.32 and 3.33 show the effect of both the n-alkyl chain lengths and percentages of quaternization on the antimicrobial effect against *S. aureus* and *E. coli* respectively. The n-alkyl chain lengths of quaternary ammonium compounds have strong influence on the antimicrobial activity in solution. For example, Gilbert P et al.¹⁷⁸ investigated the effect of n-alkyl chain lengths on the antimicrobial activities of n-alkyltrimethylammonium bromides towards *Staphylococcus aureus*, *Saccharomyces cerevisiae*, and *Pseudomonas aeruginosa*. The maximum antimicrobial activities for n-alkyltrimethylammonium bromides were observed for the n-alkyl chain lengths between 10 and 12 carbon atoms. Majumdar et al.¹⁷⁵ synthesized quaternary ammonium salt functional trimethoxysilane (QAS-TMS) and determined the antimicrobial activity of QAS-TMS in solution against *E. coli* and *S. aureus*. In general, the QAS-TMS containing one quaternary ammonium group per molecule showed more activity towards the Gram-positive bacterium *S. aureus* than the Gram-negative bacterium *E. coli*. In another approach, Majumdar et al. synthesized a quaternary ammonium substituted polyhedral oligomeric silsesquioxane (Q-POSS) and the antimicrobial properties of Q-POSSs were evaluated against *E. coli* and *S. aureus*. In contrast to QAS-TMS, the Q-POSSs were found to effective against both the *E. coli* and *S.*

aureus to equal extent. This non-linear chemical structure-antimicrobial activity relationship can be attributed to several factors: (a) the degree of affinity of QACs towards the cell wall of microorganisms, (b) the degree of agglomeration and micelle formation in solution, (c) steric interactions, (d) diffusibility of QACs through the cell wall, and (e) amphiphilic nature of the QACs.^{164, 166, 173} Studies showed that amphiphilic nature of QACs that offers both the hydrophobic and hydrophilic interactions are needed to effectively bind the target microorganism cell walls.¹⁷⁹⁻¹⁸⁰



P = Bacterial growth in D/E medium (10^{-1} dilution in D/E only)

N = No bacterial growth in D/E medium (blank D/E)

A = Growth in all three replicates well for each dilution (7 log reduction)

B = No growth in all three replicate wells for each dilution (7 log reduction)

C = Bacterial growth inhibited at different dilutions

- C1 = 5 log reduction
- C2 = 7 log reduction
- C3 = 8 log reduction

Figure 3.31. Images of array plates illustrate representative results obtained from combinatorial high throughput screening of antimicrobial activity in aqueous solution. Dilutions were presented in each row of the plates. Three replicate wells used per dilution were shown in columns.

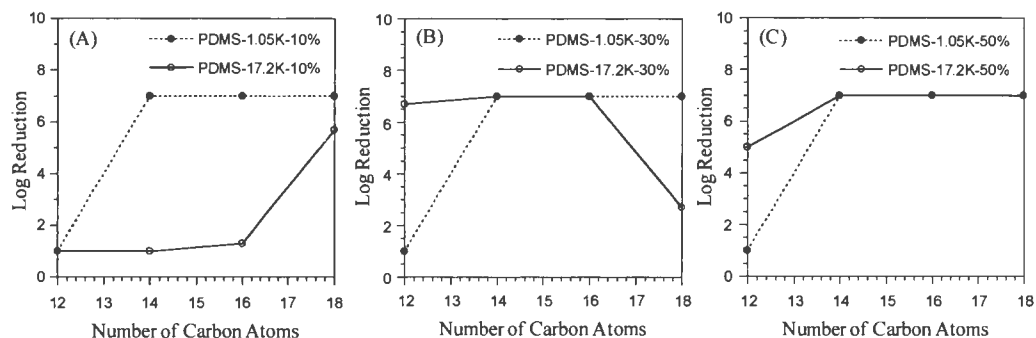


Figure 3.32. Variation of log reduction with the number of n-alkyl carbons attached to the nitrogen atom in PDMS-*b*-PCVE-*b*-PQ for (A) 10 mole %, (B) 30 mole %, and (C) 50 mole % quaternization when tested against *S. aureus*.

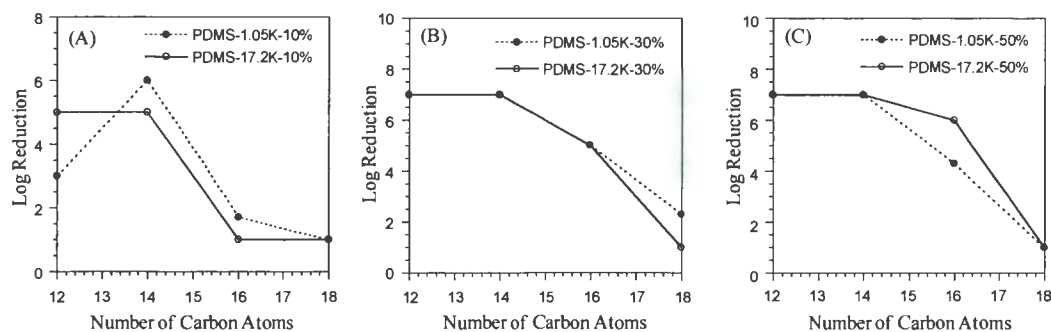


Figure 3.33. Variation of log reduction with the number of n-alkyl carbons attached to the nitrogen atom in PDMS-*b*-PCVE-*b*-PQ for (A) 10 mole %, (B) 30 mole %, and (C) 50 mole % quaternization when tested against *E. coli*.

However, the chemical structures of quaternary ammonium compounds synthesized here are totally different than that were produced by Majumdar et al. and Gilbert P. et al. The PDMS-*b*-PCVE-*b*-PQs contain pendent quaternary ammonium chloride salt moieties chemically attached to a polymer backbone. These polyquaternary ammonium salt blocks are attached to hydrophobic PDMS blocks and PCVE blocks. These quaternary ammonium compounds are generally blended with crosslinked networks, for

example, crosslinked PDMS to synthesize antimicrobial coatings that show antimicrobial activity via a contact active mechanism. The advantages of such polymeric quaternary ammonium compounds attached to blocks of PDMS are the low water and chemical solubility than monomeric and macromeric quaternary ammonium compounds. This will increase the lifetime of the antimicrobial coating as the antimicrobial agent dissolves to the environment at a lower rate than the monomeric counterpart. Additionally, due to the presence of polymeric blocks of quaternary ammonium compounds the PDMS-*b*-PCVE-*b*-PQ possesses very high charge density per molecule that will reduce the requirement of contact time and concentration to be as effective as monomeric QAC.

According to the generally accepted mechanism of bactericidal activity of cationic antimicrobial compounds, once the positive charge over nitrogen atom in QAC had interacted with the head groups of acidic phospholipids on bacterial cell wall the QAC adsorbed on to the cell wall surfaces and the hydrophobic part of QAC penetrates into the hydrophobic core of the cell wall disrupting cell integrity. The bioactivity difference in between Gram-positive and Gram-negative bacteria can be explained by the cell wall structure of these microorganisms. The multiwall cell of *E. coli* is composed of a thin, inner wall (2-3 nm) containing 10-20% peptidoglycan followed by an outer lipid bilayer (7 nm) containing phospholipids and lipopolysaccharides. On the other hand, the cell wall of *S. aureus* is a thick, single wall membrane containing 60 to 90% peptidoglycan. In general, PDMS-*b*-PCVE-*b*-PQs (polyquats) synthesized from the lower molecular weight PDMS showed high bioactivity against the Gram-positive bacterium when the n-alkyl chain lengths were above 12 carbons (C-12) (Figure 3.32). However, polyquats synthesized from

the higher molecular weight of PDMS and the percentage of quaternization above 10 mole % showed high activity against *S. aureus* when the n-alkyl chain lengths were above 12 carbons except for one polyquat sample produced from C-18 and 30 mole % quaternization. The possible reason could be nature of the interaction of the polyquat and bacterial cell wall.

Polyquats synthesized from both the low and high molecular weight PDMS showed high antimicrobial activity towards the Gram-negative bacterium when the extent of quaternization was above 10% and the chain lengths of n-alkyl attached to nitrogen were 12 and 14 carbons (Figure 3.33). Higher number of carbons in the n-alkyl chain (C-16 and C-18) did not show any significant effect on the antimicrobial activity against *E. coli*. Combing the above results, it can be concluded that PDMS-*b*-PCVE-*b*-PQs containing n-alkyl chain length of 14 carbons showed the broad spectrum antimicrobial activity against both the Gram-positive and the Gram-negative bacteria for the entire concentration of quaternization investigated in this research.

3.5. CONCLUSION

A novel monoallyl-functional AMEA initiator capable of producing very fast and quantitative initiation under a living carbocationic polymerization condition of vinyl ether was synthesized and characterized. With the AMEA, a polymer (PCVE) of 2-chloroethyl vinyl ether was produced using a living carbocationic polymerization. The narrow molecular weight distribution and quantitative incorporation of monoallyl-functionality to PCVE indicated a relatively fast and efficient initiation process associated with the use of

AMEA in the presence of $\text{Et}_{1.5}\text{AlCl}_{1.5}$ at 0 °C. The order of polymerization calculated from the percentage of conversion and reaction time was one. The AMEA possessing a monoallyl-functionality in the ester fragment attaches to the one end of PCVE. This monoallyl-functional PCVE was used to produce two block copolymers, PDMS-*b*-PCVE, consisted of high and low molecular weight PDMS using hydrosilylation. The successful block copolymer synthesis was confirmed using ^1H NMR, FTIR, and GPC. The chlorine atoms in PDMS-*b*-PCVE were replaced by a *n*-alkyldimethyl amine by varying the *n*-alkyl chain lengths of tertiary amine from 12 carbons to 18 carbons and percentage of quaternization. The antimicrobial activities of PDMS-*b*-PCVE-*b*-PQs were evaluated in solution against *E. coli* and *S. aureus*. The antimicrobial activity towards *E. coli* was found to increase when the *n*-alkyl chain were consisted of 12 and 14 carbons. However, the antimicrobial activities against *S. aureus* were the highest when the percentages of quaternization were at the higher end (30 mole % and 50 mole %) and the *n*-alkyl chains were consisted of 14 and 16 carbons. The great advantage of PDMS-*b*-PCVE-*b*-PQs possessing very high charge density per molecule over monomeric quaternary ammonium compounds is the presence of polymeric blocks of quaternary ammonium compounds that are very effective against microorganisms even at a low concentration and low contact time. Based on these results obtained in this research, it appears that the novel initiator is useful to synthesize a wide variety of polymers with various applications. The polyquaternary ammonium compounds described in this document have tremendous commercial potential.

CHAPTER 4. SYNTHESIS AND CHARACTERIZATION OF A NOVEL, HIGHLY BROMINATED, FLAME RETARDANT POLYMER PRODUCED USING CARBOCATIONIC POLYMERIZATION

4.1. ABSTRACT

A novel, highly brominated polymer (PBrVE) was synthesized from pentabromo-6-ethoxybenzene vinyl ether monomer (BrVE) using carbocationic polymerization. BrVE was synthesized from the reaction between 2-iodoethyl vinyl ether and pentabromophenol in the presence of potassium carbonate. BrVE was polymerized in the presence of an ester functional base, initiator and Lewis acid. The progress of the polymerization was characterized using Real Time FTIR by monitoring the concentration of the vinyl ether double bond in BrVE with time. The PBrVE was characterized using ¹H NMR and FTIR spectra. The thermal and rheological properties of PBrVE were compared to a commercially available brominated flame retardant, poly(pentabromobenzyl acrylate), PBrBA. Solution viscosity measurement revealed that PBrVE possesses an intrinsic viscosity which is twice as high than that of PBrBA. The glass transition temperature of PBrVE was determined to be 103 °C which was 57 °C lower than that of PBrBA. The higher molecular mobility of PBrVE resulted in a lower melt viscosity than PBrBA.

4.2. INTRODUCTION

Polymeric materials when exposed to high temperature, suffer from thermal breakdown and the decomposed products react with air oxygen providing a combustion process.¹⁸¹⁻¹⁸³ Flame retardants (FRs) are essential additives for many plastic applications.

Industries that require flame retardant plastics include electronics, automobiles, aircraft, building materials, and rail vehicles to name a few. FRs are generally inorganic and organic halogenated or non-halogenated compounds. Examples of flame retardants are antimony trioxide,¹⁸⁴⁻¹⁸⁵ chlorofluorocarbons, micas,¹⁸⁶⁻¹⁸⁷ inorganic carbonates,¹⁸⁸⁻¹⁹⁰ magnesium hydroxide,¹⁹¹⁻¹⁹⁶ alumina trihydrate,¹⁹⁷ boron containing inorganic compounds¹⁹⁸⁻²⁰⁸ (borax, zinc borate, boric acid), melamine phosphate, alkyl phosphate,²⁰⁹⁻²¹² red phosphorous,²¹³ expandable graphite,²¹⁴⁻²²⁴ etc. For plastics, organic brominated FRs (BFRs) are the most prevalent due to their effectiveness.²²⁵ Recently, a movement is going on to switch from halogenated flame retardants to environmentally friendly, non-halogenated flame retardants. However, in order to pass the industrial standard for flame retardancy test, the amount of non-halogenated fillers required can exceed 60 percent by weight.²²⁵ Thus, this alternative technology has a negative impact on the physical and mechanical properties of plastic articles.

During the combustion of a plastic in air, highly oxidizing agents, free radicals, are generated which are essential elements for propagating the flame. Halogenated materials are very useful to capture the free radicals in the gas-phase. The mechanism by which halogenated flame retardants provide flame retardancy basically involves interruption of the combustion process by halogen radicals such that the rate of heat generation is reduced, resulting in flame extinguishment.²²⁶

All four halogens are effective in trapping free radicals and the efficiency increases with the size of the halogen, i.e., I>Br>Cl>F. Thus, any organohalogen compound could be used as a flame retardant. However, the fluorinated compounds are very stable and

decompose at very high temperature generating their halogens too late to be good flame retardants. Organoiodine compounds being unstable to heat possess low shelf-life and decompose at moderate temperatures. Thus, it is difficult to blend organoiodine compounds with plastic using common processing techniques, such as extrusion molding, injection molding, etc. Only the organobromine and organochlorine compounds can be used effectively as flame retardants. Considering the free radical trapping efficiency and lower decomposition temperature, organobromine compounds are more popular than the organochlorine compounds.

Since, the bromine is the major part for a flame retardant, there is no restriction on the chemical structure to be an efficient flame retardant until the percentage of bromine is the same. The considerations for an efficient flame retardant are the long life time and good compatibility with polymer. As a result, there are more than 75 aromatic, aliphatic, and cycloaliphatic brominated compounds used as brominated flame retardants.²²⁷ Currently, there are a wide variety of commercially available BFRs most of which contain high levels of aromatic bromine. Typically, FRs need to be added at a level of 5 – 20 weight percent to pass industry standards for flame retardancy.²²⁸ At this level of additive, the FR can have dramatic effects on physical and mechanical properties and processability of the plastic. As a result, the selection of a FR for a specific application often involves the influence of the FR on properties well beyond flammability.

Depending upon the mode of incorporation into polymers, BRFs can be divided into two subgroups, such as reactive compounds and additives. Reactive BFRs such as tetrabromobisphenol-A is used as a reactive intermediate for the production of epoxy and

polycarbonate polymers.²²⁹ Additive BFRs (monomeric and polymeric) are blended with non-halogenated polymers. However, polymeric BFRs are more compatible with a base polymer than the monomeric BFRs.

Due to issues with compatibility, polymeric BFRs are often preferred over small molecule BFRs that can “bloom” (i.e. diffuse from the bulk of a molded part to the surface). Polymeric BFRs possess better compatibility with plastics. Table 4.1 shows some examples of monomeric BFRs. As shown in Table 4.2 some commercially available polymeric BFRs include brominated epoxy oligomers (BrEO), brominated polycarbonate oligomers (BrPCO), and poly(pentabromobenzyl acrylate) (PBrBA). In addition to enhancing the properties and processability of plastic materials, polymeric BFRs have certain advantages over monomeric BFRs regarding the environmental hazard classification. Large polymeric BFRs are less likely to leach out of the end product preventing their accumulation in environment.²³⁰⁻²³² Moreover, polymeric BFRs are less likely to penetrate through the cell wall of living tissues or, bioaccumulate effectively.²³³ Polymeric BFRs have better compatibility with base polymer and thus better temperature, weather, and color resistance.²³⁴ Hence, the polymeric BFRs are predicted to gain more market share than monomeric BFRs in future.²³⁵

Of these polymeric BFRs mentioned in Table 4.2, PBrBA (poly(pentabromobenzyl acrylate)) possesses the highest bromine content which should allow for lower levels of the additive to be used to obtain adequate flame retardancy. According to Smith et al.²²⁸ PBrBA can enhance the properties and processability of some thermoplastics in addition to

providing flame retardancy. Dead Sea Bromine Group has commercialized a polymeric brominated flame retardant PBrBA.

Table 4.1. The chemical structure of some commercially available monomeric brominated flame retardants.

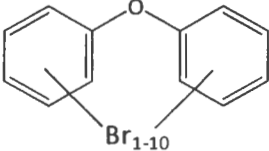
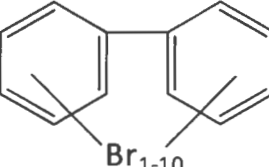
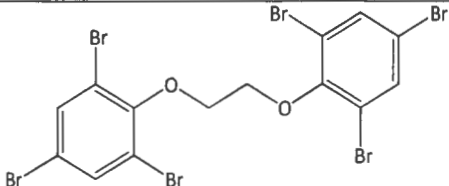
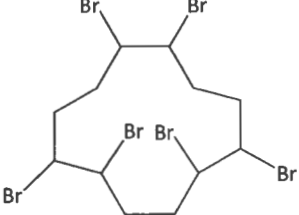
Monomeric BFRs	Chemical Structure	Formula & References
<p>PBDE (Polybrominated diphenyl ethers)</p>		<p>$C_{12}H_6Br_4O$, TetraBDE²³⁶⁻²³⁷ $C_{12}H_5Br_5O$, PentaBDE^{236, 238-241} $C_{12}H_4Br_6O$, HexaBDE²³⁶ $C_{12}H_2Br_8O$, OctaBDE^{236, 239, 242-246} $C_{12}Br_{10}O$, DecaBDE^{236, 243, 246}</p>
<p>PBB (Polybrominated Biphenyls)</p>		<p>$C_{12}H_4Br_6$, HexaBB^{236, 247-252} $C_{12}Br_{10}$, DecaBB^{236, 253-255}</p>
<p>BTBPE (1,2-bis(2,4,6-tribromophenoxy) ethane)</p>		<p>$C_{14}H_8Br_6O_2$²³⁶</p>
<p>HBCDD (Hexabromocyclodecane)</p>		<p>$C_{12}H_{18}Br_6$²⁵⁶⁻²⁶⁹</p>

Table 4.2. The chemical structure of some commercially available polymeric brominated flame retardants.

Polymeric BFRs	Chemical Structure	Reference
BrEO		Brominated epoxy oligomers ²⁷⁰⁻²⁷⁷
BrPCO		Brominated polycarbonate oligomers ²⁷⁸⁻²⁸⁸
PBrBA		Poly(pentabromo benzyl acrylate) ^{277, 289-306}

This document describes the synthesis and characterization of a novel, highly brominated polyvinylether that has essentially the same bromine content as PBrBA, but with very different physical properties.

4.3. EXPERIMENTAL

4.3.1. Materials

Table 4.3 describes the starting materials used for the investigation. Unless specified otherwise, all materials were used as received.

Table 4.3. Chemicals used.

Chemical or Abbreviation	Description	Source
CVE	2-chloroethyl vinyl ether, 99 %	Sigma-Aldrich
NaI	Sodium iodide, ≥ 99 %	Sigma-Aldrich
Acetone	ACS Grade, 99.5%	VWR Chemicals
Diethyl ether	ACS Grade, 99%	VWR Chemicals
N,N-dimethyl formamide	Anhydrous, 99.8%	Sigma-Aldrich
BrP	Pentabromophenol, 99%	Acros Organics
Magnesium sulfate	Anhydrous, ReagentPlus®, ≥ 99.5 %	Sigma-Aldrich
PBrBA (FR1025)	Polypentabromobenzyl acrylate	Dead Sea Bromine
Et3Al2Cl3	Ethylaluminum sesquichloride (25 wt. % in toluene)	Sigma-Aldrich
PBT	Polybutylene terephthalate	SABIC
BB	Bromobenzene, 99 %	Sigma-Aldrich
DBB	1,3-dibromobenzene, >97 %	TCI America
MCAC	Methyl chloroacetate, 99%, a Lewis base in cationic polymerization, distilled over calcium hydride	Sigma-Aldrich
Dibromobenzene	1,3-dibromobenzene, >97.0 %	TCI America
Methylene chloride	ACS grade, 99.5%	VWR
MeOH	Methanol, ≥ 99.8 %	Sigma-Aldrich
CDCl3	Deuterated chloroform (99.8%), contains 1% v/v TMS, NMR solvent	Alfa Aesar
C6D5Br	Deuterated bromobenzene, 99.5 %, NMR solvent	Sigma-Aldrich

4.3.2. Synthesis of 1,2,3,4,5-pentabromo-6-(2-(vinylloxy)ethoxy)benzene (BrVE)

The synthesis of BrVE consisted of the synthesis of 2-iodoethyl vinyl ether followed by the reaction of IVE with pentabromophenol.

4.3.2.1. Synthesis of 2-iodoethyl vinyl ether

IVE was synthesized using the synthesis scheme shown in Figure 4.1. A detailed procedure is as follows: 100.65 g of 2-chloroethyl vinyl ether, 200.16 g of sodium iodide and 730 g of acetone were combined in a 2-liter, 3-neck round bottom flask and heated at a temperature of 60 °C for 72 hours. Next, the reaction mixture was cooled to room temperature and diluted with 600 ml of diethyl ether. The organic layer was washed thrice with deionized water (DI) and dried with anhydrous magnesium sulfate. The product was recovered by rotary evaporation of diethyl ether and excess 2-chloroethyl vinyl ether at a temperature of 50 °C and a pressure of 60 mmHg for 1 hour. Proton NMR was used to confirm the production of 2-iodoethyl vinyl ether: ^1H NMR (CDCl_3) δ 6.44 ppm (q, 1H, $\text{OCH}=\text{C}$), 4.19, 4.05 ppm (dd, 2H, $\text{CH}_2=\text{C}$), 3.95 ppm (t, 2H, OCH_2), 3.3 ppm (t, 2H, CH_2I).

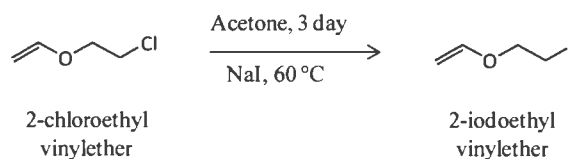


Figure 4.1. The synthetic scheme used to produce 2-iodoethyl vinyl ether.

4.3.2.2. Synthesis of BrVE

Synthesis of the BrVE monomer consisted of the reaction between pentabromophenol and 2-iodoethyl vinyl ether in the presence of a base in N,N-dimethyl formamide (Figure 4.2). A detailed procedure is as follows: 139.01 g of 2-iodoethyl vinyl ether, 266.67 g of pentabromophenol, 98.06 g of potassium carbonate, and 900 ml of N,N-

dimethyl formamide were added in a 2-liter, 3-neck round bottom flask and heated at a temperature of 80 °C for 24 hours. The reaction mixture was filtered hot to remove potassium carbonate and the product monomer (BrVE) was isolated after precipitating the filtrate into methanol. BrVE was purified after crystallization from methanol and dried at 45 °C under vacuum overnight. The product yield was 89%. Proton NMR, carbon NMR and FTIR were used to confirm the production of BrVE: ^1H NMR (CDCl_3) δ 6.55 ppm (q, 1H, $\text{OCH}=\text{C}$), 4.07 - 4.27 ppm (m, 6H, $\text{C}=\text{CH}_2$, $\text{CH}_2\text{-CH}_2$). ^{13}C NMR (CDCl_3) δ 86.95 ppm ($\text{CH}_2=\text{}$), 151.44 ppm ($=\text{CH}$), 71.53, 66.6 ppm ($\text{O-CH}_2\text{-CH}_2$), 153.7, 128.8, 125.13, 121.82 ppm ($\text{Ar C}=\text{C}$). IR (KBr) 2938 (C-H), 1612 (C=C), 1342 ($\text{Ar C}=\text{C}$), 1051 (C-O), 811, 981 ($=\text{C-H}$) cm^{-1} .

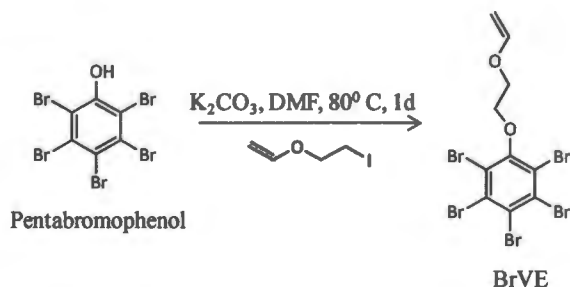


Figure 4.2. The synthetic scheme used to produce BrVE.

The purity of BrVE monomer was determined using an Agilent 1100 Series High Performance Liquid Chromatography (HPLC) fitted with an Agilent 1100 auto-sampler and a diode array detector. Sample solutions were prepared at 1 mg/ml in methanol and injected at a volume of 20 μl through a Zorbax Eclipse XDB-C18 HPLC column. The mobile phase was a mixture of water and acetonitrile (30/70 vol. %) and the column was maintained at a constant temperature of 40 °C. Pentabromophenol showed a strong peak at

a retention time of 5.47 minutes when a detector signal of 280 nm was used. Absence of any peak at a retention time of 5.47 minutes indicated that the BrVE is totally free of pentabromophenol.

4.3.3. Synthesis of the polymer of BrVE

BrVE was polymerized using a carbocationic polymerization. Prior to use, BrVE was dried at 60 °C under vacuum overnight. Polymerization solvents bromobenzene and 1,3-dibromobenzene were distilled over calcium hydride. The polymerization initiator, 1-isobutoxyethyl acetate was synthesized according to the procedure below.

4.3.3.1. Synthesis of 1-isobutoxyethyl acetate (IBEA)

The IBEA was prepared using the procedure of Aoshima and Higashimura.³⁶ A detailed description is as follows (Figure 4.3): 18 g of glacial acetic acid and 45 g of isobutyl vinyl ether were combined in a 250 ml, 2-neck round bottom flask fitted with a reflux condenser and heated at 60 °C for 3 hours. Next, the reaction mixture was cooled to room temperature and diluted with 200 ml of diethyl ether. The organic layer was washed thrice with deionized water (DI) and dried with anhydrous magnesium sulfate. The crude product was recovered by rotary evaporation of diethyl ether and the unreacted isobutyl vinyl ether under a temperature of 25 °C and a pressure of 20 millibar. The purified IBEA was collected after one time distillation over calcium hydride. Proton NMR was used to confirm the production of IBEA: ¹H NMR (CDCl₃) δ 5.87 ppm (q, 1H, O-CH-O), 3.19, 3.4 (m, 2H, O-CH₂-C), 2.05 ppm (s, 3H, O=C-CH₃), 1.8 ppm (m, 1H, C-CH-C), 1.36 ppm (d, 3H, O-C-CH₃), 0.86 ppm (dd, 6H, C-C-CH₃).

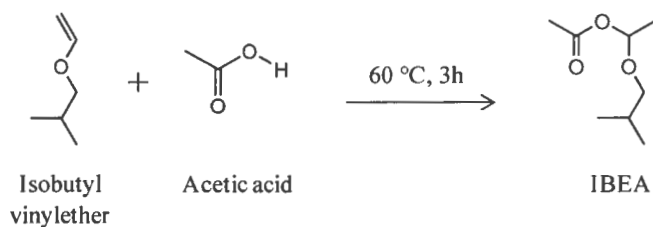


Figure 4.3. The synthetic scheme used to produce IBEA.

4.3.3.2. Determination of polymerization kinetics using gravimetric analysis

A detailed description of BrVE polymerization is as follows (Figure 4.4). Polymerization kinetic studies were carried out inside a glove box using a dry three-neck, round-bottom flask equipped with an overhead stirrer. The reaction vessel was partially submerged in a heptanes bath at 0 °C. 51.5 mg (0.32 mM) of IBEA, 36 g (64.4 mM) of BrVE ($[M]_0:[I]_0 = 200:1$), and 8.74 g (80.5 mM) of MCAc were dissolved into 600 ml of bromobenzene and cooled to 0 °C. The polymerization was started by the addition of 0.88 ml (1.61 mM) of $\text{Et}_3\text{Al}_2\text{Cl}_3$ solution ($[M]_0:[\text{Et}_{1.5}\text{AlCl}_{1.5}]_0 = 200:5$). Polymer samples as a function of time were obtained by withdrawing a known amount of reaction mixtures at different periods of time and terminating them with methanol. Each polymer sample was purified by dissolving in bromobenzene and then precipitating into diethyl ether. Polymers were isolated using centrifugation at 3500 rpm at 22 °C for 5 minutes. Polymer yield was determined gravimetrically after drying the purified polymer at 40 °C under vacuum overnight. The reduced viscosity and inherent viscosity of each polymer were measured and plotted with the percentage of monomer conversion.

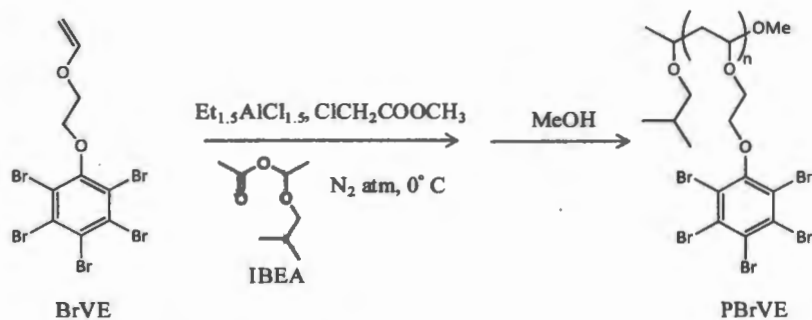


Figure 4.4. The synthetic scheme used to produce PBrVE.

4.3.3.3. Determination of polymerization kinetics using Real Time FTIR

The progress of polymerization was monitored using Real Time FTIR, ReactIR™ iC10 from Mettler Toledo, fitted with a diamond tip K6 conduit probe inside the glove box. At first, a dry 40 ml vial was fixed with the probe and the initial background spectrum was collected. As mentioned in Table 4.4; the BrVE, IBEA, MCAc, and bromobenzene were combined together in the vial to make a homogeneous solution. The solution was brought to the reaction temperature and the reaction was started by the addition of supplied ethyl aluminum sesquichloride solution. The rate of consumption of BrVE monomer was directly determined by integrating the peak area of reaction spectra between 1608 cm⁻¹ and 1678 cm⁻¹. FTIR spectra were taken at a resolution of 8 cm⁻¹ and a Mercury Cadmium Telluride detector was used to analyze the signal. From the reaction trend graph, the peak intensity of C=C bond in BrVE at different reaction time was recorded.

4.3.3.4. Synthesis of high molecular weight PBrVE (PBrVE/HMW/0C)

The synthesis of high molecular weight PBrVE (PBrVE/HMW/0C) consisted of the polymerization of BrVE in the absence of IBEA and external base, MCAc (Figure 4.5).

Table 4.4. Formulation of BrVE polymerizations.

Formula	Initial weight of reactants					[M] ₀ : [I] ₀ : [MCAc] ₀ : [Et _{1.5} AlCl _{1.5}] ₀	T ³ (°C)	Reaction Time (h)	
	BrVE (g)	IBEA (mg)	MCAc (g)	Solvent (g)					Et _{1.5} AlCl _{1.5} (g)
				BB ¹	DBB ²				
PBrVE/ BB/0C	1	1.43	0.24	235.8	--	0.022	200 : 1 : 250 : 5	0	2
PBrVE/ BB/22C	1	1.43	0.24	24.56	--	0.022	200 : 1 : 250 : 5	22	2
PBrVE/ BB/50C	1	1.43	0.24	24.56	--	0.022	200 : 1 : 250 : 5	50	2
PBrVE/ DBB/0C	1	0.75	0.24	--	32.7	0.022	200 : 0.5 :250 : 5	0	19

¹BB stands for bromobenzene

²DBB stands for dibromobenzene

³T stands for polymerization temperature

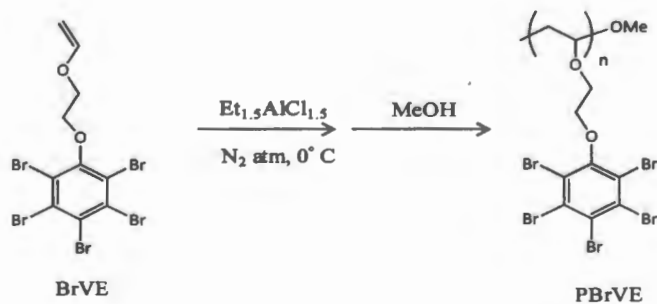


Figure 4.5. The synthetic scheme used to produce PBrVE in the absence of the IBEA and MCAc.

A detailed procedure is as follows: 84 g of BrVE was dissolved in 2063 g of bromobenzene in a 2-liter, 3-neck round bottom flask fitted with a overhead stirrer and cooled to 0 °C. The reaction was started by the addition of 1.86 g of supplied ethyl aluminum sesquichloride solution ($[M]_0:[Et_{1.5}AlCl_{1.5}]_0 = 200:5$). After 2 hours, the reaction was terminated by the addition of 1.5 liter methanol to precipitate the polymer. The

polymer was washed with excess of methanol to remove the co-initiator fragment and dried in vacuum overnight.

4.3.4. Determination of the solution viscosity of PBrVE

PBrVE is insoluble in common solvents, such as tetrahydrofuran (THF), toluene, methanol, acetone, etc. Determination of polymer molecular weight and molecular weight distribution using Gel Permeation Chromatography (GPC) was not possible due to the insolubility of PBrVE in THF, a commonly used GPC solvent. Polymer molecular weight was characterized by measuring the solution viscosity using an Ubbelohde viscometer at 25 °C according to the ASTM D 445 - 06. Each polymer sample was dissolved at a series of concentration in dibromobenzene and filtered through a 0.45 µm syringe filter from VWR. Polymer solutions were equilibrated at 25 °C for 10 minutes before measurements were taken. The time required for the liquid to travel across the volume indicated by the upper and lower marks in the viscometer was recorded. Each data was reported as the average of 3 replicate measurements. The standard deviation from the mean value of three replicate measurements was found as less than 0.2%. The reduced viscosity, inherent viscosity, and intrinsic viscosity of PBrVE were calculated according to the following formula:

$$\text{Reduced viscosity } (\eta_{\text{red}}) = \eta_{\text{sp}}/c$$

$$\text{Inherent viscosity } (\eta_{\text{inh}}) = (\ln \eta_r)/c$$

$$\text{Intrinsic viscosity } [\eta] = (\eta_{\text{sp}}/c)_{c=0} = [(\ln \eta_r)/c]_{c=0}$$

where, c = concentration of polymer in g/100 ml. Specific viscosity (η_{sp}) can be defined as follows:

$$\text{Specific viscosity } (\eta_{sp}) = \eta/\eta_0 - 1 = t/t_0 - 1$$

where, t and t_0 are the times required for the polymer solution and pure solvent to pass through a certain volume marked by two lines in the viscometer. The pure empirical relationship between η_{sp}/c and c is given by Huggins as follows:

$$\eta_{sp}/c = [\eta] + k' [\eta]^2 c \quad (1)$$

where, k' is the Huggins constant. The $[\eta]$ was calculated from the intercept at $c=0$.

There is another empirical relation also available between $[(\ln \eta_r)/c]$ and c which is described as follows:

$$(\ln \eta_r)/c = [\eta] + k'' [\eta]^2 c \quad (2)$$

where, k'' is the Kraemer constant. The $[\eta]$ was calculated from the intercept at $c=0$. The intrinsic viscosity reported was the average value of intrinsic viscosities obtained from equations (1) and (2).

4.3.5. Determination of the Specific gravity of PBrVE

A known weight (a) of PBrVE was taken in a volumetric flask and dissolved in dibromobenzene. The volume (V) of the volumetric flask was adjusted by the addition of additional amount of dibromobenzene at a temperature of 25 °C. The total weight (b) of dibromobenzene needed to adjust the volume at 25 °C was recorded. Next, the weight (c) of only dibromobenzene needed to make up the volume of the volumetric flask at 25 °C was noted. The density of PBrVE (ρ_{PBrVE}) at 25 °C was calculated according to the following equation:

$$\rho_{\text{PBrVE}} = \frac{a}{\left[V - \frac{b \times V}{c} \right]}$$

The specific gravity (SG) of PBrVE was calculated according to the following equation:

$$\text{SG} = \frac{\rho_{\text{PBrVE}}}{\rho_{\text{water}}}$$

The ρ_{water} , density of water, is considered as 0.997044 g/ml at 25 °C. The specific gravity data was reported as the average value of 3 replicate measurements. The standard deviation from the mean value of three replicate measurements was found as 0.03.

4.3.6. Instrumentation and procedures

4.3.6.1. Nuclear Magnetic Resonance (NMR) spectroscopy

A JEOL-ECA 400 (400MHz) NMR spectrometer equipped with an autosampler was used to generate proton NMR (^1H NMR) spectra. Data acquisition was completed using 16 scans in CDCl_3 as the lock solvent for BrVE and in $\text{C}_6\text{D}_5\text{Br}$ as the lock solvent for PBrVE.

4.3.6.2. Fourier Transform Infrared (FTIR) spectroscopy

FTIR experiments were carried out using a Nicolet Magna-IR 850 spectrometer Series II. The solid samples were mixed with dry potassium bromide powder and pressed to produce circular transparent films using a compression molding. FTIR spectra were taken at a rate of 1 spectrum/s with a resolution of 4 cm^{-1} .

4.3.6.3. Differential Scanning Calorimetry (DSC)

The thermal properties of PBrVE and PBrBA were determined using differential scanning calorimetry. The instrument utilized was a DSC Q1000 from TA Instruments, and sample sizes ranged from 4.5 to 5.5 mg. All polymers were subjected to a heat-cool-heat cycle by first heating samples from 30 °C to 250 °C at a heating rate of 20 °C/minute (1st heat), cooling from 250 °C to 30 °C at a cooling rate of 20 °C/minute (cooling), and reheating from 30 °C to 250 °C at a heating rate 20 °C/minute (2nd heat). The T_g reported was obtained from the 2nd heat.

4.3.6.4. Thermogravimetric Analysis (TGA)

TGA was carried out using a Q500 from TA Instruments. Samples sizes were 10 mg to 15 mg. In a ramp heating mode samples were heated from 30 °C to 700 °C at five different heating rates of 2.5, 5, 10, 20, and 40 °C/minute in air.

4.3.6.5. Refractive Index (RI) measurement

PBrVE and PBrBA were dissolved in bromobenzene at 2.6 wt. % and filtered using a 1 micron syringe filter from VWR. The polymer solutions were coated over single-side polished silicon wafers using a spin coater from Specialty Coating Systems (model P6700) at spin rates of 220, 500, and 1000 rpm and dried overnight. The refractive index of PBrVE and PBrBA were measured using a M88 J. A. Woollam spectroscopic ellipsometer.

4.3.6.6. Atomic Force Microscopy (AFM)

The roughness of the film surfaces coated over silicon wafer was characterized using an AFM consisting of a Dimension 3100® microscope coupled with a Nano-scope IIIa controller manufactured by Veeco Incorporated. Surface scanning was carried out in

tapping mode using a silicon probe and a scan rate of 1 Hz. The image collection set point was in between 0.8 to 0.9.

4.3.6.7. Rheological properties

The rheological properties of PBrVE and PBrBA in melt were characterized using an ARES rheometer from TA Instruments. Specimens were created by melt pressing powders into thin films of approximately 0.33 mm thickness using a heated press. Temperature profiles were generated using a constant strain of 5 % and a frequency of 10 rad/s. Frequency sweeps were generated by ramping frequency from 0.1 rad/s to 500 rad/s at a constant strain of 5 % and constant temperature of 230 °C.

4.4. RESULTS AND DISCUSSION

The commercially available polymeric BFRs possess quite high glass transition temperatures which can lead to undesirably high melt viscosities and reduced impact strength in plastic compositions. As a result, it was of interest to synthesize a highly brominated polymer with a relatively flexible polymer backbone. The polymer that was synthesized was PBrVE. The BrVE monomer was synthesized by the reaction between 2-iodoethyl vinyl ether and pentabromophenol (Figure 4.2). 2-iodoethyl vinyl ether was produced from 2-chloroethyl vinyl ether using the reaction scheme in Figure 4.1. The monomer was an off-white crystalline product with a melting point of 134 °C.

4.4.1. Characterization of BrVE

Successful synthesis of the BrVE was confirmed by ^1H NMR, ^{13}C NMR, DEPT-135, HETCOR, and FTIR spectra. According to the proton NMR spectrum (Figure 4.6.B),

the absorption associated with one methine and two methylene protons of the vinyl ether double bond were at 6.52 ppm, 4.07 ppm, and 4.22 ppm, respectively. The total disappearance of the proton absorption peaks at 3.3 ppm confirmed that BrVE was free from unreacted IVE.

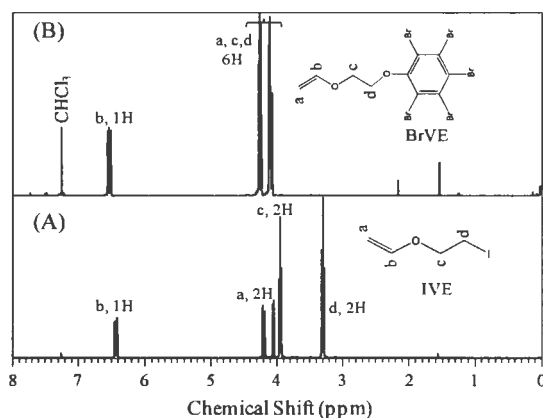


Figure 4.6. ^1H NMR spectra of (A) IVE and (B) BrVE.

The Distortionless Enhancement by Polarization Transfer (DEPT) method is useful for determining the number of hydrogen atoms attached to a given carbon atom. In a DEPT-135 spectrum, methyl and methine carbons appear as positive peaks, while the methylene carbons appear as negative peaks. As shown in Figure 4.7, the methylene carbon (number 1) and methine carbon (number 2) in the vinyl ether double bond can be seen as a negative peak at 87.3 ppm and a positive peak at 151.6 ppm, respectively. All quaternary carbons in the aromatic ring at the positions of 5, 6, 7, 8, 9, and 10 did not appear in the DEPT-135 spectrum. The position of carbons in the ethoxy group was assigned using a HETCOR spectrum (Figure 4.8). One carbon at 87.3 ppm and two protons (dd) at 4.07 and 4.22 ppm correspond to methylene group (1); one carbon at 151.6 ppm and

one proton quartet at 6.52 ppm correspond to methine group (2); one carbon at 66.6 ppm and two protons triplet at 4.1 ppm correspond to methylene group (4); one carbon at 71.4 ppm and two protons triplet at 4.26 ppm correspond to methylene group (3). As shown in the FTIR spectrum (Figure 4.9), the absorption peak between 1608 cm^{-1} and 1678 cm^{-1} confirmed the presence of vinyl ether double bond in BrVE.

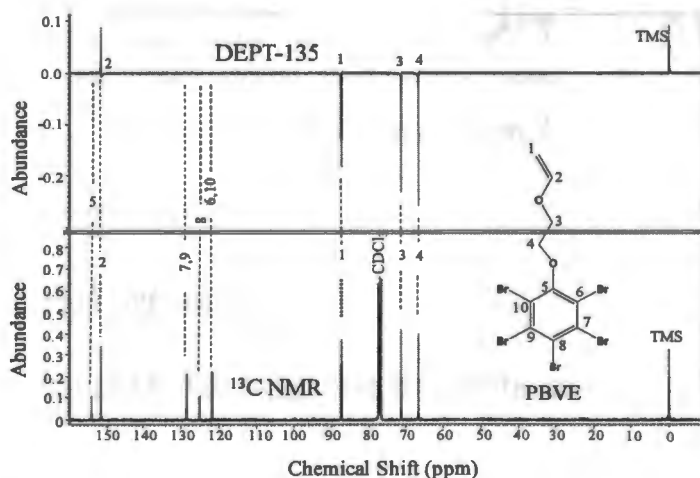


Figure 4.7. ^{13}C NMR and DEPT-135 spectra of BrVE.

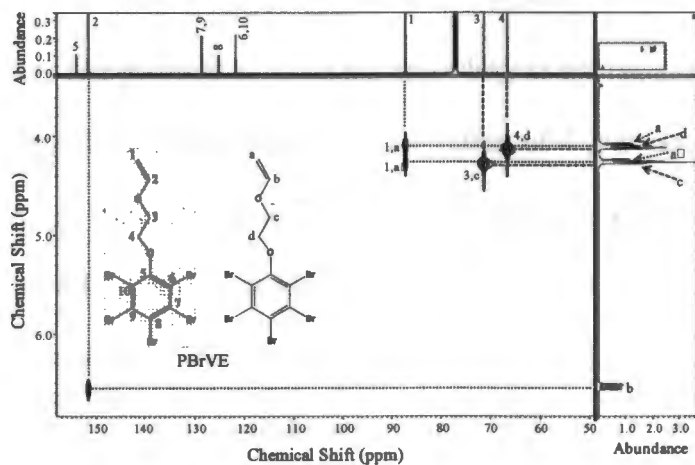


Figure 4.8. HETCOR spectrum of BrVE.

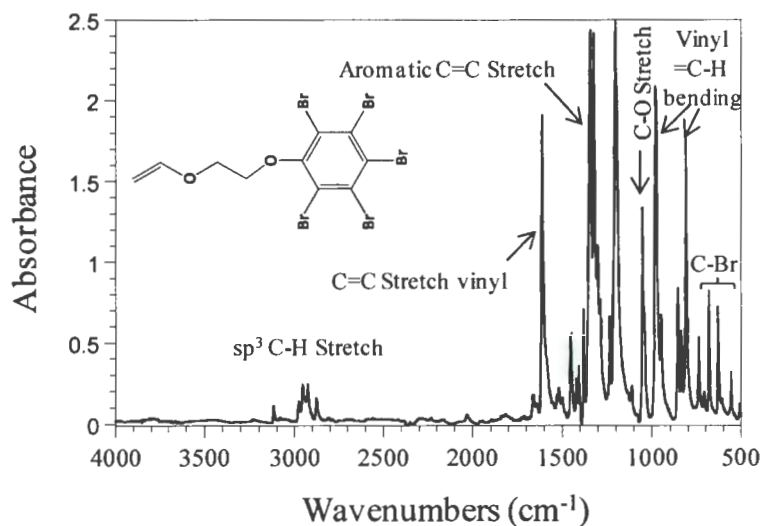


Figure 4.9. FTIR spectrum of BrVE.

4.4.2. Polymerization kinetics studies

4.4.2.1. Polymerization kinetics study using gravimetric analysis

Polymerization of the monomer, BrVE, was successfully achieved using cationic polymerization in which bromobenzene, IBEA, and $\text{Et}_3\text{Al}_2\text{Cl}_3$ were the solvent, initiator, and co-initiate, respectively. The polymer isolated was only soluble in bromobenzene and dibromobenzene. The polymer synthesized according to the reaction scheme in Figure 4.4 was dissolved in dibromobenzene at a concentration of 4 g/dL and both the reduced and inherent viscosities were plotted as a function of monomer conversion (Figure 4.10). As shown in Figure 4.10, both the reduced and inherent viscosities of PBrVE increased with the monomer conversion. This data demonstrates that carbocations generated due to the addition of co-initiator were propagating during the entire course of conversion.

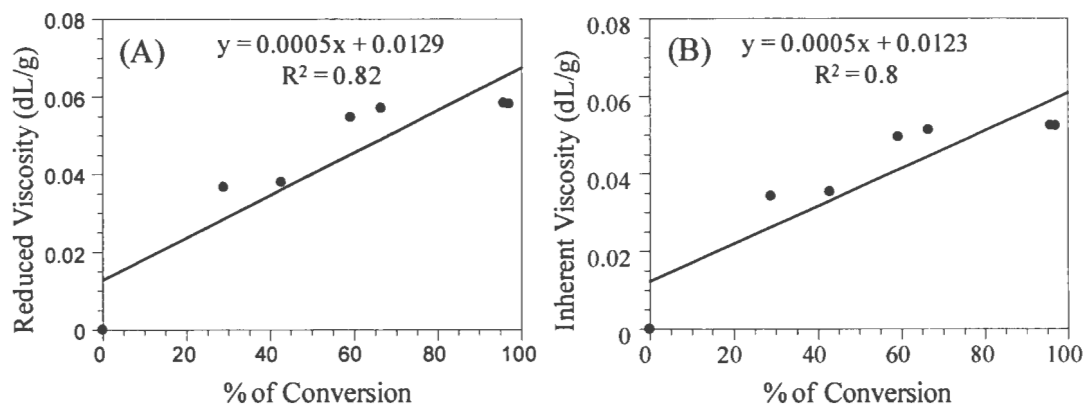


Figure 4.10. Plot of (A) reduced viscosity and (B) inherent viscosity as a function of monomer conversion for BrVE polymerization at 0 °C ($[M]_0:[IBEA]_0:[MCAc]_0:[Et_{1.5}AlCl_{1.5}]_0 = 200:1:250:5$).

4.4.2.2. Polymerization kinetic study using Real Time FTIR analysis

The progress of BrVE polymerization was monitored using Real Time FTIR experiment. Figure 4.11 shows the reaction spectra taken before the addition of $Et_{1.5}AlCl_{1.5}$ and after 2 hours of reaction at a temperature of 22 °C ($[BrVE]_0:[IBEA]_0:[MCAc]_0:[Et_{1.5}AlCl_{1.5}]_0 = 200:1:250:5$). From the reaction trend graph, the peak intensities of C=C bond in BrVE at different reaction times were recorded. From the peak intensity data, the percentage of conversion (Figure 4.12) and $\ln([M]_0/[M]_t)$ (Figure 4.13) were plotted as a function of polymerization time. The linear relation between $\ln([M]_0/[M]_t)$ and reaction time at two reaction temperatures of 0 °C and 22 °C demonstrated the first order kinetics for the polymerization of BrVE (Figure 4.13). With the increase in reaction temperature from 22 °C to 50 °C, a third order polynomial relationship was observed indicating a significant contribution from termination reactions (Figure 4.13).

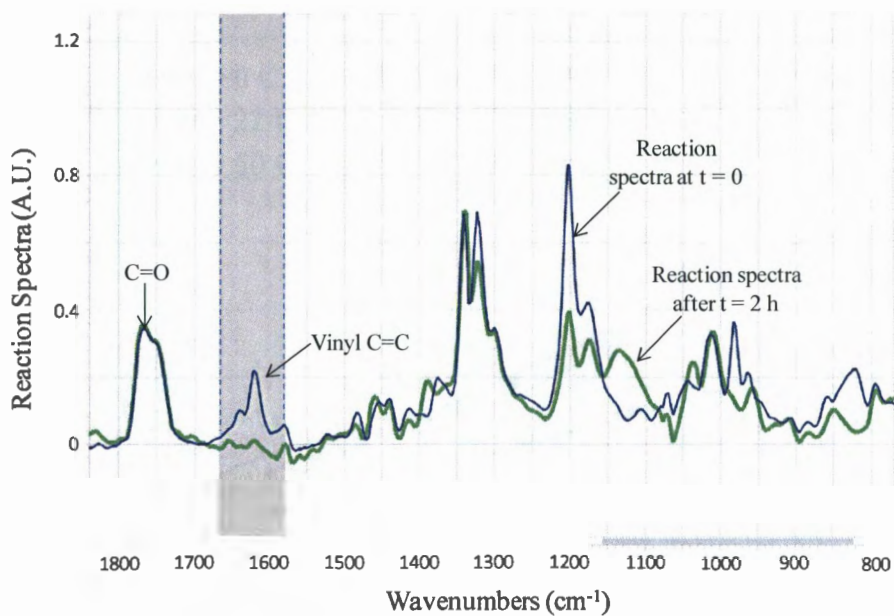


Figure 4.11. BrVE polymerization spectra before the addition of $\text{Et}_{1.5}\text{AlCl}_{1.5}$ and after 2 hours of reaction at a reaction temperature of $22\text{ }^\circ\text{C}$ ($[\text{BrVE}]_0:[\text{IBEA}]_0:[\text{MCAC}]_0:[\text{Et}_{1.5}\text{AlCl}_{1.5}]_0 = 200:1:250:5$).

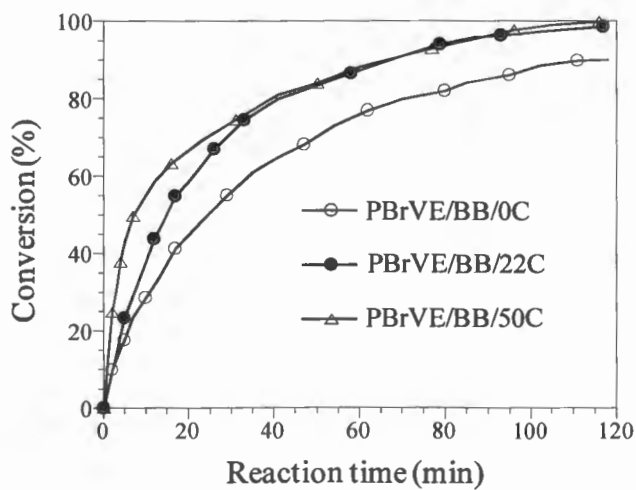


Figure 4.12. Plot of % of conversion vs. reaction time at three different reaction temperatures of $0\text{ }^\circ\text{C}$, $22\text{ }^\circ\text{C}$, and $50\text{ }^\circ\text{C}$. ($[\text{M}]_0:[\text{IBEA}]_0:[\text{MCAC}]_0:[\text{Et}_{1.5}\text{AlCl}_{1.5}]_0 = 200:1:250:5$).

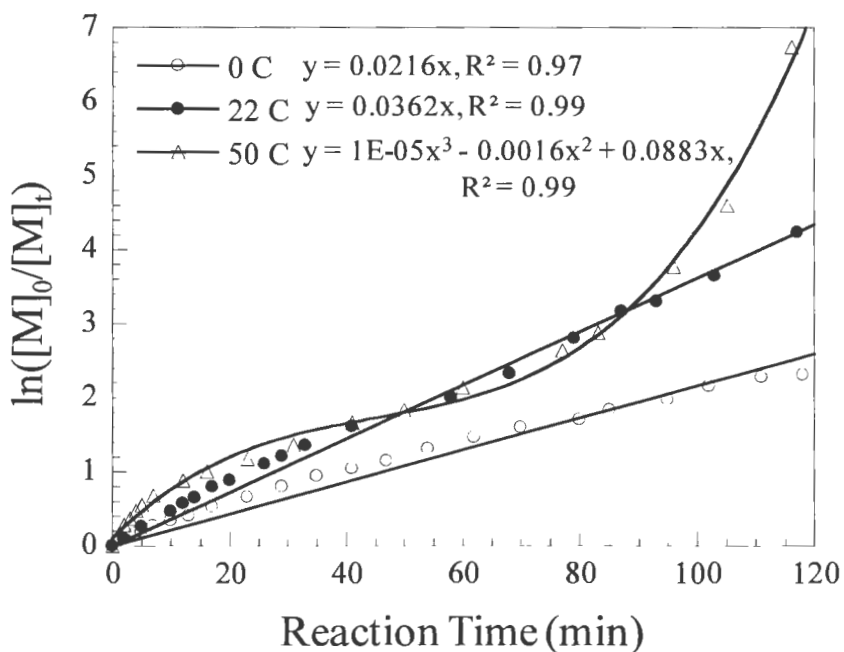


Figure 4.13. Plot of $\ln([M]_0/[M]_t)$ vs. reaction time at three different reaction temperatures of 0 °C, 22 °C, and 50 °C. ($[M]_0:[IBEA]_0:[MCAc]_0:[Et_{1.5}AlCl_{1.5}]_0 = 200:1:250:5$).

From the $\ln([M]_0/[M]_t)$ vs. reaction time plot, the energy of activation of BrVE polymerization between 0 °C to 22 °C was calculated according to the Arrhenius equation:

$$\text{Arrhenius Equation: } K = A \times \exp(-E_a/RT)$$

where, A, K, E_a , R, and T represent the pre-exponential factor, reaction rate constant, activation energy, universal gas constant, and reaction temperature, respectively.

Considering reaction temperatures at 0 °C and 22 °C,

$$K_1 = A \times \exp(-E_{a1}/RT_1) \quad K_2 = A \times \exp(-E_{a2}/RT_2)$$

$$\frac{K_1}{K_2} = \frac{A \times \exp(-E_{a1}/RT_1)}{A \times \exp(-E_{a2}/RT_2)}$$

Considering the pre-exponential factor to be constant within the temperature range,

$$0.02 / 0.037 = \exp \{ - (\Delta E_a / R)(1/273 - 1/295) \}$$

The energy of activation (ΔE_a) of BrVE polymerization was calculated to be 18.7 KJ/mole.

The percentages of conversion and intrinsic viscosities of polymers synthesized (Table 4.4) are listed in Table 4.5. The intrinsic viscosity of the polymer synthesized at 0 °C (PBrVE/BB/0C) was higher than that at 22 °C (PBrVE/BB/22C) which indicated that the carbocation generated at a reaction temperature of 0 °C propagated more uniformly for the entire range of conversion leading to higher molecular weight polymer. Lower polymerization temperature reduces the termination rate and enables one to produce higher molecular weight polymer. However, when dibromobenzene (DBB) was used as a polymerization solvent, no significant increase in the molecular weight was observed even at a reaction temperature of 0 °C. The possible reason could be the contribution of the impurity in DBB to the initiation process that possibly lowers the molecular weight and hence, the viscosity of polymer. The methyl chloroacetate complexes with the cationic propagating species through carbonyl double bond to delocalize the positive charge over the propagating species and lowers the reactivity of carbocation. Thus, the exclusion of initiator and Lewis base (i.e. PBrVE/HMW/0C) produced the highest molecular weight polymer. The inherent viscosity of PBrVE/HMW/0C at 25 °C was 0.076 dL/g. The specific gravity of PBrVE/HMW/0C measured at a temperature of 25 °C was 2.43.

Table 4.5. BrVE conversion and PBrVE intrinsic viscosity obtained for polymerizations described in Table 4.4.

Polymer	% Conversion (Gravimetry)	Intrinsic Viscosity (dL/g)
PBrVE/BB/0C	88	0.052
PBrVE/BB/22C	87	0.043
PBrVE/BB/50C	90	--
PBrVE/DBB/0C	71	0.018
PBrVE/HMW/0C (PBrVE)	95	0.076

The PBrVE/HMW/0C possesses the highest intrinsic viscosity and hence the highest molecular weight. Thus, the thermal, viscoelastic, and optical properties of PBrVE/HMW/0C were evaluated and compared with a commercially available oligomeric BFR, PBrBA. For convenience, PBrVE/HMW/0C is referred here as PBrVE. One of the advantages of PBrVE is its insolubility in most organic solvents at room temperature. It is only soluble in bromobenzene and dibromobenzene. Thus, the chance of PBrVE leaching out to the environment from finished products after contacting common organic solvents is very low.

4.4.3. Characterization of PBrVE using NMR and FTIR

The successful polymerization of BrVE was confirmed using proton NMR (Figure 4.14) and FTIR (Figure 4.15). As shown in Figure 4.14, two protons attached to the backbone methylene groups in repeating unit appeared between 1.8 ppm and 2.3 ppm. Five protons at the positions of b, c, and d in the repeating unit were between 3.8 ppm and 4.4 ppm. Absence of any peak between 1608 cm^{-1} and 1678 cm^{-1} in the FTIR spectrum of PBrVE indicated that the polymer was totally free of unreacted monomer.

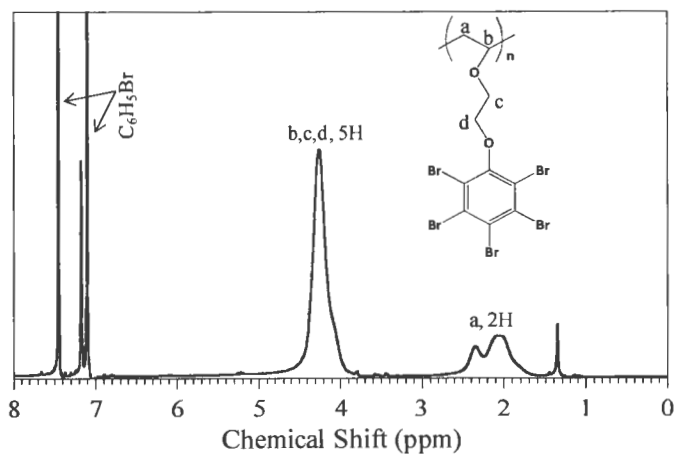


Figure 4.14. ^1H NMR spectrum for PBrVE.

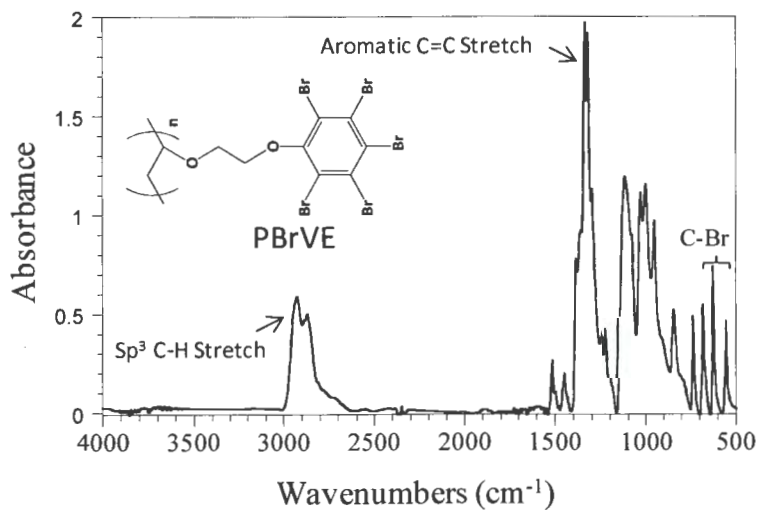


Figure 4.15. FTIR spectrum for PBrVE.

4.4.4. Comparison of the solution viscosities of PBrVE to PBrBA

Table 4.6 lists the viscometric parameters obtained for PBrVE and PBrBA. The plots of η_{sp}/c with c and $(\ln \eta_r)/c$ with c are shown in Figure 4.16. It is clear from Table 4.6 that the intrinsic viscosity of PBrVE is more than 2 times higher than that of PBrBA.

Table 4.6. Viscometric parameters for PBrVE and PBrBA.

Solution	c (g/dL)	η_r	η_{sp}	η_{sp}/c (dL/g)	$(\ln \eta_r)/c$ (dL/g)	$[\eta]$ (dL/g)
PBrVE-c1	2	1.17	0.17	0.082537	0.076392	0.079
PBrVE-c2	3	1.25	0.25	0.084738	0.075503	
PBrVE-c3	3.5	1.30	0.30	0.087765	0.076614	
PBrVE-c4	4.5	1.39	0.39	0.08758	0.073835	
PBrVE-c5	5	1.44	0.44	0.088275	0.073119	
PBrBA-c1	2	1.068	0.068	0.034	0.033	0.032
PBrBA-c2	3	1.1	0.1	0.0331	0.0316	
PBrBA-c3	3.5	1.12	0.119	0.034	0.032	
PBrBA-c4	4.5	1.155	0.155	0.0344	0.032	
PBrBA-c5	5	1.183	0.183	0.0362	0.033	

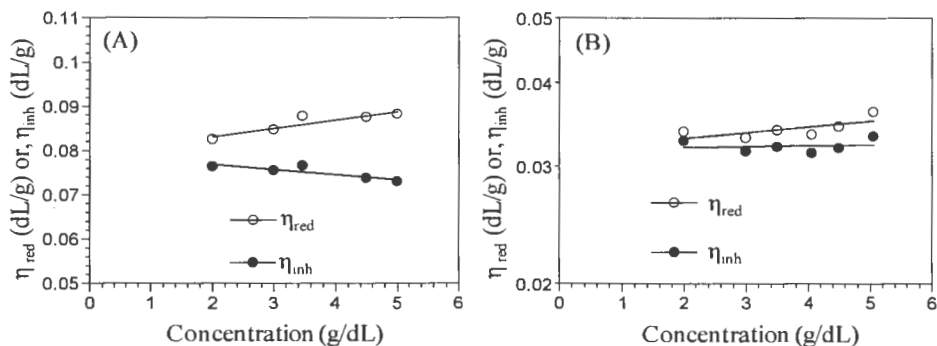


Figure 4.16. Plot of η_{sp}/c as a function of c and $(\ln \eta_r)/c$ as a function of c for (A) PBrVE and (B) PBrBA.

4.4.5. Comparison of the glass transition temperature (T_g) of PBrVE to PBrBA

The T_g of the polymer was determined using DSC. The DSC thermogram obtained from the 2nd heat (Figure 4.17) showed a glass transition value of 103 °C for PBrVE and 160 °C for PBrBA. The significantly lower glass transition temperature of PBrVE is

attributed to the flexible ethoxy linkage connecting the bulky pentabromophenyl group to the PBrVE polymer backbone compared to the ester group in PBrBA.

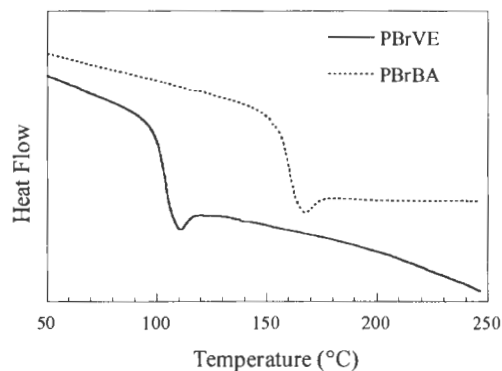


Figure 4.17. DSC thermograms for PBrVE and PBrBA.

4.4.6. Determination of thermal decomposition kinetics of PBrVE and PBrBA

TGA was performed in an air-oxidative environment with a constant increase in temperature. From the thermograms the decomposition temperature (T_0), onset temperature (T_{onset}), and ash content are listed in Table 4.7. The T_0 can be defined as the temperature of the maximum weight loss rate (dm/dt_{max}). The T_{onset} can be considered as the point when decomposition just begins. Figure 4.18 demonstrates variations of weight % and derivative of weight % as function of temperature for PBrVE and PBrBA when a heating rate of 20 °C/minute was used. Figure 4.19 shows the influence of the heating rate on the thermal decomposition of PBrVE and PBrBA. A higher rate implies the material reaches at a particular temperature within a short period of time that delays the thermal decomposition process towards higher temperature.³⁰⁷⁻³⁰⁸ For PBrVE, the values of T_{onset} and T_0 were higher than that of PBrBA. The brominated pendent group in PBrVE is attached to the

polymer backbone by ether linkage that provides an enhanced thermal stability as compared to the ester linkage in PBrBA. This enhanced thermal stability of PBrVE makes the polymer as a suitable candidate where high temperature, chemical, and weather resistances are required. Moreover, PBrVE was completely vaporized above 420 °C providing the maximum bromine free radical to the environment while some char was remaining for PBrBA.

The kinetics data obtained from TGA is useful to understand the process of decomposition which is helpful to predict other interesting properties. The rate of reaction at an isothermal conversion can be written as:

$$d\alpha/dt = k \times f(\alpha) \quad (3)$$

where, t is the time and α is the extent of decomposition = $(m_0 - m) / (m_0 - m_f)$ where, m_0 , m , and m_f are the initial, actual (at time t), and final mass of the sample. $f(\alpha)$ is the reaction rate which depends on the particular mechanism. According to Arrhenius;

$$k = A \times e^{-E/RT} \quad (4)$$

where, A , E , R , and T represent the pre-exponential factor, activation energy, universal gas constant, and absolute temperature, respectively. Combining equation (3) and (4):

$$d\alpha/dt = A \times e^{-E/RT} \times f(\alpha) \quad (5)$$

If the sample temperature is changing at a constant heating rate, the $d\alpha/dt$ can be written as:

$$d\alpha/dt = (dT/dt) \times (d\alpha/dT) = \beta \times (d\alpha/dT) \quad (6)$$

where, β represents the heating rate (dT/dt) .

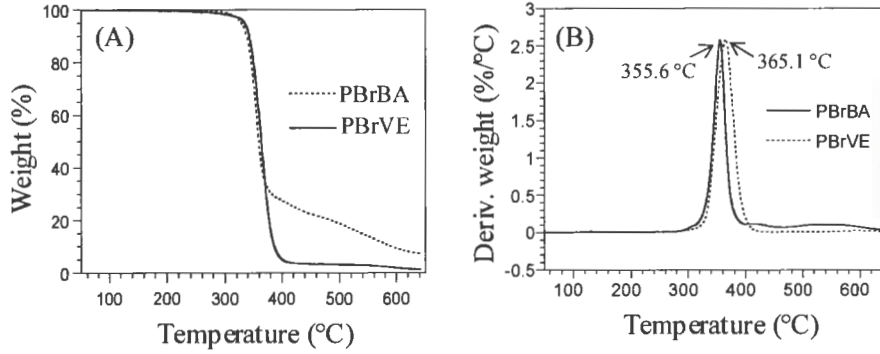


Figure 4.18. Plot of weight % as a function of temperature and (B) derivative of weight % as function of temperature for PBrVE and PBrBA when a heating rate of 20 °C/minute was used.

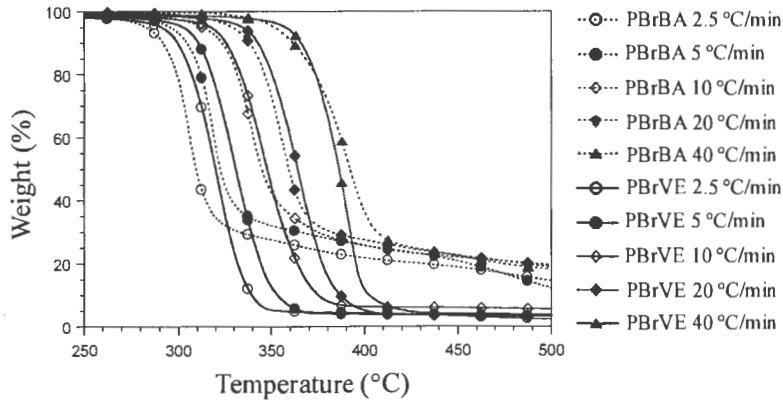


Figure 4.19. Plot of weight % as a function of temperature for PBrVE and PBrBA when five different heating rates were used.

Combining equation (5) and (6):

$$(d\alpha/dT) = (A/\beta) \times e^{-E/RT} \times f(\alpha) \quad (7)$$

Equation (7) is the basic equation of kinetic calculation.

The simplest model for $f(\alpha)$ in TGA can be given as:

$$f(\alpha) = (1 - \alpha)^n \quad (8)$$

where $(1 - \alpha)$ and n represent the amount of reactive remaining and reaction order

Combining equation (7) and (8):

$$(d\alpha/dT) = (A/\beta) \times e^{-E/RT} \times (1 - \alpha)^n \quad (9)$$

Table 4.7. Values of T_{onset} , T_0 , and ash content for BFRs.

BFRs	T_{onset} (°C)	T_0 (°C)	Wt. % remaining at 420 °C
PBrBA-2.5 °C/min	295.2	305.6	20.6
PBrBA-5 °C/min	307.4	318.5	23.9
PBrBA-10 °C/min	326.2	338.9	23.7
PBrBA-20 °C/min	341.3	355.6	25.3
PBrBA-40 °C/min	368.4	390.3	25.8
PBrVE-2.5 °C/min	304.6	322.5	3.9
PBrVE-5 °C/min	313.4	330.3	3.8
PBrVE-10 °C/min	328.5	346.9	6.1
PBrVE-20 °C/min	346.4	365.1	3.8
PBrVE-40 °C/min	371.7	390.5	5.2

4.4.6.1. Determination of activation energy using Flynn–Wall method.³⁰⁹⁻³¹⁰ This

method is relatively simple method of determining the energy of activation directly from TGA graphs. Using this method, the energy of activation can be calculated without knowing the order of decomposition. Flynn and Wall had rearranged the equation (9) using the Doyle approximation ($E/RT \geq 20$) to get the following equation:

$$(d \log \beta) / d(1/T) = -(E \times b) / R$$

where, b is a constant = 0.457. For a constant decomposition (iso-conversion), the temperatures (T) were recorded from the thermograms obtained at several heating rates (β).

Figures 4.20 and 4.21 represent the plot of $-\log\beta$ as a function of $1/T$ for PBrVE and PBrBA respectively. From the slope of the $\log\beta$ versus $1/T$ plot, the activation energies were calculated at different extent of decompositions and mentioned in Table 4.8. The average activation energies of decomposition for PBrVE and PBrBA were 29.8 Kcal/mole and 26.6 Kcal/mole respectively.

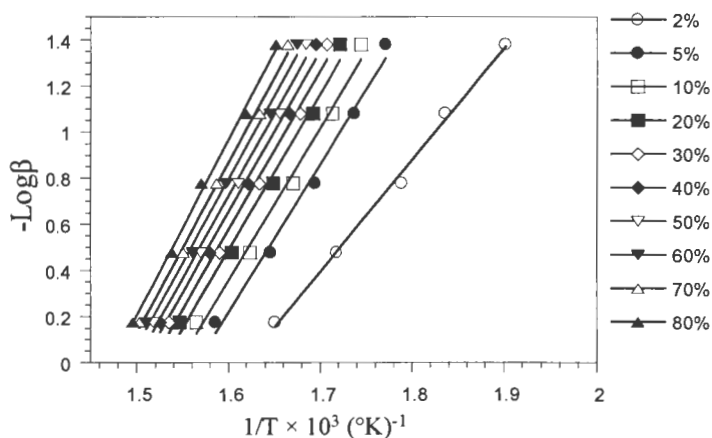


Figure 4.20. Plot of $-\log\beta$ as a function of $1/T$ for PBrVE.

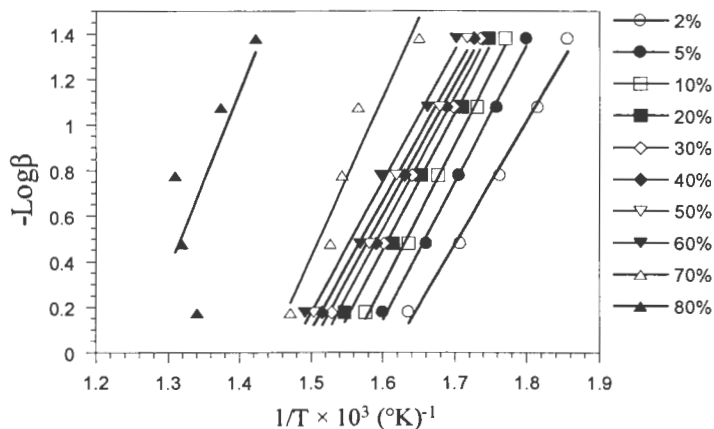


Figure 4.21. Plot of $-\log\beta$ as a function of $1/T$ for PBrBA.

Table 4.8. Activation energies at different percentage of decomposition for PBrVE and PBrBA using Flynn–Wall method.

Decomposition	PBrVE		PBrBA	
	E (Kcal/mole)	Average E (Kcal/mole)	E (Kcal/mole)	Average E (Kcal/mole)
0.02	21.03312	29.8	23.62342	26.6
0.05	28.02705		26.26956	
0.1	28.8405		26.88171	
0.2	29.44341		26.04549	
0.3	29.92974		25.32805	
0.4	30.39867		24.81944	
0.5	31.42701		24.57711	
0.6	32.135625		25.02045	
0.7	33.212685		30.35537	
0.8	33.863445		33.92823	

4.4.6.2. Determination of activation energy using Kissinger method³¹¹⁻³¹²

The activation energy can be calculated by the Kissinger method using the following equation:

$$d \ln(\beta/T_0^2) / d(1/T_0) = - E / R$$

Where β and T_0 are the heating rate and the temperature of TGA curves which correspond to the maximum decomposition rate. From the slope of the plot $\ln(\beta/T_0^2)$ versus $1/T_0$, the activation energy was calculated and listed in the Table 4.9. It was clearly demonstrated that the activation energy values calculated for PBrVE and PBrBA using Kissinger and Flynn–Wall methods agree on the basis of similar trend. Additionally, for

PBrVE the higher activation energy of decomposition indicates that the polymer possesses better thermal stability than that of PBrBA.

Table 4.9. Activation energies of decomposition for PBrVE and PBrBA determined using Kissinger method.

Heat rate (°C/ min)	PBrVE				PBrBA			
	T _o (°C)	1000/T _o (1/°K)	-ln(β/T _o ²)	E (Kcal/ mole)	T _o (°C)	1000/T _o (1/°K)	-ln(β/T _o ²)	E (Kcal/ mole)
2.5	322.5	1.68	15.96	28.4	305.6	1.73	-15.9	22.5
5	330.3	1.66	15.29		318.5	1.69	-15.25	
10	346.9	1.61	14.65		338.9	1.63	-14.62	
20	365.1	1.57	14.02		355.6	1.59	-13.99	
40	390.5	1.51	13.40		390.3	1.51	-13.4	

4.4.7. Film formation and refractive index

Figure 4.22 shows the AFM images of films produced from PBrVE and PBrBA. Table 4.10 lists the root mean square (rms) roughness and maximum roughness obtained from AFM. From the images it was clear that the PBrVE could produce a polymeric film of smooth surface finish.

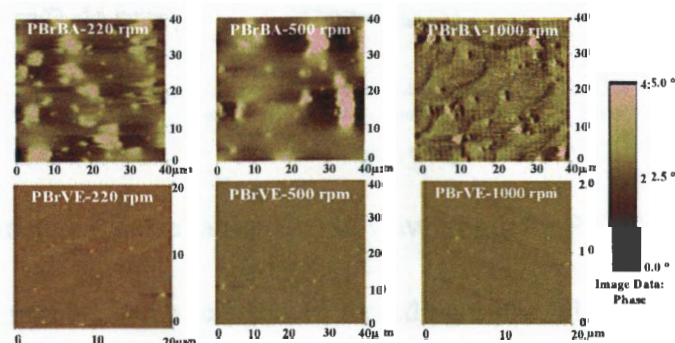


Figure 4.22. AFM images of PBrVE and PBrBA films.

Table 4.10. Results obtained from AFM experiment.

Samples	Image RMS, R_q (nm)	Image R_{max} (nm)
PBrVE, 220 rpm	1.12	57.66
PBrVE, 500 rpm	0.72	47.38
PBrVE, 1000 rpm	0.57	28.98
PBrBA, 220 rpm	27.93	310
PBrBA, 500 rpm	26.92	280.25
PBrBA, 1000 rpm	10.57	130.75

The refractive index of PBrVE and PBrBA were evaluated using a J. A. Woollam spectroscopic ellipsometer. Figure 4.23 shows the variation of refractive index with wavelengths of light for PBrVE and PBrBA. The refractive indexes at a wavelength of 589 nm were determined as 1.68 and 1.7 for PBrVE and PBrBA respectively.

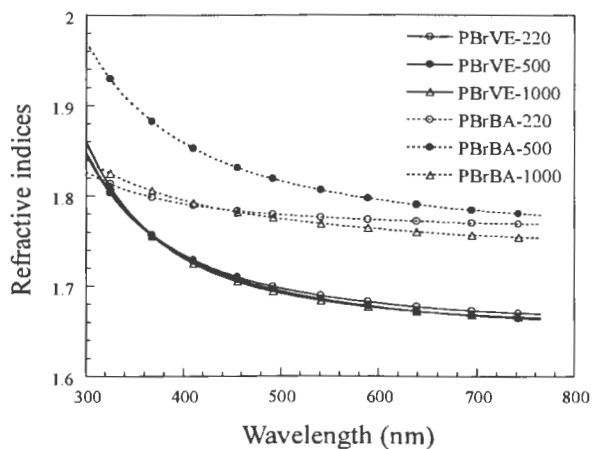


Figure 4.23. Refractive index as a function of wavelength for PBrVE and PBrBA.

The Abbe number can be calculated according to the following equation:

$$\text{Abbe number (V)} = \frac{(n_D - 1)}{(n_F - n_C)}$$

where, n_D , n_F , and n_C are refractive indexes of material at wave lengths of 589.2 nm, 486.1 nm & 656.3 nm, respectively. Abbe number of a transparent material is a measure of dispersion (refractive index variation with wavelength) in visible light. Low dispersion materials have high Abbe numbers. The Abbe numbers calculated after taking refractive indexes data from Figure 4.23 and inserting those into the equation mentioned above were 19.5 and 38.9 for PBrVE and PBrBA, respectively. The lower Abbe number for PBrVE clearly demonstrated that as opposed to the use of PBrBA, PBrVE will result a better dispersion in a medium, such as a base polymer.

4.4.8. Comparison of the rheological properties of PBrVE to PBrBA

Figures 4.24 and 4.25 represent the data obtained from a frequency sweep test and a temperature ramp test respectively. Table 4.11 listed the shear viscosity data of PBrVE and PBrBA at different temperatures.

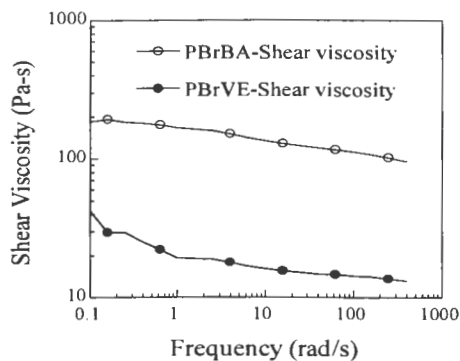


Figure 4.24. Shear viscosity as a function of frequency at 230 °C.

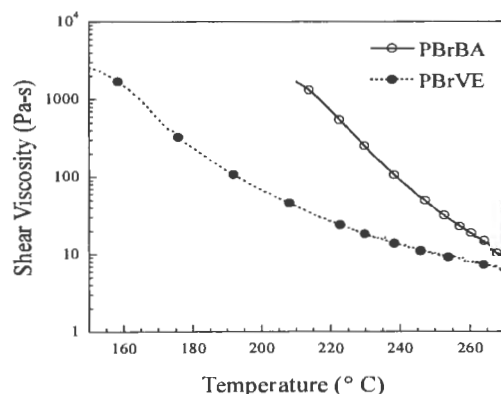


Figure 4.25. Shear viscosity as a function of temperature.

Table 4.11. Shear Viscosity values for PBrVE and PBrBA at different temperatures.

Temperature (° C)	Shear Viscosity (Pa-s)	
	PBrVE	PBrBA
210	41.176243	1702.817
230	18.222532	234.1874
260	7.8913164	18.92366
270	6.5442791	10.53209

PBrVE displayed much lower melt viscosity than the commercially available PBrBA which can be attributed largely to the higher polymer chain flexibility of PBrVE. The reduced melt viscosity and superior dispersibility of PBrVE should result in better processability, and perhaps, improved impact and optical properties of plastic compositions containing this polymer.

4.5. CONCLUSION

A novel BrVE monomer possessing high bromine content was synthesized and polymerized using a carbocationic polymerization in the presence of IBEA/ $\text{Et}_{1.5}\text{AlCl}_{1.5}$

initiating system and an ester functional base. The polymerization was optimized by varying the reaction temperature, initiator, concentration of an ester functional base, and solvent. The polymer molecular weight was characterized using a solution viscosity measurement. The polymer possessing the highest possible molecular weight (PBrVE/HMW/0C) was produced when the polymerization was carried out in the absence of a base and an initiator at a reaction temperature of 0 °C. The intrinsic viscosity of PBrVE was determined as more than 2 times higher than the commercially available BRF, PBrBA. Successful polymerization of BrVE was confirmed using ¹H NMR and FTIR. The thermal and flow properties of PBrVE was determined and compared to the PBrBA. Due to the higher flexibility of the polyvinylether polymer backbone as well as the flexibility of the ethoxy group linking the bulky pentabromophenyl group to the polymer backbone, PBrVE possessed a lower T_g. Additionally, due to the presence of thermally stable ether linkage between the pendent pentabromophenyl moiety and the polymer backbone, the PBrVE possesses better thermal and weather resistance. These results indicate that PBrVE may have utility for the development of FR plastics with improved processability.

CHAPTER 5. CHARACTERIZATION OF BLENDS OF POLYBUTYLENE TEREPHTHALATE AND POLY(PENTABROMO-6-(2-(VINILOXY)ETHOXY)BENZENE)

5.1. ABSTRACT

In this research polybutylene terephthalate (PBT) was blended with poly(pentabromo-6-(2-(viniloxy)ethoxy)benzene) (PBrVE) and the thermal, mechanical, and melt rheological properties were compared with an analogous blend prepared from PBT and poly(pentabromobenzyl acrylate) (PBrBA). Thermogravimetric analysis showed that the thermal stability of the PBT and brominated flame retardants (BFRs) blends were essentially the same as that of pure PBT. Characterization of the PBT blends using transmission electron microscopy indicated higher compatibility between PBT and PBrVE as compared to PBT and PBrBA. Additionally, the PBrVE was blended with PBT and Sb_2O_3 and the Young's modulus, flexural modulus, and flame retardancy of this blend were evaluated and compared to an analogous blend produced from PBrBA, PBT, and Sb_2O_3 . Due to the higher compatibility between PBT and PBrVE phases, the Young's modulus and flexural modulus were higher for PBrVE based PBT/ Sb_2O_3 blend than PBrBA based PBT/ Sb_2O_3 blend. Results obtained from the flame test showed that the flame retardancy of PBT/ Sb_2O_3 /PBrVE blend was the same as PBT/ Sb_2O_3 /PBrBA blend.

5.2. INTRODUCTION

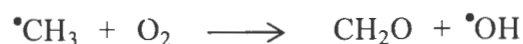
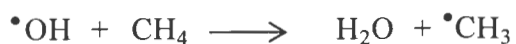
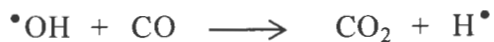
A popular engineering thermoplastic polybutylene terephthalate, PBT, is widely used in electronic, electrical and automotive applications for the last two decades. It is

important to find a suitable flame retardant for PBT. To date, the most efficient flame retardants for PBT are halogenated flame retardants. Among other non-halogenated flame retardants red phosphine and organo phosphorous compounds such as phosphorus oxynitride and phosphazenes have been used as flame retardants for PBT.³¹³ However, red phosphine is harmful due to the production of toxic phosphine gas. The phosphorus-nitrogen containing compounds are thermally stable and only start to decompose above 450 °C. Additionally, flame retardant PBT blended with organo phosphorous compounds cannot meet the industrial requirement for the UL-94 test even though the loading of organo phosphorous compounds were as high as 30 wt%.³¹⁴

BFRs are well-known for their superiority in fire safety. The growing interest for the BFR is their efficiency, good thermal stability under severe condition, and their contribution to reducing smoke toxicity. During combustion of a petroleum product (e.g. polymer) free radicals are generated. In the presence of a BFR, highly reactive free radicals, such as H[•], O[•], and OH[•] are substituted by less active bromine radical. The mechanism of inhibition process using BFRs can be described as follows:³¹⁵

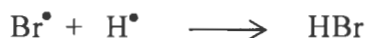


Chain propagation:

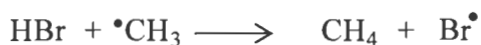
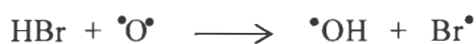
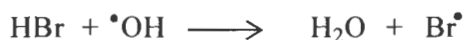




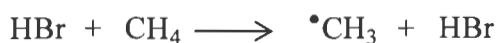
Inhibitor generation:



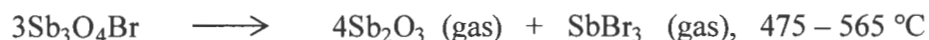
Inhibition:



Inhibitor regeneration:



Antimony trioxide is a well-known, and perhaps the most efficient, combustion decelerator when used in combination with halogenated flame retardants.³¹⁶ The efficiency of BFRs is synergized in the presence of antimony trioxide. Antimony trioxide enhances the efficiency of BFRs by enabling bromine to stay at the flame zone for longer time.³¹⁷ Antimony trioxide catalyzes the free-radical recombination and the formation of hydrogen bromide. During the combustion process, antimony trioxide in combination with BFR produces antimony bromide, an efficient gas phase inhibitor according to the following equations:³¹⁵

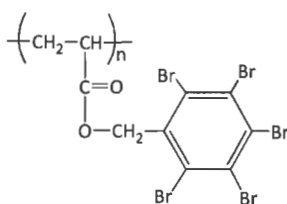


where, 'cond.' and 'gas' represent the condensed and gas phase respectively.

The evaluation of fire retardancy is carried out by various techniques, for example, the UL-94 test and cone calorimetry. UL-94 test is a small scale flame retardancy test for the flammability of plastic material. This test determines the sample's tendency to either self-extinguish or spread the flame once the specimen has been ignited. This is an important screening method of plastic acceptability with regards to its flammability behavior. In the vertical UL-94 test, a 1/2" × 5" specimen is held in the vertical position and flame is applied to its free end. The time necessary to self extinguish the flame after removal of the ignition source and the numbers of drips are counted. The three ratings, V-2, V-1, and V-0 (best) indicate that the sample was tested in a vertical position. The cone calorimeter measures an important parameter, the rate at which heat is released during combustion. From a cone calorimetry experiment, the mass loss rate and the total heat released are evaluated.³¹⁸⁻³²¹

Currently, there are a wide variety of commercially available BFRs most of which contain high levels of aromatic bromine. Typically, flame retardants (FRs) need to be added at a level of 5 – 20 weight percent to pass industry standards for flame retardancy.²²⁸

At this level of additive, the FR can have dramatic effects on physical and mechanical properties and processability of the plastic. As a result, the selection of a FR for a specific application often involves the influence of the FR on properties well beyond flammability. Polymeric BFRs possess better compatibility with plastics. Dead Sea Bromine Group has commercialized a polymeric brominated flame retardant, poly(pentabromobenzyl acrylate), PBrBA. The chemical structure of PBrBA is shown below:



PBrBA is especially suitable for engineering thermoplastics, nylon, PBT, PET, and styrenic copolymers.^{228, 290, 292, 299-300, 302, 305, 322-332} The advantages of PBrBA over other monomeric BFRs are:²²⁸ (1) non-blooming, (2) effective flame retardancy, (3) high temperature resistance, (4) good processability, (5) excellent compatibility with fiber reinforcement and polymer matrix, and (6) weather and chemical resistance.

PBrBA possesses 71 weight percentage of bromine and 30 weight percentage of polyacrylate. The polyacrylate part is a very effective processing aid in engineering polymers, such as polybutylene terephthalate (PBT) and nylons with and without glass reinforce.²²⁸ It lowers the melt viscosity significantly during injection molding enabling the production of large and complicated connectors with good surface finish.

In this research PBT was blended with PBrVE and the thermal, mechanical, and melt rheological properties were compared with an analogous blend prepared from PBT

and PBrBA. Next, the PBrVE was blended with PBT and Sb₂O₃ and the flame retardancy of this blend was evaluated with an analogous blend produced from PBT, PBrBA, and Sb₂O₃.

5.3. EXPERIMENTAL

5.3.1. Materials

Table 5.1 describes the starting materials used for the investigation. Unless specified otherwise, all materials were used as received.

Table 5.1. Chemicals used.

Chemical or Abbreviation	Description	Source
PBrVE	Polymer of 1,2,3,4,5-pentabromo-6-(2-(vinylloxy)ethoxy)benzene, produced using carbocationic polymerization	Synthesized previously (Intrinsic viscosity = 0.079 dL/g, T _g = 103 °C)
PBrBA (FR1025)	Polypentabromobenzyl acrylate, produced using free-radical polymerization	Dead Sea Bromine (Intrinsic viscosity = 0.032 dL/g, T _g = 160 °C)
PBT	Polybutylene terephthalate	SABIC
Sb ₂ O ₃	Antimony(III) oxide, powder, 5 μm, ReagentPlus [®] , 99%	Sigma-Aldrich

5.3.2. Polymer blend preparation

5.3.2.1. PBT/BFR Blends produced using melt extrusion process

Polymer blends were produced using a Leistritz Micro 18 GL-40 D co-rotating twin screw extruder. Table 5.2 lists the compositions of PBT-based blend. Dry blends of

polymers and additives were produced by manually shaking in a plastic bag. The dry blends were dried in an air oven at 100 °C for 12 hours before extrusion. Extrusion was done at a screw speed of 200 rpm. Table 5.3 lists the processing parameters of PBT-based blends. A Brabender[®] gravimetric feeder was used to control the feed rate of the extruder. Extruded polymer strands were cooled in a water bath and immediately pelletized using a chopper (Scheer-Bay BT 25) with a chopper speed of 230 rpm.

Table 5.2. Compositions of PBT-based blends produced from PBrVE and PBrBA.

Polymer	PBT (wt. %)	PBrVE (wt. %)	PBrBA (wt. %)	Sb ₂ O ₃ (wt. %)
PBT	100	--	--	--
PBT/PBrVE	90	10	--	--
PBT/PBrBA	90	--	10	--
PBT/Sb ₂ O ₃	97	--	--	3
PBT/PBrVE/Sb ₂ O ₃	89	8	--	3
PBT/PBrBA/Sb ₂ O ₃	89	--	8	3

Table 5.3. Parameters of melt extrusion process used to produce PBT-based blends.

Parameters	PBT-based blends		
	Set	PBT/PBrVE	PBT/PBrBA
Zone 1 (°C)	221	221	221
Zone 2 (°C)	232	232	232
Zone 3 (°C)	238	237	237
Zone 4 (°C)	238	237	237
Zone 5 (°C)	240	239	239
Zone 6 (°C)	243	242	242
Zone 7 (°C)	243	242	242
Gate adapter (°C)	238	237	237

5.3.2.2. Production of molded bars using injection molding process

Extruded granules were dried in an air oven at 100 °C overnight before using to a single plasticating screw injection molding (Techno Plas, 5080) to produce dumb-bell shaped specimens possessing a dimension according to ASTM D638 (type I). Additionally, rectangular shaped molded bars possessing a dimension of 158.7 mm × 12.7 mm × 3.2 mm were produced to conduct the Izod impact test, flexural test, and vertical burning test. Table 5.4 lists the processing parameters of PBT-based granules. As mentioned in Table 5.4, a nozzle temperature of 254 °C was maintained to process the PBT/PBrVE blend. On the contrary, for the PBT/PBrBA blend a nozzle temperature of 310 °C was necessary to avoid nozzle frosting.

Table 5.4. Parameters for injection molding process.

Parameters	PBT-based blends		
	Set	PBT/PBrVE	PBT/PBrBA
Barrel Zone 1 (°C)	254	254	254
Barrel Zone 2 (°C)	252	251	251
Barrel Zone 3 (°C)	246	245	245
Barrel Zone 4 (°C)	238	238	238

5.3.3. Instrumentation and procedures

5.3.3.1. Differential Scanning Calorimetry (DSC)

The thermal properties of extruded blends were determined using differential scanning calorimetry. The instrument utilized was a DSC Q1000 from TA Instruments, and sample sizes ranged from 4.5 to 5.5 mg. All PBT/BFR were subjected to a heat-cool-

heat cycle by first heating samples from 30 °C to 250 °C at a heating rate of 20 °C/minute (1st heat), holding at 250 °C for 3 minutes, cooling from 250 °C to 30 °C at a cooling rate of 20 °C/minute (cooling), holding at 30 °C for 5 minutes, and reheating from 30 °C to 250 °C at a heating rate 20 °C/minute (2nd heat).

5.3.3.2. Thermogravimetric Analysis (TGA)

TGA was carried out using a Q500 from TA Instruments. Samples sizes were 18 mg to 22 mg. Experiments were conducted by heating samples from 25 °C to 850 °C at a heating rate of 10 °C /min in an air atmosphere.

5.3.3.3. Measurement of mechanical properties - tensile test

Tensile test for dumb bell shaped specimens (ASTM D 638, type I) was carried out using an Instron 5567 (load frame displacement control) tensile tester fitted with a 30 KN load cell. The displacement rate of the movable clamp was set as 5 mm/minute. Data reported was the average of 5 replicate measurements.

5.3.3.4. Measurement of mechanical properties - flexural test

Flexural test for molded bars possessing a dimension of 158.7 mm × 12.7 mm × 3.2 mm was carried out using an Instron 5567 (load frame displacement control) fitted with a 2 KN load cell. The experiment was carried out according to the ASTM D790-03. The crosshead speed of the movable clamp was set as 1.4 mm/minute and the length of the support was 51.6 mm. Data reported was the average of 5 replicate measurements.

5.3.3.5. Measurement of mechanical properties - Izod impact test

Izod impact test for molded bars possessing a dimension of 158.7 mm × 12.7 mm × 3.2 mm was carried out according to the ASTM D256.

5.3.3.6. Transmission Electron Microscopy (TEM)

For TEM, thin films were cut from dumb-bell shaped specimen using a RMC MTXL ultramicrotome at room temp. Images were taken using a JEOL JEM-100 CX II electron microscope. ImageJ 1.43 software was used to calculate the area of dispersed domains.

5.3.3.7. Rheological properties

Specimens were created by melt pressing pellets into thin films of approximately 0.33 mm thickness using a heated press. Rheological properties were determined with an ARES Rheometer from TA Instruments. Frequency sweeps were generated by ramping frequency from 0.1 rad/s to 500 rad/s at a constant strain of 5% and two constant temperatures of 230 °C and 255 °C.

5.3.3.8. Flame retardant test-vertical burning

For PBT/Sb₂O₃ and PBT/Sb₂O₃/BFRs blends, molded bars possessing a dimension of 158.7 mm × 12.7 mm × 3.2 mm were produced using injection molding. Flame retardant test of these bars was conducted using Triton's flame test chamber that was built as per specifications of ASTM D-6413. The test set up was modified to get a close match to the UL-94 Vertical Burn test protocol (UL-94V). Testing was performed without preconditioning the samples. A detailed procedure is as follows: Samples were held vertically. Each sample was exposed to a flame of 10 seconds. As shown in Figure 5.1, the test specimen was held at one end in the vertical position at a height of 12 inches above the cotton. A burner flame (1.5 inches flame height using methane gas) was applied to the free end of the test specimen for a period of 10 seconds. The flame was then removed. The

following characteristics were recorded during 10 seconds flame exposure: (1) time to ignition, (2) time to self extinguish, and (3) nature of drips. For each blend, there are total four samples were tested.

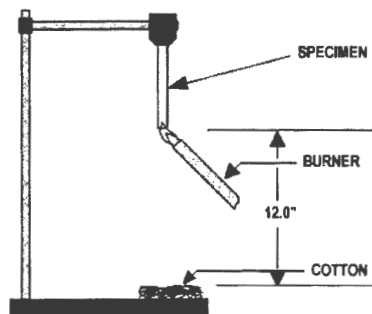


Figure 5.1. Schematic representation of flame test set up.

5.4. RESULTS AND DISCUSSION

Due to the high levels of bromination associated with BFRs, there generally is inherently poor compatibility between the matrix polymer and the BFR. For small molecule BFRs, this poor compatibility can lead to blooming of the FR. For polymeric BFRs, poor compatibility can lead to die swelling during extrusion and poor mechanical properties due to relatively high interfacial tension between BFR-rich domains and the matrix polymer. For applications requiring transparency, high interfacial tension between BFR-rich domains and the polymer matrix can result in dispersed-phase domain sizes large enough to scatter visible light which generates opacity.

PBT is a semicrystalline polymer and BFRs (PBrVE and PBrBA) are amorphous polymer. The interfacial tension between PBT and BFR phases in PBT/BFR blends is

usually high due to the difference in the densities of crystalline and amorphous phases. Higher interfacial tension between two phases leads to poor dispersion of phases and reduces mechanical strength of blend. The free energy of mixing (ΔG_{mix}) of PBT and BFRs interfaces is positive. Otherwise, molecular mixing of PBT and BFRs phases would continue to competition and at the equilibrium the interfaces would vanish. The interfacial tension and the interface density across the interface are the key factor for predicting the thermal and mechanical properties of PBT/BFRs blends.³³³⁻³³⁴ The presence of small molecules weakens the interface mechanically. Since, PBrVE has higher molecular weight than the PBrBA; the improved compatibility between PBT and PBrVE phases will result better dispersion of PBrVE in PBT.

Reiter et al.³³⁵ studied the effect of molecular weight distribution on the immiscible polymer blend interface. They found that the lower molecular weight fractions (short chains) preferentially accumulate at the interface. Presences of shorter chains (oligomers) at the interface weaken the integrality of polymer blend, because shorter chains have fewer interactions with neighboring larger chains. The commercially available PBrBA is synthesized using a free radical polymerization of BrBA (2,3,4,5,6-Pentabromobenzyl acrylate). In contrast to the relatively longer life time of a propagating carbocation in cationic polymerization, the life time of a propagating free radical is very short in free radical polymerization which leads to a polymer with broad molecular weight distribution. Moreover, the molecular weight of PBrVE ($[\eta] = 0.079 \text{ dL/g}$) is much higher than that of PBrBA ($[\eta] = 0.037 \text{ dL/g}$). Considering the higher molecular weight and relatively narrow molecular weight distribution, PBrVE is expected to be more compatible with large PBT

molecule. Thus, due to the better dispersion of PBrVE and PBT phases, the mechanical performance of PBT/PBrVE blend should be better than that of PBT/PBrBA blend.

5.4.1. Measurement of thermal properties of PBT and PBT/BFRs blends

Figure 5.2.A shows the plot of heat flow as a function of temperature for PBT and PBT/BFR blends when the second heating cycle was selected from DSC thermograms. The melting temperatures and the heat of melting were calculated from these graphs. Figure 5.2.B shows the plot of heat flow as a function of temperature when the first cooling cycle was selected from DSC thermograms. The heat of crystallization and crystallization points were calculated from these graphs. The data obtained from these thermograms are listed in Table 5.5. Each data reported is the average of 3 replicate measurements. The heat of melting (ΔH_m) and heat of crystallization (ΔH_c) of PBT and PBT/BFR blends were calculated after integrating the area under peak. Data obtained from Table 5.5 shows that the ΔH_m of neat PBT was reduced by 2% and 5.4% due to the addition of PBrVE and PBrBA respectively.

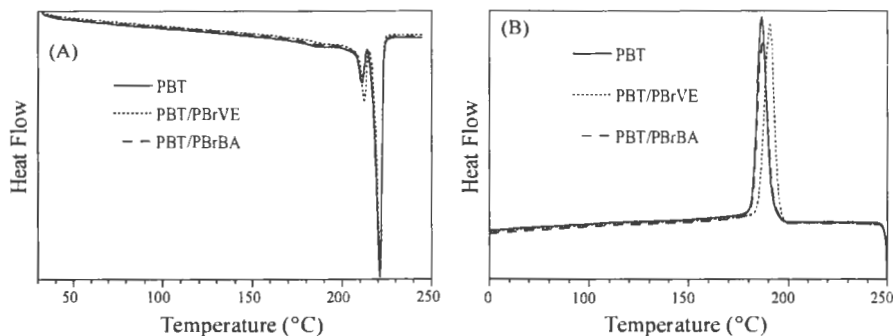


Figure 5.2. DSC thermograms obtained from (A) second heating and (B) first cooling for PBT, PBT/PBrVE, and PBT/PBrBA.

Table 5.5. Data obtained from DSC thermograms of PBT, PBT/PBrVE, and PBT/PBrBA.

Blends		ΔH_m	T_{m1}	T_{m2}	ΔH_c	T_c
		(J/g)	(°C)	(°C)	(J/g)	(°C)
PBT	Average	48.3	211.2	221.3	57.9	186.8
	Standard Deviation	0.75	0.15	0.17	0.81	0.21
PBT/PBrVE	Average	47.3	211.8	221.3	55.8	189.9
	Standard Deviation	0.25	0.37	0.13	0.23	0.86
PBT/PBrBA	Average	45.7	210.7	220.9	54.5	186.7
	Standard Deviation	0.48	0.18	0.22	0.41	0.34

The possible reason could be the difference in the extent of phase miscibility of BFRs with the PBT. Due to the lower interfacial tension between PBT and PBrVE phases, the property of PBT/PBrVE blend is close to that of pure PBT. Additionally, agglomeration of PBrBA phases, caused by the poor interaction between PBT and PBrBA phases, results in the formation of larger domains in PBT/PBrBA blend.

5.4.2. Thermogravimetric analysis of PBT, PBT/PBrVE, and PBT/PBrBA

TGA was performed in an air-oxidative environment with a constant increase in temperature. Figure 5.3 shows the plot of weight percentage as a function of temperature for PBT and PBT/BFR blends when the samples were heated at a constant heating rate. From the thermograms, three important parameters, for example, the decomposition temperature (T_0), onset temperature (T_{onset}), and ash content are listed in Table 5.6. The T_0 can be defined as the temperature of the maximum weight loss rate (dm/dt_{max}). The T_{onset} can be considered as the point when decomposition just begins. The thermal stability of plastic compositions is an important property that can affect processability.

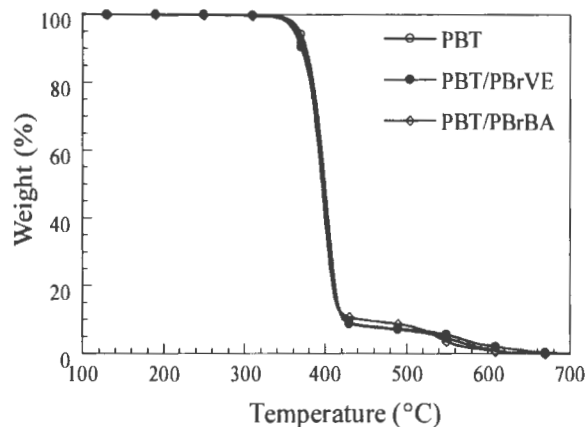


Figure 5.3. TGA thermograms obtained for pure PBT, PBT/PBrVE, and PBT/PBrBA in an air atmosphere.

Table 5.6. Values of the T_{onset} , T_0 , and ash content for pure PBT, PBT/PBrVE, and PBT/PBrBA.

BFRs	T_{onset} (°C)	T_0 (°C)	Wt. % remaining at 430 °C	Ash content (Wt. %) at 700 °C
PBT	380.4	401.9	8.7	0.01
PBT/PBrVE	376.6	400.2	9.1	0.01
PBT/PBrBA	376.6	396.9	10.7	0.08

As shown in Table 5.6, the T_{onset} of PBT/BFRs blend was slightly lower than that of pure PBT. This can be explained by the fact that the onset temperatures of PBrVE and PBrBA were 51.9 °C and 54.2 °C lower than that of pure PBT. However, the decomposition temperature (T_0) of PBT/PBrVE blend was slightly higher than that of PBT/PBrBA blend. Since, the ether linkage in PBrVE is thermally stable than the ester linkage in PBrBA, the T_0 of the PBT/PBrVE blend is slightly higher than that of PBT/PBrBA blend.

5.4.3. Tensile testing of PBT/BFRs and PBT/BFRs/Sb₂O₃ blends

In order to determine the effect of BFRs on the mechanical properties of neat PBT and PBT/Sb₂O₃, tensile tests were carried out. Figure 5.4.A shows the plot of tensile stress as a function of tensile strain for PBT and PBR/BFRs blends. Figure 5.4.B shows the plot of tensile stress as a function of tensile strain for PBT/Sb₂O₃ and PBT/Sb₂O₃/BFRs blends. Table 5.7 lists the data obtained from tensile testing of blends. From the tensile test, the following five important parameters are obtained: (1) Young's modulus, (2) tensile stress at yield, (3) maximum tensile stress, (4) toughness, and (5) % of elongation. Young's modulus is calculated from the region of the tensile stress versus tensile strain plot, where the material behaves as a perfect elastic body. Young's modulus (E) can be written as:

$$E = \sigma / \varepsilon$$

where, σ and ε are the tensile stress and strain respectively. The Young's modulus is a fundamental measurement of material stiffness. The higher the value of E, the more resistance the material is to be stretched. Toughness is measured by the area under the stress-strain curve. The area has the unit of energy per unit volume and the work necessary to deform the material is the toughness. The deformation may be elastic or non-elastic (permanent). The Young's modulus of the PBT and PBT/BFRs blends were calculated from the initial slope of the stress-strain graph. A tough plastic, such as polybutylene terephthalate, exhibits a yield point followed by extensive elongation at almost constant stress. This is called the plastic flow which happens in the non-linear viscoelastic region. Extension at a constant stress in the plastic flow region is called as cold drawing. The cold drawing begins with necking which is defined as the narrowing down a portion of the

material to a smaller cross-section. The neck grows at the expense of the consumption of the entire sample at either end.³³⁶

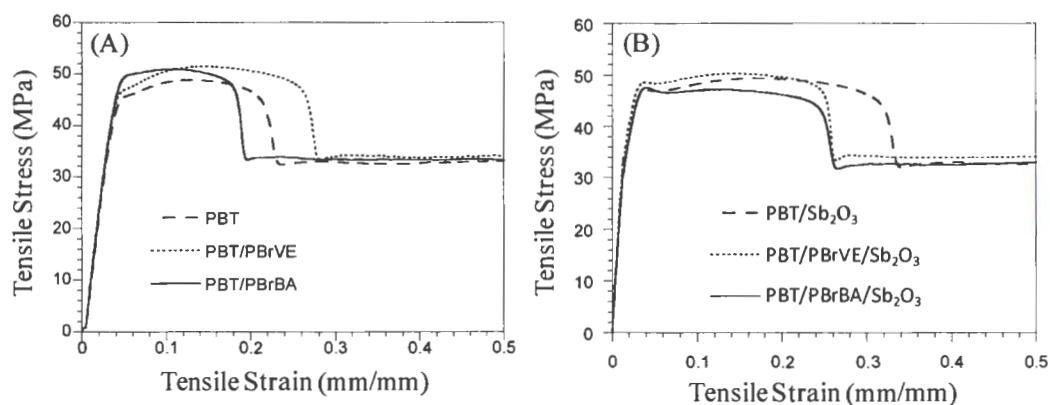


Figure 5.4. Plot of tensile stress as a function of tensile strain for (A) PBT, PBT/PBrVE, and PBT/PBrBA; and (B) PBT/Sb₂O₃, PBT/Sb₂O₃/PBrVE, and PBT/Sb₂O₃/PBrBA.

Data obtained from Table 5.7 shows that for PBT/BFR blends, the addition of PBrVE and PBrBA increased the Young's modulus of neat PBT by 5.3% and 2.3% respectively. Moreover, due to the better compatibility between PBT and PBrVE, the values of toughness at the yield and maximum tensile stress are higher for PBT/PBrVE. Antimony trioxide (Sb₂O₃) is a reinforcing filler for PBT. In addition to Sb₂O₃, PBrVE increased the modulus of PBT/Sb₂O₃ blend by 11.1%, whereas PBrBA reduced the modulus by 4.4%. Due to addition of less compatible PBrBA to PBT/Sb₂O₃, PBrBA forms relatively larger glassy domains which reduce the modulus of PBT/Sb₂O₃. Orientation of the semicrystalline polymer is more important than the glassy, amorphous polymer. The addition of PBrVE increased the tensile stress at yield for PBT/Sb₂O₃ by 3.8%, where as it remained constant after the incorporation of PBrBA. However, the toughness of

PBT/Sb₂O₃/PBrVE and PBT/Sb₂O₃/PBrBA blends at yield points were essentially the same as PBT/Sb₂O₃. The percentages of elongation for all of the blends exceed a value of 50% which is common for a tough plastic.³³⁶

Table 5.7. Data obtained from tensile test for PBT, PBT/PBrVE, and PBT/PBrBA samples with and without Sb₂O₃.

Sample		Young's modulus (MPa)	Tensile stress at yield (offset 0.2 %) (MPa)	Energy at yield (offset 0.2 %) (J)	Maximum tensile stress (MPa)	Energy at maximum tensile stress (J)	Percent elongation (%)
PBT	Average ± SD	1461.2 ± 39.9	33.9 ± 1.1	1.21 ± 0.08	48.28 ± 0.61	13.65 ± 1.7	> 50
PBT/PBrVE	Average ± SD	1538 ± 24.9	34.7 ± 1.4	1.2 ± 0.1	51.44 ± 0.13	15.7 ± 0.6	> 50
PBT/PBrBA	Average ± SD	1495.1 ± 35.7	33.7 ± 1.8	1.18 ± 0.1	49.91 ± 1.11	12.3 ± 1.3	> 50
PBT/Sb ₂ O ₃	Average ± SD	2768.5 ± 52.7	31.12 ± 0.36	0.45 ± 0.01	49.6 ± 0.14	15.5 ± 0.3	> 50
PBT/Sb ₂ O ₃ /PBrVE	Average ± SD	3074 ± 108.8	32.3 ± 1.1	0.42 ± 0.03	50.1 ± 0.4	12.65 ± 0.5	> 50
PBT/Sb ₂ O ₃ /PBrBA	Average ± SD	2645.6 ± 138.5	31.2 ± 0.55	0.47 ± 0.04	47.8 ± 0.3	2.64 ± 0.05	> 50

5.4.4. Flexural testing of PBT/Sb₂O₃/BFR blends

In order to determine the effect of BFRs on the mechanical properties of the neat PBT/Sb₂O₃ blends, flexural tests were carried out. Figure 5.5 shows the plot of flexural stress as a function of flexural strain for neat PBT/Sb₂O₃ and PBT/Sb₂O₃/BFR blends. Table 5.8 shows the mechanical properties for all blends measured by flexural testing. Due

to the addition of PBrVE, the maximum flexural strength of PBT/Sb₂O₃ blend was increased by 2%, whereas it was the same when PBrBA was added. Moreover, PBrBA reduced the modulus of elasticity of PBT/Sb₂O₃ blend by 5%. The non-reinforcing nature of PBrBA for the PBT/Sb₂O₃ blend also confirmed with the results obtained from tensile testing. PBT being more compatible with PBrVE than PBrBA, a higher degree of dispersion was achieved for PBT/Sb₂O₃/PBrVE. The inferior compatibility between PBrBA and PBT phases causes the reduction in the modulus of elasticity of PBT/Sb₂O₃/PBrBA.

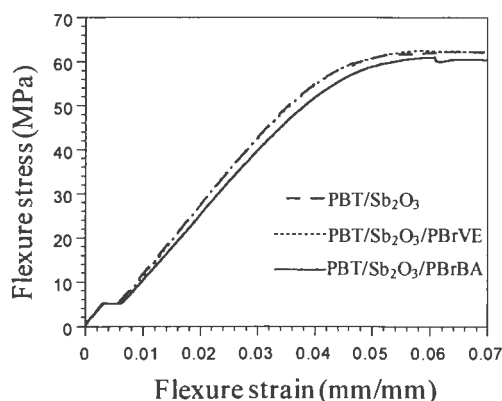


Figure 5.5. Plot of flexural stress as a function of flexural strain for PBT/Sb₂O₃, PBT/Sb₂O₃/PBrVE, and PBT/Sb₂O₃/PBrBA.

Table 5.8. Data obtained from flexural test for PBT/Sb₂O₃, PBT/Sb₂O₃/PBrVE, and PBT/Sb₂O₃/PBrBA.

Sample		Modulus of Elasticity (MPa)	Maximum Flexural Strength (MPa)
PBT/Sb ₂ O ₃	Average ± SD	1582.2 ± 63.6	61.2 ± 0.6
PBT/Sb ₂ O ₃ /PBrVE	Average ± SD	1581.2 ± 31.4	62.6 ± 0.6
PBT/Sb ₂ O ₃ /PBrBA	Average ± SD	1506.2 ± 33.5	61.8 ± 1.3

5.4.5. Izod impact testing of PBT/Sb₂O₃ and PBT/Sb₂O₃/BFR blends

To determine the effect of BFRs on the mechanical properties of PBT/Sb₂O₃ blend, Izod impact tests were carried out. Table 5.9 lists the data obtained from the experiment. Impact resistance is the energy required to fracture a sample when struck with a sharp blow. Data obtained from Table 5.9 shows that after addition of PBrVE and PBrBA to PBT/Sb₂O₃, the impact strength increased by 4.4% and 1.5% respectively. Toughening of PBT/Sb₂O₃ blend due to the addition of BFRs could be explained by the formation of crazes by the BFR domains and shear yielding which absorbs energy locally.

Table 5.9. Izod impact strength data for PBT/Sb₂O₃, PBT/Sb₂O₃/PBrVE, and PBT/Sb₂O₃/PBrBA.

Sample		Impact Strength (KJ/m ²)
PBT/Sb ₂ O ₃	Average ± SD	2.75 ± 0.26
PBT/Sb ₂ O ₃ /PBrVE	Average ± SD	2.87 ± 0.11
PBT/Sb ₂ O ₃ /PBrBA	Average ± SD	2.79 ± 0.19

5.4.6. Comparison of the rheological properties of a PBT/PBrVE blend to a PBT/PBrBA blend

For PBT and PBT/BFR blends, frequency sweeps were generated at two constant temperatures of 230 °C and 255 °C. Figures 5.6.A and 5.6.B display melt viscosity as a function of frequency at 230 °C and 255 °C, respectively. At 230 °C, which is just 10 °C above the PBT melting temperature, the blend containing 10 wt. % PBrVE showed significant shear sensitivity that was not observed with either pure PBT or the blend

containing PBrBA. At high frequency (i.e. ~ 500 rad/s), the melt viscosity of the PBT/PBrVE blend was 57 % lower than that of either pure PBT or the PBT/PBrBA blend. This high shear sensitivity observed for PBT/PBrVE would be expected to enhanced processability with regard to creating injection molded parts with relatively thin walls, such as those encountered in the electronics industry. At 255 °C, the melt viscosity of the PBT/PBrVE blend was approximately 33 % lower than the PBT/PBrBA blend over the entire frequency range and approximately 53 % lower than PBT. The lower viscosity of the PBT/PBrVE blend can be largely attributed to both the lower T_g and melt flow temperature of PBrVE as compared to PBrBA.

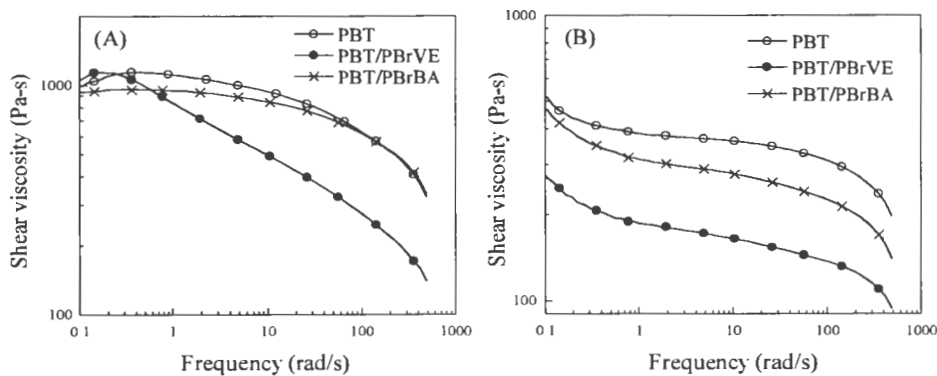


Figure 5.6. Shear viscosity as a function of frequency for PBT, PBT/PBrVE, and PBT/PBrBA at (A) 230 °C and (B) 255 °C.

5.4.7. Comparison of the morphology of a PBT/PBrVE blend to a PBT/PBrBA blend

To investigate the difference in blend compatibility associated with the use of PBrVE as opposed to PBrBA, the morphology of the PBT/BFR blends were characterized using transmission electron microscopy (TEM). Figure 5.7 shows the TEM micrographs of

the PBT/PBrVE and PBT/PBrBA blends. As shown in Figure 5.7, the dispersed phases of the PBT/PBrVE blend appear to be somewhat smaller than the dispersed phases of the PBT/PBrBA blend suggesting lower interfacial tension between PBT and PBrVE as compared to PBT and PBrBA. From the TEM images, the average dispersed phase size was determined. The results showed that the areas of the PBrVE domains in the PBT/PBrVE blend were 27 % smaller than the PBrBA domains in the PBT/PBrBA blend.

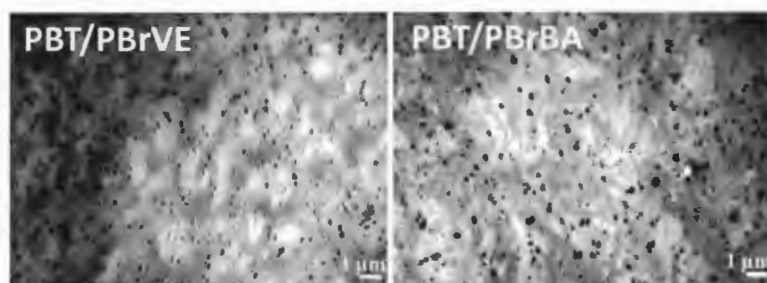


Figure 5.7. TEM micrographs of the PBT/PBrVE and PBT/PBrBA blends.

5.4.8. Flame retardancy testing for PBT/Sb₂O₃, PBT/Sb₂O₃/PBrVE, and PBT/Sb₂O₃/PBrBA blends using a vertical burn test

To investigate the difference in fire safety associated with the use of PBrVE as opposed to PBrBA, the flame retardancy tests were conducted for PBT/Sb₂O₃ and PBT/Sb₂O₃/BFR blends. From the flame retardancy test, the values of three important parameters are listed in Table 5.10: (1) time to ignition, (2) time to self extinguish, and (3) nature of drips. Time to ignite is the time for the test specimen to ignite in seconds during each flame exposure. The time to self-extinguish is the duration (seconds) of flaming combustion of the test specimen after the flame exposure. The nature of drips is the

occurrence of flaming drips during the flaming combustion of the test specimen. If the drips do not ignite the cotton they are classified as non-flaming drips and if the drips ignite the cotton they were classified as flaming drips.

Table 5.10. Results obtained from vertical burn flame retardant test for PBT/Sb₂O₃ and PBT/Sb₂O₃/BFR blend.

Blends	Time to ignition (s)	Time to self extinguish (s)	Nature of drips
PBT/Sb ₂ O ₃ -S1	7	3	Flaming
PBT/Sb ₂ O ₃ -S2	4	3	Flaming
PBT/Sb ₂ O ₃ -S3	5	>60	Flaming
PBT/Sb ₂ O ₃ -S4	6	>60	Flaming
Average Value ± SD (PBT/Sb ₂ O ₃)	5.5 ± 1.3	3 ± 0	
PBT/PBrBA/ Sb ₂ O ₃ -S1	4	0	No drips
PBT/PBrBA/ Sb ₂ O ₃ -S2	6	0	No drips
PBT/PBrBA/ Sb ₂ O ₃ -S3	6	0	No drips
PBT/PBrBA/ Sb ₂ O ₃ -S4	6	0	No drips
Average Value ± SD (PBT/PBrBA/Sb ₂ O ₃)	5.5 ± 1	0	
PBT/PBrVE/ Sb ₂ O ₃ -S1	6	0	Non- flaming
PBT/PBrVE/ Sb ₂ O ₃ -S2	4	0	Non-flaming
PBT/PBrVE/ Sb ₂ O ₃ -S3	6	0	Non-flaming
PBT/PBrVE/ Sb ₂ O ₃ -S4	6	0	No drips
Average Value ± SD (PBT/PBrVE/Sb ₂ O ₃)	5.5 ± 1	0	

For each blend there are total four samples (S1 to S4) were tested. Data obtained from Table 5.10 shows that after the flame exposure, both the PBT/PBrVE/Sb₂O₃ and PBT/PBrBA/Sb₂O₃ blends were able to self-extinguish almost immediately (time = 0

second). Additionally, none of the drips produced from PBT/PBrVE/Sb₂O₃ and PBT/PBrBA/Sb₂O₃ blends were flaming. Since, the bromine is the major part for a flame retardant, there is no restriction on the chemical structure to be an efficient flame retardant until the percentage of bromine is the same. PBrVE and PBrBA have essentially the same percentage of bromine (71%).

5.5. CONCLUSION

The novel PBrVE was blended with an engineering thermoplastic polymer, PBT and the thermal, mechanical, and viscoelastic properties were evaluated and compared to an analogous blend prepared from PBrBA and PBT. Thermogravimetric analysis showed the thermal stability of the PBT/BFR blends was essentially the same as that of pure PBT. Result obtained from TEM images indicated that the PBT is more compatible with the higher molecular weight PBrVE than the oligomeric PBrBA. Blending PBrVE with PBT resulted in lower melt viscosity and better blend compatibility than an analogous blend based on PBrBA. Additionally, BFRs were blended with PBT/Sb₂O₃; and flame retardancy and mechanical properties were compared. Data obtained from tensile and flexural tests showed that for PBT/Sb₂O₃ blend, PBrVE and PBrBA can be considered as reinforcing filler and non-reinforcing filler, respectively. Results obtained from the flame tests showed that the flame retardancy of PBT/Sb₂O₃/BFR blends were the same. These results indicate that PBrVE may have utility for the development of FR plastics with improved processability, impact and, perhaps, improved optical properties.

CHAPTER 6. COATINGS DERIVED FROM NOVEL, SOYBEAN OIL-BASED POLYMERS PRODUCED USING LIVING CARBOCATIONIC POLYMERIZATION

6.1. ABSTRACT

A process was developed to obtain vinyl ether-functional monomers containing fatty acid pendent groups directly from soybean oil (SBO) using base-catalyzed transesterification. In addition, a carbocationic polymerization process was developed for the vinyl ether monomers that allowed for high molecular weight polymers to be produced without consuming any of the vinyl groups present in the fatty acid portion of the monomers. Compared to SBO, which possesses on average 4.5 vinyl groups per molecule, the polyvinylethers based on the soybean oil-derived vinyl ether monomers (polyVESFA) possess tens to thousands of vinyl groups per molecule depending on the polymer molecular weight produced. As a result of this difference, coatings based on polyVESFA were shown to possess much higher crosslink density at a given degree of functional group conversion compared to analogs based on conventional SBO. In addition, the dramatically higher number of functional groups per molecule associated with polyVESFA results in gel-points being reached at much lower functional group conversion, which was shown to dramatically reduce cure-time compared to SBO-based analogs. Based on the results obtained, it appears that these new renewable materials may have tremendous commercial utility in the coatings industry.

6.2. INTRODUCTION

At present, organic chemicals are almost entirely derived from building blocks that are obtained from natural gas, petroleum, and coal.³³⁷ Approximately 13 percent of the crude oil used in the United States currently goes into the production of nonfuel chemicals.³³⁸ Since fossil resources are limited, there is an ongoing need to develop useful chemicals from renewable resources. Renewable resources that have been used to produce chemicals include plant oils, polysaccharides, sugars, and wood. Of these, plant oils are the most important renewable raw materials for the chemical industry.³³⁹ Chemicals derived from plant oils have been used to produce surfactants, components for cosmetics, lubricants, polymers, coatings, and flooring materials. The utility of a plant oil for a given application depends on the composition of the fatty acids contained in the oil. The most important molecular parameters of the fatty acids are the stereochemistry of the double bonds, their degree of unsaturation, and the length of the carbon chain. With regard to the length of the carbon chain, coconut oil and palm kernel oil are particularly suited for the production of surfactants and cosmetics because they possess relatively high fractions of short and medium chain length (mainly 12 and 14 carbon atoms) fatty acids; while soybean, rapeseed, and sunflower oil, which possess longer chain fatty acids (18 carbon atoms), are used in polymer and lubricant applications.³³⁹ The nature of the unsaturation is of paramount importance for coating applications since the double bonds are the functional groups responsible for the formation of crosslinks during coating film formation. The degree of unsaturation is typically expressed by the iodine value (i.e. amount of iodine in grams that can react with double bonds present in 100 g of sample). Based on iodine value,

plant oils are divided into three classes, namely, drying (iodine value > 150), semi-drying ($120 < \text{iodine value} < 150$), and non-drying (iodine value < 120). In the 1950s, the most common plant oil used in paint formulations was linseed oil.³⁴⁰ Since this time, the volume of linseed oil has declined while the volume of soybean oil (SBO) has increased to the extent that it is now the predominant plant oil used in the coatings industry.³⁴¹ SBO, classified as a “semi-drying” oil, is comprised of both saturated and unsaturated fatty acids. The unsaturated fatty acids include 9% alpha-linolenic acid, 51% linoleic acid, and 25% oleic acid, and the saturated fatty acids include 4% stearic acid and 11% palmitic acid.³⁴²

Historically, crosslinking with coatings based on plant oils was achieved by a process referred to as autoxidation. The mechanism of crosslinking with autoxidation has been studied in detail using Fourier transform infrared (FTIR) spectroscopy and other spectroscopic techniques.³⁴³⁻³⁴⁶ The process starts with the abstraction of a bisallylic hydrogen atom, trapping of the radical by oxygen, and subsequent hydrogen abstraction to form hydroperoxides. A variety of crosslinks including those that generate new alkyl, ether, and peroxy groups are formed by the various radical coupling reactions involved in autoxidation. The double bonds present in the fatty acid portion of plant oils have been derivatized to enable other mechanisms of crosslinking beyond autoxidation. The most common derivatization involves conversion of the double bonds to epoxide groups.³⁴⁷ Epoxidized plant oils have been used to generate thermoset coatings using the common methods of curing epoxide-functional resins such as with amines,³⁴⁸⁻³⁴⁹ anhydrides,³⁵⁰ and cationic photocure.³⁵¹⁻³⁵³ Epoxidized plant oils have been further derivatized by reaction of the epoxide groups with both acrylic acid to produce acrylate-functional plant oils^{339, 354-355}

and methanol to produce polyol functional plant oil.³⁵⁶⁻³⁵⁷ Vulcanized vegetable oil (VVO) has been used in rubber industry for a long time as valuable processing aid.³⁵⁸⁻³⁵⁹ The double bonds present in the fatty acid portion of plant oils can easily be crosslinked with sulfur to form VVO.³⁶⁰

A primary drawback associated with the use of plant oil-based materials for many coating applications is their relatively high molecular mobility which leads to relatively low glass transition temperatures (T_g) and low modulus. As a means to increase thermo-mechanical properties of plant oil-based coatings, it was of interest to produce novel polymers in which the pendent groups of the polymers contain plant oil-derived fatty acids. As shown schematically in Figure 6.1, the primary difference in polymers possessing the molecular architecture of interest to that of the natural plant oil triglyceride is the number of functional groups per molecule. For example, if the average number of double bonds per triglyceride for a given plant oil is “X,” then the number of double bonds for a corresponding polymer derived from that same plant oil would be $DPX/3$ where “DP” is the degree of polymerization for the polymer. For SBO, the average number of double bonds per triglyceride is 4.5. Thus, polymers of interest derived from SBO possessing DPs of 10, 50, 100, 500, and 1,000 would possess on average 15, 75, 150, 750, and 1500 double bonds per polymer molecule, respectively. The benefit of having higher numbers of functional groups per molecule is that, at a given degree of functional group conversion, crosslink density will be higher. Thus, at a given functional group conversion, thermo-mechanical properties would be expected to increase with increasing polymer molecular weight. To further illustrate the difference in crosslink network formation for the polymers

of interest to their corresponding plant oil, theoretical gel points (p_c) were calculated using a modification of the equation shown below, which was derived by Flory.³⁶¹

$$p_c = 1/[1 + (f - 2)]^{1/2} \quad (I)$$

This equation applies to a blend of a multifunctional precursor with an average number of functional groups per molecule of “ f ” and a difunctional precursor. The functional groups present on the multifunctional precursor can only react with the functional groups of the difunctional precursor and vice-versa (i.e. precursors cannot react with themselves). In addition, the equation applies to a blend involving a stoichiometric ratio of functional groups. Figure 6.2 shows the relationship between theoretical gel point (i.e. degree of conversion that results in the production of a crosslinked network) and DP of polymers possessing a fatty acid pendent group in the repeat unit. To generate this plot, equation (I) was modified by substituting $DP\gamma$ for f where γ is the average number of functional groups per fatty acid pendent group. From Figure 6.2, it can be seen that increasing DP of a polymer possessing a fatty acid pendent group dramatically decreases the gel-point. Even the use of short oligomers with a DP around 10 can be used to generate a crosslinked network at relatively low functional group conversion. This analysis illustrates that increasing the number of functional groups per molecule enables shorter cure times and higher crosslink densities at a given extent of conversion. This characteristic was expected to be very useful considering the fact that complete conversion of functional groups is often not possible due to reaction kinetic considerations as well as energy input/cost limitations associated with some curing processes. In addition, this concept could be used to enable useful coating materials to be produced from non-drying

oils, such as castor, almond, peanut, and olive oil, and faster curing materials from semi-drying oils, such as corn, cotton seed, and sesame oil.

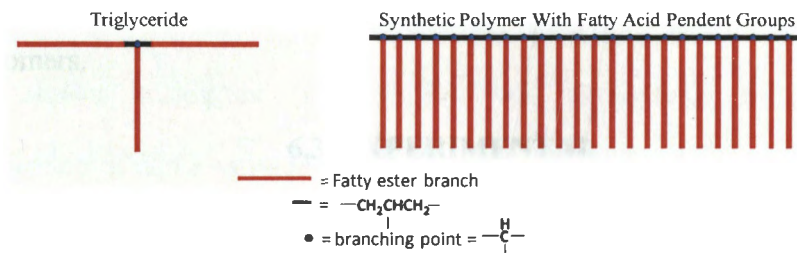


Figure 6.1. A schematic illustrating the difference in molecular architecture between a plant oil triglyceride and a synthetic polymer containing a fatty acid pendent group in the repeat unit.

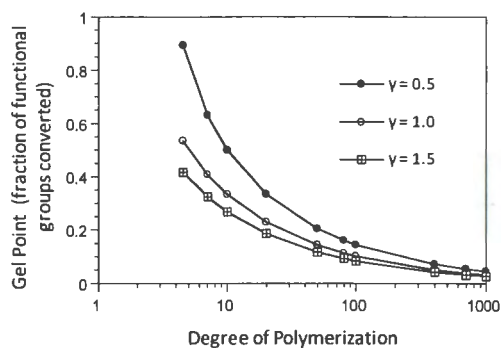


Figure 6.2. The relationship between theoretical gel-point (i.e. degree of conversion that results in the production of a crosslinked network) and DP of polymers possessing a fatty acid pendent group in the repeat unit. To generate this plot, equation (I) was modified by substituting $DP\gamma$ for f where γ is the average number of functional groups per fatty acid pendent group.

This document describes the synthesis of vinyl ether-functional monomers (VESFA) containing fatty acid pendent groups directly from soybean oil. A carbocationic polymerization process was developed for VESFA that allowed for high molecular weight polymers. The utility of this polymer in coating compositions was investigated by

comparing properties to analogous coatings derived from conventional SBO. In addition, a copolymer of VESFA and vinyl ether-functional polyethylene glycol monomer (VEPEG) was produced without consuming any of the vinyl groups present in the fatty acid portion of the monomers.

6.3. EXPERIMENTAL

6.3.1. Materials

Table 6.1 describes the starting materials used for the investigation. Unless specified otherwise, all materials were used as received.

Table 6.1. A list of the starting materials used for the investigation.

Chemical name	Description	Source
SBO	Soybean oil, RBD (technical grade)	Cargill
EGVE	Ethylene glycol vinyl ether, > 95%	TCI America
PEGMVE (R500)	Polyethylene glycol monovinylether, Molecular weight = 550 g/mole (approx.)	Clariant
IE (Iodoethane)	ReagentPlus [®] , 99%	Sigma-Aldrich
KOH	Potassium hydroxide, ≥ 85%	Sigma-Aldrich
Et _{1.5} AlCl _{1.5}	Ethylaluminum sesquichloride (25 wt. % in toluene)	Sigma-Aldrich
MCAc	Methyl chloroacetate, 99%, Distilled over calcium hydride before use	Sigma-Aldrich
Toluene	ACS grade, 99.5%	EMD Chemicals
MeOH	Methanol, ≥ 99.8 %	Sigma-Aldrich
n-hexane	ACS grade, 98.5%	VWR
Magnesium sulfate	Anhydrous, ReagentPlus [®] , ≥99.5%	Sigma-Aldrich
CDCl ₃	Deuterated chloroform, 99.9%	Sigma-Aldrich
D ₂ O	Deuterium Oxide, 99.8%	TCI America
Cobalt octoate	Cobalt 2-ethylhexanoate, 12% Cobalt	OMG Americas
Zirconium octoate	Zirconium 2-ethylhexanoate, 18% Zirconium	OMG Americas
Nuxtra [®] Zinc	Zinc carboxylate in mineral spirits, 8%	Dura Chemicals
Stearic acid	Reagent grade, 95%	Sigma-Aldrich
ZnO	Zinc Oxide powder, >99%	Sigma-Aldrich
S	Sulfur Powder, precipitated, 99.5%	Alfa-Aesar
TMTD	Tetramethylthiuram disulfide, 97%	Sigma-Aldrich

6.3.2. Synthesis of the vinyl ether of SBO fatty acids (VESFA) and polymer of VESFA (polyVESFA)

6.3.2.1. Synthesis of the VESFA

As shown in Figure 6.3, VESFA was synthesized using base-catalyzed transesterification of SBO with ethylene glycol vinyl ether (EGVE). A detailed procedure is as follows: 20 g of SBO, 20 g of EGVE, and 0.56 g of anhydrous KOH were added to a two-neck, 100 ml, round-bottom flask and stirred at 70 °C for 3 hours under a blanket of nitrogen. Next, the reaction mixture was cooled down to room temperature and diluted with 120 ml of n-hexane. The hexane layer was washed once with 30 ml acidic, deionized water (pH 4.0) and then multiple times with pure deionized water until the wash water was neutral. The hexane layer was then dried with magnesium sulfate. The product was recovered by rotary evaporation of the n-hexane and drying under vacuum (15 – 20 mm of Hg) overnight.

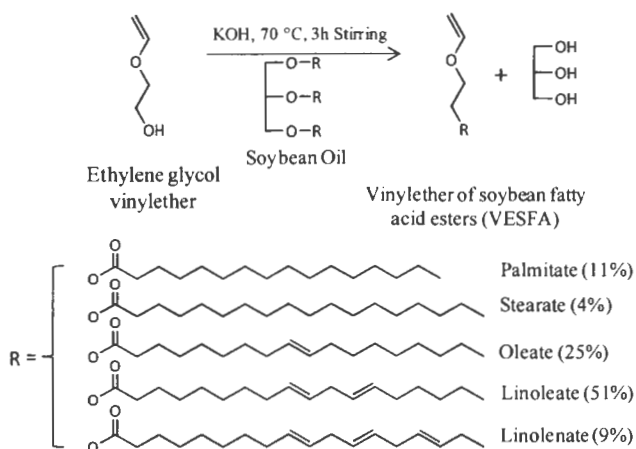


Figure 6.3. The synthetic scheme used to produce VESFA.

6.3.2.2. Synthesis of the polyVESFA

PolyVESFA was prepared using living cationic polymerization as shown in Figure 6.4. The cationogen, 1-isobutoxyethyl acetate (IBEA), was prepared using the procedure of Aoshima and Higashimura.³⁶ The polymerization solvent, toluene, was dried over calcium hydride before use. A detailed polymerization procedure is as follows: Prior to use, VESFA was dried with magnesium sulfate. The dry VESFA was polymerized at 0 °C within a glove box in a three-neck, round-bottom flask baked at 200 °C prior to use. 23.4 mg of initiator (i.e. IBEA) and 256 g of VESFA ($[\text{VESFA}]_0:[\text{IBEA}]_0 = 5000:1$) were dissolved in 1600 ml of dry toluene and chilled to 0 °C. The polymerization was initiated by the addition of 36.05 ml of ethylaluminum sesquichloride solution (25 wt. % in toluene) ($[\text{VESFA}]_0:[\text{Et}_{1.5}\text{AlCl}_{1.5}]_0 = 200:18$). The reaction was terminated after 17 hours by the addition of 1600 ml of chilled methanol which caused the polymer to precipitate. The polymer was isolated and washed multiple times with methanol. The purified polymer was collected as a viscous liquid after centrifuging at 4500 rpm at 21 °C for 10 minutes and drying under vacuum (5 – 7 mm of Hg) overnight.

6.3.2.3. Kinetic study of the polymerization of VESFA

6.3.2.3.1. Determination of the effect of an external base (MCAc) and a co-initiator (Lewis acid) on the polymerization of VESFA. The determination of the effect of an external base on the rate of polymerization is described as follows: VESFA, IBEA solution, MCAc, and dry toluene were combined in a dry 40 ml vial according to the formulation as described in Table 6.2 and cooled to 0 °C inside a glove box.

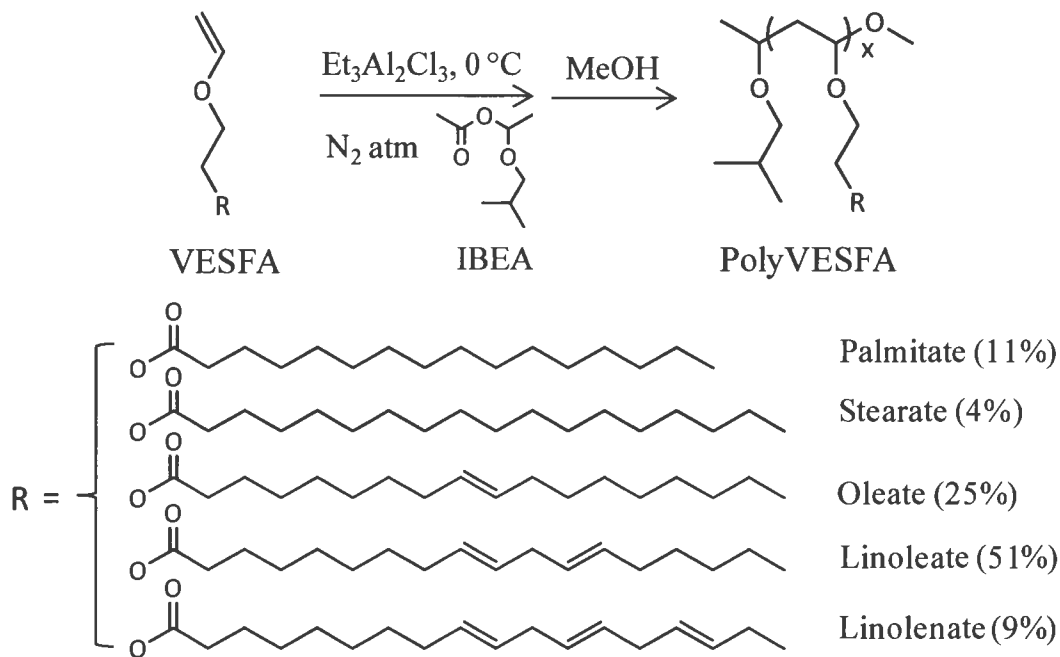


Figure 6.4. The synthetic scheme used to produce polyVESFA.

Each polymerization was initiated by the addition of supplied ethyl aluminum sesquichloride solution (Lewis acid). After 17 hours, each reaction was terminated by the addition of 6 ml of chilled methanol which causes the polymer to precipitate. The polymer was isolated and washed multiple times with methanol. The purified polymer was collected as a viscous liquid after centrifuging at 4500 rpm at 21 °C for 10 minutes and drying under vacuum (5 – 7 mm of Hg) overnight. The percentage of conversion of each polymer was calculated gravimetrically and the number average molecular weight was measured using a gel permeation chromatography. Each polymerization was carried out three times. The average and standard deviation values for % conversion, GPC number average molecular weight, and PDI were reported.

Table 6.2. Compositions used to compare the effect of a Lewis acid ($\text{Et}_{1.5}\text{AlCl}_{1.5}$) and MCAc to the polymerization of VESFA.

Sample name	VESFA (g)	IBEA Solution ¹ (mg)	MCAc (mg)	Toluene (g)	$\text{Et}_{1.5}\text{AlCl}_{1.5}$ Solution (ml)	$[\text{VESFA}]_0$: $[\text{IBEA}]_0$: $[\text{MCAc}]_0$: $[\text{Et}_{1.5}\text{AlCl}_{1.5}]_0$
MCAc/LA-250/5	1	65	387	5.22	0.039	200:1:250:5
MCAc/LA-0/5	1	65	--	5.22	0.039	200:1:0:5
MCAc/LA-250/18	1	65	387	5.15	0.141	200:1:250:18
MCAc/LA-0/18	1	65	--	5.15	0.141	200:1:0:18
MCAc/LA-250/30	1	65	387	5.08	0.235	200:1:250:30
MCAc/LA-0/30	1	65	--	5.08	0.235	200:1:0:30

¹IBEA solution: 0.5 g of IBEA dissolved in 13.7 g of toluene.

6.3.2.3.2. Determination of the VESFA polymerization kinetics in the absence of an external base. The kinetic study in the absence of an external base is described as follows: VESFA, IBEA, and dry toluene were combined in a dry 250 ml round bottom flask and chilled to 0 °C inside a glove box. Table 6.3 describes the compositions used to determine the VESFA polymerization kinetic. The reaction was started by the addition of supplied ethyl aluminum sesquichloride solution. Known weight of aliquot was withdrawn at different time intervals and terminated by the addition of chilled methanol which causes the polymer to precipitate. Each polymer was isolated and washed multiple times with methanol. The purified polymer was collected as a viscous liquid after centrifuging at 4500 rpm at 21 °C for 10 minutes and drying under vacuum (5 – 7 mm of Hg) overnight. The percentage of conversion of each polymer was calculated gravimetrically and the number average molecular weight was measured using a gel permeation chromatography.

Table 6.3. Compositions used to determine the VESFA polymerization kinetic in the absence of an external base.

Sample name	VESFA (g)	IBEA (mg)	Toluene (g)	Et _{1.5} AlCl _{1.5} Solution (μ l)	[VESFA] ₀ : [IBEA] ₀ : [Et _{1.5} AlCl _{1.5}] ₀
MCAc/LA-0/5	7	16	36.55	274	200 : 1 : 5
MCAc/LA-0/10	7	16	36.38	548	200 : 1 : 10
MCAc/LA-0/18	7	16	36.08	987	200:1: 18

6.3.3. Synthesis of polyethylene glycol-functional monovinylether monomer (VEPEG) and the polymer of VEPEG (polyVEPEG)

6.3.3.1. Synthesis of VEPEG

A VEPEG was synthesized by end-capping a commercially available polyethylene glycol monovinylether, PEGMVE, as follows: 20 g of iodoethane (IE) and 8.08 g of potassium hydroxide were added to a 500 ml, round-bottom flask and stirred at 300 rpm at 40 °C. Then, 58.8 g of PEGMVE was added drop-wise to the reaction mixture. After the addition was complete, the temperature was raised to 64 °C and stirring continued for 12 hours under a blanket of nitrogen. The reaction mixture was cooled to room temperature and then diluted with 300 ml of methylene chloride. The organic layer was filtered as a clear liquid and washed three times with 300 ml of DI water. The organic layer was then dried with anhydrous magnesium sulfate and the product monomer was recovered by rotary evaporation of volatiles. The monomer was dried with magnesium sulfate before use.

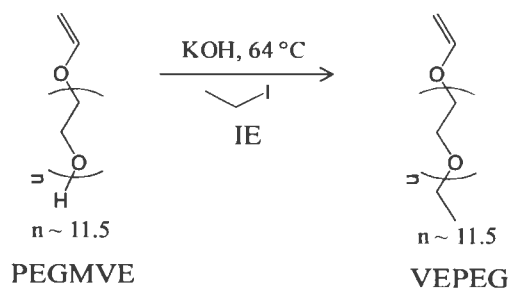


Figure 6.5. The synthetic scheme used to produce VEPEG.

6.3.3.2. Synthesis of polyVEPEG

VEPEG was polymerized at 0 °C within a glove box in a test tube dried at 250 °C under vacuum just before use. 1 g of VEPEG and 1.4 mg of IBEA were dissolved in 5.25 g of dry toluene and chilled to 0 °C. The polymerization was initiated with the addition of 0.208 ml of ethyl aluminum sesquichloride solution (25 wt. % in toluene) ($[\text{VEPEG}]_0:[\text{IBEA}]_0:[\text{Et}_{1.5}\text{AlCl}_{1.5}]_0 = 200:1:44$). After 12 hours, the reaction was terminated with addition of 10 ml of methanol. The polymer was soluble in methanol. Finally, the polyVEPEG was recovered by rotary evaporation of all the volatiles and drying under vacuum overnight.

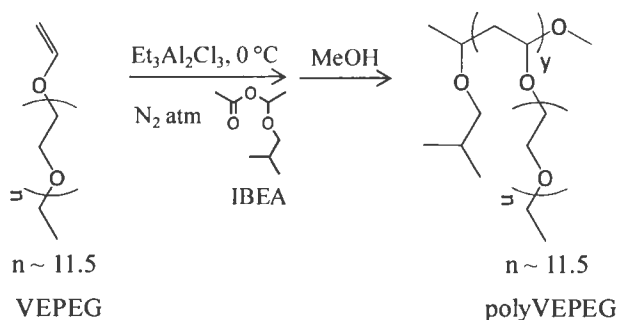


Figure 6.6. The synthetic scheme used to produce polymer of VEPEG.

6.3.3.3. Synthesis of the random copolymer of VEPEG and VESFA (polyVESFA-*r*-VEPEG)

VESFA and VEPEG were copolymerized at 0 °C within a glove box in a test tube dried at 250 °C under vacuum just before use. 1 g of VEPEG, 0.61 g of VESFA, and 2.77 mg of IBEA were dissolved in 8.43 g of dry toluene and chilled to 0 °C. The polymerization was initiated with the addition of 0.417 ml of ethyl aluminum sesquichloride solution (25 wt. % in toluene) ($[\text{VESFA}]_0:[\text{VEPEG}]_0:[\text{IBEA}]_0:[\text{Et}_{1.5}\text{AlCl}_{1.5}]_0 = 100:100:1:44$). After 12 hours, the reaction was terminated with addition of 20 ml of methanol. The copolymer was soluble in methanol. Finally, the copolymer was recovered by rotary evaporation of all the volatiles and drying under vacuum overnight. A high-throughput Symyx Rapid GPC was used to determine the molecular weight of polyVEPEG.

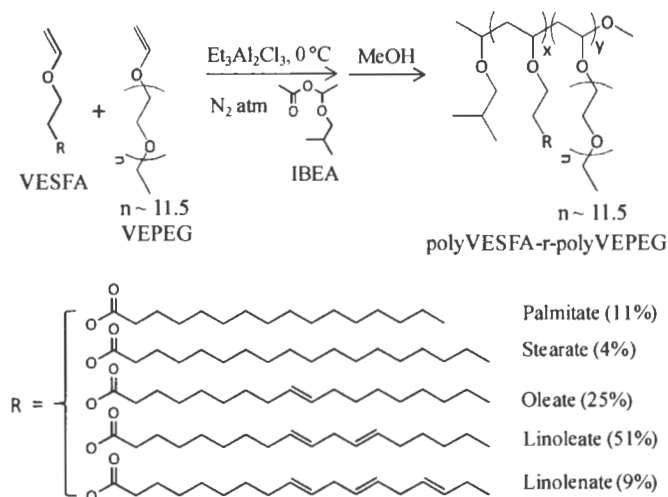


Figure 6.7. The synthetic scheme used to produce copolymer of VESFA and VEPEG.

6.3.4. Comparison of polyVESFA with SBO

6.3.4.1. Comparison of polyVESFA with SBO in an air drying system

Table 6.4 describes the compositions of a series of coatings produced to compare the difference between polyVESFA and SBO in autoxidation-curable systems.

Table 6.4. Compositions used to compare the difference between polyVESFA and SBO in autoxidation-curable systems.

Coating ID	polyVESFA (g)	SBO (g)	Cobalt octoate (mg)	Zirconium octoate (mg)	Nuxtra® Zinc (mg)
polyVESFA-HCo	5	--	4.2	27.7	250
polyVESFA-LCo	5	--	1.3	27.7	250
SBO-HCo	--	5	4.2	27.7	250
SBO-LCo	--	5	1.3	27.7	250

6.3.4.2. Comparison of polyVESFA with SBO in a sulfur vulcanizable system

Table 6.5 describes the compositions produced to compare the difference between polyVESFA and SBO in a sulfur vulcanizable system. A detailed procedure is as follows: polyVESFA, stearic acid, and zinc oxide were added in a 20 ml vial and mixed homogeneously at 40 °C using a high speed homogenizer at a stir speed of 15,000 r.p.m. for 3 minutes. Next, sulfur and tetramethylthiuram disulfide were added and stirred at room temperature using a stir speed of 7,000 rpm for 2 minutes.

Table 6.5. Compositions used to compare the difference between polyVESFA and SBO in a sulfur vulcanization system.

Formulations	polyVESFA (g)	SBO (g)	Stearic acid (mg)	Zinc Oxide (g)	Sulfur (g)	Tetramethyl thiuram disulfide (mg)
polyVESFA/S	2.33	---	12	0.139	0.081	12
SBO/S	---	7.17	36	0.429	0.252	37

6.3.5. Instrumentation and procedures

An MBraun glove box system equipped with a cold well and a chiller from FTSTM Systems was used for the cationic polymerization of TVE. Normal heptane was used as cooling medium.

6.3.5.1. Gel Permeation Chromatography (GPC)

A high-throughput Symyx Rapid GPC equipped with an evaporative light scattering detector (PL-ELS 1000) and 2xPLgel Mixed-B columns of 10 μm particle size was used to determine the molecular weight and molecular weight distribution of polymer. Polymer solutions of 3 mg/ml were prepared in THF and the temperature of the column was maintained at 45 $^{\circ}\text{C}$. Molecular weight data was reported relative to polystyrene standards.

6.3.5.2. Nuclear Magnetic Resonance (NMR) spectroscopy.

A JEOL-ECA 400 (400MHz) nuclear magnetic resonance (NMR) spectrometer equipped with an autosampler was used to generate proton NMR (^1H NMR) spectra. Data acquisition was completed using 16 scans in CDCl_3 as the lock solvent. For polyVEPEG, D_2O was used as a NMR solvent.

6.3.5.3. Fourier Transform Infrared (FTIR) spectroscopy

A Nicolet Manga-850 FTIR instrument was employed to measure FTIR spectra. Samples were coated on dry potassium bromide disc, and the measurements were carried out in the range of wavelengths from 600 cm^{-1} to 3900 cm^{-1} using 64 scans with a data spacing of 0.964 cm^{-1} .

6.3.5.4. Differential Scanning Calorimetry (DSC)

The thermal properties of polymers and SBO were determined using differential scanning calorimetry (DSC). The instrument utilized was a DSC Q1000 from TA Instruments, and sample sizes ranged from 4.5 to 5.5 mg. Samples were first heated from $30\text{ }^{\circ}\text{C}$ to $70\text{ }^{\circ}\text{C}$ at a heating rate of $10\text{ }^{\circ}\text{C}/\text{minute}$ (1st heat), cooled from $70\text{ }^{\circ}\text{C}$ to $-120\text{ }^{\circ}\text{C}$ at a cooling rate of $10\text{ }^{\circ}\text{C}/\text{minute}$ (cooling), and reheated from $-120\text{ }^{\circ}\text{C}$ to $120\text{ }^{\circ}\text{C}$ at a heating rate $10\text{ }^{\circ}\text{C}/\text{minute}$ (2nd heat). The T_g reported was obtained from the 2nd heat.

6.3.5.5. Thermogravimetric Analysis (TGA)

TGA was carried out using a Q500 from TA Instruments. Samples sizes were 10 mg to 15 mg. In a ramp heating mode samples were heated from $30\text{ }^{\circ}\text{C}$ to $800\text{ }^{\circ}\text{C}$ at a heating rates of $20\text{ }^{\circ}\text{C}/\text{minute}$ in air.

6.3.5.6. Rheological properties

Rheological properties were determined with an ARES Rheometer from TA Instruments. For measuring viscosity, liquid samples were placed between a cone and plate and viscosity monitored as a function of shear rate at a temperature of $25\text{ }^{\circ}\text{C}$. For monitoring cure kinetics of sulfur vulcanizable system, liquid samples were placed in between two parallel plates and heated for 2 hours at $140\text{ }^{\circ}\text{C}$ using a constant frequency of

10 rad/s and strain of 0.3%. Measurement was carried out using an auto-strain mode that was created by applying a maximum strain of 5% and a strain adjustment of 25%.

6.3.5.7. Drying time measurement

Cure characteristics of coatings designed to cure by autoxidation were determined using a BK 3-Speed Drying Recorder produced by MICKLE Laboratory Engineering Co. Ltd. With this device, a needle carrier holding 6 hemispherical ended needles travel across the length of six 305×25 mm recently coated glass strips. The coatings were cast on the glass strips using a 25 mm cube film applicator to produce wet films about 75 microns in thickness. A weight of 5 g was attached to each hemispherical needle to characterize coating film properties. Coating cure was characterized by determining open time, dust-free time, and tack-free time as defined by Klaasen and van der Leeuw.³⁶²

6.4. RESULTS AND DISCUSSION

6.4.1. VESFA and polyVESFA synthesis and characterization

6.4.1.1. VESFA synthesis and characterization

The novel monomer, VESFA, was synthesized from EGVE and SBO using base catalyzed transesterification, as shown in Figure 6.3. This process is similar to that used to produce biodiesel with the exception that EGVE was used instead of methanol.³⁶³ VESFA was isolated as a light yellow liquid. Since SBO is based on a mixture of 5 different fatty acids, VESFA is also a mixture of 5 different vinyl ethers in which each component of the vinyl ether mixture is based on a different fatty acid from SBO. Successful synthesis of VESFA was confirmed by ¹H NMR, ¹³C NMR, DEPT-135, and FTIR spectra. Figure 6.8

shows the ^1H NMR spectrum obtained for VESFA. As shown in Figure 6.8, one methine and two methylene protons in the vinyl double bond of VESFA appeared at 6.5, 4.2, and 4.0 ppm, respectively. Table 6.6 lists the integration values of proton from the ^1H NMR spectrum and the theoretical value according the formula of VESFA. Integration of this spectrum confirmed that the composition of fatty acids in the VESFA sample was the same as that for SBO.

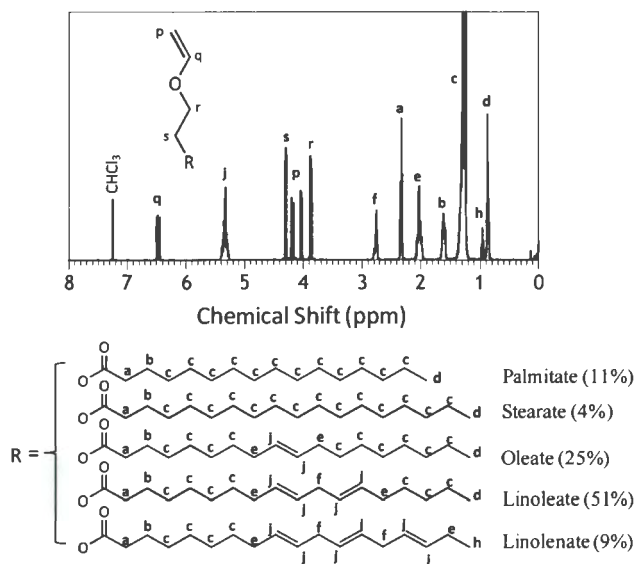


Figure 6.8. ^1H NMR spectrum obtained for VESFA.

Table 6.6. Theoretical and experimental integration values of proton obtained for VESFA.

Integration Value of protons	$\int q$	$\int j$	$\int s$	$\int p$	$\int r$	$\int f$	$\int a$	$\int e$	$\int b$	$\int c$	$\int (h+d)$
Theoretical	0.33	1.01	0.67	0.67	0.67	0.46	0.67	1.13	0.67	5.54	1.0
^1H NMR	0.29	1.0	0.63	0.63	0.63	0.47	0.67	1.1	0.72	5.54	1.0

The Distortionless Enhancement by Polarization Transfer (DEPT) method is useful for determining the number of hydrogen atoms attached to a given carbon atom. In a

DEPT-135 spectrum, methyl and methine carbons appear as positive peaks, while the methylene carbons appear as negative peaks. As shown in Figure 6.9, The methylene carbon (number 1) and methine carbon (number 2) in the vinyl double bond can be seen as a negative peak at 86.9 ppm and as a positive peak at 151.5 ppm, respectively. All methine carbons in the unsaturation of fatty acid fragment at the position numbers of 11 and 12 produce positive peaks at 127.9 ppm and 129.9 ppm. Two methylene carbons in the ethyl spacer in between vinyl ether and fatty acid produce negative peaks at 65.8 and 62.4 ppm. FTIR spectrum of VESFA (Figure 6.10) confirms the presence of unsaturation in the vinyl ether double bond (C=C) and carbonyl (C=O) group at 1614 cm^{-1} and 1740 cm^{-1} respectively. The peak absorption due to the C=C unsaturation in the fatty acid can be seen at 2973 cm^{-1} .

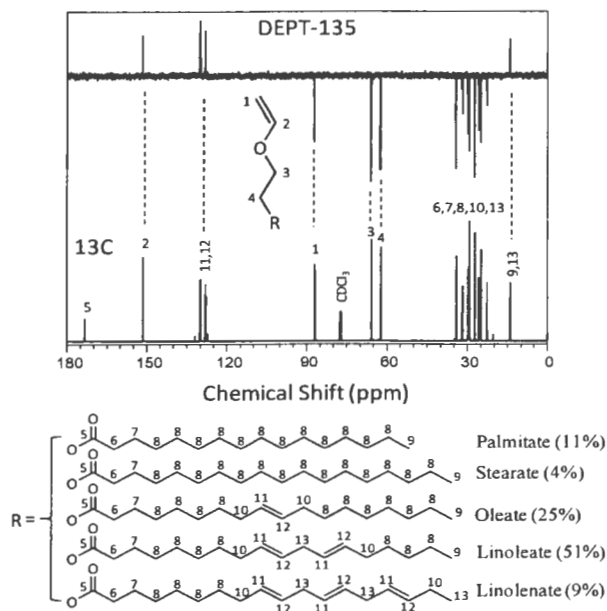


Figure 6.9. ^{13}C NMR and DEPT-135 spectra obtained for VESFA.

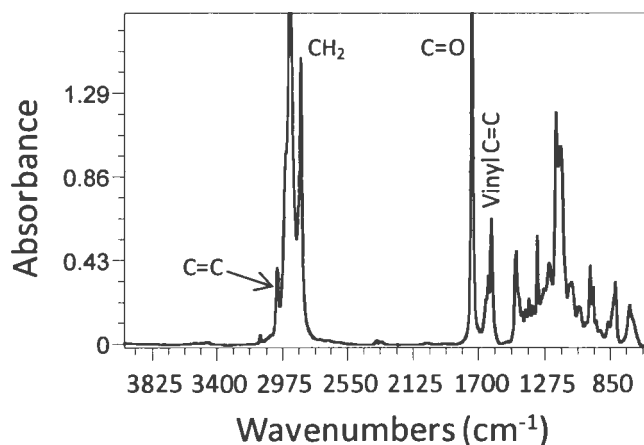


Figure 6.10. FTIR spectrum obtained for VESFA.

6.4.1.2. PolyVESFA synthesis and characterization

As shown in Figure 6.4, VESFA was polymerized using cationic polymerization based on an initiator system comprised of IBEA as the cationogen and $\text{Et}_{1.5}\text{AlCl}_{1.5}$ as the coinitiator. With this system, complexation of the Lewis acid coinitiator with the acetate group of IBEA dissociates the carbon-oxygen bond to produce a carbocation at the oxygen-stabilized secondary carbon atom of IBEA. This carbocation initiates polymerization by addition to the vinyl ether group of a monomer molecule. Polymerization is terminated by the addition of methanol which reacts with carbocationic polymer chain ends to produce methyl ether end groups.

The chemical structure of the polyVESFA was characterized using ^1H NMR, ^{13}C NMR, and FTIR. As shown in Figure 6.11, peaks associated with the vinyl ether group of VESFA (6.5 and 4.0 ppm) are not present while peaks associated with the vinyl groups of the fatty acid groups (5.3 ppm) are retained. This result indicates that the reactivity of the

carbocationic species generated during the polymerization process, which includes the initiating carbocations and chain propagating carbocations, were reactive enough to polymerize the vinyl ether groups of the VESFA, but not so reactive that they add to double bonds of the fatty acid portion of VESFA. Selectivity of the polymerization process toward the vinyl ether functionality was critical to prevent gelation during polymerization and to preserve pendent group unsaturation for application of the polyVESFA in coating applications. Table 6.7 lists the integration values of proton from the ^1H NMR spectrum and the theoretical value according the formula of polyVESFA. Integration of this spectrum confirmed that the composition of fatty acids in the polyVESFA sample was the same as that for VESFA.

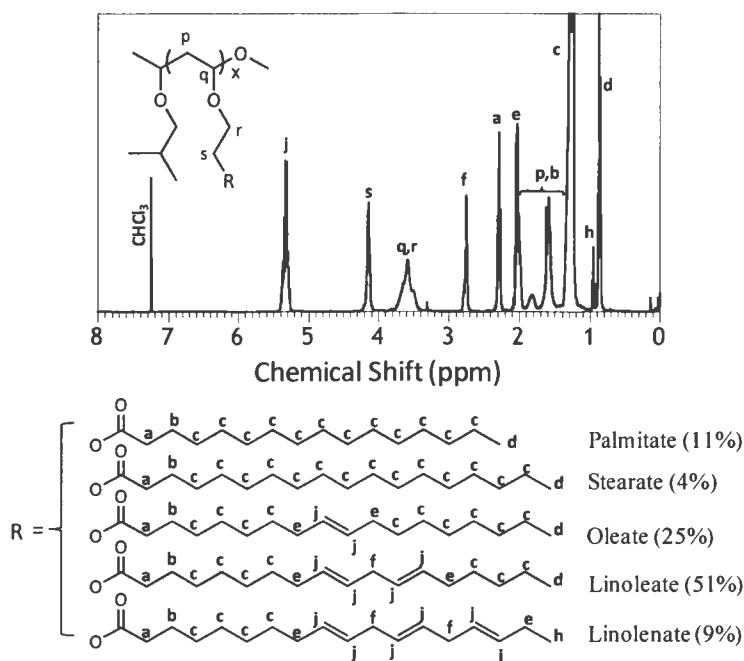


Figure 6.11. ^1H NMR spectrum obtained for polyVESFA.

Table 6.7. Theoretical and experimental integration values of proton obtained for polyVESFA.

Integration Value of protons	$\int j$	$\int s$	$\int q+r$	$\int f$	$\int a$	$\int e$	$\int p+b$	$\int c$	$\int h+d$
Theoretical	1.01	0.67	1.0	0.46	0.67	1.13	1.34	5.54	1.0
$^1\text{H NMR}$	1.03	0.66	0.95	0.47	0.68	1.1	1.14	5.75	1.0

The ^{13}C NMR and FTIR spectra of polyVESFA were shown in Figures 6.12 and 6.13 respectively. As shown in Figure 6.12, peaks associated with the vinyl ether group of VESFA (151.5 and 86.9 ppm) are not present while peaks associated with the vinyl groups of the fatty acid groups (127.9 and 129.9 ppm) are retained. As shown in the FTIR spectrum (Figure 6.13) of polyVESFA, absorption peaks associated with the C=C unsaturation of the vinyl ether (1614 cm^{-1}) are disappeared while the C=C unsaturation of the fatty acid (2973 cm^{-1}) are retained.

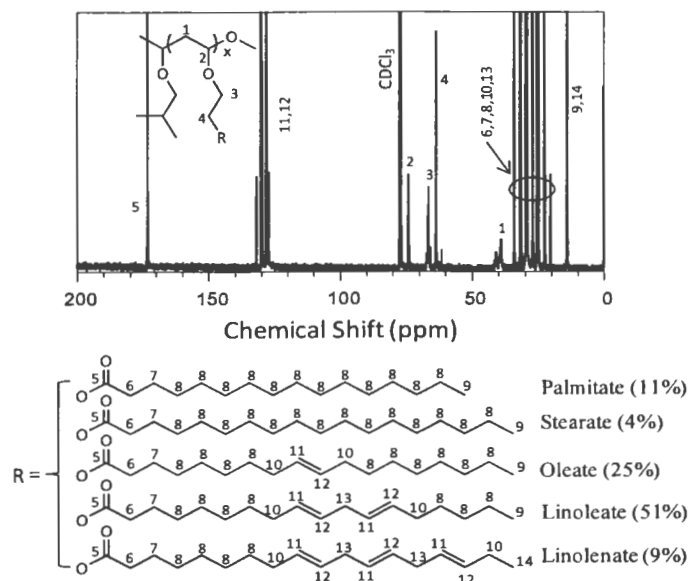


Figure 6.12. ^{13}C NMR spectrum obtained for polyVESFA.

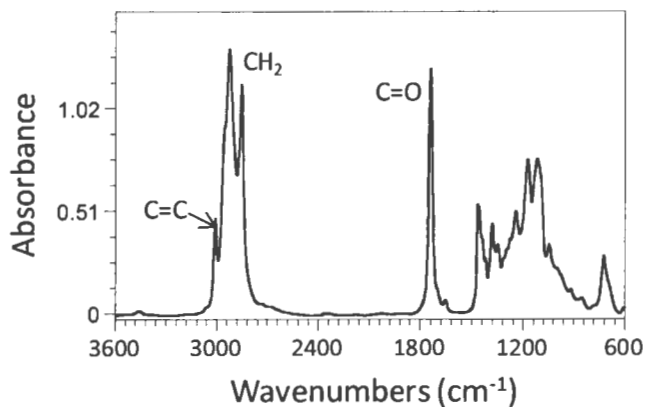


Figure 6.13. FTIR spectrum obtained for polyVESFA.

GPC chromatograms of polyVESFA, VESFA, and SBO are shown in Figure 6.14. The absence of any peak in the GPC chromatogram of polyVESFA at a retention time of 237 seconds demonstrated that the polyVESFA is totally free from unreacted VESFA. Table 6.8 lists the values of GPC number average molecular weight and PDI for SBO, VESFA, and polyVESFA.

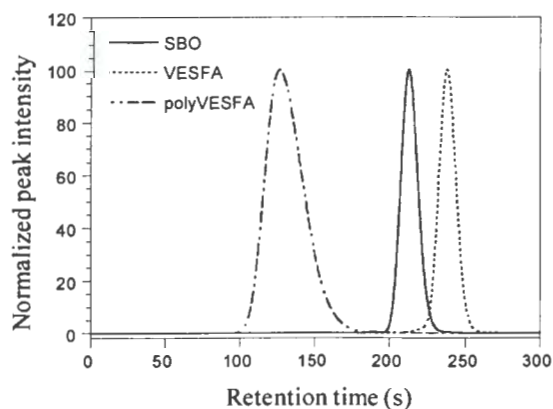


Figure 6.14. Plot of normalized peak intensity as a function of retention time for GPC chromatograms of SBO, VESFA, and polyVESFA.

Table 6.8. GPC number average molecular weight and PDI.

Sample	GPC Mn (g/mole)	PDI
SBO	1,010	1.08
VESFA	403	1.06
polyVESFA	39,140	1.17

6.4.1.3. Polymerization kinetic study

The initiation process of a vinyl ether polymerization initiated by $\text{IBEA}/\text{Et}_{1.5}\text{AlCl}_{1.5}$ is consisted of the formation of oxygen-stabilized secondary carbon atom of initiating species followed by the addition to the vinyl ether group of a monomer molecule. The secondary carbocation generated at the propagating species is very reactive and short living in the absence of an external base. As mentioned in the Introduction, an added base containing an ester group complexes with the propagating species to delocalize the positive charge over the propagating center and reduces the reactivity of the carbocation. However, VESFA possesses one ester group per monomer that provides an added stability to the propagating center and excludes the necessity of an external base (e.g. MCAc). This conception is supported by the following results.

6.4.1.3.1. Determination of the effect of an external base (MCAc). Polymers obtained after polymerizations mentioned in Table 6.2 were characterized using gravimetric analysis and GPC. Figures 6.15, 6.16.A, and 6.16.B demonstrate the effect of a Lewis acid ($\text{Et}_{1.5}\text{AlCl}_{1.5}$) and MCAc on the conversion, GPC number average molecular weight, and molecular weight distribution (PDI) after 17 hours of reaction.

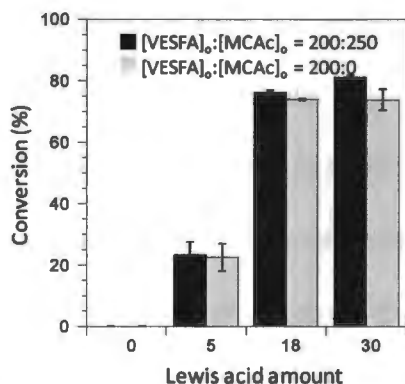


Figure 6.15. Plot of % of conversion as a function of Lewis acid amount after 17 hours of polymerization when carried out both in the presence ($[\text{VESFA}]_0:[\text{MCAc}]_0 = 200:250$) and absence ($[\text{VESFA}]_0:[\text{MCAc}]_0 = 200:0$) of an external base (MCAc). The X-axis indicates the value of the ratio $[\text{Et}_{1.5}\text{AlCl}_{1.5}]_0 : [\text{VESFA}]_0$, when $[\text{VESFA}]_0$ was selected as 200.

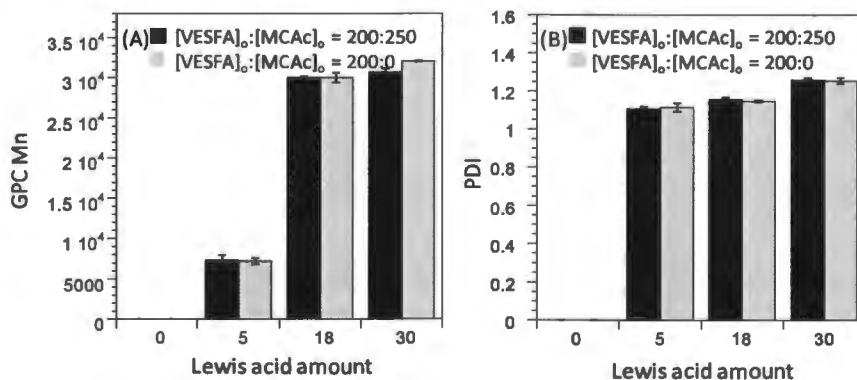


Figure 6.16. Plot of (A) GPC number average molecular weight and (B) PDI as a function of Lewis acid amount after 17 hours of polymerization when carried out both in the presence ($[\text{VESFA}]_0:[\text{MCAc}]_0 = 200:250$) and absence ($[\text{VESFA}]_0:[\text{MCAc}]_0 = 200:0$) of an external base (MCAc). The X-axis indicates the value of the ratio $[\text{Et}_{1.5}\text{AlCl}_{1.5}]_0 : [\text{VESFA}]_0$, when $[\text{VESFA}]_0$ was selected as 200.

The Lewis acid (LA) concentrations presented here are the initial molar ratios of LA to VESFA when the initial molar concentration of VESFA was selected as 200. Results

showed that the external base does not have influence on the percent of conversion and hence the molecular weight. However, when the LA concentration is low ($[\text{VESFA}]_0$: $[\text{Et}_{1.5}\text{AlCl}_{1.5}]_0 = 200:5$), the polymerization rate is relatively low (23% conversion after 17 hours of reaction) indicating the stability of the carbocationic propagating species by the ester groups of VESFA. With the increase in the LA concentration from 5 to 30, the reactivity of the propagating species increases as indicated by the increase in both % of conversion and PDI. The mechanism of stabilization of carbocationic propagating species in the presence of ester groups from VESFA can be shown in Figure 6.17.

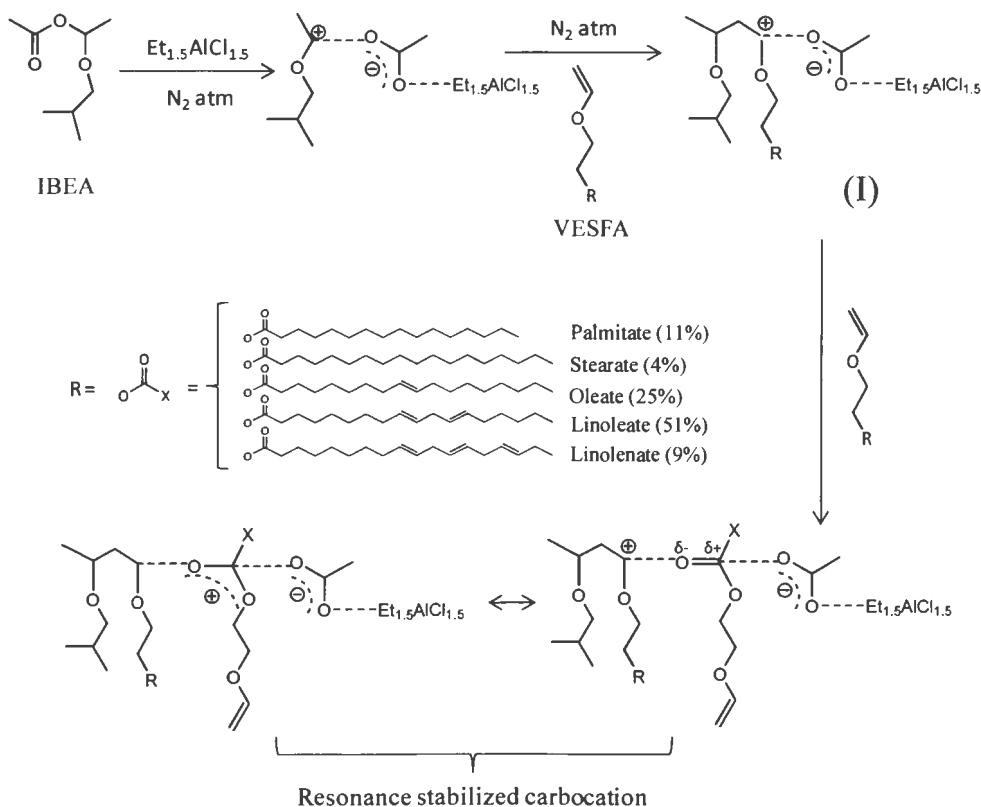


Figure 6.17. Stabilization of carbocation in the presence of ester group of VESFA.

The acetate counter ion produced after dissociation of IBEA is not sufficient to provide the stability of propagating species (I). The acetate groups from the VESFA complexes with the propagating carbocation to add stability that will enable it to undergo living carbocationic polymerization. The order of polymerization of VESFA in the absence of an added base was determined at different LA concentrations (Figure 6.18.A). A first order polymerization was achieved when the LA concentration was selected as 10 and 18. At these concentrations, the plot of $\ln\{[M]_0/[M]_t\}$ as a function of polymerization time yielded a straight line passing through the origin with a correlation coefficient (R^2) of 0.99. From the slope of the lines, the polymerization rate constants were evaluated and compared. The rate of reaction for a first order reaction can be presented as follows:

$$\frac{d[\text{VESFA}]}{dt} = -kt$$

where, k and t are the reaction rate (h^{-1}) and reaction time (h) respectively. The reaction rates obtained from the slope of the straight lines (Figure 6.18.A) were 0.0436 h^{-1} and 0.0821 h^{-1} when the LA concentrations of 10 and 18 were used. Thus, with the increase in LA concentration from 10 to 18, the rate of reaction increased almost double. However, with a relatively lower LA concentration, such as 5, the reaction rate was too slow to complete 45 % of the polymerization after 120 hours. The order reaction with such a low amount of LA followed a polynomial distribution with an order of 2. This may be due to the addition of rate constant from side reaction (e.g. termination, chain transfer, etc) to the rate of propagation. This may be an indicative of the fact that the propagating carbocation

generated by the $\text{IBEA}/\text{Et}_{1.5}\text{AlCl}_{1.5}$ initiating system cannot stay ‘alive’ for such a long reaction time of 120 hours.

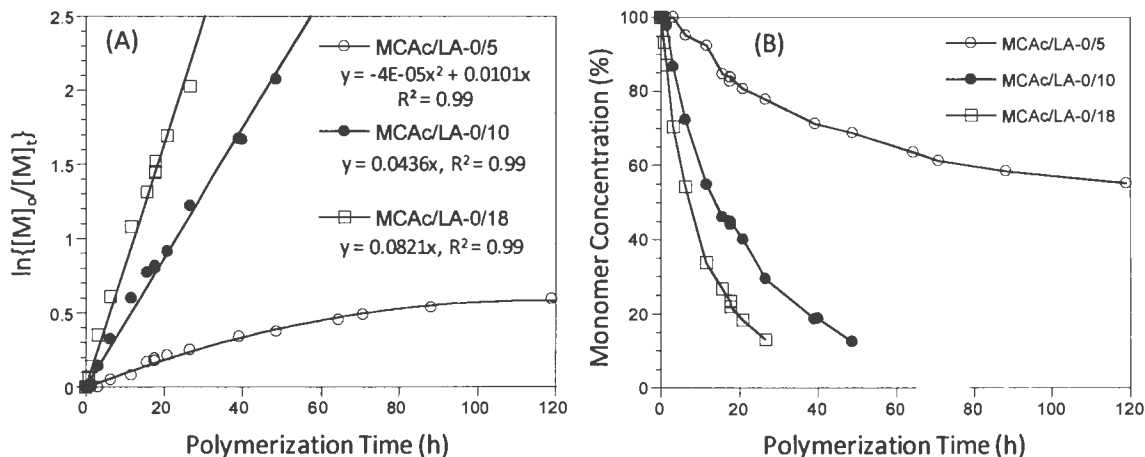


Figure 6.18. Plot of (A) $\ln\{[M]_0/[M]_t\}$ and (B) monomer concentration as a function of polymerization time. The symbols MCAc/LA-0/5, MCAc/LA-0/10, and MCAc/LA-0/18 represent the condition of polymerizations in the absence of an external base when the LA was used at three different molar concentrations of 5, 10, and 18, respectively.

6.4.1.3.2. Determination of the kinetics of VESFA polymerization in the absence of an external base. The living carbocationic polymerization of VESFA in the absence of an

external base (MCAc) was demonstrated by the linear relationship between the GPC number average molecular weight and the percent of conversion (Figure 6.19) when a LA concentration of 18 was used. A plot of number average molecular weight obtained from GPC analysis as a function of VESFA monomer conversion yielded a straight line that passed through the origin with a slope of 485.3 and correlation coefficient of 0.98.

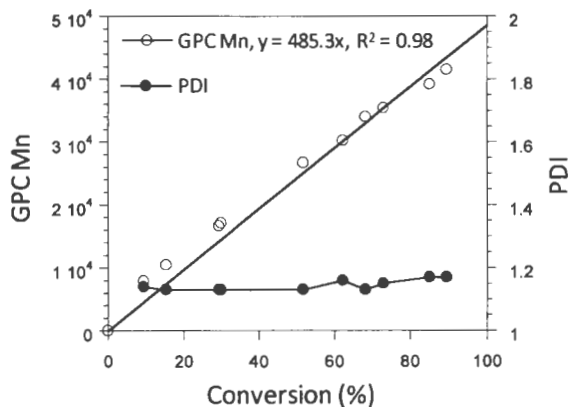


Figure 6.19. Plot of GPC number average molecular weight and PDI as a function of % of conversion for the polymerization of VESFA. ([VESFA]₀: [IBEA]₀: [Et_{1.5}AlCl_{1.5}]₀ was used as 200:1:18).

6.4.2. Characterization of polyVEPEG and polyVESFA-*r*-VEPEG

The proton NMR spectra obtained for VEPEG was shown in Figure 6.20. As shown in Figure 6.20, the two methyl protons and one methine protons associated with the vinyl ether double bond of VEPEG were at 3.9 ppm, 4.1 ppm, and 6.4 ppm, respectively. Successful synthesis of VEPEG was confirmed after integrating and comparing the peak areas associated with the three methyl protons at 1.17 ppm to the two methylene of vinyl ether double bond at 3.9 ppm and 4.1 ppm. The absence of proton absorption peak associated with the hydroxyl group of PEGMVE between 3.42 ppm and 3.45 ppm and the generation of a new peak associated with the OCH₂ group between 3.45 ppm to 3.5 ppm confirmed that the VEPEG was totally free from unreacted PEGMVE. As shown in the FTIR spectrum of VEPEG (Figure 6.21), the peaks associated with the C=C bond of vinyl ether can be easily seen at 1620 cm⁻¹. The absence of any peak associated with the

hydroxyl group between 3150 cm^{-1} and 3550 cm^{-1} also confirmed that the VEPEG was totally free from unreacted PEGMVE.

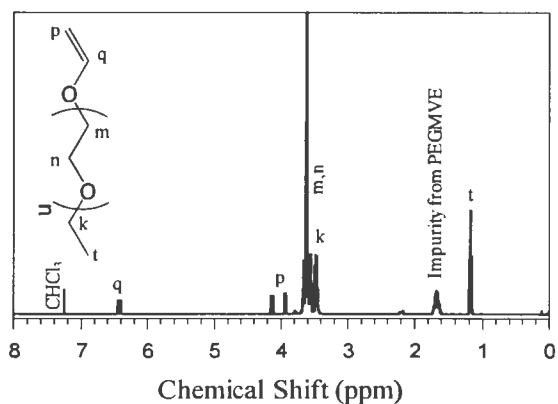


Figure 6.20. ^1H NMR spectrum obtained for VEPEG.

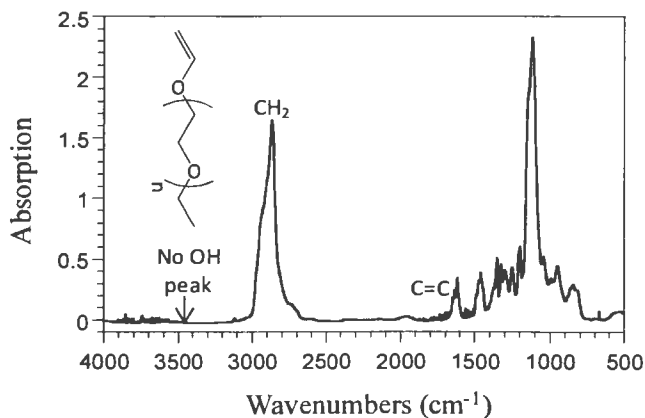


Figure 6.21. FTIR spectrum obtained for VEPEG.

The proton NMR spectra obtained for polyVEPEG and polyVESFA-r-polyVEPEG were shown in Figures 6.22 and 6.23 respectively. The polymerization of VEPEG was confirmed by the absence of peaks associated with the vinyl ether at 3.9 ppm, 4.1 ppm, and 6.4 ppm. The GPC number average molecular weight and molecular weight distribution

obtained for polyVEPEG were 14,200 g/mole and 1.21 respectively. The synthesis of random copolymer of VESFA and VEPEG was carried out according to the polymerization scheme shown in Figure 6.7. Considering the equal reactivity of carbocation generated from both the monomers, simultaneous initiation of VESFA and VEPEG can produce the random copolymer. The successful synthesis of the copolymer was confirmed by the total disappearance of protons associated with the vinyl ether double bond at 6.4 ppm and 4.2 ppm.

The GPC number average molecular weight and molecular weight distribution was found as 14,750 and 1.22 respectively. The polyVESFA is not soluble in methanol. On the other hand, polyVEPEG is soluble in methanol. The copolymer synthesized from VEPEG and VESFA is nicely soluble in methanol. This provides a strong evidence for the formation of a copolymer of both the monomers.

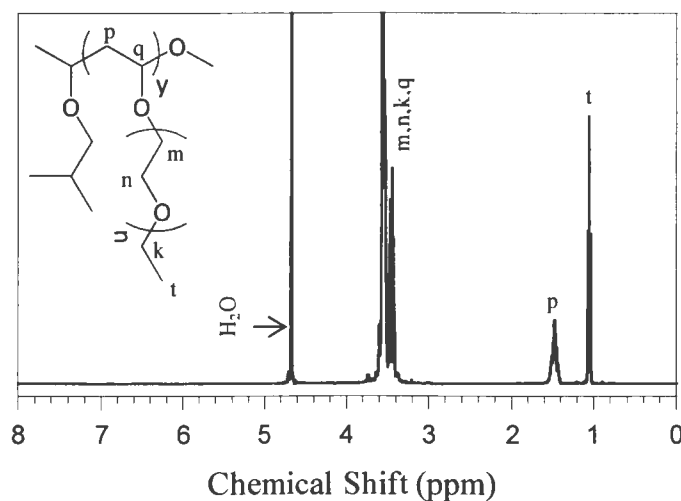


Figure 6.22. ¹H NMR spectrum obtained for polyVEPEG.

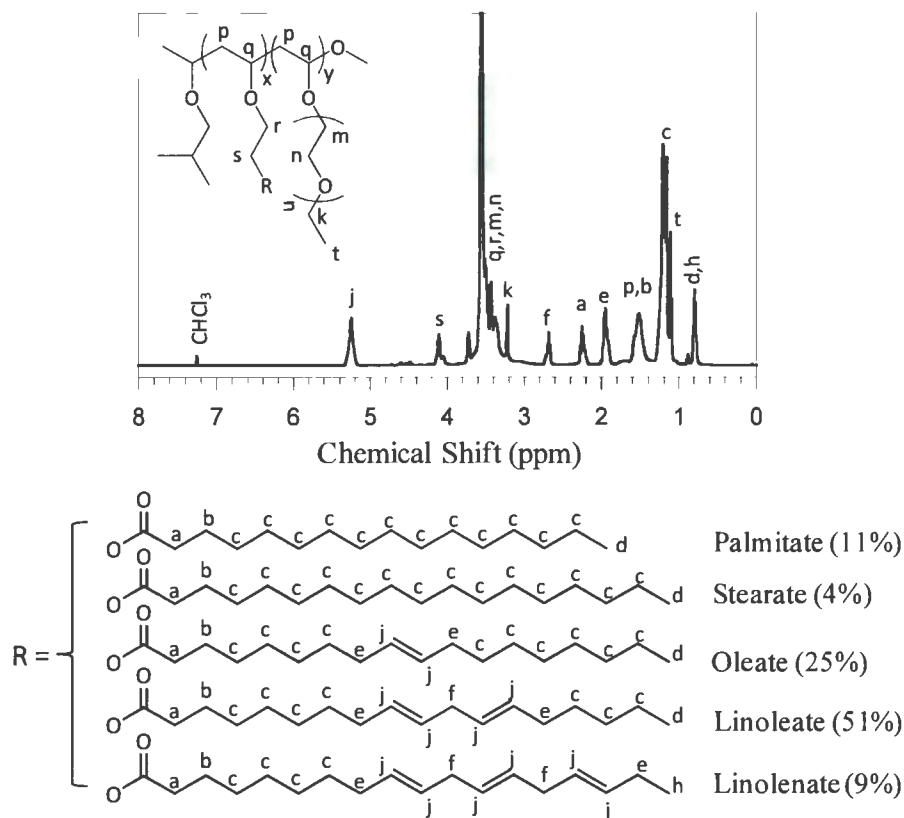


Figure 6.23. ^1H NMR spectrum obtained for polyVESFA-r-polyVEPEG.

6.4.3. Property comparison of polyVESFA with SBO

The basic properties of the polyVESFA were compared to SBO. Figures 6.24.A and 6.24.B provide a comparison of the thermal properties of polyVESFA, SBO, and VESFA. Figure 6.25 provides a comparison of thermogravimetric analysis for SBO, VESFA, and polyVESFA. The DSC thermograms displayed in Figure 6.24.A show very different thermal properties between polyVESFA and SBO. After cooling from 70 °C to -120 °C at 10°C/minute, the SBO sample exhibited a small endotherm at -77 °C which was immediately followed by a significant crystallization exotherm and two endotherms with

peak temperatures of $-39\text{ }^{\circ}\text{C}$ and $-25\text{ }^{\circ}\text{C}$. This behavior suggests that the original crystallites formed during the controlled cooling were quite imperfect resulting in a relatively low melting temperature and immediate recrystallization to produce the higher temperature endotherms. In contrast, polyVESFA displayed a glass transition temperature at $-98\text{ }^{\circ}\text{C}$ and a very diffuse, weak endotherm with a peak temperature of $-28\text{ }^{\circ}\text{C}$. The weak, diffuse endotherm indicates that incorporating the fatty acids into a polymer as pendant groups greatly reduces the crystallizability of the fatty acid chains. Considering the higher viscosity and corresponding reduced molecular mobility associated with a polymeric structure as compared to a triglyceride, it is not surprising that crystallization of the fatty acids chains in polyVESFA was reduced compared to SBO.

The TGA was performed in an air-oxidative environment with a constant increase in temperature. From the thermograms, three important parameters, for example, the decomposition temperature (T_0), onset temperature (T_{onset}), and ash content are listed in Table 6.9. The T_0 can be defined as the temperature of the maximum weight loss rate (dm/dt_{max}). The T_{onset} can be considered as the point when decomposition just begins. As shown in Figure 6.25, the decomposition temperature of polyVESFA was slightly higher than that of SBO. According to the data in Table 6.9, polyVESFA shows 6.2% and 5% increase in the T_{onset} and T_0 as compared to SBO.

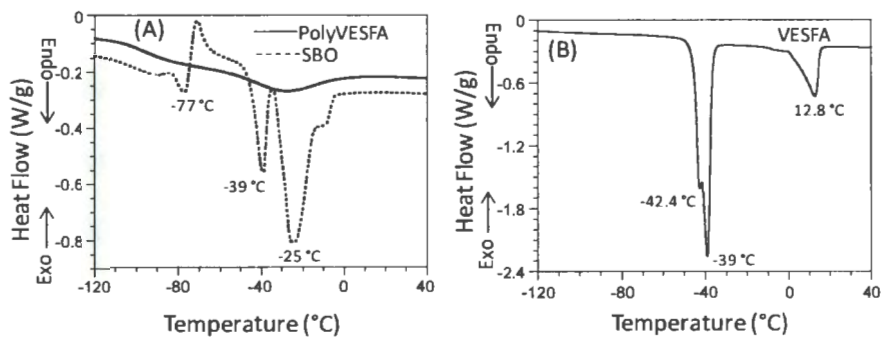


Figure 6.24. (A) DSC thermograms for polyVESFA, SBO, and (B) VESFA.

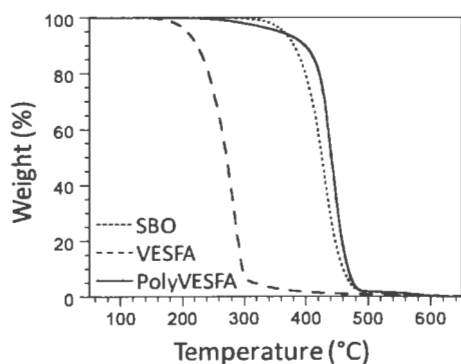


Figure 6.25. TGA thermograms for VESFA, polyVESFA, and SBO.

Table 6.9. Data obtained from TGA thermograms of VESFA, polyVESFA, and SBO.

Sample	Tonset (°C)	T0 (°C)	Ash content (%) 800 °C
SBO	394.8	428.2	0.1
VESFA	247.2	286.2	0.3
polyVESFA	419.3	449.2	0.03

Figure 6.26 provides a comparison of the rheological properties of a polyVESFA sample to SBO. From Figure 6.26, it can be seen that the polyVESFA possessed a viscosity that was about two orders of magnitude higher than that of SBO at shear rates

below 2000 s^{-1} which is consistent with the major difference in molecular weight between the two materials. In addition, the viscosity of the polyVESFA sample showed significantly more shear sensitivity than SBO. Increasing shear rate from approximately 1000 s^{-1} to $10,000\text{ s}^{-1}$ reduced the viscosity of polyVESFA by approximately an order of magnitude. The shear sensitivity of the polyVESFA indicates that the molecular weight of the polyVESFA was high enough to enable significant polymer chain entanglement.

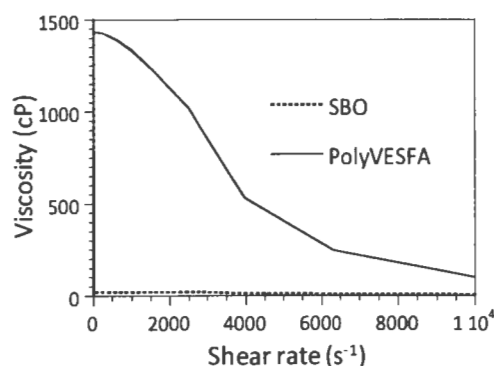


Figure 6.26. Plot of viscosity as a function of shear rate for polyVESFA and SBO.

6.4.4. Coatings cured using autoxidation

SBO is classified as semi-drying oil. Based on the fatty acid composition of SBO, each triglyceride contains on average 4.5 double bonds. With this degree of unsaturation, it would be expected that the development of a crosslinked network from SBO using autoxidation would require much longer drying times compared to a drying oil such as linseed oil which possesses on average 6.3 double bonds per triglyceride.³⁴² For polyVESFA, the number of double bonds per polymer molecule is equal to 1.5DP since each repeat unit contains one fatty acid group with the average number of double bonds per

fatty acid chain being 1.5. Thus, for a polyVESFA possessing a DP of 100, the average number of double bonds per polymer molecule is 150. With this extraordinarily high number of double bonds per molecule, a crosslinked network can be developed even at very low extents of autoxidation. To demonstrate this fact, four coating compositions were prepared by adding autoxidation catalysts to polyVESFA and SBO. The four coating compositions prepared are described in Table 6.10. Table 6.10 shows variations in open time, dust-free time, and tack-free time for the four different compositions.

Table 6.10. Cure characteristics obtained for coatings based on polyVESFA and SBO and cured using autoxidation. The composition of the coatings is described in Table 6.4.

Formulation	Open time (hr)	Dust-free time (hr)	Tack-free time (hr)
polyVESFA-HCo	2.5	5	6.1
polyVESFA-LCo	5.3	8.5	11.8
SBO-HCo	15	21	40
SBO-LCo	28	> 48	> 48

For the two coatings based on the high level of the cobalt drier (i.e. polyVESFA-HCo and SBO-HCo), open time, dust-free time, and tack-free time were all dramatically reduced with the use of polyVESFA as compared to SBO. For the polyVESFA-based coating, open time, dust-free time, and tack-free time were reduced by a factor of 6, 4, and 6.5, respectively, compared to the SBO-based coating. For the coatings based on the lowest level of cobalt drier (i.e. polyVESFA-LCo and SBO-LCo), SBO-LCo remained tacky even after 48 hours at ambient conditions. In contrast, the analogous coating based on polyVESFA was tack-free after 11.8 hours. These results clearly show the utility of

increasing the number of double bonds per molecule by incorporating the fatty acid groups of SBO into a polymeric structure.

6.4.5. Coatings cured using sulfur vulcanization

To understand the utility of polyVESFA as compared to SBO in the production of sulfur vulcanized rubber, a conventional vulcanization system was investigated. For sulfur vulcanizable system, a simple experiment was conducted in which the cure kinetics of a blend of polyVESFA and sulfur was compared to that of an analogous blend of SBO and sulfur. The cure kinetics was characterized by monitoring shear storage modulus and shear viscosity as function of time at 140 °C. As shown in Figure 6.27, shear storage modulus for the polyVESFA/S blend began to decrease from 54 Pa to 2 Pa for the first 30 seconds of reaction time and then started to increase just after 3 minutes. Next, the shear storage modulus increased sharply over a time period of 27 minutes to a maximum value of 198 KPa and after 15 minutes the modulus started to decrease slowly to a final value of 173 KPa for a total heating period of 2 hours at 140 °C. Similarly, the shear viscosity decreased for first 30 seconds and then started to increase sharply to the maximum value of 19,740 Pa-s. After 15 minutes the viscosity began to decrease slowly to a final value of 17,280 Pa-s for a total heating time of 2 hours. Initially, the sudden drop of shear modulus and viscosity were observed due to the increase in polymer chain mobility and the plasticization effect of stearic acid melting at 140 °C. Devulcanization effect was observed due to overheating after 45 minutes of reaction causing slight reduction in both the shear storage modulus and viscosity. This result indicates that the crosslinked network started

developing almost immediately and full crosslinking was achieved within about 0.5 hours. In contrast, within the 2 hours of experiment, no significant increase in shear storage modulus and viscosity were observed for the SBO/S blend.

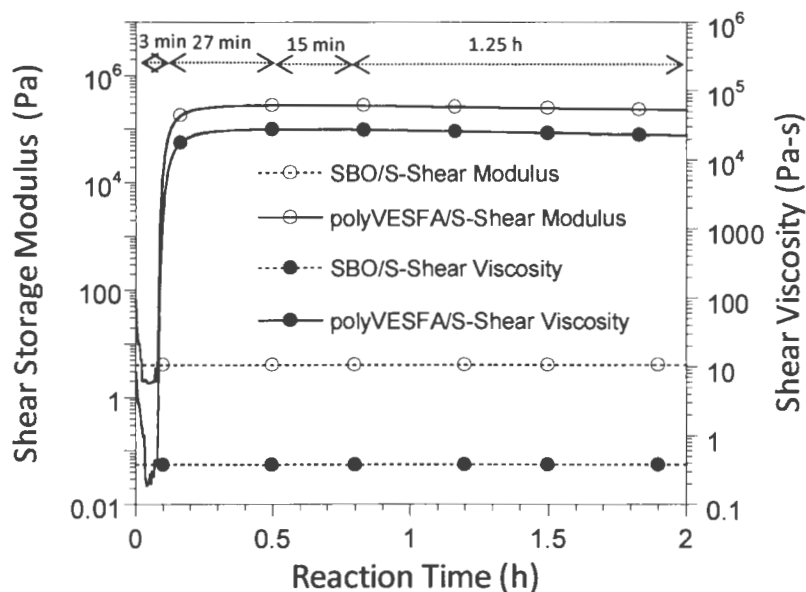


Figure 6.27. Shear storage modulus and shear viscosity as a function of vulcanization time at 140 °C for SBO/S and polyVESFA/S cure systems.

Assuming the kinetics of the reaction between the unsaturation in fatty acids and the sulfur were the same for the two blends, which seems reasonable considering the unsaturation present in polyVESFA and SBO are chemically equivalent, then the dramatic difference in shear modulus and viscosity response as a function of time can only be attributed to the difference in the number of double bonds per molecule. As discussed in the *Introduction* and illustrated in Figure 6.2, increasing the number of functional groups per molecule decreases the gel-point dramatically. Even though the extent of conversion of

the double bonds-sulfur reaction for the two systems may have been the same at any point in time during the cure process, the much higher unsaturation content per molecule for polyVESFA resulted in the gel-point being reached at much lower conversion/cure time providing elasticity to the material as indicated by the increase in shear modulus. This dramatic reduction in the time required for the development of the crosslinked network associated with the use of polyVESFA in a sulfur vulcanizable cured system could have tremendous commercial utility considering energy cost and production rate affects associated with thermal curing.

6.5. CONCLUSION

A novel VESFA monomer was produced by transesterification reaction between soybean oil and ethylene glycol vinyl ether. The VESFA was polymerized using a living carbocationic polymerization in the absence of an added base. The addition of an external base has no effect on the percentage of monomer conversion and molecular weight of polymer. The carbonyl group in the ester functional VESFA acts as a base to provide the stability of the carbocationic propagating species generated by $\text{IBEA}/\text{Et}_{1.5}\text{AlCl}_{1.5}$. Thermal analysis demonstrated that incorporating the fatty acids into a polymer as pendent groups greatly reduces the crystallizability of the fatty acid chains. Viscosity analysis revealed that the polyVESFA possessed a higher viscosity than that of SBO which is consistent with the major difference in molecular weight between the two materials. In addition, the viscosity of the polyVESFA sample showed significantly more shear sensitivity than SBO. It was clearly demonstrated that the use of polyVESFA or its derivatives in place of SBO

or its derivatives offers tremendous advantages in a variety of coating systems. For coating systems based on cure by autoxidation, it was demonstrated that use of polyVESFA can reduce drying-time by a factor of 4 to 6.5. For coating systems based on cure by sulfur vulcanization, it was shown that use of polyVESFA can develop a crosslinked network within 30 minutes of reaction, whereas SBO was in liquid state after 2 hours of vulcanization. All of these results can be attributed to a higher number of functional groups per molecule associated with the use of polyVESFA as opposed to SBO. A higher number of functional groups per molecule results in the gel-point being reached at much lower conversion and the obtainment of a higher crosslink density at a given degree of functional group conversion. Based on the results described in this document, it appears that the novel SBO-based polymer, polyVESFA, has tremendous commercial potential.

CHAPTER 7. SYNTHESIS, CHARACTERIZATION, AND APPLICATION OF A NOVEL EPOXY-FUNCTIONAL POLYMER OF VESFA (E- POLYVESFA) AND DERIVATIVES OF E-POLYVESFA

7.1. ABSTRACT

A novel epoxidized polymer (E-polyVESFA) of soybean oil (SBO) was synthesized and the thermal and viscoelastic properties were compared to commercially available epoxidized soybean oil (E-SBO). Additionally, acrylated polymer (A-polyVESFA) and alcohol-functional polymer (OH-polyVESFA) of SBO were synthesized from E-polyVESFA and characterized using proton NMR and FTIR. The use of E-polyVESFA as opposed to E-SBO in an epoxy-amine cure system reduced cure time at 120 °C by more than an order of magnitude. For cationic photo-cure system it was demonstrated that the use of E-polyVESFA substantially increased cure rate, ultimate function group conversion during photocure. Glass transition temperature (T_g) and crosslink density of cured films were significantly higher for the E-polyVESFA-based materials. Similar to the result obtained from the cationic photo-cure systems, the use of A-polyVESFA in the place of A-SBO increases the ultimate conversion, T_g and crosslink density. Modulus measurement of polyurethane film produced from OH-polyVESFA showed higher crosslink density and T_g than an analogous film derived from alcohol functional SBO. Compared to E-SBO, which possesses on average 4.5 epoxides per molecule, the epoxidized polymer based on the soybean oil-derived vinyl ether monomers possess tens to thousands of epoxy groups per molecule depending on the polymer molecular weight produced. As a result, coatings based on E-polyVESFA and its derivatives were shown to possess much higher crosslink

density at a given degree of functional group conversion compared to analogs based on conventional E-SBO.

7.2. INTRODUCTION

In general, the importance of renewable resource-based products in industry is very clear because these are non-toxic and biodegradable.³⁶⁴ Approximately 13 percent of crude oil used in the United States currently goes into the production of nonfuel chemicals.³³⁸ Since fossil resources are limited, there is an ongoing need to develop useful chemicals from renewable resources. Renewable resources that have been used to produce chemicals include plant oils, polysaccharides, sugars, and wood. Of these, plant oils are the most important renewable raw materials for the chemical industry.³³⁹ In the year of 2004, world total productions of oil from seven major crops are shown in Figure 7.1. Production continues to achieve the target rate of 3 - 4 % growth per year.³⁶⁵

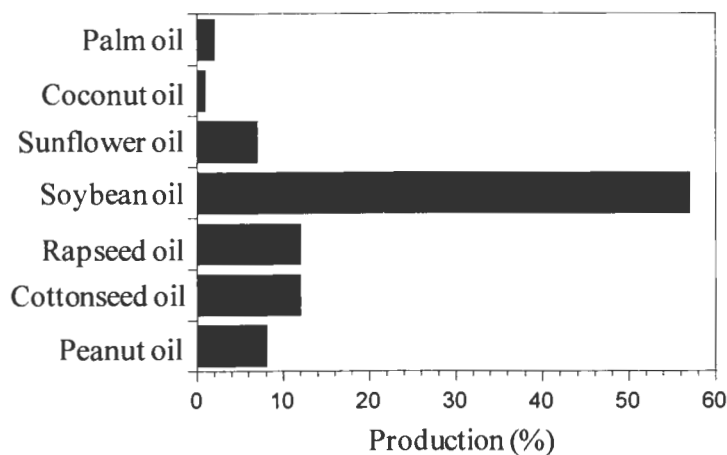


Figure 7.1. World production of oil from seven major crops.³⁶⁵

Soybean oil is the most widely used vegetable oil for non-food applications due to its low cost and availability. Soybean oil has a relatively high amount of unsaturation that could be epoxidized by the reaction with hydrogen peroxide³⁶⁶ and performic acid.³⁴⁷ Studies show that epoxidized soybean oil can be used in thermosetting polymers using the common methods of curing epoxide-functional resins such as with amines,³⁴⁸⁻³⁴⁹ anhydrides,³⁵⁰ and cationic photocure.³⁵¹⁻³⁵³ Epoxidized plant oils have been further derivatized by reaction of the epoxide groups with acrylic acid to produce acrylate-functional plant oils.³³⁹ Similar to other liquid, multifunctional acrylates, acrylate-functional plant oils have been used in radiation-curable coatings.³⁵⁴⁻³⁵⁵ In addition to serving as a starting material for the generation of acrylate-functional plant oils, epoxidized plant oils have been used to generate plant oil-based polyols by reaction of the epoxide groups with, for example, methanol.³⁵⁶ These polyols can be formulated with isocyanates to produce polyurethane coatings.³⁵⁶⁻³⁵⁷

Ultraviolet curing is one of the most efficient processes to rapidly transform liquid coatings to solid film. This well established technology offers numerous advantages over conventional curing technologies. The benefits of photocure systems in general include low or no volatile organic content, very rapid cure, and relatively low cost production. The overall production cost is usually less than bake systems. However, curing of thick article and film shrinkage due to very rapid and solvent less cure are the major problems in photocure systems.

Epoxidized soybean oil (E-SBO) has been extensively used in cationic photopolymerization to produce surface coatings and polymer composites. A major

disadvantage of E-SBO relative to more conventional epoxy resins such as bisphenol-A-based epoxy resins is the relatively low reactivity resulting from disubstitution of the epoxy groups.³⁶⁷ Cycloaliphatic epoxides are popular in cationic photopolymerization due to their faster reactivity. Since cycloaliphatic epoxides tend to produce high T_g crosslinked networks that can be brittle, vegetable oil-based epoxides can be used to impart flexibility and toughness.³⁶⁸

Cationic UV curing, based on the generation of acid using photochemical reaction followed by the cationic polymerization was first proposed in the decade of 1970s.³⁶⁹ Cationic UV curing coating is an important part in the UV curing market. It has been estimated that approximately eight percentage of industrial chemicals cured by photochemical route are cured by cationic polymerization.³⁷⁰ Compared to free radical photocure systems, cationic photocure systems are not inhibited by oxygen and radical impurities, and can lead to very long active center life-times.³⁷¹⁻³⁷² Additionally, cationic photocure coating possesses better flexibility and the system releases fewer volatile organic compounds.³⁷⁰ However, the cationic photocure system is chain transfer reaction was observed in the presence of water, alcohol, and base. The disadvantage of UV cure system is the cost of the equipment and materials.³⁵¹

A typical cationic UV photocure system consisted of an epoxide, a cationic initiator and additional ingredients such as other epoxides, polyols and additives. Alcohol and polyols react with epoxides. In the presence of UV light, the cationic photoinitiator generates cationic species that initiates the cationic ring opening polymerization of epoxides.

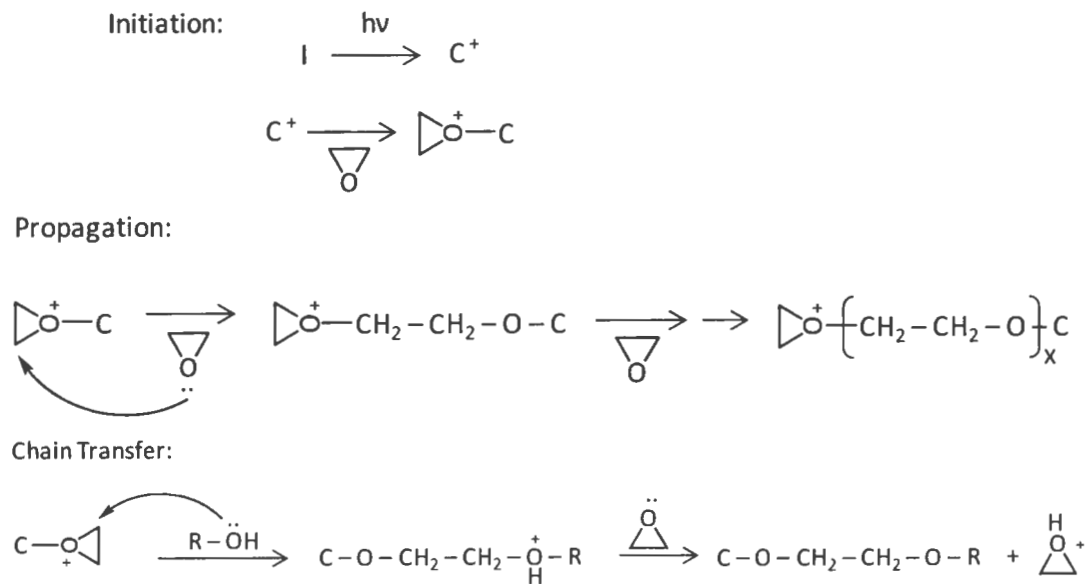


Figure 7.2. Schematic representation of cationic photopolymerization in presence of alcohols.³⁷³⁻³⁷⁴

The cationic photoinitiators belong to three main categories, for example, diazonium salts,³⁷⁵⁻³⁷⁶ onium salts^{375, 377} and organometallic complexes³⁷⁸⁻³⁸¹ (Figure 7.3). Onium salts (iodonium salt and sulfonium salt) are commonly used as cationic photoinitiator. They are stable, non-hygroscopic and efficient photoinitiator consisting of positive charge central atom and counter anion. Upon light radiation, these salts generate cation radicals and Brønsted acids (Figure 7.4). The cationic species reacts with epoxides to initiate the polymerization. The protonation of an epoxy group with such ‘super acids’ is very fast and quantitative.³⁷⁴ The quantitative yield of super acid (HB) was observed both in the presence and absence of a proton donor (RH) such as a solvent.³⁷³

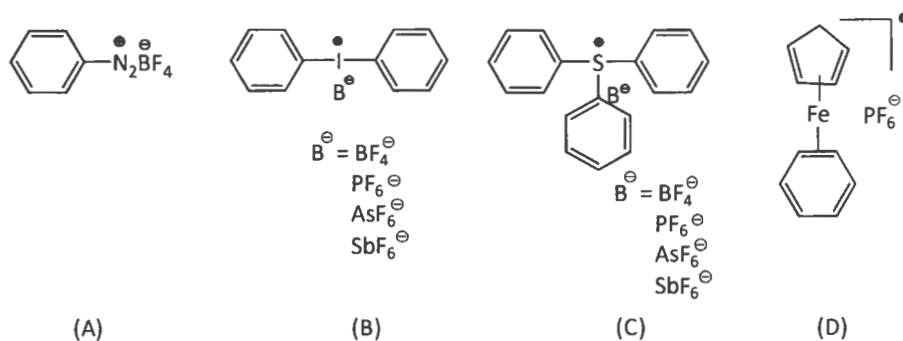


Figure 7.3. Chemical structure of (A) diazonium salt, (B) iodonium salt, (C) sulfonium salt, and (D) iron-arene salt.³⁷³

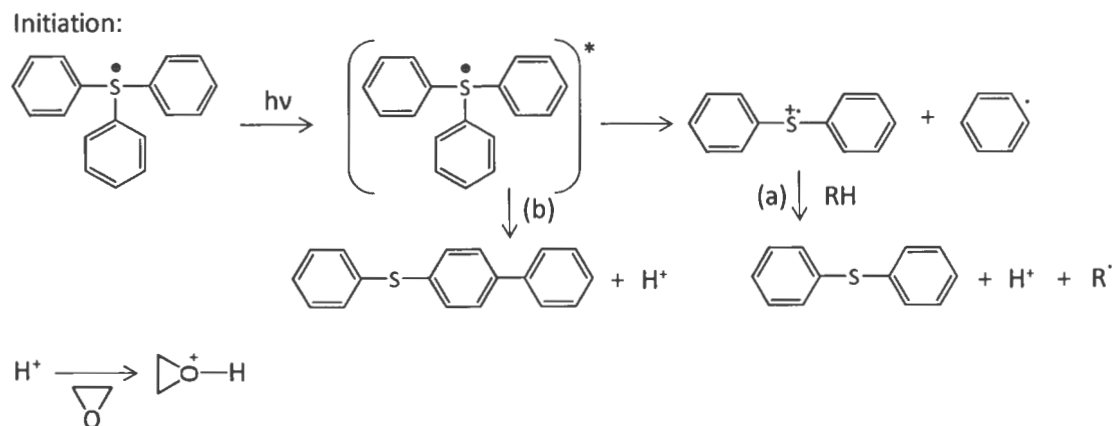
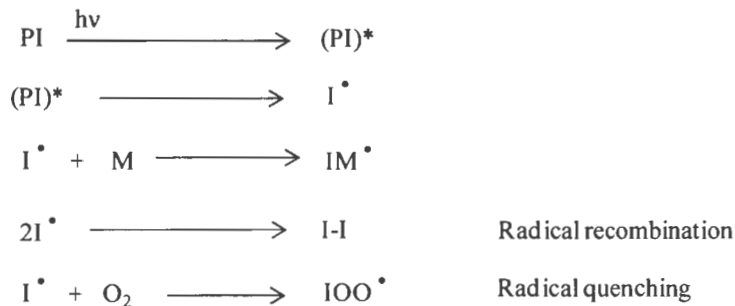


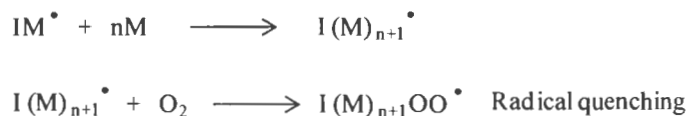
Figure 7.4. Photolysis of sulfonium salt and generation of protons in the (a) presence and (b) absence of proton donor.^{373, 375}

In contrast to the cationic photopolymerization, free radical polymerization is associated with the generation of free radical in the initiation stage followed by the addition of free radical to vinyl double bond. In general, free radical photopolymerization consists of following steps:

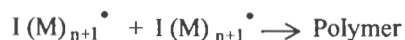
Initiation:



Propagation:



Termination:



The types of photo-initiator used in the free radical photopolymerization are cleavage type and bimolecular type (Figure 7.5). Cleavage type photo-initiators are the most effective that start initiation without a co-initiator. In the excited state, the bimolecular type initiator abstract hydrogen radical from synergist (co-initiator), such as alcohol, amine, and thiol and produces free radicals that initiate polymerization.

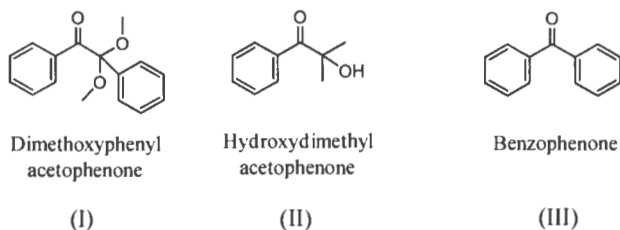


Figure 7.5. Free radical photoinitiator: Cleavage type (I and II), Bimolecular type (III).

Inhibition of oxygen is a major problem in free-radical photopolymerization. Oxygen preferentially scavenges the propagating free radical to form relatively unreactive

peroxy free radical that reacts with itself or other propagating radicals by coupling and disproportionation reaction to form inactive products.³⁸²⁻³⁸³ However, bimolecular type photo-initiators in combination with synergist are less affected by oxygen inhibition.³⁸⁴

A primary drawback related to the use of epoxidized vegetable oil in coatings application is their low modulus and low glass transition temperature (T_g) due to relatively low functional groups per triglyceride molecule. As a means to increase the thermo-mechanical properties of coatings derived from epoxidised vegetable oils is the synthesis of novel polymer from vegetable oil containing pendent fatty acids where the unsaturation in fatty acid can be converted to epoxide. The major difference of these epoxidized polymers to the epoxidized triglycerides is the number of epoxide groups per molecule. As the DP increases, the polymer possessing epoxides in the fatty acid pendent group dramatically decreases the gel-point. Thus, increasing the number of functional groups per molecule enables shorter cure times and higher crosslink densities at a given extent of conversion. The advantage of possessing higher number of functional groups per molecule is that, at a given degree of functional group conversion, the crosslink density, modulus, and T_g will be higher.

This document describes the epoxidation of polymer (polyVESFA) synthesized from SBO to produce epoxidized polyVESFA. This novel polymer is being referred to as the epoxidized polymer of the vinyl ether of soybean oil fatty acid esters (E-polyVESFA). The utility of this polymer in coating compositions was investigated by comparing properties to analogous coatings derived from E-SBO.

7.3. EXPERIMENTAL

7.3.1. Materials

Table 7.1 describes the starting materials used for the investigation.

Table 7.1. A list of the starting materials used for the investigation.

Chemical or Trade name	Description	Source
PolyVESFA	Polymer of the vinyl ether of soybean oil fatty acid esters	Synthesized previously
3-chloroperoxy benzoic acid	Epoxidizing agent, $\leq 77\%$	Sigma-Aldrich
Magnesium sulfate	Anhydrous, ReagentPlus®, $\geq 99.5\%$	Sigma-Aldrich
MeOH	Methanol, $\geq 99.8\%$	Sigma-Aldrich
Methylene chloride	ACS grade 99.5%	VWR
ESO	Vikoflex 7170, Epoxidized soybean oil	Arkema
CYRACURE® UVR-6000 (EHMOx)	3-Ethyl-3-hydroxymethyl-oxetane, Reactive diluent	Dow Chemical
CYRACURE® UVI-6974	Bis[4-(diphenylsulfonio)phenyl]sulfide bis(hexafluoroantimonate), 50 wt. % salt in propylene carbonate, Cationic photoinitiator	Dow Chemical
Tone™ 031 (Polyol)	Tri-functional liquid polyol	Dow Chemical
CDCl ₃	Deuterated chloroform	Sigma-Aldrich
TETA	Triethylenetetramine, technical grade (60 %)	Sigma-Aldrich
HDDA	1,6-Hexanediol diacrylate	Sartomer
IRGACURE® 184	1-Hydroxycyclohexyl phenyl ketone, Free-radical photoinitiator	BASF
HBF ₄	Tetrafluoroboric acid solution, 48 wt. % in H ₂ O	Sigma-Aldrich
Tolonate® IDT 70 B	Aliphatic polyisocyanate based on isophorone diisocyanate trimer (70 % solids in butyl acetate), Equivalent weight on delivery form = 342 g	Perstorp
DBTDL	Dibutyltin dilaurate, 95%	Sigma-Aldrich

7.3.2. Synthesis of E-polyVESFA

PolyVESFA was epoxidized using the synthetic scheme shown in Figure 7.6. A detailed procedure is as follows: 60 g of polyVESFA was dissolved in 1200 ml of methylene chloride in a 2-liter round-bottom flask and 71 g of 3-chloroperoxybenzoic acid added with vigorous stirring. The reaction was continued for 4 hours at room temperature at a stirrer speed of 650 rpm. After the reaction was complete, the polymer was precipitated into methanol, isolated by centrifugation, and dried under vacuum (5 – 7 mm of Hg) overnight.

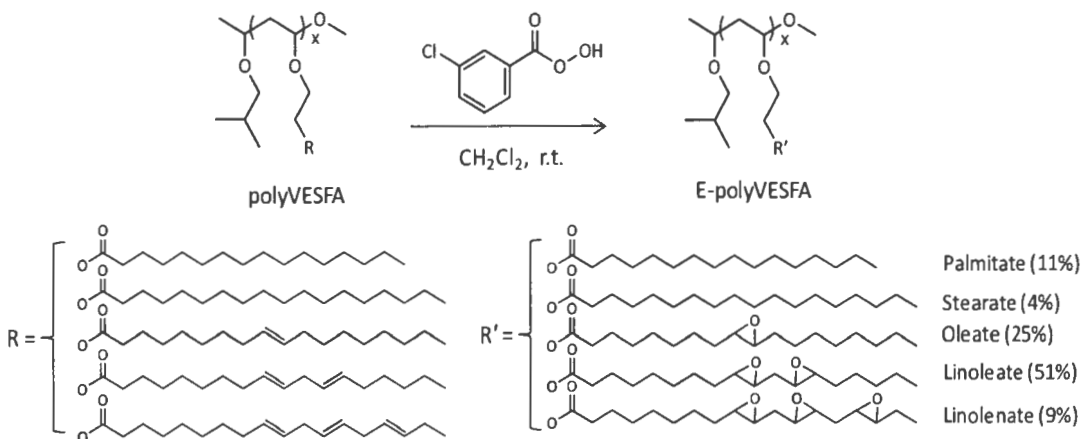


Figure 7.6. The synthetic scheme used to produce E-polyVESFA.

7.3.3. Synthesis of acrylated polyVESFA (A-polyVESFA) and acrylated soybean oil (A-SBO)

7.3.3.1. Synthesis of acrylated polyVESFA (A-polyVESFA)

An acrylate-functional derivative of polyVESFA was synthesized from E-polyVESFA using the synthetic scheme shown in Figure 7.7. A detailed procedure is as

follows: In a 1 liter round-bottom flask, 88.4 g of E-polyVESFA, 107 mg of hydroquinone, and 1.44 g of potassium acetate were dissolved in 435 g of toluene. The rapidly stirring solution was heated to 110 °C and 21.52 g of acrylic acid was added drop-wise over the period of 1 hour. After 42 hours of reaction, the temperature was cooled to room temperature and the toluene was removed by rotary evaporation. The crude material was diluted with methylene chloride and washed with DI water to remove unreacted acrylic acid and catalyst residue. The organic layer was dried with anhydrous magnesium sulfate. The product was isolated by rotary evaporation of methylene chloride and drying under vacuum (5 – 7 mm of Hg) overnight.

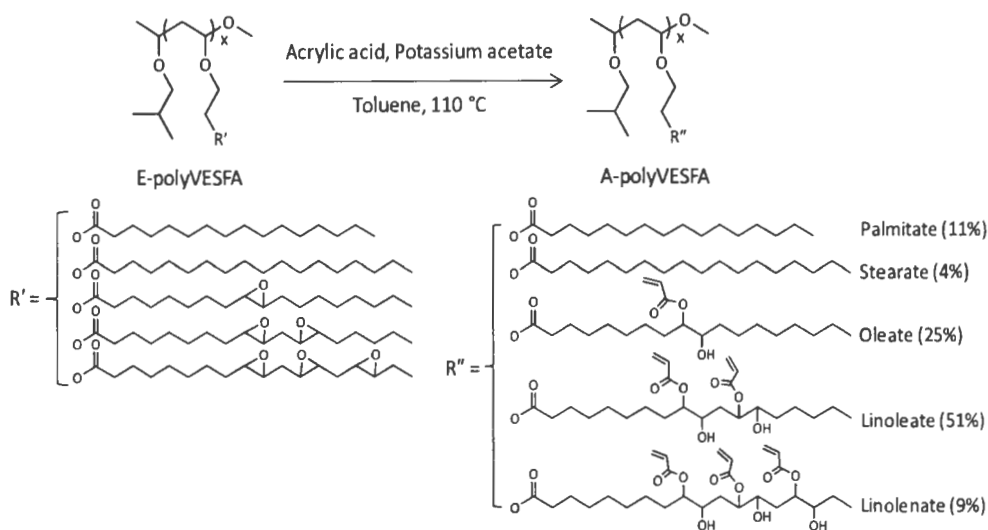


Figure 7.7. The synthetic scheme used to produce A-polyVESFA.

7.3.3.2. Synthesis of acrylated soybean oil (A-SBO)

The synthesis procedure of an acrylate-functional derivative of SBO from commercially available E-SBO is described as follows: In a 1 liter round-bottom flask, 100

g of E-SBO, 121 mg of hydroquinone, and 1.62 g of potassium acetate were dissolved in 493 g of toluene. The rapidly stirring solution was heated to 110 °C and 30.38 g of acrylic acid was added drop-wise over the period of 1 hour. After 42 hours of reaction, the temperature was cooled to room temperature and the toluene was removed by rotary evaporation. The crude material was diluted with methylene chloride and washed with DI water to remove unreacted acrylic acid and catalyst residue. The organic layer was dried with anhydrous magnesium sulfate. The product was isolated by rotary evaporation of methylene chloride and drying under vacuum (5 – 7 mm of Hg) overnight.

7.3.4. Synthesis of alcohol-functional polyVESFA (OH-polyVESFA) and soybean oil (OH-SBO)

7.3.4.1. Synthesis of OH-polyVESFA

An OH-polyVESFA was synthesized from E-polyVESFA using the synthetic scheme shown in Figure 7.8. A detailed procedure is as follows: 33.15 g of methanol and 1.94 g of tetrafluoroboric acid solution were combined in a 1-liter round bottom flask and the temperature was maintained at 30 °C. A solution of 60 g E-polyVESFA and 340 g toluene was added to the vessel with continuous stirring and the temperature was raised to 50 °C. After 1 hour of reaction, 3.8 ml of ammonium hydroxide solution (30% v/v NH₄OH in water) was added to neutralize the acidity of the reaction mixture and cooled to room temperature. The organic layer was washed with 300 ml of deionized water thrice and dried with anhydrous magnesium sulfate. The polymer was stored as a solution in toluene at a concentration of 20.5 weight percent solid.

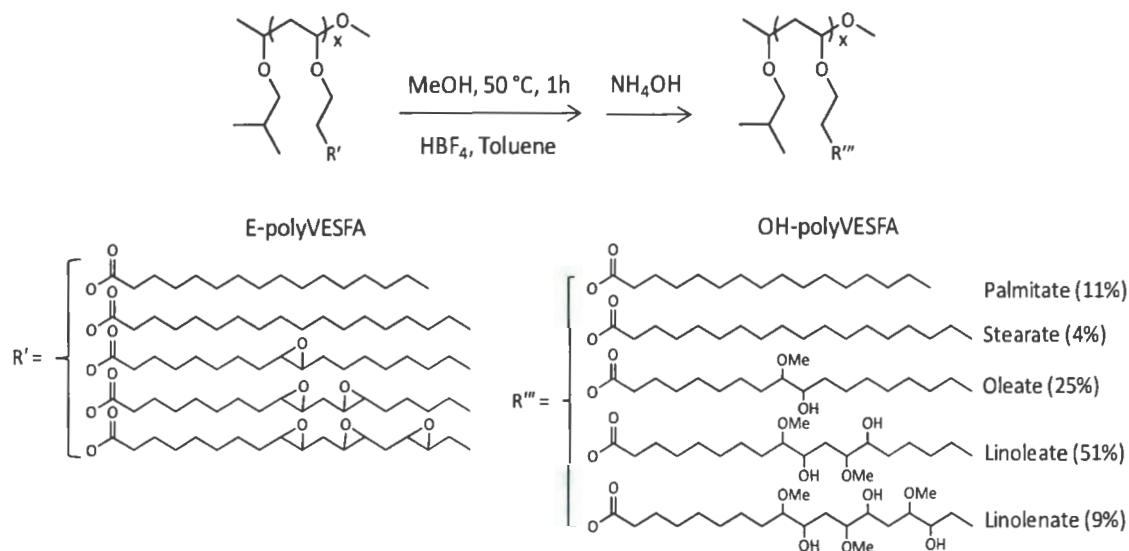


Figure 7.8. The synthetic scheme used to produce OH-polyVESFA.

7.3.4.2. Synthesis of alcohol-functional soybean oil (OH-SBO)

The synthesis procedure of an OH-SBO from commercially available E-SBO is described as follows: 41.26 g of methanol and 2.41 g of tetrafluoroboric acid solution were combined in a 1-liter round bottom flask and the temperature was maintained at 30 °C. A solution of 60 g E-SBO and 340 g toluene was added to the vessel with continuous stirring and the temperature was raised to 50 °C. After 1 hour of reaction, 4.75 ml of ammonium hydroxide solution (30% v/v NH₄OH in water) was added to neutralize the acidity of the reaction mixture and cooled to room temperature. The organic layer was washed with 300 ml of deionized water thrice and dried with anhydrous magnesium sulfate. The product was collected after rotary evaporation of toluene and dried under vacuum overnight.

7.3.5. Coating preparation to compare the difference between E-polyVESFA and E-SBO in epoxy-amine cure systems

An example of the production of epoxy-amine curable liquid coatings is as follows: An epoxy-amine curable liquid coating was prepared by mixing E-polyVESFA and TETA together using a FlackTek mixer at 3500 rpm for 3 minutes. An analogous reference coating was produced by replacing E-polyVESFA with commercially available ESO. Table 7.2 describes the compositions of the coatings produced.

Table 7.2. Compositions used to compare the difference between E-polyVESFA and E-SBO in epoxy-amine cure systems.

Formulation	Wt. of E-polyVESFA (g)	Wt. of E-SBO (g)	Wt. of TETA (g)
E-polyVESFA/TETA	10.53	---	1.47
E-SBO/TETA	---	10.22	1.78

7.3.6. Coating preparation to compare the difference between E-polyVESFA and E-SBO in cationic photocure systems

7.3.6.1. Preparation of liquid coatings

An example of the production of a series of liquid coatings is as follows: A series of radiation curable liquid coatings were prepared by mixing E-polyVESFA, EHMOx, Tone™ 031, and Cyracure® UVI-6974 photoinitiator together using a FlackTek mixer at 3500 rpm for 3 minutes. An analogous series of reference coatings was produced by

replacing E-polyVESFA with commercially available ESO. Table 7.3 describes the compositions of the coatings produced.

Table 7.3. Compositions used to compare the difference between E-polyVESFA and E-SBO in cationic photocure systems.

Sample ID	Wt. % E-polyVESFA	Wt. % ESO	Wt. % EHMOx	Tone™ 031 Wt. %	Wt. % CYRACURE® UVI-6974	Clarity
100S-HI	--	95.2	--	--	4.8	Hazy
100P-HI	95.2	--	--	--	4.8	Hazy
100S-LI	--	97.6	--	--	2.4	Hazy
100P-LI	97.6	--	--	--	2.4	Hazy
80/10/10S/Ox/To-LI	--	78	9.8	9.8	2.4	Hazy
80/10/10P/Ox/To-LI	78	--	9.8	9.8	2.4	Clear
70/30S/Ox-HI	--	66.6	28.6	--	4.8	Clear
70/30P/Ox-HI	66.6	--	28.6	--	4.8	Hazy
70/30S/Ox-LI	--	68.3	29.3	--	2.4	Clear
70/30P/Ox-LI	68.3	--	29.3	--	2.4	Clear
70/20/10S/Ox/To-LI	--	68.3	19.5	9.8	2.4	Clear
70/20/10P/Ox/To-LI	68.3	--	19.5	9.8	2.4	Hazy
70/10/20S/Ox/To-LI	--	68.3	9.8	19.5	2.4	Hazy
70/10/20P/Ox/To-LI	68.3	--	9.8	19.5	2.4	Hazy

7.3.6.2. Preparation of cured free films

Each liquid coating mixture was cast over Teflon® coated glass using a square draw down bar (BYK Gardner) to produce wet films about 200 microns in thickness. The films were cured by passing coated substrates once or twice under a F300 UVA lamp from

Fusion UV Systems (UVA light intensity $\sim 1420 \text{ mW/cm}^2$ as measured by UV Power Puck[®] II from EIT Inc.) equipped with a bench top conveyor belt set at a belt speed of 24 feet/min. Free films were characterized using dynamic mechanical thermal analysis.

7.3.6.3. Characterization of cured coatings

Each liquid coating mixture was cast on two cold rolled steel Q-panels, two aluminum Q-panels, and one glass panel using a square draw down bar (BYK Gardner) to produce wet films about 200 microns in thickness. The coatings were cured by passing coated substrates once under a F300 UVA lamp from Fusion UV Systems (UVA light intensity $\sim 1420 \text{ mW/cm}^2$ as measured by UV Power Puck[®] II from EIT Inc.) equipped with a bench top conveyor belt set at a belt speed of 24 feet/min. Cured coatings were characterized by MEK double rubs (ASTM D 5402-93), pencil hardness test (ASTM D 3363-00), Konig pendulum hardness test (ASTM D 4366-95), impact resistance test (ASTM D 2794-93), and crosshatch adhesion test (ASTM D 3359-97).

7.3.7. Coating preparation to compare the difference between A-polyVESFA and A-SBO in free-radical photocure systems

7.3.7.1. Preparation of liquid coatings

An example of the production of a series of liquid coatings is as follows: A series of radiation curable liquid coatings were prepared by mixing A-polyVESFA, HDDA, and Irgacure[®] 184 photoinitiator together using a FlackTek mixer at 3500 rpm for 3 minutes. An analogous series of reference coatings was produced by replacing A-polyVESFA with A-SBO. Table 7.4 describes the compositions of the coatings produced.

Table 7.4. Compositions used to compare the difference between A-polyVESFA and A-SBO in free-radical photocure systems.

Sample ID	Wt. % A-polyVESFA	Wt. % A-SBO	Wt. % HDDA	Wt. % IRGACURE [®] 184
60/40 A-VESFA/HDDA HI	58.3	----	39.3	2.4
60/40 A-VESFA/HDDA LI	59.4	----	39.6	1.0
60/40 A-SBO/HDDA HI	----	58.3	39.3	2.4
60/40 A-SBO/HDDA LI	----	59.4	39.6	1.0

7.3.8. Coating preparation to compare the difference between OH-polyVESFA and OH-SBO in polyurethane coating systems

7.3.8.1. Preparation of liquid coatings

The reaction scheme to synthesize a polyurethane coating is shown in Figure 7.9. An example of the production of a liquid coating is as follows: A polyol-isocyanate curable liquid coating was prepared by mixing OH-polyVESFA, Tolonate[®] IDT, DBTDL, and toluene together using a FlackTek mixer at 3500 rpm for 3 minutes. An analogous reference coating was produced by replacing OH-polyVESFA with OH-SBO. Table 7.5 describes the compositions of the coatings produced.

7.3.8.2. Preparation of cured free films

Each liquid coating solution was cast over stamped temple of 1 mm in depth glued over Teflon[®] coated glass. The coatings were cured by heating coated substrates in an air oven at 80 °C for overnight. Free films were characterized using dynamic mechanical thermal analysis.

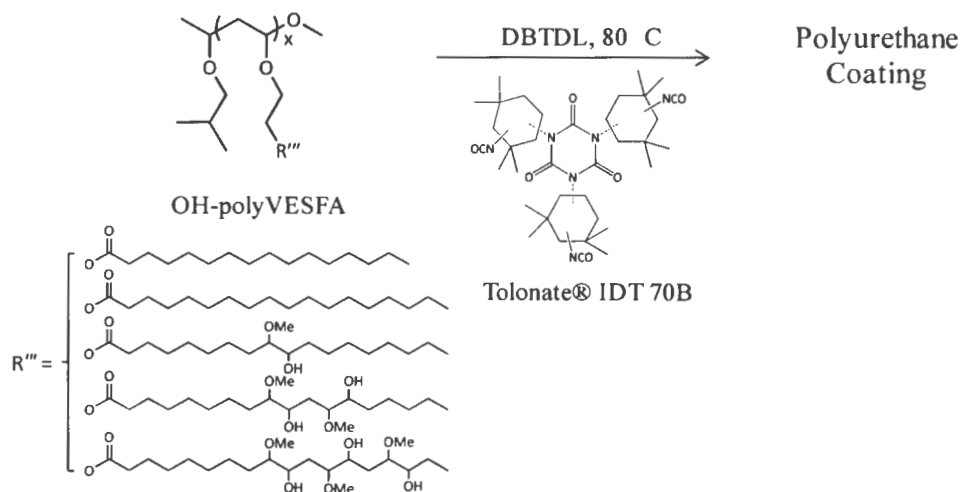


Figure 7.9. The synthetic scheme used to produce polyurethane coating.

Table 7.5. Compositions used to compare the difference between OH-polyVESFA and OH-SBO in polyurethane coating systems.

Sample ID	OH-polyVESFA solution ¹ (g)	OH-SBO ² (g)	Tolonate® IDT ³ (g)	DBTDL solution ⁴ (mg)	Toluene (g)
OH-polyVESFA/IDT	10	--	2.4	74.6	--
OH-SBO/IDT	--	5	7.13	200	21.2

¹ OH-polyVESFA solution: OH-polyVESFA dissolved in toluene at 20.5 wt. % solid.

² OH-SBO: Used as 100% solid.

³ Tolonate® IDT: Used as supplied (70 wt. % solid in butyl acetate).

⁴ DBTDL solution: 1 wt% DBTDL in toluene and butyl acetate mixture.

7.3.9. Instrumentation and procedures

7.3.9.1. Nuclear Magnetic Resonance (NMR) spectroscopy

A JEOL-ECA 400 (400MHz) nuclear magnetic resonance (NMR) spectrometer equipped with an autosampler was used to generate proton NMR (¹H NMR) spectra. Data acquisition was completed using 16 scans in CDCl₃ as the lock solvent.

7.3.9.2. Fourier Transform Infrared (FTIR) spectroscopy

A Nicolet Magna-850 FTIR instrument was employed to measure FTIR spectra. Samples were coated on dry potassium bromide disc, and the measurements were carried out in the range of wavenumbers from 600 cm^{-1} to 3900 cm^{-1} using 64 scans with a data spacing of 0.964 cm^{-1} .

7.3.9.3. Real-Time FTIR (RT-FTIR)

RT-FTIR experiments were carried out using a Nicolet Magna-IR 850 spectrometer Series II. The light source was a LESCO Super Spot MK II 100W DC UVA mercury vapor short lamp. Samples were spin-coated onto a KBR plate at 4000 rpm for 20 seconds and exposed to ultraviolet (UV) light. FTIR spectra were taken at a rate of 1 spectrum/s with a resolution of 4 cm^{-1} . Experiments were carried out in air at 25 °C and the UV light intensity was 59 mW/cm^2 as measured using a UV Power Puck II from EIT Inc. For cationic and free-radical photocure systems, samples were exposure to UV light for 3 minutes and 30 seconds respectively.

7.3.9.4. Differential Scanning Calorimetry (DSC)

The thermal properties of polymers and SBO-derivatives were determined using differential scanning calorimetry (DSC). The instrument utilized was a DSC Q1000 from TA Instruments, and sample sizes ranged from 4.5 to 5.5 mg. Samples were first heated from 30 °C to 70 °C at a heating rate of 10 °C/minute (1st heat), cooled from 70 °C to -120 °C at a cooling rate of 10 °C/minute (cooling), and reheated from -120 °C to 120 °C at a heating rate 10 °C/minute (2nd heat). The T_g reported was obtained from the 2nd heat.

7.3.9.5. Photo-Differential Scanning Calorimetry (Photo-DSC)

Photo-DSC experiments were performed using a DSC Q1000 from TA Instruments which was equipped with a photocalorimetric accessory. Experiments were carried out using a UV light (320–500 nm) intensity of 50 mW/cm² and a temperature of 30 °C. Liquid sample sizes ranged from 4.5 to 5.5 mg. For cationic photocure systems, samples were equilibrated for 1 minute before exposure to UV light for 7 minutes followed by a temperature ramp from 0 °C to 200 °C at a rate of 10 °C/min under nitrogen to determine the residual heat associated with thermal cure of residual (unreacted functional groups). For free-radical photocure systems, samples were equilibrated for 1 minute before exposure to UV light for 30 seconds.

7.3.9.6. Thermogravimetric Analysis (TGA)

Thermogravimetric analysis (TGA) was carried out using a Q500 from TA Instruments. Samples (15 to 25 mg) were heated from 30 °C to 800 °C at a heating rate of 20 °C/minute.

7.3.9.7. Dynamic Mechanical Analysis (DMA)

Viscoelastic properties of cured free films were characterized using a TA800 dynamic mechanical thermal analyzer from TA Instruments. Temperature was ramped from -40 °C to 120 °C using a heating rate of 5 °C/min, strain rate of 0.02 %, and frequency of 1 Hz.

7.3.9.8. Rheological properties

Rheological properties were determined with an ARES Rheometer from TA Instruments. For monitoring epoxy amine cure kinetics, liquid samples were placed in

between two parallel plates and heated for 20 hours at 120 °C using a constant frequency of 2 rad/s and strain of 1%. For measuring viscosity of E-polyVESFA and E-SBO, liquid samples were placed between a cone and plate and viscosity was monitored as a function of shear rate at a temperature of 25 °C.

7.4. RESULTS AND DISCUSSION

7.4.1. Characterization and property comparison of E-polyVESFA with E-SBO (ESO)

7.4.1.1. Characterization of E-polyVESFA and E-SBO

E-polyVESFA was produced according to the synthetic scheme shown in Figure 7.6. The successful synthesis of E-polyVESFA was confirmed by ^1H NMR (Figure 7.10), ^{13}C NMR (Figure 7.11), and FTIR (Figure 7.12) spectra.

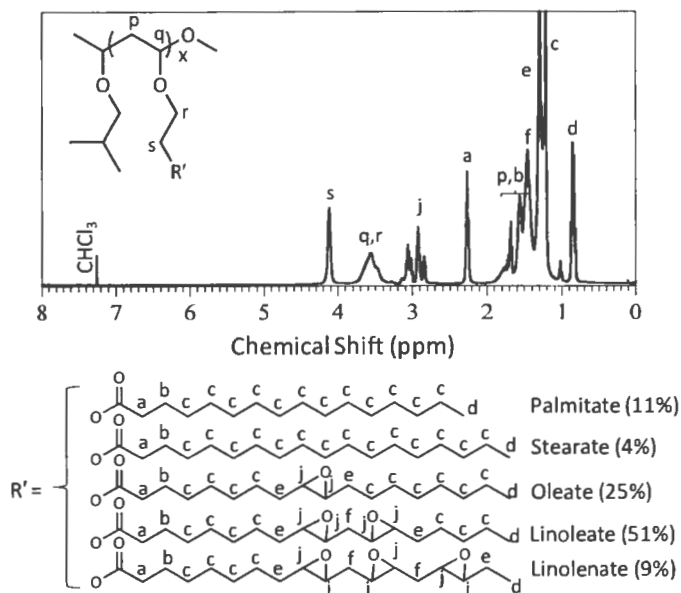


Figure 7.10. ^1H NMR spectrum obtained for E-polyVESFA.

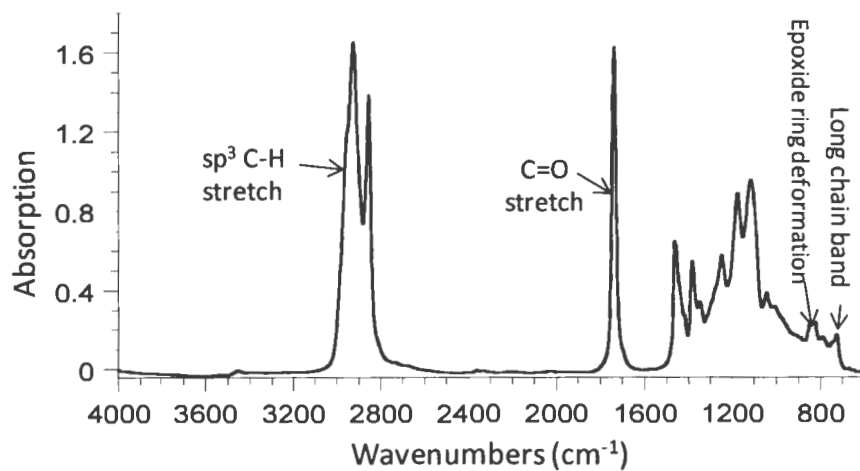


Figure 7.12. FTIR spectrum obtained for E-polyVESFA.

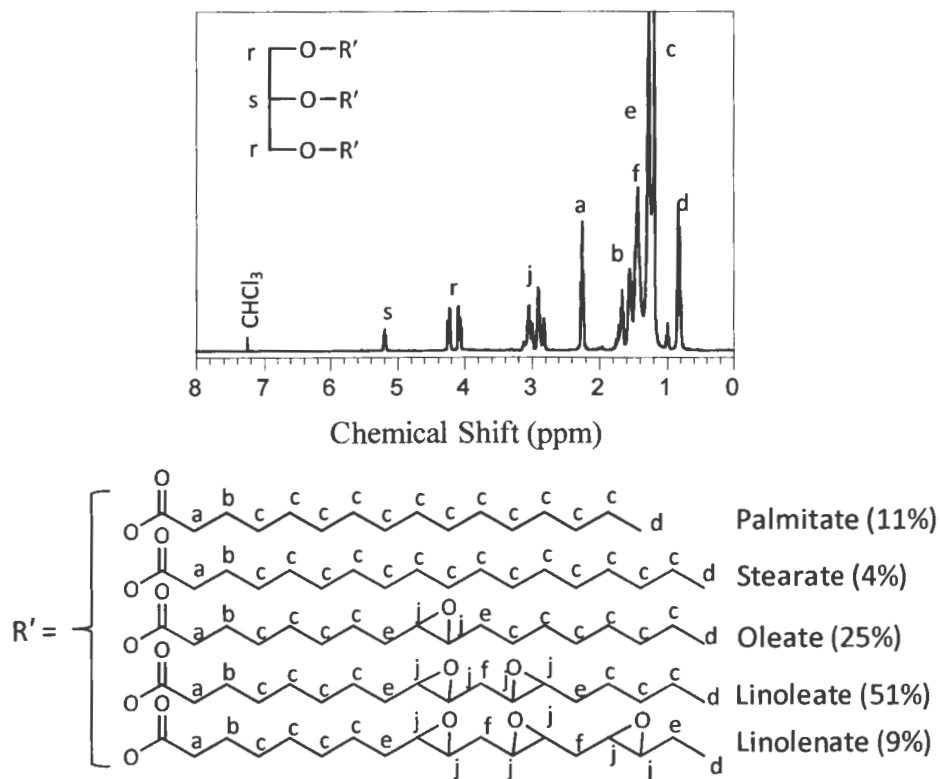


Figure 7.13. ¹H NMR spectrum obtained for E-SBO.

7.4.1.2. Property comparison of E-polyVESFA with E-SBO

The basic properties of the E-polyVESFA were compared to E-SBO. Figures 7.14.A and 7.14.B provide a comparison of the thermal properties of E-polyVESFA, E-SBO. The DSC thermograms displayed in Figure 7.14.A showed very different thermal properties between E-polyVESFA and E-SBO. After cooling from 70 °C to -120 °C at 10°C/minute, the E-SBO sample exhibited a small endotherm at -60.3 °C which was followed by a significant crystallization exotherm and two endotherms with peak temperatures of -29.3°C, -15.7 °C and -5.8 °C, respectively. This behavior suggests that the original crystallites formed during the controlled cooling were quite imperfect resulting in a relatively low melting temperature and recrystallization to produce the higher temperature endotherms.

In contrast, E-polyVESFA displayed a glass transition temperature at -58.0 °C and a very weak, diffuse melting transition with an enthalpy of melting of 5.97 J/gm and a peak maximum at -21.7 °C. The weak, diffuse endotherm indicates that incorporating the fatty acids into a polymer as pendent groups greatly reduces the crystallizability of the fatty acid chains. Considering the higher viscosity and corresponding reduced molecular mobility associated with a polymeric structure as compared to a triglyceride, it is not surprising that crystallization of the fatty acids chains in E-polyVESFA was reduced compared to SBO. The TGA was performed in an air-oxidative environment with a constant increase in temperature. As shown in Figure 7.14.B, the decomposition temperature of E-polyVESFA was slightly higher than that of E-SBO. Figure 7.15 provides a comparison of the rheological properties of a E-polyVESFA sample to E-SBO.

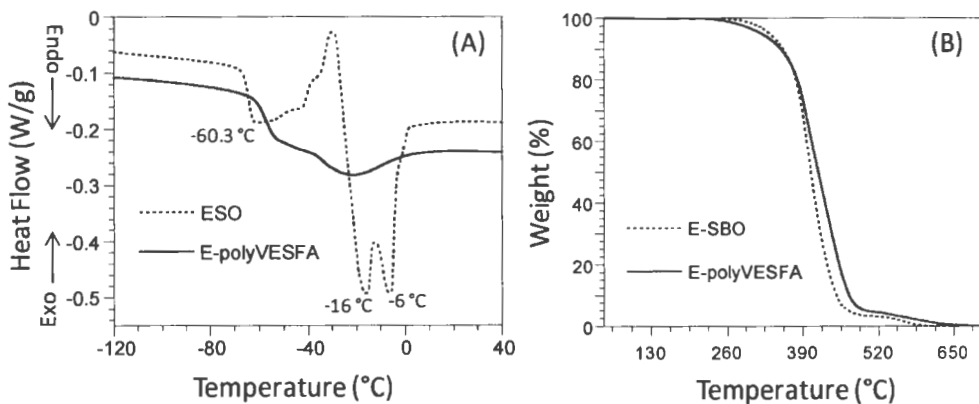


Figure 7.14. (A) DSC thermograms for E-polyVESFA and E-SBO. (B) TGA thermograms for E-polyVESFA and E-SBO.

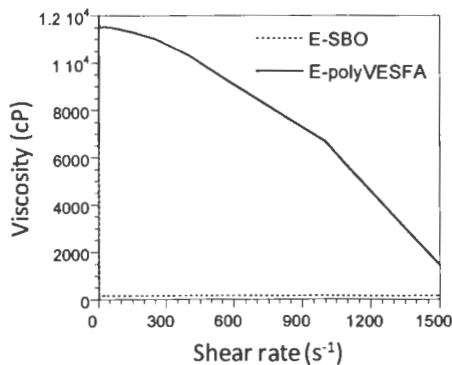


Figure 7.15. Plot of viscosity as a function of shear rate for E-polyVESFA and E-SBO.

From Figure 7.15, it can be seen that the E-polyVESFA possessed a viscosity that was about two orders of magnitude higher than that of E-SBO at shear rates below 1000 s⁻¹ which is consistent with the major difference in molecular weight between the two materials. In addition, the viscosity of the E-polyVESFA sample showed significantly more shear sensitivity than E-SBO. The shear sensitivity of the E-polyVESFA indicates that the molecular weight of the polyVESFA was high enough to enable significant polymer chain entanglement. The epoxy equivalent weight determined according to the

ASTM D 1652 – 97 for E-polyVESFA and E-SBO were 290 g/eq and 232 g/eq respectively.

7.4.2. Characterization of coatings to compare the difference between E-polyVESFA and E-SBO in epoxy-amine cure systems

The epoxy group is a very versatile functionality for producing coatings since curing can be accomplished by a variety of methods including amine-cure, anhydride-cure, and cationic photocure. To understand the utility of E-polyVESFA as E-SBO in the production of coatings, an amine-cured system was investigated. For amine-cure, a simple experiment was conducted in which the cure kinetics of a blend of E-polyVESFA and TETA was compared to that of an analogous blend of E-SBO and TETA. A 1/1 stoichiometry between the epoxy groups and NH groups was used, and cure kinetics were characterized by monitoring shear modulus as function of time at 120 °C. As shown in Figure 7.16, the shear modulus for the E-polyVESFA/TETA blend began to increase after just 25 minutes at 120 °C and increased sharply over a time period of 4 hours. This result indicates that the crosslinked network was developed relatively rapidly and full crosslinking was achieved within about 5 hours. In contrast, it took over 15 hours at 120 °C for an increase in shear modulus to be observed for the E-SBO/TETA blend.

Assuming the kinetics of the reaction between the epoxy groups and the NH groups were the same for the two blends, which seems reasonable considering the epoxy groups present in E-polyVESFA and E-SBO are chemically equivalent, then the dramatic difference in shear modulus response as a function of time can only be attributed to the

difference in the number of epoxy groups per molecule. As discussed in the *Introduction*, increasing the number of functional groups per molecule decreases the gel-point dramatically. Even though the extent of conversion of the epoxy-amine reaction for the two systems may have been the same at any point in time during the cure process, the much higher epoxy content per molecule for E-polyVESFA resulted in the gel-point being reached at much lower conversion/cure time providing elasticity to the material as indicated by the increase in shear modulus. This dramatic reduction in the time required for the development of the crosslinked network associated with the use of E-polyVESFA in an amine-cured system could have tremendous commercial utility considering energy cost and production rate affects associated with thermal curing.

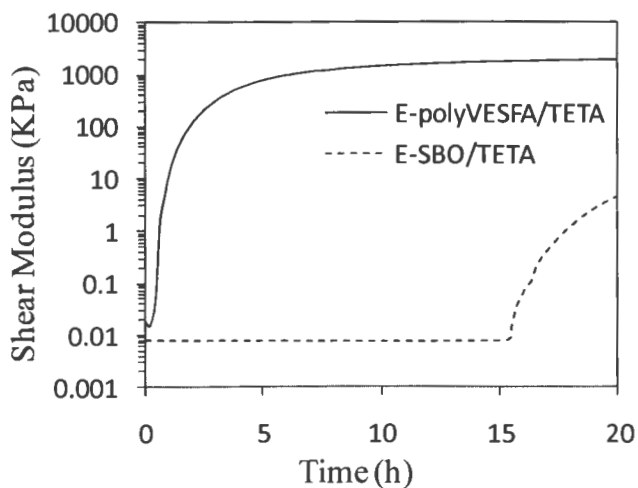


Figure 7.16. Shear modulus as a function time at 120 °C for a blend of E-polyVESFA and TETA as well as E-SBO and TETA. A 1/1 stoichiometry between the epoxy groups and NH groups was used.

7.4.3. Characterization of coatings to compare the difference between E-polyVESFA and E-SBO in cationic photocure systems

Cationic photocure has become a very important method for producing thermoset coatings. The benefits of photocure systems in general include low or no volatile organic content, very rapid cure, and relatively low cost production. Compared to free radical photocure systems, cationic photocure systems are not inhibited by oxygen and can lead to very long active center life-times.³⁸⁵ To understand the basic differences between E-SBO and E-polyVESFA in a cationic photocure system, the series of coatings described in Table 7.3 were prepared and characterized with respect to cure rate and viscoelastic properties. Cure rate was characterized using both RT-FTIR and photo-DSC.

7.4.3.1. Characterization using Real-Time FTIR (RT-FTIR)

RT-FTIR experiments were conducted by monitoring the change in absorbance of epoxides from 860 cm^{-1} to 800 cm^{-1} as a function of UV exposure time. Absorbance over this wavelength range corresponds to both epoxy ring motions and oxetane ring motions. As shown in Figure 7.17, the coatings based on blends of E-polyVESFA and EHMOx showed significantly higher rates of cure than the corresponding coatings based on E-SBO and EHMOx.

Considering the fact that the chemical structure of the epoxy groups in E-SBO and E-polyVESFA are the same and the concentration of epoxy groups in the two materials is similar (epoxy equivalent weight for E-SBO and E-polyVESFA are 232 g/mole and 290 g/mole , respectively), it was somewhat surprising that reaction rates were so different. The

most plausible explanation for the difference can be based on differences in gel-point. As discussed earlier in this document, the much higher number of functional groups per molecule associated with E-polyVESFA as compared to E-SBO results in gelation occurring at lower reaction conversion.

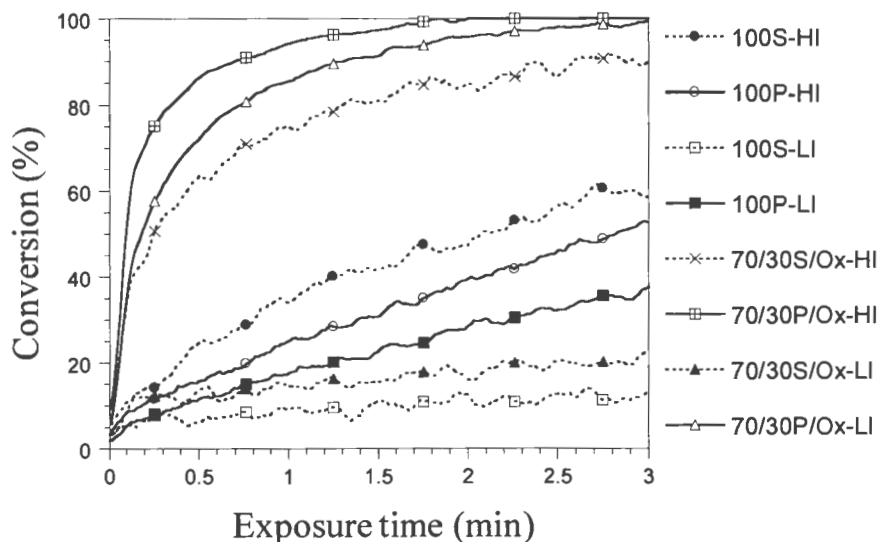


Figure 7.17. Results obtained from RT-FTIR experiments on the coatings described in Table 7.3 when the change of absorption in epoxides was monitored as a function of UV exposure time.

The result of reaching the gel-point at low reaction conversion is a rapid rise in viscosity and major changes in diffusion characteristics. Gelation essentially prevents polymer molecule translational diffusion (i.e. diffusion of entire polymer chains) and can significantly limit polymer segmental diffusion (i.e. diffusion of pendent groups or portions of polymer chains). Compared to polymer translational and segmental diffusion, monomer diffusion is reduced to a much lower extent. Assuming termination reactions are

bimolecular reactions that do not involve the monomer (i.e. EHMOx), it would be expected that, at a given degree of functional group conversion, the relative rate of termination to propagation would be lower for the more highly crosslinked medium because diffusion limitations would have a greater effect on reducing termination rate as compared to propagation rate. This phenomenon has been referred to by Ito and coworker³⁸⁶ as a “cation isolation effect” and essentially results in a higher concentration of propagating species during polymerization/cure enabling faster polymerization/cure.

7.4.3.2. Characterization using photo DSC

With photo-DSC, heat flow from a sample is monitored as a function of UV exposure time. For the coatings described in to Table 7.3, the plot of heat flow (W/g) as a function of UV light exposure time (s) was shown in Figure 7.18. From the photo-DSC graphs, the maximum heat flow (H_{max}) can be related to the rate of polymerization,³⁸⁷ and the total heat evolved (ΔH) can be related to the percentage of conversion. The ΔH was calculated after integrating the peak area under the curve. The ΔH is related to the percentage of total conversion according to the following equation:

$$\% \text{ of Total Conversion} = \frac{\Delta H_{\text{Photopolymerization}}}{\Delta H_{\text{Photopolymerization}} + \Delta H_{\text{Residual Heat}}} \times 100\%$$

where, $\Delta H_{\text{Photopolymerization}}$ and $\Delta H_{\text{Residual Heat}}$ represent the heat of reaction evolved during photo-polymerization and thermal polymerization respectively. Figure 7.19 shows the thermograms obtained from thermal cure that was applied immediately after photo-DSC experiments on the coatings described in Table 7.3. Table 7.6 lists the time period

associated with the onset of cure (i.e. induction time), the time period associated with the peak maximum of the heat flow (i.e. time to peak maximum), and the percent of conversion obtained by UV light exposure for both the control and experimental coatings.

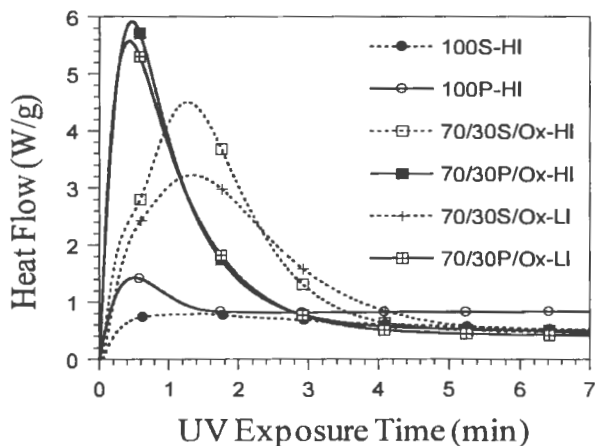


Figure 7.18. Results obtained from photo-DSC experiments on the coatings described in Table 7.3.

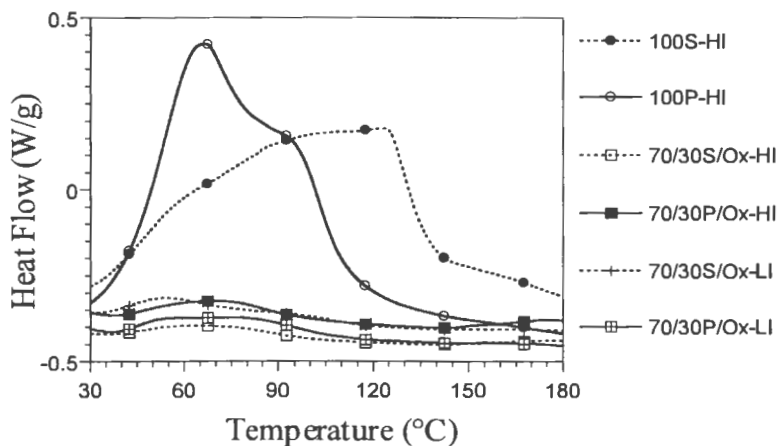


Figure 7.19. Results obtained from thermal cure that was applied immediately after photo-DSC experiments on the coatings described in Table 7.3.

Table 7.6. Data obtained from photo-DSC experiments on the coatings described in Table 7.3.

Sample ID	Induction time (secs)	Time to peak maximum (secs)	% of conversion (2 minutes UV exposure)	% of conversion (7 minutes UV exposure)
100S-HI	3.6	54.6	9.3	39.2
100P-HI	0	28.8	16.7	44.3
70/30S/Ox-HI	1.8	75.6	36.8	98.6
70/30P/Ox-HI	0.6	27.6	64.4	97.6
70/30S/Ox-LI	3.6	78.6	26.7	97.1
70/30P/Ox-LI	0.6	25.8	62.1	97.1

From Table 7.6, it can be seen that the coatings based on E-polyVESFA possess faster cure rates as indicated by the shorter time period associated with peak of the reaction exotherm and higher extent of conversion after 2 minute and 7 minutes UV exposure. Data obtained from Table 7.6 shows that the induction time and the time to peak maximum of heat flow was lower for coatings derived from E-polyVESFA than that derived from E-SBO analog.

As shown in Figure 7.18, the relative rates of cure obtained with photo-DSC gave similar results to those obtained with RT-FTIR. Coatings based on blends of E-polyVESFA and EHMOx showed higher rates of cure than the corresponding coatings based on E-SBO and EHMOx. One discrepancy was observed between the RT-FTIR data and the photo-DSC data. This discrepancy had to do with the relative rates of cure between coatings based on pure E-polyVESFA (i.e. 100P-HI) and pure E-SBO (i.e. 100S-HI). Based on RT-FTIR, the rate of cure obtained with the E-SBO coating was slightly higher

than that of the E-polyVESFA coating while just the opposite result was obtained with photo-DSC. At present, the root cause of this discrepancy is not known; however, it should be understood that the heat flow measured from photo-DSC is a composite of both the polymerization exotherm as well as heat released from the conversion of UV energy into thermal energy, while RT-FTIR is a direct measure of the consumption of functional groups.

7.4.3.3. Coating characterization

Table 7.7 lists the physical parameters of cured coatings produced according to the formulation in Table 7.3. These coatings were cured by passing coated substrates once under a UVA lamp at a belt speed of 24 feet/min. All of the coatings derived from the E-polyVESFA were able to form tack-free films immediately after passing through the UV light. However, only 70/30S/Ox-HI and 70/30S/Ox-LI coatings derived from E-SBO formed tack-free film immediately after cure. The coating, 100S-LI was not able to form solid film even after 18 hours dark cure. The dramatic difference in formation in tack-free film after UV light exposure as a function of time can only be attributed to the difference in the number of epoxy groups per molecule. As discussed in the “Introduction”, increasing the number of functional groups per molecule decreases the gel-point dramatically. Even though the extent of conversion of the epoxides for the two systems may have been the same at any point in time during the cure process, the much higher epoxy content per molecule for E-polyVESFA resulted in the gel-point being reached at much lower conversion/cure time providing elasticity to the material as indicated by the tack-free film.

This dramatic reduction in the time required for the development of the crosslinked network associated with the use of E-polyVESFA in an cationic photo-cured system could have tremendous commercial utility considering energy cost and production rate.

Table 7.7. Properties of coatings produced from E-polyVESFA and E-SBO in cationic photocure systems cured at a belt speed of 24 ft/min with 1 pass.

Sample ID	Thickness (μm)	Pencil hardness	König pendulum hardness (s)	Reverse impact (in-lb)	MEK double rubs	Cross hatch adhesion
100S-HI*	98.7	6B	46	48	24	0B
100P-HI	103	1H	55	10	1050	0B
100S-LI**	--	--	--	--	--	--
100P-LI	105	1H	65	10	1150	0B
80/10/10S/Ox/To-LI*	99.4	HB	26	152	103	0B
80/10/10P/Ox/To-LI	99	3H	18	36	485	0B
70/30S/Ox-HI	98	4H	20	148	147	0B
70/30P/Ox-HI	102	4H	34	36	581	0B
70/30S/Ox-LI	99.7	4H	20	152	188	1B
70/30P/Ox-LI	102	4H	50	36	683	0B
70/20/10S/Ox/To-LI*	100.2	HB	17	164	42	0B
70/20/10P/Ox/To-LI	101	2H	18	64	245	0B
70/10/20S/Ox/To-LI‡	--	--	--	--	--	--
70/10/20P/Ox/To-LI	97	F	21	40	234	0B

*Coatings were liquid state after passing through UV light and became solid after 18 hours of dark cure.

**Coatings were still in the liquid state after 18 hours of dark cure.

‡Coating was liquid state after passing through UV light and became soft and tacky after 18 hours of dark cure.

The pencil hardness determines the resistance of coating materials to scratch effect on the surface. The addition of EHMO_x increases the pencil hardness of coatings. Addition of 10 wt. % (80/10/10P/O_x/To-LI) and 30 wt. % (70/30P/O_x-LI) of EHMO_x to 100P-LI increases the pencil hardness from 1H to 3H and 4H respectively. However, the addition of a polyol reduces the pencil hardness as in case of 70/20/10P/O_x/To-LI and 70/10/20P/O_x/To-LI. Similar trend was observed with the coatings derived from E-SBO. The coating derived from pure E-SBO (100S-HI) was too soft to provide any significant resistance against scratch effect. The coating prepared from the formulation 70/10/20S/O_x/To-LI was too soft to measure the hardness. In general, coatings produced from E-polyVESFA showed superior pencil hardness than analogous coatings derived from E-SBO which could be due to the higher number of branching point per molecule and hence the higher cross-link density.

The pendulum hardness is sensitive in detecting the coatings hardness where hardness is defined as the resistance to deformation. The interaction between the pendulum and the coating depends upon the elastic and viscoelastic properties of coating. The amplitude of the oscillation of pendulum touching on the surface reduces with softer surface. Coatings possessing higher modulus and toughness can resist the dampening of the pendulum. With the addition of a polyol, the pendulum hardness of coatings obtained from the both E-polyVESFA and ESO reduces. In general, coatings produced from E-polyVESFA possessed higher pendulum hardness than E-SBO analog.

Impact resistance of coating is its ability to resist cracking caused by rapid deformation (impact). This is important during the manufacture and service of articles. It

was found from Table 7.7 that coatings derived from E-polyVESFA were brittle possessing lower impact resistance than those derived from E-SBO. A polyol was added to increase the impact resistance of coatings derived from E-polyVESFA. For example, the addition of 10 weight percent of polyol (70/20/10P/Ox/To-LI) in the place of EHMOx at 70/30P/Ox/-LI could increase the impact resistance by 77%. However, polyol reduced the crosslink density, hardness and MEK double rubs of coatings. The brittleness nature of coating produced from E-polyVESFA could be due to the presence of higher number of functional groups per molecule that reduces the flexibility of crosslinked network. The MEK double rubs test describes the coating resistance against organic solvent, such as methyl ethyl ketone (MEK). Coatings derived from E-polyVESFA possessing higher cross-linked density would reduce the swelling of network in the presence of MEK and hence, the higher numbers of double rubs were required to breakdown the network. However, the film thickness has a big influence on the result. Due to extensive shrinkage during curing, the coatings derived from pure E-SBO (100S-HI) produced non-uniform surface. This could be the possible reason for early failure of sample during MEK double rubs. In general, cationic radiation curing formulation is developed as solventless system. Thus, curing of such system generates stress between the coating and substrate interface. This could be the reason that all of these coatings showed poor result in cross hatch adhesion test.

7.4.3.4. Characterization using DMA

The viscoelastic properties of the photo-cured coating materials were investigated by measuring storage modulus as a function of temperature on cured free films. The

effects of photo-initiator content and UV light energy on the viscoelastic properties of free films produced from E-polyVESFA and E-SBO are shown in Figure 7.20. Table 7.8 lists the values of T_g , storage modulus, and crosslink density obtained from these graphs. The crosslink density (moles of crosslinks per unit volume) of cured film can be calculated from the storage moduli in the rubbery plateau region according to the following equation:

$$\nu = E' / 3RT$$

where, ν , E' , R , and T are the moles of elastically effective network chains per unit volume (crosslink density), storage moduli in the rubbery plateau region, universal gas constant (8.314×10^7 dynes/K.mole), and temperature (in Kelvin) corresponding to the storage moduli in the rubbery plateau region.

As shown in Figure 7.20, the storage modulus and glass transition temperatures of cured films produced from E-polyVESFA were higher than the analogous films produced from E-SBO. This result is due to the much higher number of epoxy groups per molecular for E-polyVESFA as compared to E-SBO which translates to a higher degree of crosslinking at a given extent of cure. According to the data from Table 7.8, the coatings produced from the lower amount of photo-initiator showed higher crosslink density and T_g . This can be explained by considering the fact that the lower concentration of photoinitiator actually increases the concentration of reactive groups which are responsible for the higher modulus and T_g . The total energy of light exposed when coatings were passed once and twice through the UV chamber at a belt speed of 24 ft/minute were 1420 mW/cm^2 and 2840 mW/cm^2 respectively as measured by a UV Power Puck II from EIT Inc. As the amount of UV light was increased from 1420 mW/cm^2 to 2840 mW/cm^2 , the storage

modulus of 70/30P/Ox-HI and 70/30P/Ox-LI were increased by 2.9% and 0.8% respectively. On the other hand, the increment of storage modulus for E-SBO derived analogous coatings (70/30S/Ox-HI and 70/30S/Ox-LI) were 22.3% and 8% respectively. This data demonstrates that the effect of amount of light has a lesser effect on the ultimate curing of coatings produced from E-polyVESFA. The faster cure rate of epoxides in 70/30P/Ox compared to 70/30S/Ox was also confirmed in Real-Time FTIR experiments. The faster polymerization/cure rate of coating derived from E-polyVESFA could be useful in the production line in industry regarding the faster production rate and low energy consumption.

The effect of a reactive diluent and a polyol on the crosslink density and T_g of cured film are shown in Figures 7.21 and 7.22. Table 7.9 lists the values of storage modulus and T_g of these films. As shown in Figure 7.21, the film produced from pure E-polyVESFA (i.e. 100P-LI) showed a T_g of approximately 33.4 °C and the difference in storage moduli before and after the T_g was relatively small, which is indicative of a relatively high crosslink density. This result is in stark contrast to that observed for the film prepared from pure E-SBO (i.e. 100S-HI) which was too liquid-like to measure. This result is due to the much higher number of epoxy groups per molecular for E-polyVESFA as compared to E-SBO which translates to a higher degree of crosslinking at a given extent of cure. Similarly, the blends of E-polyVESFA and EHMOx enabled the production of films with higher T_g and higher crosslink density than analogous blends based on E-SBO. However, the polyol reduced both the crosslink density and T_g of cured coatings.

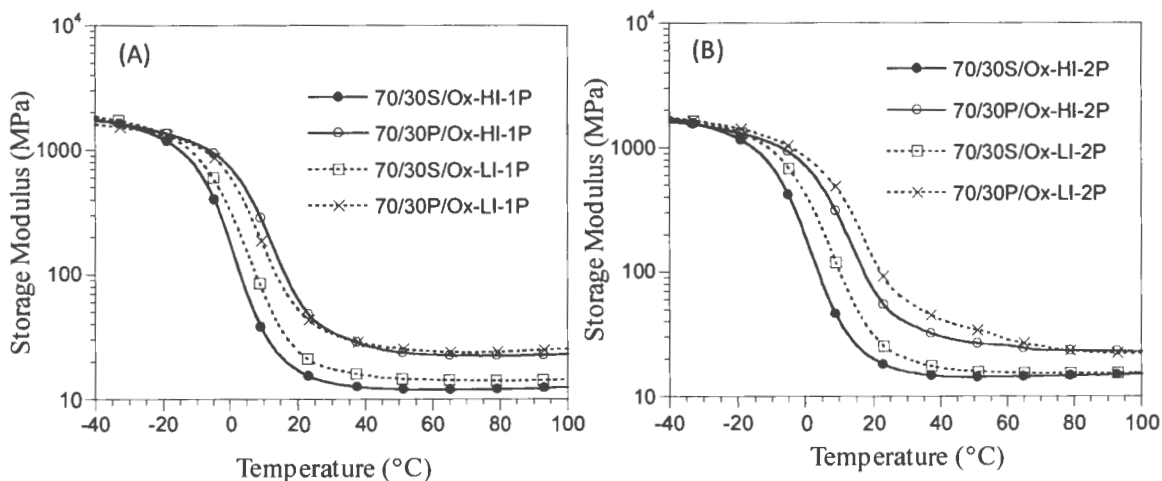


Figure 7.20. Viscoelastic properties obtained for free films produced from E-polyVESFA and E-SBO in cationic photocure systems using (A) one and (B) two passes under the UVA lamp.

Table 7.8. Storage modulus, crosslink densities, and T_g of free films produced from E-polyVESFA and E-SBO in cationic photocure systems using one and two passes under the UVA lamp.

Sample ID	Storage modulus (MPa) at 90 °C	Crosslink density at 90 °C (mol/lit)	T_g (°C)
70/30S/Ox-HI-1P	12.15	1.34	4.7
70/30P/Ox-HI-1P	22.48	2.48	15.7
70/30S/Ox-LI-1P	14.21	1.57	10.8
70/30P/Ox-LI-1P	24.65	2.72	11.8
70/30S/Ox-HI-2P	14.86	1.64	5.0
70/30P/Ox-HI-2P	23.13	2.55	16.6
70/30S/Ox-LI-2P	15.36	1.7	12.1
70/30P/Ox-LI-2P	24.81	2.74	18.9

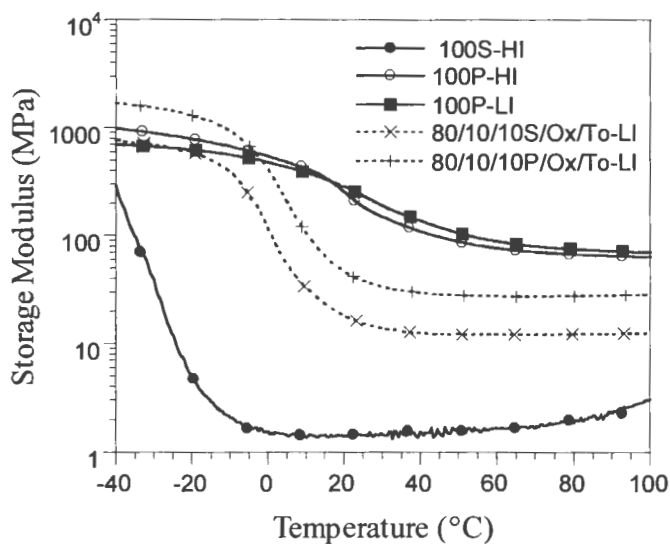


Figure 7.21. Viscoelastic properties obtained for free films produced from E-polyVESFA and E-SBO in cationic photocure systems using one pass under the UVA lamp.

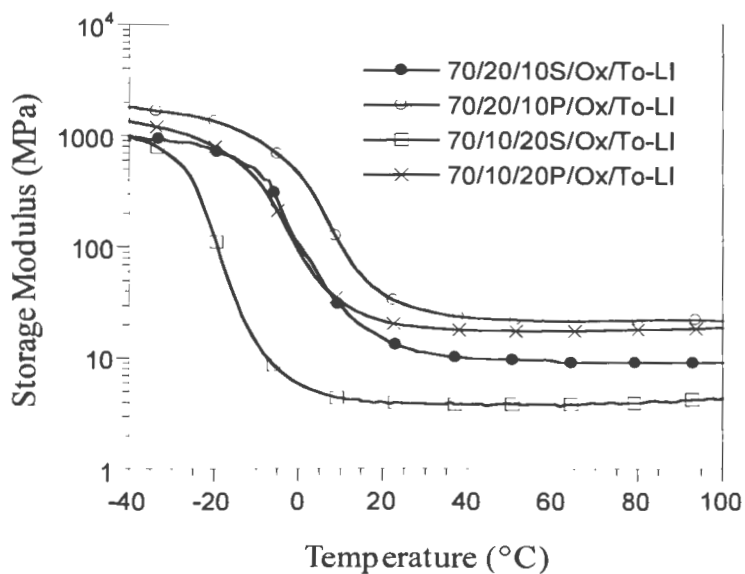


Figure 7.22. Viscoelastic properties obtained for free films produced from E-polyVESFA and E-SBO in cationic photocure systems using one pass under the UVA lamp.

Table 7.9. Data obtains from DMA experiments for E-polyVESFA and E-SBO based coatings in cationic photocure systems using one pass under the UVA lamp.

Sample ID	Storage modulus (MPa) at 90 °C	Crosslink density at 90 °C (mol/lit)	T _g (°C)
100S-HI	2.31	0.26	-29.9
100P-HI	64.83	7.16	26
100S-LI	Not Cured	--	---
100P-LI	71.88	7.94	33.4
80/10/10S/Ox/To-LI	12.35	1.36	0.8
80/10/10P/Ox/To-LI	27.96	3.09	7.6
70/30S/Ox-HI	12.15	1.34	4.8
70/30P/Ox-HI	22.48	2.48	15.7
70/30S/Ox-LI	14.21	1.57	10.8
70/30P/Ox-LI	24.65	2.72	12.4
70/20/10S/Ox/To-LI	9.09	1.0	2.3
70/20/10P/Ox/To-LI	22.18	2.45	8.9
70/10/20S/Ox/To-LI	4.18	0.46	- 14.5
70/10/20P/Ox/To-LI	18.34	2.03	0.1

7.4.4. Characterization of A-polyVESFA and A-SBO

A-polyVESFA was produced from E-polyVESFA using the synthetic scheme described in Figure 7.7. Successful synthesis of A-polyVESFA was confirmed using ¹H NMR and FTIR. Figure 7.23 displays the ¹H NMR spectrum for A-polyVESFA which shows peaks between 5.7 and 6.4 ppm associated with the protons of the acrylate vinyl group. The % of acrylation was confirmed by integrating the ¹H NMR spectrum. For the preparation of A-polyVESFA, the molar ratio of E-polyVESFA to acrylic acid was selected as 1: 0.98. After integrating and comparing the proton absorption in the areas between 2.8

ppm and 3.2 ppm in ^1H NMR spectra of E-polyVESFA and A-polyVESFA, the % of conversion calculated was 97.3. The proton absorption peak at 0.8 ppm was used to normalize the integration values. From the FTIR spectrum shown in Figure 7.24, the broad band centered at 3450 cm^{-1} attributed to the hydroxyl group produced by epoxy ring opening with acrylic acid can be easily seen. In addition, peaks at 1616 cm^{-1} associated with the acrylate vinyl group can be seen. Successful synthesis of A-SBO was confirmed using ^1H NMR. Figure 7.25 displays the ^1H NMR spectrum for A-SBO which shows peaks between 5.7 and 6.5 ppm associated with the protons of the acrylate vinyl group.

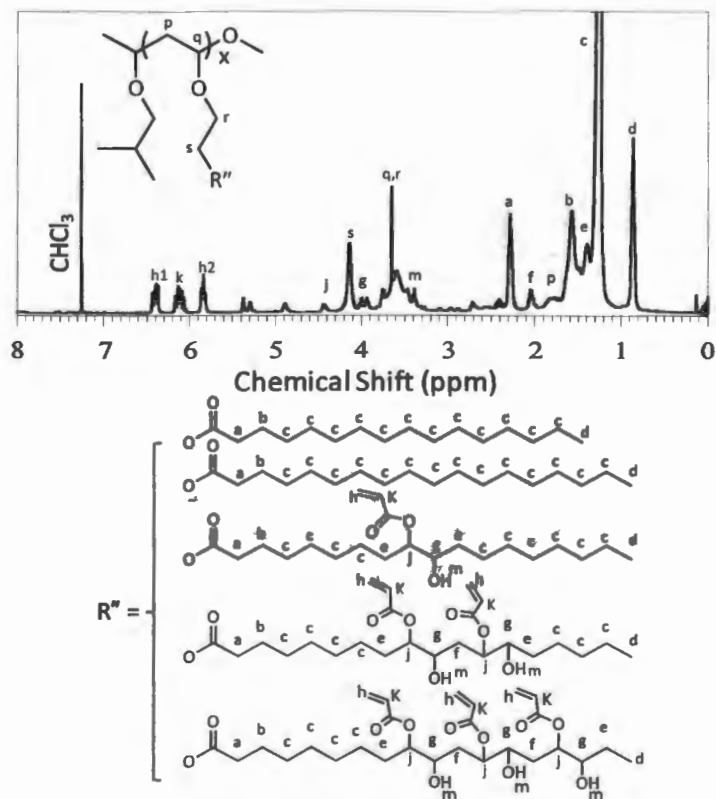


Figure 7.23. ^1H NMR spectrum obtained for A-polyVESFA.

7.4.5. Characterization of coatings to compare the difference between A-polyVESFA and A-SBO in free-radical photocure systems

To understand the utility of A-polyVESFA as compared to A-SBO, the photocurable compositions shown in Table 7.4 were produced. With these compositions, HDDA was used as a reactive diluent. Differences in cure kinetics were characterized using both RT-FTIR and photo-DSC. Figure 7.26 displays a typical profile of a free-radical photopolymerization reaction which shows the percentage of monomer conversion with UV light exposure time for a multifunctional acrylate in air.³⁷³ The characteristics 'S' shaped graph consisted of a very short induction time (t_i) due to oxygen inhibition followed by a sharp increase in the rate of polymerization (R_p) and a strong decrease in the R_p at the glassy state. The development of crosslinked network upon the UV light exposure of a free-radical photocure system is consisted of the following three steps: (1) change in refractive index, (2) change in tackiness, and (3) insolubilization of the film.³⁸⁸ In a Real Time FTIR experiment, the degree of conversion and R_p of an acrylate curing system can be defined by the following equations:³⁸⁷

$$R_p = -\frac{d[M]}{dt} = [M]_0 \frac{A(t_1) - A(t_2)}{(t_2 - t_1)A(t_0)}$$

$$\text{Percentage of Conversion} = \frac{A(t_0) - A(t)}{A(t_0)} \times 100$$

where, $A(t_1)$, $A(t_2)$, $A(t_0)$, and $A(t)$ are the absorbance at any time t_1 , t_2 , before UV exposure, and after UV exposure, respectively. $[M]_0$ represents the initial acrylate double bond concentration before UV exposure.

RT-FTIR experiments were conducted by monitoring the change in absorbance between 1645 cm^{-1} to 1608 cm^{-1} , which corresponds to C=C stretching of the acrylate vinyl groups, as a function of UV exposure time. As shown in Figure 7.27, the rate of acrylate polymerization was very fast for all 4 compositions. Table 7.10 describes the average data obtained from the percentage of conversion versus UV light exposure time graph in a Real-Time FTIR experiment. The standard deviations from the mean value of three replicate measurements were found to be less than 3%.

Upon irradiation with UV light, the polymerization for E-polyVESFA/HDDA-HI and E-SBO/HDDA-HI coatings started without any induction time, and the rate of polymerization increased sharply. However, the polymerization for coatings possessing the lower level of photoinitiator started slowly with an induction time followed by a sharp and a moderate increase in polymerization rate for E-polyVESFA/HDDA-LI and E-SBO/HDDA-LI coatings respectively. The biggest difference between the coatings was the ultimate extent of conversion achieved during photopolymerization. The use of the higher level of photoinitiator enabled significantly higher levels of acrylate conversion to be achieved. This result is to be expected considering that polymerization rate is a function of the concentration of free radicals present in the polymerizing medium and a faster rate allows for higher extents of conversion to be achieved before the material becomes vitrified and/or the radicals are terminated. The more interesting result that was obtained related to the differences in ultimate conversion obtained as a function of the composition of the soybean-based component. At either photoinitiator concentration, a significantly higher ultimate acrylate conversion was achieved with A-polyVESFA as compared to A-SBO.

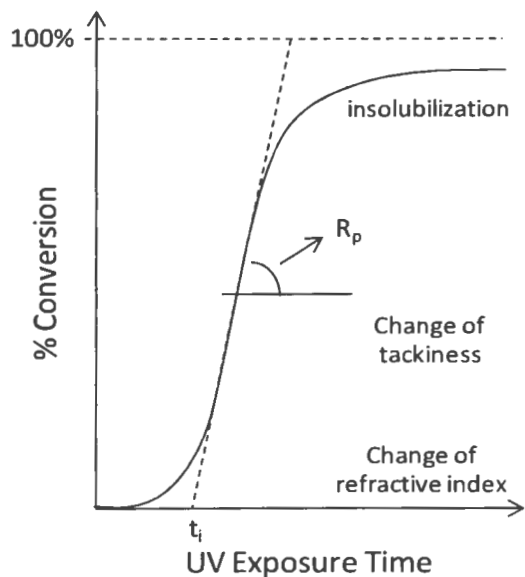


Figure 7.26. % of conversion as a function of UV exposure time for a free-radical photo curable system in air.^{373, 388}

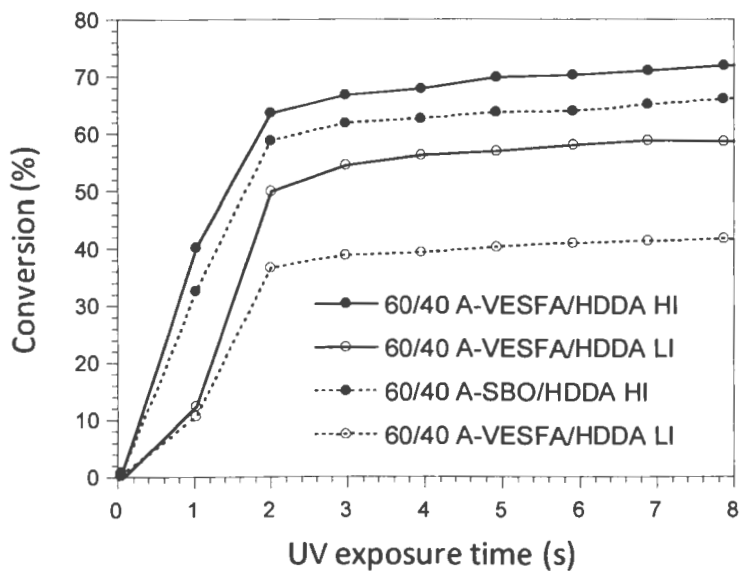


Figure 7.27. Real time FTIR results for the acrylate-based coatings described in Table 7.4.

Table 7.10. Real time FTIR data obtained for A-polyVESFA/HDDA and A-SBO/HDDA curing.

Formulation	Induction time (s)	Rp (s ⁻¹)	Percentage of conversion after 2 secs.	Percentage of conversion after 8 secs.
60/40 A-VESFA/HDDA HI	0	41.7	63	72
60/40 A-VESFA/HDDA LI	0.7	41.7	50	60
60/40 A-SBO/HDDA HI	0	33.3	59	67
60/40 A-SBO/HDDA LI	0.6	28.1	37	42

This result can be attributed to the much higher number of acrylate groups per molecule for A-polyVESFA which results in the gel-point being reached at a much lower conversion compared to analogous coatings based on A-SBO. The much higher inhibition of polymer translational and segmental diffusion compared to monomer diffusion that accompanies gelation results in a reduction in the rate of termination relative to propagation, ultimately increasing overall polymerization/cure rate.

With photo-DSC, heat flow from the sample is monitored as a function of UV exposure time. For the coatings described in to Table 7.4, the plot of heat flow (W/g) as a function of UV light exposure time (s) was shown in Figure 7.28. From the photo-DSC graphs, the maximum heat flow (H_{max}) can be related to rate of polymerization,³⁸⁷ and the total heat evolved (ΔH) can be related to the percentage of conversion. The ΔH was calculated after integrating the peak area under the curve. The ΔH is related to the percentage of conversion according to the following equation:

$$\text{Percent of Conversion} = \frac{\Delta H}{\Delta H_0} \times 100$$

where, ΔH_0 is the theoretical total heat of reaction. ΔH_0 can be calculated after considering the heat of polymerization of acrylate as 86.1 KJ/mole³⁸⁹ using the following equations :

$$\Delta H_0 = \text{Total moles of acrylate} \times (86.1 \text{ KJ/mole})$$

$$\text{Total moles of acrylate} = \frac{Wt_1 \times \% \text{ of Acrylation}}{(\text{AEW of A-polyVESFA}) \times 100} + \frac{Wt_2 \times \% \text{ of Purity}}{(\text{AEW of HDDA}) \times 100}$$

where, Wt_1 , Wt_2 represent the weight of A-polyVESFA and HDDA respectively. The percentage of acrylation of E-polyVESFA and E-SBO calculated using proton NMR spectra was 97%. The theoretical acrylate equivalent weight (AEW) of A-polyVESFA and A-SBO calculated based on the epoxy equivalent weight of E-polyVESFA and E-SBO were 362 g/mole and 304 g/mole, respectively. The average data obtained from photo-DSC experiments were listed in Table 7.11. The standard deviations from the mean value of three replicate measurements were found to be less than 4%.

As shown in Figure 7.28, the relative rates of cure obtained with photo-DSC gave similar results to those obtained with RT-FTIR. In general, the use of A-polyVESFA results in faster cure than A-SBO. All the coating formulations containing higher amount photoinitiator showed an increase in ΔH_{max} (faster cure rate) relative to coating formulations containing lower amount of photoinitiator. The ΔH and percentage of conversion values reported in Table 7.11 were calculated for 30 seconds of UV light exposure.

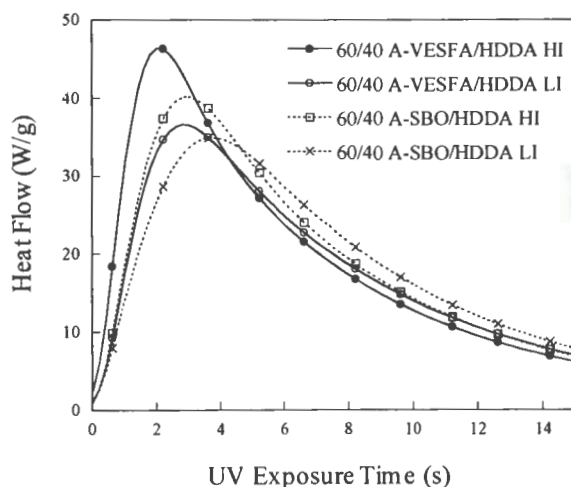


Figure 7.28. Photo-DSC results for the acrylate-based coatings described in Table 7.4.

Table 7.11. Induction time and time to peak max values of Photo-DSC results for the acrylate-based coatings.

Sample ID	Induction time (s)	Time to peak maximum (s)	ΔH_{max} (J/mole)	ΔH (J/mole)	Conversion % (30 sec of UV exposure)
60/40 A-VESFA/HDDA HI	0.2	2	45	297	68.6
60/40 A-VESFA/HDDA LI	0.2	3	36	296	67.5
60/40 A-SBO/HDDA HI	0.2	3	41	319	69.5
60/40 A-SBO/HDDA LI	0.3	4.3	33	316	68.1

Data obtained from Real-Time FTIR indicated that a higher degree of ultimate conversion could be achieved for A-polyVESFA/HDDA coatings than that with A-SBO/HDDA. However, the total heat of reaction (ΔH) and the percentage of conversion calculated for A-polyVESFA/HDDA coatings were almost similar to that for A-SBO/HDDA coatings. This can be easily explained by the fact that the DSC measures the total heat generated during the exposure of UV light. The epoxy equivalent weight for E-

SBO is 20% lower than the E-polyVESFA. Considering the percentage of acrylation in A-SBO and A-polyVESFA are the same (97%) it can be easily understood that the total moles of acrylate functional groups are higher for A-SBO than that for A-polyVESFA.

7.4.6. Characterization of OH-polyVESFA and OH-SBO

OH-polyVESFA was produced from E-polyVESFA using the synthetic scheme described in Figure 7.8. Successful synthesis of OH-polyVESFA was confirmed using ^1H NMR and FTIR. Figure 7.29 displays the ^1H NMR spectrum for OH-polyVESFA which showed peaks between 3.2 and 3.3 ppm associated with the protons of the methoxy group. The % of methanolysis was confirmed by integrating the ^1H NMR spectrum. For the preparation of OH-polyVESFA, the molar ratio of E-polyVESFA to methanol was selected as 1 : 5.8. After integrating and comparing the proton absorption peaks in the areas between 2.8 ppm and 2.9 ppm in ^1H NMR spectra of E-polyVESFA and OH-polyVESFA, the percentage of conversion calculated was 99.9. The proton absorption peak at 0.8 ppm was used to normalize the integration values. From the FTIR spectrum (Figure 7.30) the broad band centered at 3400 cm^{-1} attributed to the hydroxyl group produced by epoxy ring opening with methanol can be easily seen. Successful synthesis of OH-SBO was confirmed using ^1H NMR. Figure 7.31 displays the ^1H NMR spectrum for OH-SBO which showed peaks between 3.1 and 3.2 ppm associated with the protons of the methoxy group.

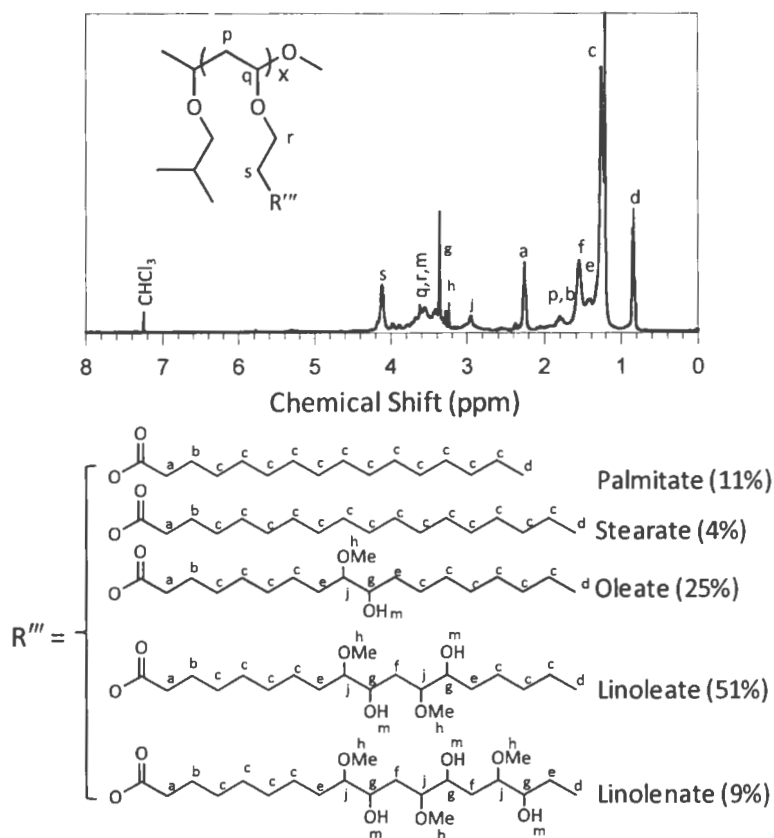


Figure 7.29. ^1H NMR spectrum obtained for OH-polyVESFA.

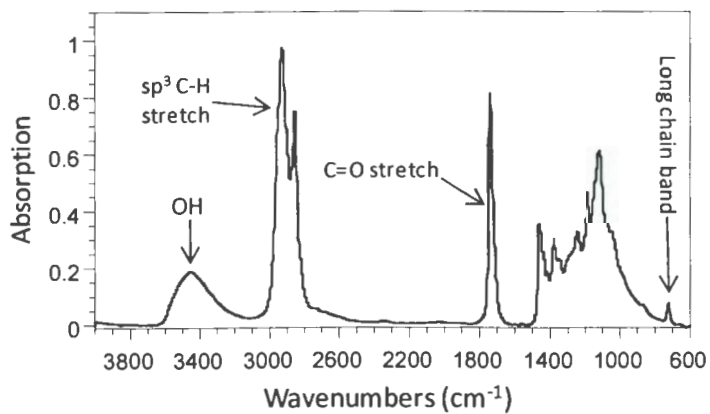


Figure 7.30. FTIR spectrum obtained for OH-polyVESFA.

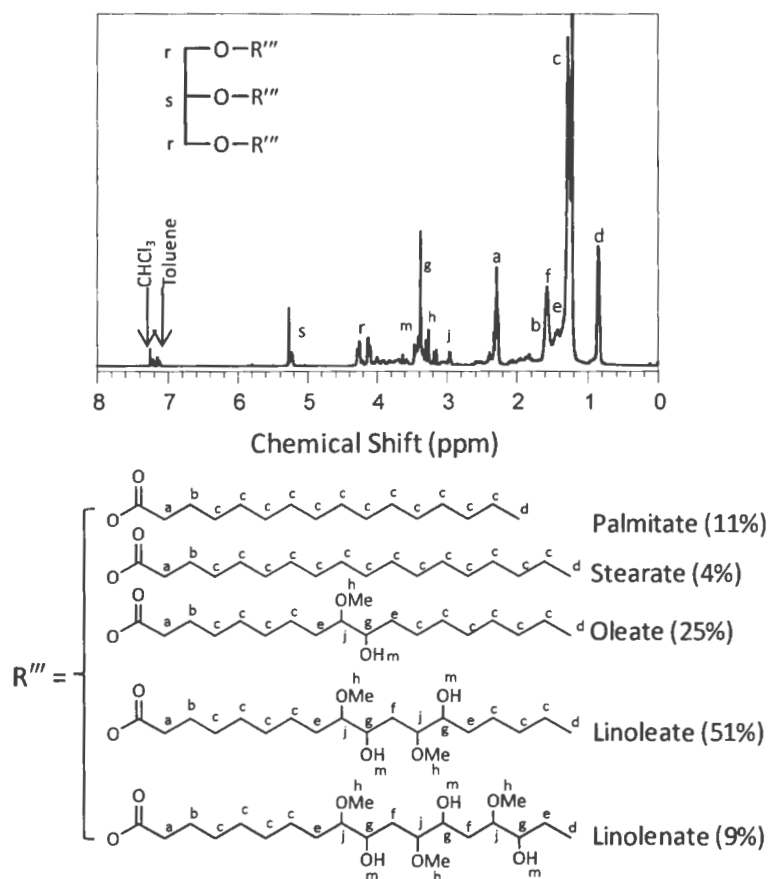


Figure 7.31. ^1H NMR spectrum obtained for OH-SBO.

7.4.7. Characterization of coatings to compare the difference between OH-polyVESFA and OH-SBO in polyurethane coating systems

The viscoelastic properties of the polyurethane coating were investigated by measuring storage modulus as a function of temperature on cured free films. Table 7.12 lists the values of T_g , storage modulus, and crosslink density obtained from these graphs. The cross linking density (moles of crosslinks per unit volume) was calculated from the storage moduli in the rubbery plateau region. As shown in Figure 7.32, the storage modulus

and glass transition temperatures of cured films produced from OH-polyVESFA were higher than the analogous films produced from OH-SBO. This result is due to the much higher number of hydroxyl groups per molecular for OH-polyVESFA as compared to OH-SBO which translates to a higher degree of crosslinking at a given extent of cure.

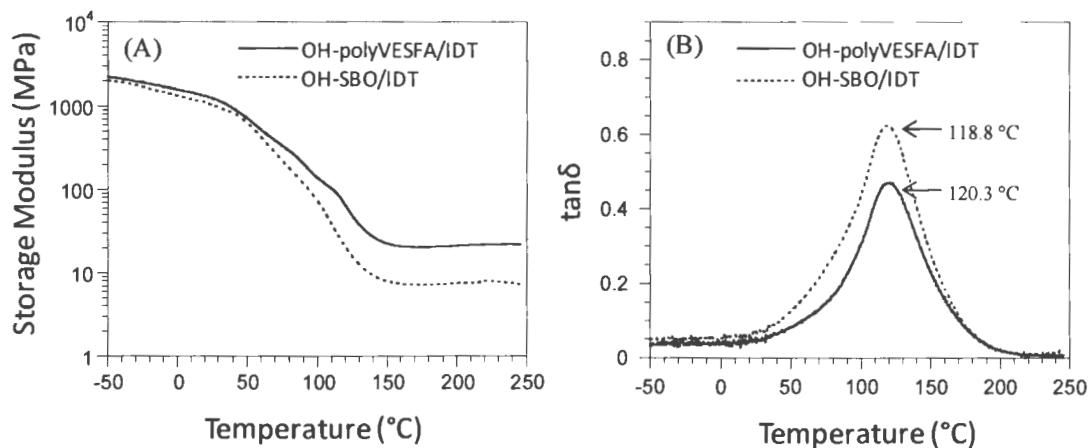


Figure 7.32. Viscoelastic properties obtained for free films produced from OH-polyVESFA and OH-SBO in a polyurethane coating system.

Table 7.12. Storage modulus and T_g obtained for free films produced from OH-polyVESFA and OH-SBO in a polyurethane coating system.

Formulation	Storage Modulus (MPa) at 170 °C	Crosslink Density (mole/lit) at 170 °C	T_g (°C)
OH-polyVESFA/IDT	20.49	1.85	120.3
OH-SBO/IDT	7.29	0.66	118.8

7.5. CONCLUSION

A novel epoxidized polymer, E-polyVESFA, was synthesized from polyVESFA and the physical properties were compared to commercially available epoxidized soybean

oil, E-SBO. Thermal analysis demonstrated that incorporating the fatty acids into a polymer as pendent groups greatly reduces the crystallizability of the fatty acid chains. Viscosity analysis revealed that the E-polyVESFA possessed a higher viscosity than that of E-SBO which is consistent with the major difference in molecular weight between the two materials. In addition, the viscosity of the E-polyVESFA sample showed significantly more shear sensitivity than E-SBO. In epoxy-amine cure systems, the use of E-polyVESFA as opposed to E-SBO reduced cure time at 120 °C by more than an order of magnitude. For cationic photocure systems, the use of E-polyVESFA substantially increased cure rate and ultimate function group conversion during photocure. In addition, T_g and crosslink density of cured films were significantly higher for the E-polyVESFA-based materials. Physical properties measurement for coatings derived from E-polyVESFA showed higher MEK double rubs, pencil hardness, and pendulum hardness compared to E-SBO based coatings. However, the E-polyVESFA based coatings were more brittle than the E-SBO based analog. Acrylated polymer, A-polyVESFA, and alcohol-functional polymer, OH-polyVESFA, were synthesized from E-polyVESFA and characterized using proton NMR and FTIR. Similar to the results obtained for the cationic photocure systems, the use of A-polyVESFA in place of A-SBO in free-radical photocure systems resulted in faster cure. The T_g and crosslink density of cured films produced from polyurethane coating were higher for the OH-polyVESFA-based materials. All of these results can be attributed to a higher number of functional groups per molecule associated with the use of E-polyVESFA, A-polyVESFA, and OH-polyVESFA as opposed to E-SBO and its derivatives. A higher number of functional groups per molecule results in the gel-point being reached at much

lower conversion and the obtainment of a higher crosslink density at a given degree of functional group conversion. Based on the results described in this document, it appears that the novel E-polyVESFA has tremendous commercial potential.

CHAPTER 8. GENERAL CONCLUSION

The objective of the research was to the synthesis and characterization of novel polyvinylethers using carbocationic polymerization. In a living carbocationic polymerization of vinyl ether, the initiation is very fast and quantitative. Moreover, the propagating species does not take part in side reactions, such as chain termination and chain transfer. Thus, end-functional polymers were synthesized by the following two steps: (1) initiation from functionalized initiator and (2) termination from functionalized terminator. The major advantage of living carbocationic polymerization is the synthesis of well defined polymers with narrow molecular weight distribution. Additionally, using living carbocationic polymerization, block copolymers of vinyl ether were synthesized and characterized. Four unique carbocationic polymerizations of vinyl ether were investigated here.

In Chapter 2, a novel TVE monomer containing Triclosan as a biocide moiety was synthesized and polymerized using living carbocationic polymerization initiated by IBEA/ $\text{Et}_{1.5}\text{AlCl}_{1.5}$. The monoallyl-functional PTVE was achieved by terminating the living polymerization with 2-allyloxyethanol. The incorporation of monoallyl-functionality in PTVE enabled the formation of Triclosan tethered polydimethylsiloxane graft copolymer possessing excess Si-H groups. The excess hydride was used to synthesize both PDMS-g-PTVE/P and PDMS-g-PTVE/S copolymers. The PDMS-g-PTVE/P copolymers were transparent rubbery two phase materials. The PDMS-g-PTVE/P coatings based on the PDMS-6K exhibited higher antimicrobial activity than analogous coatings based on PDMS-63K. Antimicrobial activity of these leachate non-toxic coatings revealed that the

surfaces produced from PDMS-6K provided excellent reduction in *S. epidermidis* biofilm retention (80% – 97%) and moderate reduction in both *C. albicans* (42% – 58%) and *C. lytica* (45% - 50%) biofilm retention. The PDMS-g-PTVE/P coating surfaces produced from PDMS-6K provided enough PTVE concentration at the coating/water interface, so that PTVE can effectively interact with the microorganism cell wall to damage the bacterial extra cellular process. However, the surfaces generated from PDMS-g-PTVE/S coatings were one phase and hydrophobic materials. Due to crosslinking, the PDMS-g-PTVE/S coating surfaces were unable to provide enough concentration of the PTVE moiety at the coating/water interface which is necessary to damage the bacterial extra cellular process effectively. *S. epidermidis* is considered as one of the major organism responsible for biomedical failure due to infection, so these coatings can be a used in implantable devices as long-term antimicrobial coatings towards *S. epidermidis*.

In Chapter 3, a novel monoallyl-functional AMEA initiator capable of producing very fast and quantitative initiation under a living carbocationic polymerization condition of vinyl ether was synthesized and characterized. With the AMEA, a monoallyl-functional PCVE was produced using a living carbocationic polymerization. A series of PDMS-*b*-PCVE-*b*-PQs were synthesized using hydrosilylation between monoallyl-functional PCVE and hydride terminated PDMS followed by quaternization with *n*-alkyldimethyl amine by varying the *n*-alkyl chain lengths of tertiary amine from 12 carbons to 18 carbons and percentage of quaternization. The antimicrobial activity of PDMS-*b*-PCVE-*b*-PQs in solution towards *E. coli* was found to increase when the *n*-alkyl chain were consisted of 12 and 14 carbons. However, the antimicrobial activities towards *S. aureus* were the highest

when the percentages of quaternization were at the higher end (30 mole % and 50 mole %) and the n-alkyl chains were consisted of 14 and 16 carbons. The great advantage of PDMS-*b*-PCVE-*b*-PQs possessing very high charge density per molecule over monomeric quaternary ammonium compounds is the presence of polymeric blocks of quaternary ammonium compounds that are very effective against microorganisms even at a low concentration and low contact time. Based on these results obtained in this research, it appears that the novel initiator is useful to synthesize wide varieties of polymers with various applications. The polyquaternary ammonium compounds described in this document have tremendous commercial potential.

In Chapter 4, a novel BrVE monomer possessing high bromine content was synthesized and polymerized using a carbocationic polymerization in the presence of IBEA/Et_{1.5}AlCl_{1.5} initiating system and an ester functional base. The polymer possessing the highest possible molecular weight (PBrVE/HMW/0C) was produced when the polymerization was carried out in the absence of a base and an initiator at a reaction temperature of 0 °C. Due to the higher flexibility of the polyvinylether polymer backbone as well as the flexibility of the ethoxy group linking the bulky pentabromophenyl group to the polymer backbone, PBrVE possessed a lower T_g. Additionally, due to the presence of thermally stable ether linkage between the pendent pentabromophenyl moiety and the polymer backbone, the PBrVE possesses better thermal and weather resistance.

In Chapter 5, the PBrVE was blended with PBT and the thermal, mechanical, and viscoelastic properties were evaluated and compared to an analogous blend prepared from PBrBA and PBT. BFRs were blended with PBT/Sb₂O₃; and flame retardancy and

mechanical properties were compared. Data obtained from mechanical tests showed that the use of PBrVE as opposed to the use of PBrBA increases the Young's modulus, flexural modulus, and impact resistance of PBT/Sb₂O₃ blend. Results obtained from the flame tests showed that the flame retardancy of PBT/Sb₂O₃/BFR blends were the same. Blending PBrVE with the PBT resulted in lower melt viscosity and better blend compatibility than an analogous blend based on PBrBA. These results indicate that PBrVE may have utility for the development of FR plastics with improved mechanical properties, processability and, perhaps, improved optical properties.

In Chapter 6, a novel monomer, VESFA was produced by transesterification reaction between soybean oil and ethylene glycol vinyl ether and polymerized using a living carbocationic polymerization in the absence of an added base. The carbonyl group in the ester functional VESFA acts as a base to provide the stability of the carbocationic propagating species. It was clearly demonstrated that the use of polyVESFA in place of SBO offers tremendous advantages in a variety of coating systems. For coating systems based on cure by autoxidation, it was demonstrated that use of polyVESFA can reduce drying-time by a factor of 4 to 6.5. For coating systems based on cure by sulfur vulcanization, it was shown that use of polyVESFA can develop a crosslinked network within 30 minutes of reaction, whereas SBO was in liquid state after 2 hours of vulcanization. All of these results can be attributed to a higher number of functional groups per molecule associated with the use of polyVESFA as opposed to SBO.

In Chapter 7, a novel E-polyVESFA was synthesized from polyVESFA and the physical properties were compared to commercially available E-SBO. In epoxy-amine cure

systems, the use of E-polyVESFA as opposed to E-SBO reduced cure time at 120 °C by more than an order of magnitude. For cationic photocure systems, the use of E-polyVESFA substantially increased cure rate and ultimate function group conversion during photocure. Physical properties measurement for coatings derived from E-polyVESFA showed higher MEK double rubs, pencil hardness, and pendulum hardness compared to E-SBO based coatings. However, the E-polyVESFA based coatings were more brittle than the E-SBO based analog. Acrylated polymer (A-polyVESFA) and alcohol-functional polymer (OH-polyVESFA) were synthesized from E-polyVESFA and the coatings properties were compared with analogous coating systems derived from A-SBO and OH-SBO. Similar to the results obtained for the cationic photocure systems, the use of A-polyVESFA in place of A-SBO in free-radical photocure systems resulted in faster cure. The T_g and crosslink density of cured films produced from polyurethane coating were higher for the OH-polyVESFA-based materials. All of these results can be attributed to a higher number of functional groups per molecule associated with the use of E-polyVESFA, A-polyVESFA, and OH-polyVESFA as opposed to E-SBO and its derivatives. Based on the results described in this document, it appears that the novel SBO-based polymer, E-polyVESFA, has tremendous commercial potential.

Living carbocationic polymerization can be achieved by judicious choice of initiator, co-initiator, Lewis base, solvent, and polymerization temperature. In conclusion, the carbocationic polymerization, specially living carbocationic polymerization is a powerful polymerization technique to synthesize a variety of well-defined functional polymers and copolymers.

LITERATURE CITED

1. Williams, G., Kinetics of the catalyzed polymerization of styrene. I. Experimental methods and some general features of stannic chloride catalysis. *Journal of the Chemical Society* **1938**, 246-53.
2. Gandini, A.; Cheradame, H., Cationic polymerization. Initiation processes with alkenyl monomers. *Advances in Polymer Science* **1980**, 34-35, 1-289.
3. Odian, G., *Principles of Polymerization*. 2nd ed.; John Wiley & Sons: New York, 1981; p 340-412.
4. Szwarc, M., "Living" polymers. *Nature (London, United Kingdom)* **1956**, 178, 1168-9.
5. Olah, G. A., Stable carbocations. CXVIII. General concept and structure of carbocations based on differentiation of trivalent (classical) carbenium ions from three-center bound penta- of tetracoordinated (nonclassical) carbonium ions. Role of carbocations in electrophilic reactions. *Journal of the American Chemical Society* **1972**, 94 (3), 808-20.
6. Sagane, T.; Lenz, R. W., Molecular weight effects on the liquid-crystalline properties of poly(vinyl ether)s with pendant cyanobiphenyl mesogenic groups. *Macromolecules* **1989**, 22 (9), 3763-7.
7. Namikoshi, T.; Hashimoto, T.; Kodaira, T., Living cationic polymerization of vinyl ethers with a urethane group. *Journal of Polymer Science, Part A: Polymer Chemistry* **2004**, 42 (12), 2960-2972.
8. Namikoshi, T.; Hashimoto, T.; Kodaira, T., Living cationic polymerization of vinyl ethers with a tricyclodecane or tricyclodecene unit: Synthesis of new poly(vinyl ether)s with high glass-transition temperature. *Journal of Polymer Science, Part A: Polymer Chemistry* **2004**, 42 (14), 3649-3653.

9. Namikoshi, T.; Hashimoto, T.; Urushisaki, M., Living cationic polymerization of vinyl ether with a cyclic acetal group. *Journal of Polymer Science, Part A: Polymer Chemistry* **2007**, *45* (21), 4855-4866.
10. Matsumoto, K.; Kubota, M.; Matsuoka, H.; Yamaoka, H., Water-soluble fluorine-containing amphiphilic block copolymer: synthesis and aggregation behavior in aqueous solution. *Macromolecules* **1999**, *32* (21), 7122-7127.
11. Kennedy, J. P.; Feinberg, S. C., Cationic polymerization with boron halides. VI. Polymerization of styrene with boron trifluoride, boron trichloride, and boron tribromide. *Journal of Polymer Science, Polymer Chemistry Edition* **1978**, *16* (9), 2191-7.
12. Kennedy, J. P.; Huang, S. Y.; Feinberg, S. C., Cationic polymerization with boron halides. IV. Elucidation and control of initiation and termination by the help of model experiments. *Journal of Polymer Science, Polymer Chemistry Edition* **1977**, *15* (12), 2869-92.
13. Kennedy, J. P.; Huang, S. Y.; Feinberg, S. C., Cationic polymerization with boron halides. III. Boron trichloride coinitiator for olefin polymerization. *Journal of Polymer Science, Polymer Chemistry Edition* **1977**, *15* (12), 2801-19.
14. Biswas, M.; Kabir, G. M. A., Some aspects of the polymerization of butyl vinyl ether by chromyl chloride. *Journal of Polymer Science, Polymer Chemistry Edition* **1979**, *17* (3), 673-81.
15. Biswas, M.; Kabir, G. M. A., Polymerization of iso-butyl vinyl ether by oxychlorides of group V and VI elements. *European Polymer Journal* **1978**, *14* (10), 861-5.
16. Taninaka, T.; Uemura, H.; Minoura, Y., Cationic polymerization of styrene initiated by phosphorus oxychloride. *European Polymer Journal* **1978**, *14* (3), 199-202.

17. Reibel, L.; Kennedy, J. P.; Chung, D. Y. L., Cationic polymerizations by aromatic initiating systems. II. Correlation between cationic model and polymerization reactions with the p-methylbenzyl chloride/triethyl aluminum system. *Journal of Polymer Science, Polymer Chemistry Edition* **1979**, *17* (9), 2757-68.
18. Di Maina, M.; Cesca, S.; Giusti, P.; Ferraris, G.; Magagnini, P. L., Studies on polymerizations initiated by syncatalytic systems based on aluminum organic compounds, 6. Comparison with isobutene polymerizations initiated by ethylaluminum dichloride or aluminum trichloride. *Makromolekulare Chemie* **1977**, *178* (8), 2223-34.
19. Kennedy, J. P., Novel sequential copolymers by elucidating the mechanism of initiation and termination of carbocationic polymerizations. *Journal of Polymer Science, Polymer Symposia* **1976**, *56* (Int. Symp. Cationic Polym., 4th), 1-11.
20. Magagnini, P. L.; Cesca, S.; Giusti, P.; Priola, A.; Di Maina, M., Studies on polymerizations initiated by syncatalytic systems based on aluminum organic compounds, 7. Reaction mechanisms. *Makromolekulare Chemie* **1977**, *178* (8), 2235-48.
21. Okamura, S.; Higashimura, T., Cationic polymerization of styrene. *Journal of Polymer Science* **1956**, *21*, 289-99.
22. Puskas, J. E.; Kaszas, G., Living carbocationic polymerization of resonance-stabilized monomers. *Progress in Polymer Science* **2000**, *25* (3), 403-452.
23. Storey, R. F.; Chisholm, B. J.; Brister, L. B., Kinetic Study of the Living Cationic Polymerization of Isobutylene Using a Dicumyl Chloride/TiCl₄/Pyridine Initiating System. *Macromolecules* **1995**, *28* (12), 4055-61.
24. Higashimura, T.; Sawamoto, M., Living polymerization and selective dimerization: two extremes of the polymer synthesis by cationic polymerization. *Advances in Polymer Science* **1984**, *62* (Initiators, Poly-React., Opt. Act.), 49-94.
25. Higashimura, T.; Nishii, H., Selective dimerization of styrene to 1,3-diphenyl-1-butene by acetyl perchlorate. *Journal of Polymer Science, Polymer Chemistry Edition* **1977**, *15* (2), 329-39.

26. Higashimura, T.; Hiza, M.; Hasegawa, H., Cationic oligomerization of methylstyrenes: effects of the methyl group and catalysts on product distributions. *Macromolecules* **1979**, *12* (6), 1058-61.
27. Kishimoto, Y.; Aoshima, S.; Higashimura, T., Living cationic polymerization of vinyl monomers by organoaluminum halides. 4. Polymerization of isobutyl vinyl ether by ethylaluminum dichloride (EtAlCl₂) in the presence of ether additives. *Macromolecules* **1989**, *22* (10), 3877-82.
28. Sawamoto, M.; Okamoto, C.; Higashimura, T., Hydrogen iodide/zinc iodide: a new initiating system for living cationic polymerization of vinyl ethers at room temperature. *Macromolecules* **1987**, *20* (11), 2693-7.
29. Kojima, K.; Sawamoto, M.; Higashimura, T., Living cationic polymerization of isobutyl vinyl ether by hydrogen iodide/Lewis acid initiating systems: effects of Lewis acid activators and polymerization kinetics. *Macromolecules* **1989**, *22* (4), 1552-7.
30. Schappacher, M.; Deffieux, A., Activated α -chloro ether and α -bromo ether end groups as propagating species for the living cationic polymerization of vinyl ethers. *Macromolecules* **1991**, *24* (8), 2140-2.
31. Schappacher, M.; Deffieux, A., Nature of active species in the living cationic polymerization of vinyl ethers initiated by hydrogen halide/zinc halide systems. *Macromolecules* **1991**, *24* (14), 4221-3.
32. Kamigaito, M.; Maeda, Y.; Sawamoto, M.; Higashimura, T., Living cationic polymerization of isobutyl vinyl ether by hydrogen chloride/Lewis acid initiating systems in the presence of salts: in-situ direct NMR analysis of the growing species. *Macromolecules* **1993**, *26* (7), 1643-9.
33. Kim, Y. H.; Heitz, T., α -Halogenated carboxylic acids and their corresponding zinc salts in the living polymerization of isobutyl vinyl ether. *Makromolekulare Chemie, Rapid Communications* **1990**, *11* (11), 525-33.

34. Kamigaito, M.; Sawamoto, M.; Higashimura, T., Living cationic polymerization of isobutyl vinyl ether by RCOOH/Lewis acid initiating systems: effects of carboxylate ions and Lewis acid activators. *Macromolecules* **1991**, *24* (14), 3988-92.
35. Aoshima, S.; Higashimura, T., Living cationic polymerization of vinyl monomers by organoaluminum halides. 1. Ethylaluminum dichloride/ester initiating systems for living polymerization of vinyl ethers. *Polymer Bulletin (Berlin, Germany)* **1986**, *15* (5), 417-23.
36. Aoshima, S.; Higashimura, T., Living cationic polymerization of vinyl monomers by organoaluminum halides. 3. Living polymerization of isobutyl vinyl ether by ethyldichloroaluminum in the presence of ester additives. *Macromolecules* **1989**, *22* (3), 1009-13.
37. Higashimura, T.; Kishimoto, Y.; Aoshima, S., Living cationic polymerization of vinyl monomers by organoaluminum halides. Ethylaluminum dichloride/dioxane initiating system for living polymerization of isobutyl vinyl ether. *Polymer Bulletin (Berlin, Germany)* **1987**, *18* (2), 111-15.
38. Miyamoto, M.; Sawamoto, M.; Higashimura, T., Synthesis of monodisperse living poly(vinyl ethers) and block copolymers by the hydrogen iodide/iodine initiating system. *Macromolecules* **1984**, *17* (11), 2228-30.
39. Miyamoto, M.; Sawamoto, M.; Higashimura, T., Living polymerization of isobutyl vinyl ether with hydrogen iodide/iodine initiating system. *Macromolecules* **1984**, *17* (3), 265-8.
40. Sawamoto, M.; Higashimura, T., Living cationic polymerization of vinyl monomers: mechanism and synthesis of new polymers. *Makromolekulare Chemie, Macromolecular Symposia* **1986**, *3*, 83-97.
41. Higashimura, T.; Miyamoto, M.; Sawamoto, M., Mechanisms of living polymerization of vinyl ethers by the hydrogen iodide/iodine initiating system. *Macromolecules* **1985**, *18* (4), 611-16.

42. Miyamoto, M.; Sawamoto, M.; Higashimura, T., Synthesis of telechelic living poly(vinyl ethers). *Macromolecules* **1985**, *18* (2), 123-7.
43. Sugihara, S.; Hashimoto, K.; Matsumoto, Y.; Kanaoka, S.; Aoshima, S., Thermosensitive polyalcohols: Synthesis via living cationic polymerization of vinyl ethers with a silyloxy group. *Journal of Polymer Science, Part A: Polymer Chemistry* **2003**, *41* (21), 3300-3312.
44. Sugihara, S.; Matsuzono, S.-I.; Sakai, H.; Abe, M.; Aoshima, S., Syntheses of amphiphilic block copolymers by living cationic polymerization of vinyl ethers and their selective solvent-induced physical gelation. *Journal of Polymer Science, Part A: Polymer Chemistry* **2001**, *39* (18), 3190-3197.
45. Cramail, H.; Deffieux, A., Living cationic polymerization of cyclohexyl vinyl ether. *Macromolecular Chemistry and Physics* **1994**, *195* (1), 217-27.
46. Hashimoto, T.; Makino, Y.; Urushisaki, M.; Sakaguchi, T., Living cationic polymerization of 2-adamantyl vinyl ether. *Journal of Polymer Science, Part A: Polymer Chemistry* **2008**, *46* (5), 1629-1637.
47. Rodriguez-Parada, J. M.; Percec, V., Poly(vinyl ether)s and poly(propenyl ether)s containing mesogenic groups: a new class of side-chain liquid-crystalline polymers. *Journal of Polymer Science, Part A: Polymer Chemistry* **1986**, *24* (6), 1363-78.
48. Percec, V.; Lee, M., Molecular engineering of liquid crystalline polymers by living polymerization. 10. Influence of molecular weight on the phase transitions of poly{ ω -[(4-cyano-4'-biphenyl)oxy]alkyl vinyl ether}s with nonyl and decanyl alkyl groups. *Macromolecules* **1991**, *24* (10), 2780-8.
49. Yoshida, T.; Seno, K.-I.; Kanaoka, S.; Aoshima, S., Stimuli-responsive reversible physical networks. I. Synthesis and physical network properties of amphiphilic block and random copolymers with long alkyl chains by living cationic polymerization. *Journal of Polymer Science, Part A: Polymer Chemistry* **2005**, *43* (6), 1155-1165.

50. Yoshida, T.; Kanaoka, S.; Watanabe, H.; Aoshima, S., Stimuli-responsive reversible physical networks. II. Design and properties of homogeneous physical networks consisting of periodic copolymers synthesized by living cationic polymerization. *Journal of Polymer Science, Part A: Polymer Chemistry* **2005**, *43* (13), 2712-2722.
51. Seno, K.-I.; Date, A.; Kanaoka, S.; Aoshima, S., Synthesis and solution properties of poly(vinyl ether)s with long alkyl chain, biphenyl, and cholesteryl pendants. *Journal of Polymer Science, Part A: Polymer Chemistry* **2008**, *46* (13), 4392-4406.
52. D'Agosto, F.; Charreyre, M.-T.; Delolme, F.; Dessalces, G.; Cramail, H.; Deffieux, A.; Pichot, C., Kinetic study of the "living" cationic polymerization of a galactose carrying vinyl ether. MALDI-TOF MS analysis of the resulting glycopolymers. *Macromolecules* **2002**, *35* (21), 7911-7918.
53. Minoda, M.; Yamaoka, K.; Yamada, K.; Takaragi, A.; Miyamoto, T., Synthesis of functional polymers bearing pendant mono-and oligo-saccharide residues. *Macromolecular Symposia* **1995**, *99* (Functional Polysaccharides), 169-77.
54. Okada, M., Molecular design and syntheses of glycopolymers. *Progress in Polymer Science* **2001**, *26* (1), 67-104.
55. Yamada, K.; Yamaoka, K.; Minoda, M.; Miyamoto, T., Survey of a catalyst system for living cationic polymerization of glucose-carrying vinyl ethers with acetyl and isopropylidene protecting groups. *Polymer International* **2001**, *50* (5), 531-537.
56. Yamada, K.; Yamaoka, K.; Minoda, M.; Miyamoto, T., Controlled synthesis of amphiphilic block copolymers with pendant glucose residues by living cationic polymerization. *Journal of Polymer Science, Part A: Polymer Chemistry* **1997**, *35* (2), 255-261.
57. Minoda, M.; Sawamoto, M.; Higashimura, T., Block copolymers of 2-hydroxyethyl vinyl ether and alkyl vinyl ether by living cationic polymerization: new nonionic macromolecular amphiphiles. *Macromolecules* **1987**, *20* (9), 2045-9.

58. Kamigaito, M.; Sawamoto, M.; Higashimura, T., Living cationic polymerization of isobutyl vinyl ether by trimethylsilyl iodide: Lewis acid systems on the presence of acetone: initiation via a silyloxycarbocation. *Macromolecules* **1990**, *23* (23), 4896-901.
59. Sawamoto, M.; Aoshima, S.; Higashimura, T., Synthesis of new functional polymers by living cationic polymerization. *Makromolekulare Chemie, Macromolecular Symposia* **1988**, *13-14*, 513-26.
60. Aoshima, S.; Ebara, K.; Higashimura, T., Living cationic polymerization of vinyl ethers with a functional group. 4. Synthesis of poly(vinyl ether) macromers with a methacrylate head. *Polymer Bulletin (Berlin, Germany)* **1985**, *14* (5), 425-31.
61. Haucourt, N. H.; Goethals, E. J.; Schappacher, M.; Deffieux, A., Reactivation of acetal-terminated poly(vinyl ethers). *Makromolekulare Chemie, Rapid Communications* **1992**, *13* (6), 329-36.
62. Kamigaito, M.; Sawamoto, M.; Higashimura, T., Living cationic polymerization of isobutyl vinyl ether by trimethylsilyl halide/zinc halide initiating systems: effects of carbonyl compounds. *Makromolekulare Chemie* **1993**, *194* (2), 727-38.
63. Chakrapani, S.; Jerome, R.; Teyssie, P., Novel initiator systems for the end-functionalization of poly(vinyl ethers). *Macromolecules* **1990**, *23* (11), 3026-8.
64. Sawamoto, M.; Enoki, T.; Higashimura, T., End-functionalized polymers by living cationic polymerization. 1. Mono- and bifunctional poly(vinyl ethers) with terminal malonate or carboxyl groups. *Macromolecules* **1987**, *20* (1), 1-6.
65. Reyntjens, W.; Jonckheere, L.; Goethals, E.; Du Prez, F., Thermosensitive polymer structures based on segmented copolymer networks. *Macromolecular Symposia* **2001**, *164* (Reactive Polymers), 293-300.
66. Sawamoto, M.; Enoki, T.; Higashimura, T., End-functionalized polymers by living cationic polymerization. 3. Ring-substituted anilines as functional end-capping agents for the synthesis of poly(isobutyl vinyl ether) with a terminal amine, carboxylic acid, or ester group. *Polymer Bulletin (Berlin, Germany)* **1987**, *18* (2), 117-22.

67. Fukui, H.; Sawamoto, M.; Higashimura, T., Multifunctional coupling agents for living cationic polymerization. 2. Bifunctional silyl enol ethers for living poly(vinyl ethers). *Macromolecules* **1993**, *26* (26), 7315-21.
68. Verma, A.; Nielsen, A.; McGrath, J. E.; Riffle, J. S., Preparation of ester-terminated poly(alkyl vinyl ether) oligomers and block copolymers using a combination of living cationic and group-transfer polymerization. *Polymer Bulletin (Berlin, Germany)* **1990**, *23* (6), 563-70.
69. Goethals, E. J.; Haucourt, N. H.; Verheyen, A. M.; Habimana, J., Synthesis of poly(vinyl ether) macromonomers using an iodine-free initiator. *Makromolekulare Chemie, Rapid Communications* **1990**, *11* (12), 623-7.
70. Aoshima, S.; Ikeda, M.; Nakayama, K.; Kobayashi, E.; Ohgi, H.; Sato, T., Synthesis of poly(vinyl alcohol) graft copolymers by living cationic polymerization in the presence of added bases I. Design and synthesis of poly(vinyl alcohol) graft copolymers with well-controlled poly(vinyl ether) grafts. *Polymer Journal (Tokyo, Japan)* **2001**, *33* (8), 610-616.
71. Alam, S.; Chisholm, B. J., Synthesis and characterization of graft copolymers containing blocks of biocide moieties. *Abstracts of Papers, 235th ACS National Meeting, New Orleans, LA, United States, April 6-10, 2008* **2008**, POLY-424.
72. Hashimoto, T.; Namikoshi, T.; Irie, S.; Urushisaki, M.; Sakaguchi, T.; Nemoto, T.; Isoda, S., Synthesis and microphase-separated structure of poly(tricyclodecyl vinyl ether)-block-poly(n-butyl vinyl ether)-block-poly(tricyclodecyl vinyl ether): new triblock copolymer as thermoplastic elastomer composed solely of poly(vinyl ether) backbones. *Journal of Polymer Science, Part A: Polymer Chemistry* **2008**, *46* (5), 1902-1906.
73. Sugihara, S.; Kanaoka, S.; Aoshima, S., Thermosensitive Random Copolymers of Hydrophilic and Hydrophobic Monomers Obtained by Living Cationic Copolymerization. *Macromolecules* **2004**, *37* (5), 1711-1719.

74. Kugel, A. J.; Jarabek, L. E.; Daniels, J. W.; Vander Wal, L. J.; Ebert, S. M.; Jepperson, M. J.; Stafslie, S. J.; Pieper, R. J.; Webster, D. C.; Bahr, J.; Chisholm, B. J., Combinatorial materials research applied to the development of new surface coatings XII: Novel, environmentally friendly antimicrobial coatings derived from biocide-functional acrylic polyols and isocyanates. *Journal of Coatings Technology and Research* **2009**, *6* (1), 107-121.
75. Vidaver, A. K., Antimicrobial use in plant agriculture. *Frontiers in Antimicrobial Resistance* **2005**, 465-470.
76. Singley, J. E. R., J., , *Krik-Othmer Encyclopedia of Chemical Technology*. 5 ed.; 2007; Vol. 26.
77. Ogaki, A., The antiseptics for water-based architectural coatings. *Techno-Cosmos* **2003**, *16*, 32-37.
78. Bognolo, G., Antimicrobial agents for cosmetics. *Chimica Oggi* **2005**, *23* (6), 20-21, 24-25.
79. Thomas, J.; Choi, S.-B.; Fjeldheim, R.; Boudjouk, P., Silicones Containing Pendant Biocides for Antifouling Coatings. *Biofouling* **2004**, *20* (4/5), 227-236.
80. Majumdar, P.; Lee, E.; Patel, N.; Ward, K.; Stafslie, S.; Daniels, J.; Chisholm, B. J.; Boudjouk, P.; Callow, M. A.; Callow, J. A.; Thompson, S. E. M., Combinatorial materials research applied to the development of new surface coatings IX: an investigation of novel antifouling/fouling-release coatings containing quaternary ammonium salt groups. *Biofouling* **2008**, *24* (3), 185-200.
81. Stafslie, S.; Daniels, J.; Chisholm, B.; Christianson, D., Combinatorial materials research applied to the development of new surface coatings III. Utilization of a high-throughput multiwell plate screening method to rapidly assess bacterial biofilm retention on antifouling surfaces. *Biofouling* **2007**, *23* (1/2), 37-44.

82. Khwaldia, K.; Arab-Tehrany, E.; Desobry, S., Biopolymer coatings on paper packaging materials. *Comprehensive Reviews in Food Science and Food Safety* **2010**, *9* (1), 82-91.
83. Jarvis William, R., The Lowbury Lecture. The United States approach to strategies in the battle against healthcare-associated infections, 2006: transitioning from benchmarking to zero tolerance and clinician accountability. *The Journal of hospital infection* **2007**, *65 Suppl 2*, 3-9.
84. Klevens, R. M. E., J.R.; Richards, C.L. Jr.; Horan, T.C.; Gaynes, R.P.; Pollock, D.A.; Cardo, D.M., Estimating Health Care-Associated Infections and Deaths in U.S. Hospitals 2002. *Public Health Reports* **2007**, *122*, 160-166.
85. Bryers James, D., Medical biofilms. *Biotechnology and bioengineering* **2008**, *100* (1), 1-18.
86. Hall-Stoodley, L.; Stoodley, P., Evolving concepts in biofilm infections. *Cellular Microbiology* **2009**, *11* (7), 1034-1043.
87. Ramage, G.; Mowat, E.; Jones, B.; Williams, C.; Lopez-Ribot, J., Our Current Understanding of Fungal Biofilms. *Critical Reviews in Microbiology* **2009**, *35* (4), 340-355.
88. Xu, K. D.; McFeters, G. A.; Stewart, P. S., Biofilm resistance to antimicrobial agents. *Microbiology (Reading, United Kingdom)* **2000**, *146* (3), 547-549.
89. Brown, M. R. W.; Allison, D. G.; Gilbert, P., Resistance of bacterial biofilms to antibiotics: a growth-rate related effect? *Journal of Antimicrobial Chemotherapy* **1988**, *22* (6), 777-80.
90. Borriello, G.; Werner, E.; Roe, F.; Kim, A. M.; Ehrlich, G. D.; Stewart, P. S., Oxygen limitation contributes to antibiotic tolerance of *Pseudomonas aeruginosa* in biofilms. *Antimicrobial Agents and Chemotherapy* **2004**, *48* (7), 2659-2664.

91. Francolini, I.; Donelli, G., Prevention and control of biofilm-based medical-device-related infections. *FEMS Immunology and Medical Microbiology* **2010**, *59* (3), 227-238.
92. Klotz, S. A.; Chasin, B. S.; Powell, B.; Gaur, N. K.; Lipke, P. N., Polymicrobial bloodstream infections involving *Candida* species: analysis of patients and review of the literature. *Diagnostic Microbiology and Infectious Disease* **2007**, *59* (4), 401-406.
93. Harriott, M. M.; Noverr, M. C., *Candida albicans* and *Staphylococcus aureus* form polymicrobial biofilms: Effects on antimicrobial resistance. *Antimicrobial Agents and Chemotherapy* **2009**, *53* (9), 3914-3922.
94. Shirtliff, M. E.; Peters, B. M.; Jabra-Rizk, M. A., Cross-kingdom interactions: *Candida albicans* and bacteria. *FEMS Microbiology Letters* **2009**, *299* (1), 1-8.
95. Adam, B.; Baillie George, S.; Douglas, L. J., Mixed species biofilms of *Candida albicans* and *Staphylococcus epidermidis*. *Journal of medical microbiology* **2002**, *51* (4), 344-9.
96. Tiller, J. C.; Sprich, C.; Hartmann, L., Amphiphilic conetworks as regenerative controlled releasing antimicrobial coatings. *Journal of Controlled Release* **2005**, *103* (2), 355-367.
97. Worley, S. D.; Li, F.; Wu, R.; Kim, J.; Wei, C. I.; Williams, J. F.; Owens, J. R.; Wander, J. D.; Bargmeyer, A. M.; Shirtliff, M. E., A novel N-halamine monomer for preparing biocidal polyurethane coatings. *Surface Coatings International, Part B: Coatings Transactions* **2003**, *86* (B4), 273-277.
98. Chainer, J., Home steel home. AK steel partners with AgION to build world's first antimicrobial steel house. *AISE Steel Technology* **2001**, *78* (9), 59-60.
99. Pai, M. P.; Pendland, S. L.; Danziger, L. H., Antimicrobial-coated/bonded and -impregnated intravascular catheters. *Annals of Pharmacotherapy* **2001**, *35* (10), 1255-1263.

100. Schierholz, J. M.; Beuth, J.; Rump, A.; Konig, D. P.; Pulverer, G., Novel strategies to prevent catheter-associated infections in oncology patients. *Journal of Chemotherapy (Firenze, Italy)* **2001**, *13* (Spec. Issue, 1), 239-250.
101. Edge, M.; Seal, K.; Allen, N. S.; Turner, D.; Robinson, J., The enhanced performance of biocidal additives in paints and coatings. *Special Publication - Royal Society of Chemistry* **2002**, *270* (Industrial Biocides), 84-94.
102. Boelens, J. J.; Tan, W.-F.; Dankert, J.; Zaat, S. A. J., Antibacterial activity of antibiotic-soaked polyvinylpyrrolidone-grafted silicone elastomer hydrocephalus shunts. *Journal of Antimicrobial Chemotherapy* **2000**, *45* (2), 221-224.
103. Johnson James, R.; Kuskowski Michael, A.; Wilt Timothy, J., Systematic review: antimicrobial urinary catheters to prevent catheter-associated urinary tract infection in hospitalized patients. *Annals of internal medicine* **2006**, *144* (2), 116-26.
104. John, T.; Rajpurkar, A.; Smith, G.; Fairfax, M.; Triest, J., Antibiotic pretreatment of hydrogel ureteral stent. *Journal of endourology / Endourological Society* **2007**, *21* (10), 1211-6.
105. Corchero, J. L.; Villaverde, A., Biomedical applications of distally controlled magnetic nanoparticles. *Trends in Biotechnology* **2009**, *27* (8), 468-476.
106. Xie, J.; Huang, J.; Li, X.; Sun, S.; Chen, X., Iron oxide nanoparticle platform for biomedical applications. *Current Medicinal Chemistry* **2009**, *16* (10), 1278-1294.
107. Bakker, D. P.; Huijs, F. M.; de Vries, J.; Klijnstra, J. W.; Busscher, H. J.; van der Mei, H. C., Bacterial deposition to fluoridated and non-fluoridated polyurethane coatings with different elastic modulus and surface tension in a parallel plate and a stagnation point flow chamber. *Colloids and Surfaces, B: Biointerfaces* **2003**, *32* (3), 179-190.
108. Graham, P.; Stone, M.; Thorpe, A.; Joint, I.; Nevell, T.; Tsibouklis, J., The prevention of biofilm formation and marine settlement on protective coatings prepared from low-surface-energy materials. *Proceedings in Marine Science* **2000**, *1* (Solent Science: A Review), 213-214.

109. Hyde, F. W.; Alberg, M.; Smith, K., Comparison of fluorinated polymers against stainless steel, glass and polypropylene in microbial biofilm adherence and removal. *Journal of Industrial Microbiology & Biotechnology* **1997**, *19* (2), 142-149.
110. Brash, J. L.; Uniyal, S., Dependence of albumin-fibrinogen simple and competitive adsorption on surface properties of biomaterials. *Journal of Polymer Science, Polymer Symposia* **1979**, *66* (Med. Polym.: Chem. Probl.), 377-89.
111. Townsin, R. L., The ship hull fouling penalty. *Biofouling* **2003**, *19 Suppl*, 9-15.
112. Yebra, D. M.; Kiil, S.; Dam-Johansen, K., Antifouling technology-past, present and future steps towards efficient and environmentally friendly antifouling coatings. *Progress in Organic Coatings* **2004**, *50* (2), 75-104.
113. Ferry, J. D.; Carritt, D. E., Action of antifouling paints. Solubility and rate of solution of cuprous oxide in sea water. *Journal of Industrial and Engineering Chemistry (Washington, D. C.)* **1946**, *38*, 612-17.
114. Turley, P. A.; Fenn, R. J.; Ritter, J. C.; Callow, M. E., Pyrithiones as antifoulants: Environmental fate and loss of toxicity. *Biofouling* **2005**, *21* (1), 31-40.
115. Finnie, A. A., Improved estimates of environmental copper release rates from antifouling products. *Biofouling* **2006**, *22* (5), 279-291.
116. Jelic-Mrcelic, G.; Sliskovic, M.; Antolic, B., Biofouling communities on test panels coated with TBT and TBT-free copper based antifouling paints. *Biofouling* **2006**, *22* (5), 293-302.
117. Thomas, K. V., The environmental fate and behaviour of antifouling paint booster biocides: A review. *Biofouling* **2001**, *17* (1), 73-86.
118. Kiil, S.; Weinell, C. E.; Pedersen, M. S.; Dam-Johansen, K., Analysis of Self-Polishing Antifouling Paints Using Rotary Experiments and Mathematical Modeling. *Industrial & Engineering Chemistry Research* **2001**, *40* (18), 3906-3920.

119. Kiil, S.; Dam-Johansen, K.; Weinell, C. E.; Pedersen, M. S.; Codolar, S. A., Dynamic simulations of a self-polishing antifouling paint exposed to seawater. *Journal of Coatings Technology* **2002**, *74* (929), 45-54.
120. Rascio, V. J. D.; Giudice, C. A.; Del Amo, B., Research and development of soluble matrix antifouling paints for ships, offshore platforms, and power stations. A review. *Corrosion Reviews* **1988**, *8* (1-2), 87-153.
121. Brady, R., Jr., Clean hulls without poisons: devising and testing nontoxic marine coatings. *Journal of Coatings Technology* **2000**, *72* (900), 44-56.
122. Dobretsov, S.; Dahms, H.-U.; Qian, P.-Y., Inhibition of biofouling by marine microorganisms and their metabolites. *Biofouling* **2006**, *22* (1/2), 43-54.
123. Brady, R. F., Jr.; Singer, I. L., Mechanical factors favoring release from fouling release coatings. *Biofouling* **2000**, *15* (1-3), 73-81.
124. Baier, R. E.; Shafrin, E. G.; Zisman, W. A., Adhesion: mechanisms that assist or impede it. *Science (Washington, DC, United States)* **1968**, *162* (3860), 1360-8.
125. Berglin, M.; Gatenholm, P., The barnacle adhesive plaque: morphological and chemical differences as a response to substrate properties. *Colloids and Surfaces, B: Biointerfaces* **2003**, *28* (2-3), 107-117.
126. Singer IL, K. J., Patterson M, Mechanical aspects of silicone coating for hard foulant control. *Biofouling* **2000**, *16*, 301 – 309.
127. Kohl, J. G.; Singer, I. L., Pull-off behavior of epoxy bonded to silicone duplex coatings. *Progress in Organic Coatings* **1999**, *36* (1-2), 15-20.
128. Zhang Newby, B.-m.; Chaudhury, M. K., Effect of Interfacial Slippage on Viscoelastic Adhesion. *Langmuir* **1997**, *13* (6), 1805-1809.
129. Zhang Newby, B.-m.; Chaudhury, M. K.; Brown, H. R., Macroscopic evidence of the effect of interfacial slippage on adhesion. *Science (Washington, D. C.)* **1995**, *269* (5229), 1407-9.

130. Chen, Z.; Chisholm, B. J.; Stafslie, S.; He, J.; Patel, S., Novel, UV-curable coatings containing a tethered biocide: synthesis, characterization, and antimicrobial activity. *Journal of Biomedical Materials Research, Part A* **2010**, *95A* (2), 486-494.
131. Chisholm, B. J.; Christianson, D. A.; Stafslie, S. J.; Gallagher-Lein, C.; Daniels, J., Novel, environmentally friendly, antifouling/fouling release coatings developed using combinatorial methods. *ACS Symposium Series* **2009**, *1002* (Smart Coatings II), 127-141, 4 plates.
132. Chisholm, B. J.; Christianson, D. A.; Stafslie, S. J.; Gubbins, N.; Daniels, J., An evaluation of the concept of tethering triclosan, an organic biocide, to coating matrix to create novel, environmentally-friendly, antifouling coatings. *FutureCoat Proceedings, New Orleans, LA, United States, Nov. 1-3, 2006* **2006**, 006/1-006/26.
133. Majumdar, P.; Lee, E.; Patel, N.; Stafslie, S. J.; Daniels, J.; Chisholm, B. J., Development of environmentally friendly, antifouling coatings based on tethered quaternary ammonium salts in a crosslinked polydimethylsiloxane matrix. *Journal of Coatings Technology and Research* **2008**, *5* (4), 405-417.
134. Chisholm, B. J.; Stafslie, S. J.; Christianson, D. A.; Gallagher-Lein, C.; Daniels, J. W.; Rafferty, C.; Vander Wal, L.; Webster, D. C., Combinatorial materials research applied to the development of new surface coatings. VIII: Overview of the high-throughput measurement systems developed for a marine coating workflow. *Applied Surface Science* **2007**, *254* (3), 692-698.
135. Webster Dean, C.; Chisholm Bret, J.; Stafslie Shane, J., Mini-review: combinatorial approaches for the design of novel coating systems. *Biofouling* **2007**, *23* (3-4), 179-92.
136. Owens, D. K.; Wendt, R. C., Estimation of the surface free energy of polymers. *Journal of Applied Polymer Science* **1969**, *13* (8), 1741-7.

137. Stafslie, S. J.; Bahr, J. A.; Feser, J. M.; Weisz, J. C.; Chisholm, B. J.; Ready, T. E.; Boudjouk, P., Combinatorial Materials Research Applied to the Development of New Surface Coatings I: A Multiwell Plate Screening Method for the High-Throughput Assessment of Bacterial Biofilm Retention on Surfaces. *Journal of Combinatorial Chemistry* **2006**, *8* (2), 156-162.
138. Stafslie, S.; Daniels, J.; Mayo, B.; Christianson, D.; Chisholm, B.; Ekin, A.; Webster, D.; Swain, G., Combinatorial materials research applied to the development of new surface coatings IV. A high-throughput bacterial biofilm retention and retraction assay for screening fouling - release performance of coatings. *Biofouling* **2007**, *23* (1/2), 45-54.
139. Baldassarri, L.; Simpson, W. A.; Donelli, G.; Christensen, G. D., Variable fixation of staphylococcal slime by different histochemical fixatives. *European journal of clinical microbiology & infectious diseases : official publication of the European Society of Clinical Microbiology* **1993**, *12* (11), 866-8.
140. Casse, F.; Stafslie, S. J.; Bahr, J. A.; Daniels, J.; Finlay, J. A.; Callow, J. A.; Callow, M. E., Combinatorial materials research applied to the development of new surface coatings V. Application of a spinning water-jet for the semi-high throughput assessment of the attachment strength of marine fouling algae. *Biofouling* **2007**, *23* (1/2), 121-130.
141. Sommer, S.; Ekin, A.; Webster, D. C.; Stafslie, S. J.; Daniels, J.; Vander Wal, L. J.; Thompson, S. E. M.; Callow, M. E.; Callow, J. A., A preliminary study on the properties and fouling-release performance of siloxane-polyurethane coatings prepared from poly(dimethylsiloxane) (PDMS) macromers. *Biofouling* **2010**, *26* (8), 961-972.
142. Peters, M. A.; Belu, A. M.; Linton, R. W.; Dupray, L.; Meyer, T. J.; DeSimone, J. M., Termination of Living Anionic Polymerizations Using Chlorosilane Derivatives: A General Synthetic Methodology for the Synthesis of End-Functionalized Polymers. *Journal of the American Chemical Society* **1995**, *117* (12), 3380-8.

143. Kawakami, Y.; Miki, Y.; Tsuda, T.; Murthy, R. A. N.; Yamashita, Y., Silicone macromers for graft polymer synthesis. *Polymer Journal (Tokyo, Japan)* **1982**, *14* (11), 913-17.
144. White, G. F.; Russell, N. J.; Tidswell, E. C., Bacterial scission of ether bonds. *Microbiological Reviews* **1996**, *60* (1), 216-32.
145. McMurry, L. M.; Oethinger, M.; Levy, S. B., Triclosan targets lipid synthesis. *Nature (London)* **1998**, *394* (6693), 531-532.
146. Gomez Escalada, M.; Russell, A. D.; Maillard, J. Y.; Ochs, D., Triclosan-bacteria interactions: single or multiple target sites? *Letters in Applied Microbiology* **2005**, *41* (6), 476-481.
147. Campbell, J. W.; Cronan, J. E., Jr., Bacterial fatty acid biosynthesis: Targets for antibacterial drug discovery. *Annual Review of Microbiology* **2001**, *55*, 305-332.
148. Heath, R. J.; Rubin, J. R.; Holland, D. R.; Zhang, E.; Snow, M. E.; Rock, C. O., Mechanism of triclosan inhibition of bacterial fatty acid synthesis. *Journal of Biological Chemistry* **1999**, *274* (16), 11110-11114.
149. Villalain, J.; Mateo, C. R.; Aranda, F. J.; Shapiro, S.; Micol, V., Membranotropic Effects of the Antibacterial Agent Triclosan. *Archives of Biochemistry and Biophysics* **2001**, *390* (1), 128-136.
150. Stewart, M. J.; Parikh, S.; Xiao, G.; Tonge, P. J.; Kisker, C., Structural Basis and Mechanism of Enoyl Reductase Inhibition by Triclosan. *Journal of Molecular Biology* **1999**, *290* (4), 859-865.
151. Chaffin, W. L.; Lopez-Ribot, J. L.; Casanova, M.; Gozalbo, D.; Martinez, J. P., Cell wall and secreted proteins of *Candida albicans*: identification, function, and expression. *Microbiology and molecular biology reviews : MMBR* **1998**, *62* (1), 130-80.

152. Kapteyn, J. C.; Hoyer, L. L.; Hecht, J. E.; Muller, W. H.; Andel, A.; Verkleij, A. J.; Makarow, M.; Van Den Ende, H.; Klis, F. M., The cell wall architecture of *Candida albicans* wild-type cells and cell wall-defective mutants. *Molecular Microbiology* **2000**, *35* (3), 601-611.
153. Higashimura, T.; Ebara, K.; Aoshima, S., Living cationic polymerization of vinyl ethers with a functional group. VII. Polymerization of vinyl ethers with a silyloxy group and synthesis of polyalcohols and related functional polymers. *Journal of Polymer Science, Part A: Polymer Chemistry* **1989**, *27* (9), 2937-50.
154. Van Meirvenne, D.; Haucourt, N.; Goethals, E. J., A new initiating system for the "living" polymerization of vinyl ethers leading to hydroxy-terminated polymers. *Polymer Bulletin (Berlin, Germany)* **1990**, *23* (2), 185-90.
155. Shohi, H.; Sawamoto, M.; Higashimura, T., End-functionalized polymers of p-alkoxystyrenes by living cationic polymerization. 1. p-Methoxystyrene. *Macromolecules* **1992**, *25* (1), 53-7.
156. Ruckenstein, E.; Zhang, H., Monomer [1-(Isobutoxy)ethyl Methacrylate] That Can Undergo Anionic Polymerization and Can Also Be an Initiator for the Cationic Polymerization of Vinyl Ethers. Preparation of Comblike Polymers. *Macromolecules* **1997**, *30* (22), 6852-6855.
157. Sauvet, G.; Fortuniak, W.; Kazmierski, K.; Chojnowski, J., Amphiphilic block and statistical siloxane copolymers with antimicrobial activity. *Journal of Polymer Science, Part A: Polymer Chemistry* **2003**, *41* (19), 2939-2948.
158. Majumdar, P.; Lee, E.; Patel, N.; Stafslie, S. J.; Daniels, J.; Thorson, C. J.; Chisholm, B. J., Medical device coatings based on polysiloxanes containing tethered quaternary ammonium salts. *Polymer Preprints (American Chemical Society, Division of Polymer Chemistry)* **2008**, *49* (1), 852-853.

159. Games, L. M.; King, J. E.; Larson, R. J., Fate and distribution of a quaternary ammonium surfactant, octadecyltrimethylammonium chloride (OTAC), in wastewater treatment. *Environmental Science and Technology* **1982**, *16* (8), 483-8.
160. Van Ginkel, C. G.; Kolvenbach, M., Relations between the structure of quaternary alkyl ammonium salts and their biodegradability. *Chemosphere* **1991**, *23* (3), 281-9.
161. Gottenbos, B.; Busscher, H. J.; van der Mei, H. C.; Nieuwenhuis, P., Pathogenesis and prevention of biomaterial centered infections. *Journal of Materials Science: Materials in Medicine* **2002**, *13* (8), 717-722.
162. Nishihara, T.; Okamoto, T.; Nishiyama, N., Biodegradation of didecyldimethylammonium chloride by *Pseudomonas fluorescens* TN4 isolated from activated sludge. *Journal of Applied Microbiology* **2000**, *88* (4), 641-647.
163. Laopaiboon, L.; Hall, S. J.; Smith, R. N., The effect of a quaternary ammonium biocide on the performance and characteristics of laboratory-scale rotating biological contactors. *Journal of Applied Microbiology* **2002**, *93* (6), 1051-1058.
164. Tashiro, T., Antibacterial and bacterium adsorbing macromolecules. *Macromolecular Materials and Engineering* **2001**, *286* (2), 63-87.
165. Davies, A.; Bentley, M.; Field, B. S., Comparison of the action of Vantocil, cetrimide, and chlorhexidine on *Escherichia coli* and its spheroplasts and the protoplasts of gram-positive bacteria. *Journal of Applied Bacteriology* **1968**, *31* (4), 448-61.
166. Juergensen, L.; Busnarda, J.; Caux, P.-Y.; Kent, R. A., Fate, behavior, and aquatic toxicity of the fungicide DDAC in the Canadian environment. *Environmental Toxicology* **2000**, *15* (3), 174-200.
167. Tomlinson, E.; Brown, M. R. W.; Davis, S. S., Effect of colloidal association on the measured activity of alkylbenzyldimethylammonium chlorides against *Pseudomonas aeruginosa*. *Journal of Medicinal Chemistry* **1977**, *20* (10), 1277-82.

168. Ioannou, C. J.; Hanlon, G. W.; Denyer, S. P., Action of disinfectant quaternary ammonium compounds against *Staphylococcus aureus*. *Antimicrobial Agents and Chemotherapy* **2007**, *51* (1), 296-306.
169. Patel, R. N.; Singh, N.; Gundla, V. L. N.; Chauhan, U. K., Copper(II) complexes of tridentate N,N,N',N'',N'''-pentamethyldiethylenetriamine: Superoxide dismutase and inhibitory activity against bacteria and fungi. *Spectrochimica Acta, Part A: Molecular and Biomolecular Spectroscopy* **2007**, *66A* (3), 726-731.
170. Ahlstrom, B.; Thompson, R. A.; Edebo, L., The effect of hydrocarbon chain length, pH, and temperature on the binding and bactericidal effect of amphiphilic betaine esters on *Salmonella typhimurium*. *APMIS : acta pathologica, microbiologica, et immunologica Scandinavica* **1999**, *107* (3), 318-24.
171. Gottenbos, B.; van der Mei, H. C.; Klatter, F.; Nieuwenhuis, P.; Busscher, H. J., In vitro and in vivo antimicrobial activity of covalently coupled quaternary ammonium silane coatings on silicone rubber. *Biomaterials* **2002**, *23* (6), 1417-1423.
172. Dizman, B.; Elasri, M. O.; Mathias, L. J., Synthesis and antimicrobial activities of new water-soluble bis-quaternary ammonium methacrylate polymers. *Journal of Applied Polymer Science* **2004**, *94* (2), 635-642.
173. Chen, C. Z.; Beck-Tan, N. C.; Dhurjati, P.; Van Dyk, T. K.; LaRossa, R. A.; Cooper, S. L., Quaternary Ammonium Functionalized Poly(propyleneimine) Dendrimers as Effective Antimicrobials: Structure-Activity Studies. *Biomacromolecules* **2000**, *1* (3), 473-480.
174. Majumdar, P.; Lee, E.; Gubbins, N.; Stafslie, S. J.; Daniels, J.; Thorson, C. J.; Chisholm, B. J., Synthesis and antimicrobial activity of quaternary ammonium-functionalized POSS (Q-POSS) and polysiloxane coatings containing Q-POSS. *Polymer* **2009**, *50* (5), 1124-1133.

175. Majumdar, P.; Lee, E.; Gubbins, N.; Christianson, D. A.; Stafslie, S. J.; Daniels, J.; VanderWal, L.; Bahr, J.; Chisholm, B. J., Combinatorial Materials Research Applied to the Development of New Surface Coatings XIII: An Investigation of Polysiloxane Antimicrobial Coatings Containing Tethered Quaternary Ammonium Salt Groups. *Journal of Combinatorial Chemistry* **2009**, *11* (6), 1115-1127.
176. Pant, R. R.; Rasley, B. T.; Buckley, J. P.; Lloyd, C. T.; Cozzens, R. F.; Santangelo, P. G.; Wynne, J. H., Synthesis, mobility study and antimicrobial evaluation of novel self-spreading ionic silicone oligomers. *Journal of Applied Polymer Science* **2007**, *104* (5), 2954-2964.
177. Dey, B. P.; Engley, F. B., Jr., Comparison of Dey and Engley (D/E) neutralizing medium to letheen medium and standard methods medium for recovery of *Staphylococcus aureus* from sanitized surfaces. *Journal of Industrial Microbiology* **1995**, *14* (1), 21-5.
178. Gilbert, P.; Al-Taae, A., Antimicrobial activity of some alkyltrimethylammonium bromides. *Letters in Applied Microbiology* **1985**, *1* (6), 101-4.
179. Dubnickova, M.; Rezanka, T.; Koscova, H., Adaptive changes in fatty acids of *E. coli* strains exposed to a quaternary ammonium salt and an amine oxide. *Folia Microbiologica (Prague, Czech Republic)* **2006**, *51* (5), 371-374.
180. Walsh, S. E.; Maillard, J. Y.; Russell, A. D.; Catrenich, C. E.; Charbonneau, D. L.; Bartolo, R. G., Activity and mechanisms of action of selected biocidal agents on Gram-positive and -negative bacteria. *Journal of Applied Microbiology* **2003**, *94* (2), 240-247.
181. Zhang, S.; Horrocks, A. R., A review of flame retardant polypropylene fibres. *Progress in Polymer Science* **2003**, *28* (11), 1517-1538.
182. Montero, B.; Ramirez, C.; Rico, M.; Torres, A.; Cano, J.; Lopez, J., Mechanism of thermal degradation of an inorganic-organic hybrid based on an epoxy-POSS. *Macromolecular Symposia* **2008**, *267* (Nanostructured Polymers and Polymer Nanocomposites), 74-78.

183. Lawson, D. F., Recent developments in the flammability of elastomeric materials. *Rubber Chemistry and Technology* **1986**, *59* (3), 455-81.
184. Kong, S. H.; Ahn, S. H.; Hwang, S. D.; Oh, I. H.; Son, S. B.; Lee, H. J. Flame-retardant high-impact vinyl aromatic resin compositions having good fluidity. 2009-628258, 20100152342, 20091201., 2010.
185. Zhang, P.; Song, L.; Lu, H.; Wang, J.; Hu, Y., The influence of expanded graphite on thermal properties for paraffin/high density polyethylene/chlorinated paraffin/antimony trioxide as a flame retardant phase change material. *Energy Conversion and Management* **2010**, *51* (12), 2733-2737.
186. Baral, D.; De, P. P.; Nando, G. B., Thermal characterization of mica-filled thermoplastic polyurethane composites. *Polymer Degradation and Stability* **1999**, *65* (1), 47-51.
187. Pinto, U. A.; Visconte, L. L. Y.; Gallo, J.; Nunes, R. C. R., Flame retardancy in thermoplastic polyurethane elastomers (TPU) with mica and aluminum trihydrate (ATH). *Polymer Degradation and Stability* **2000**, *69* (3), 257-260.
188. Sultan, B.-A.; Jungkvist, J. Flame-retardant polyolefin compositions comprising a high amount of inorganic fillers. 2009-EP3788, 2009146831, 20090527., 2009.
189. Grasselli, G.; Bareggi, A.; Scelza, C.; Frigerio, M.; Veggetti, P.; Belli, S. Production of self-extinguishing electric cables comprising insulating layers of expanded flame-retardant polymers. 2003-IT855, 2005062315, 20031224., 2005.
190. Morgan, A. B.; Cogen, J. M.; Opperman, R. S.; Harris, J. D., The effectiveness of magnesium carbonate-based flame retardants for poly(ethylene-co-vinyl acetate) and poly(ethylene-co-ethyl acrylate). *Fire and Materials* **2007**, *31* (6), 387-410.
191. Bown, R.; Hooper, J. J.; Riley, A. M.; Skuse, D. R. Cost effective methods for making magnesium hydroxide and uses of magnesium hydroxide as a flame retardant. 2009-GB50822, 2010004341, 20090710., 2010.

192. Dharmarajan, N.; Yu, T. C.; Metzler, D. K., Metallocene plastomer based thermoplastic olefin compounds designed for roof membrane applications. *Annual Technical Conference - Society of Plastics Engineers* **2001**, *59th* (Vol. 2), 1694-1698.
193. Holloway, L. R., Application of magnesium hydroxide as a flame retardant and smoke suppressant in elastomers. *Rubber Chemistry and Technology* **1988**, *61* (2), 186-93.
194. Innes, J. D.; Cox, A. W., Magnesium hydroxide flame retardant and smoke suppressant. *Proceedings of the International Conference on Fire Safety* **1997**, *24*, 127-138.
195. Jeencham, R.; Suppakarn, N.; Jarukumjorn, K., Effect of flame retardant on flame retardancy and mechanical properties of glass fiber/polypropylene composites. *Advanced Materials Research (Durnten-Zurich, Switzerland)* **2011**, 264-265 (Pt. 1, Advances in Materials and Processing Technologies II), 652-656.
196. Sener, A. A.; Demirhan, E., The investigation of using magnesium hydroxide as a flame retardant in the cable insulation material by cross-linked polyethylene. *Materials & Design* **2008**, *29* (7), 1376-1379.
197. Lawson, D. F.; Kay, E. L.; Roberts, D. T., Jr., Mechanism of smoke inhibition by hydrated fillers. *Rubber Chemistry and Technology* **1975**, *48* (1), 124-31.
198. Dogan, M.; Bayramli, E., Effect of boron-containing materials on the flammability and thermal degradation of polyamide 6 composites containing melamine. *Journal of Applied Polymer Science* **2010**, *118* (5), 2722-2727.
199. Dogan, M.; Yilmaz, A.; Bayramli, E., Synergistic effect of boron containing substances on flame retardancy and thermal stability of intumescent polypropylene composites. *Polymer Degradation and Stability* **2010**, *95* (12), 2584-2588.
200. Dogan, M.; Yilmaz, A.; Bayramli, E., Effect of boron containing materials on flammability and thermal degradation of polyamide-6 composites containing melamine cyanurate. *Polymers for Advanced Technologies* **2011**, *22* (5), 560-566.

201. Hogt, A. H.; Spijkerman, G. K.; Tonnaer, H. Fire resistant polyolefin composition comprising brominated flame retardant with low amounts of synergist and radical initiator. 2009-EP61032, 2010023236, 20090827., 2010.
202. Ibibikcan, E.; Kaynak, C., Use of boron compounds as synergistic flame retardants in low density polyethylene: Ethylene vinyl acetate blends and nanocomposites. *Abstracts of Papers, 241st ACS National Meeting & Exposition, Anaheim, CA, United States, March 27-31, 2011* **2011**, I+EC-76.
203. Katovic, D.; Vukusic, S. B.; Grgac, S. F.; Lozo, B.; Banic, D., Flame retardancy of paper obtained with environmentally friendly agents. *Fibres & Textiles in Eastern Europe* **2009**, *17* (3), 90-94.
204. Keibal, N. A.; Bondarenko, S. N.; Kablov, V. F.; Gonoshilov, D. G., Polyamide fibers with improved properties. *Fibre Chemistry* **2009**, *41* (3), 186-188.
205. Park, D.-H. Fire resistant resin composition for electrical cables coatings. 2008-KR4382, 2010013851, 20080728., 2010.
206. Rogunova, M. Impact-resistant, flame retardant thermoplastic molding composition. 2008-US13193, 2009105087, 20081125., 2009.
207. Rogunova, M. Impact-resistant and flame-retardant thermoplastic molding compositions. 2007-998697, 20090143514, 20071130., 2009.
208. Rogunova, M. Impact-resistant, flame retardant thermoplastic molding composition. 2008-12947, 20090143513, 20080206., 2009.
209. Choi, J.-K.; Jung, D.-S.; Lee, S.-H.; Hwang, Y.-Y.; Seo, B.-H. Flame-retardant rubber-modified styrene resin compositions. 2006-KR4974, 2008001983, 20061124., 2008.
210. Chung, Y.-j.; Kim, Y.; Kim, S., Flame retardant properties of polyurethane produced by the addition of phosphorous containing polyurethane oligomers (II). *Journal of Industrial and Engineering Chemistry (Amsterdam, Netherlands)* **2009**, *15* (6), 888-893.

211. Okada, K.; Maeda, Y.; Motoshige, R.; Noro, M. Flame-retardant thermoplastic resin composition for moldings. 1999-300467, 1022312, 19990122., 2000.
212. Prindle, J. C.; Nalepa, C. J.; Kumar, G. Flame retardant styrenic polymer compositions. 1997-250142, 806451, 19970428., 1997.
213. Hylton, R. R., Techniques for identification of silver migration in plastic encapsulated devices assembled with molding compound containing red phosphorus flame retardant material. *ISTFA 2008, Conference Proceedings from the International Symposium for Testing and Failure Analysis, 34th, Portland, OR, United States, Nov. 2-6, 2008* **2008**, 112-120.
214. Barikani, M.; Askari, F.; Barmar, M., A comparison of the effect of different flame retardants on the compressive strength and fire behaviour of rigid polyurethane foams. *Cellular Polymers* **2010**, *29* (6), 343-357.
215. Kandare, E.; Chukwunonso, A. K.; Kandola, B. K., The effect of fire-retardant additives and a surface insulative fabric on fire performance and mechanical property retention of polyester composites. *Fire and Materials* **2011**, *35* (3), 143-155.
216. Lavietes, D.; Bryson, M. L. Fire-resistant coated fiber mat rolls for roofings with graphite-containing coatings. 2009-505278, 20110011021, 20090717., 2011.
217. Milliren, C. M.; Worthington, M. J. Fire-retardant polyurethane foam and process for preparing the same. 2011-14456, 20110184079, 20110126., 2011.
218. Schmutter, B. E. Fire-resistant multilayer panels with heat-reflecting fibrous layers, metallic impact-resistant layers and intumescent layers. 2007-974494, 7887898, 20071011., 2011.
219. Sittisart, P.; Farid, M. M., Fire retardants for phase change materials. *Applied Energy* **2011**, *88* (9), 3140-3145.

220. Swindells, D. J.; Scheirs, J.; Cranston, R. W.; Dean, F. G.; Fullston, D.; Prins, M. W. Heat and flame-resistant protective coating compositions for fabrics and construction materials. 2010-AU1177, 2011029151, 20100910., 2011.
221. Tsai, K.-C.; Kuan, H.-C.; Chou, H.-W.; Kuan, C.-F.; Chen, C.-H.; Chiang, C.-L., Preparation of expandable graphite using a hydrothermal method and flame-retardant properties of its halogen-free flame-retardant HDPE composites. *Journal of Polymer Research* **2011**, *18* (4), 483-488.
222. Zhang, X.-G.; Ge, L.-L.; Zhang, W.-Q.; Tang, J.-H.; Ye, L.; Li, Z.-M., Expandable graphite-methyl methacrylate-acrylic acid copolymer composite particles as a flame retardant of rigid polyurethane foam. *Journal of Applied Polymer Science* **2011**, *122* (2), 932-941.
223. Zhu, H.; Zhu, Q.; Li, J.; Tao, K.; Xue, L.; Yan, Q., Synergistic effect between expandable graphite and ammonium polyphosphate on flame retarded polylactide. *Polymer Degradation and Stability* **2011**, *96* (2), 183-189.
224. Duquesne, S.; Delobel, R.; Le Bras, M.; Camino, G., A comparative study of the mechanism of action of ammonium polyphosphate and expandable graphite in polyurethane. *Polymer Degradation and Stability* **2002**, *77* (2), 333-344.
225. Austin, J. R.; Chao, H. S. I., Improving the mechanical properties of non-halogenated flame retardant compounds. *Proceedings of International Wire and Cable Symposium* **2009**, *58th*, 564-568.
226. Green, J., Mechanisms for flame retardancy and smoke suppression - A review. *Journal of Fire Sciences* **1996**, *14* (6), 426-442.
227. Alae, M.; Arias, P.; Sjodin, A.; Bergman, A., An overview of commercially used brominated flame retardants, their applications, their use patterns in different countries/regions and possible modes of release. *Environment international* **2003**, *29* (6), 683-9.

228. Smith, R.; Georlette, P.; Finberg, I.; Reznick, G., Development of environmentally friendly multifunctional flame retardants for commodity and engineering plastics. *Polymer Degradation and Stability* **1996**, *54* (2-3), 167-173.
229. Maas, C. J. J.; De Nooijer, H. C. J.; Pai-Paranjape, V.; Siripurapu, S.; Van Den Bogerd, J. A.; Volkers, A. A. Flame retardant thermoplastic polymer composition, method of manufacture, and articles formed therefrom. 2009-566914, 20100075125, 20090925., 2010.
230. Gouteux, B.; Alae, M.; Mabury Scott, A.; Pacepavicius, G.; Muir Derek, C. G., Polymeric brominated flame retardants: are they a relevant source of emerging brominated aromatic compounds in the environment? *Environmental science & technology* **2008**, *42* (24), 9039-44.
231. Alae, M.; Arias, P.; Sjödin, A.; Bergman, A., An overview of commercially used brominated flame retardants, their applications, their use patterns in different countries/regions and possible modes of release. *Environ. Int.* **2003**, *29* (6), 683-689.
232. Meironyte, D.; Noren, K.; Bergman, A., Analysis of polybrominated diphenyl ethers in Swedish human milk. A time-related trend study, 1972-1997. *Journal of Toxicology and Environmental Health, Part A* **1999**, *58* (6), 329-341.
233. Gouteux, B.; Alae, M.; Mabury, S. A.; Pacepavicius, G.; Muir, D. C. G., Polymeric Brominated Flame Retardants: Are They a Relevant Source of Emerging Brominated Aromatic Compounds in the Environment? *Environmental Science & Technology* **2008**, *42* (24), 9039-9044.
234. Weil, E. D.; Levchik, S., Current practice and recent commercial developments in flame retardancy of polyamides. *Journal of Fire Sciences* **2004**, *22* (3), 251-264.
235. Watanabe, I.; Sakai, S.-i., Environmental release and behavior of brominated flame retardants. *Environ. Int.* **2003**, *29* (6), 665-682.

236. Sjodin, A.; Patterson, D. G.; Bergman, A., A review on human exposure to brominated flame retardants - particularly polybrominated diphenyl ethers. *Environ. Int.* **2003**, *29* (6), 829-839.
237. de Boer, J.; Dao, Q. T.; van Leeuwen, S. P. J.; Kotterman, M. J. J.; Schobben, J. H. M., Thirty year monitoring of PCBs, organochlorine pesticides and tetrabromodiphenylether in eel from The Netherlands. *Environmental Pollution (Oxford, United Kingdom)* **2010**, *158* (5), 1228-1236.
238. Hulzebos, E.; Gerner, I., Weight factors in an Integrated Testing Strategy using adjusted OECD principles for (Q)SARs and extended Klimisch codes to decide on skin irritation classification. *Regulatory Toxicology and Pharmacology* **2010**, *58* (1), 131-144.
239. Kemmlein, S.; Herzke, D.; Law, R. J., Brominated flame retardants in the European chemicals policy of REACH-Regulation and determination in materials. *Journal of Chromatography, A* **2009**, *1216* (3), 320-333.
240. Krishnan, K.; Adamou, T.; Aylward, L. L.; Hays, S. M.; Kirman, C. R.; Nong, A., Biomonitoring Equivalents for 2,2',4,4',5-pentabromodiphenylether (PBDE-99). *Regulatory Toxicology and Pharmacology* **2011**, *60* (2), 165-171.
241. Zhang, F.-X.; Hu, W.; Yu, H.-X.; Sun, H.; Shen, O.-X.; Wang, X.-R.; Liu, H.-L.; Lam, M. H. W.; Giesy, J. P.; Zhang, X.-W., Endocrine disruption effects of 2,2',4,4',6-pentabromodiphenylether (BDE100) in reporter gene assays. *Journal of Environmental Monitoring* **2011**, *13* (4), 850-854.
242. Allchin, C. R.; Law, R. J.; Morris, S., Polybrominated diphenylethers in sediments and biota downstream of potential sources in the UK. *Environmental Pollution* **1999**, *105* (2), 197-207.
243. Antignac, J.-P.; Cariou, R.; Maume, D.; Marchand, P.; Monteau, F.; Zalko, D.; Berrebi, A.; Cravedi, J.-P.; Andre, F.; Le Bizec, B., Exposure assessment of fetus and newborn to brominated flame retardants in France: preliminary data. *Molecular Nutrition & Food Research* **2008**, *52* (2), 258-265.

244. Hamm, S., Polybrominated diphenyl ethers in sewage sludge and effluents of sewage plants from a central regions of Germany. *Organohalogen Compounds* **2004**, 66 (Dioxin 2004), 1629-1634.
245. Sandal, S.; Yilmaz, B.; Chen, C.-H.; Carpenter, D. O., Comparative effects of technical toxaphene, 2,5-dichloro-3-biphenylol and octabromodiphenylether on cell viability, [Ca²⁺]_i levels and membrane fluidity in mouse thymocytes. *Toxicology Letters* **2004**, 151 (3), 417-428.
246. Yasuhiro, H.; Shunichi, S.; Shinichi, S., Impact of PBDD/DFs in life cycle assessments of recycling of TV cabinet back covers. *Organohalogen Compounds* **2008**, 70, 1418-1421.
247. Dannan, G. A.; Moore, R. W.; Besaw, L. C.; Aust, S. D., 2,4,5,3',4',5'-Hexabromobiphenyl is both a 3-methylcholanthrene- and a phenobarbital-type inducer of microsomal drug metabolizing enzymes. *Biochemical and Biophysical Research Communications* **1978**, 85 (1), 450-8.
248. Johansson, A.-K.; Sellstroem, U.; Lindberg, P.; Bignert, A.; de Wit, C. A., Polybrominated diphenyl ether congener patterns, hexabromocyclododecane, and brominated biphenyl 153 in eggs of peregrine falcons (*Falco peregrinus*) breeding in Sweden. *Environmental Toxicology and Chemistry* **2009**, 28 (1), 9-17.
249. Lindberg, P.; Sellstrom, U.; Haggberg, L.; de Wit Cynthia, A., Higher brominated diphenyl ethers and hexabromocyclododecane found in eggs of peregrine falcons (*Falco peregrinus*) breeding in Sweden. *Environmental science & technology* **2004**, 38 (1), 93-6.
250. Millis, C. D.; Mills, R. A.; Sleight, S. D.; Aust, S. D., Toxicity of 3,4,5,3',4',5'-hexabrominated biphenyl and 3,4,3',4'-tetrabrominated biphenyl. *Toxicology and Applied Pharmacology* **1985**, 78 (1), 88-95.
251. Millis, C. D.; Mills, R. A.; Sleight, S. D.; Aust, S. D., Toxicity of 3,4,5,3',4',5'-hexabrominated biphenyl and 3,4,3',4'-tetrabrominated biphenyl. *Toxicology and applied pharmacology* **1985**, 78 (1), 88-95.

252. von der Recke, R.; Vetter, W., GC-ECNI-MSMS residue pattern of hexabrominated biphenyls in marine mammals and fish. *Organohalogen Compounds* **2007**, *69*, 505/1-505/4.
253. Fan, C.-Y.; Besas, J.; Kodavanti, P. R. S., Changes in mitogen-activated protein kinase in cerebellar granule neurons by polybrominated diphenyl ethers and polychlorinated biphenyls. *Toxicology and Applied Pharmacology* **2010**, *245* (1), 1-8.
254. Lebeuf, M.; Couillard, C. M.; Legare, B.; Trottier, S., Effects of DeBDE and PCB-126 on Hepatic Concentrations of PBDEs and Methoxy-PBDEs in Atlantic Tomcod. *Environmental Science & Technology* **2006**, *40* (10), 3211-3216.
255. Teclechiel, D.; Sundstrom, M.; Marsh, G., Synthesis of polybrominated diphenyl ethers via symmetrical tetra- and hexabrominated diphenyliodonium salts. *Chemosphere* **2009**, *74* (3), 421-7.
256. Aylward, L. L.; Hays, S. M., Biomonitoring-based risk assessment for hexabromocyclododecane (HBCD). *International Journal of Hygiene and Environmental Health* **2011**, *214* (3), 179-187.
257. Eggesbo, M.; Thomsen, C.; Jorgensen, J. V.; Becher, G.; Oyvind Odland, J.; Longnecker, M. P., Associations between brominated flame retardants in human milk and thyroid-stimulating hormone (TSH) in neonates. *Environmental Research* **2011**, *111* (6), 737-743.
258. Gosciny, S.; Vandevijvere, S.; Maleki, M.; Van Overmeire, I.; Windal, I.; Hanot, V.; Blaude, M.-N.; Vleminckx, C.; Van Loco, J., Dietary intake of hexabromocyclododecane diastereoisomers (α -, β -, and γ -HBCD) in the Belgian adult population. *Chemosphere* **2011**, *84* (3), 279-288.
259. Ibhazehiebo, K.; Iwasaki, T.; Shimokawa, N.; Koibuchi, N., 1,2,5,6,9,10- α Hexabromocyclododecane (HBCD) impairs thyroid hormone-induced dendrite arborization of Purkinje cells and suppresses thyroid hormone receptor-mediated transcription. *Cerebellum* **2011**, *10* (1), 22-31.

260. Ibhazehiebo, K.; Iwasaki, T.; Xu, M.; Shimokawa, N.; Koibuchi, N., Brain-derived neurotrophic factor (BDNF) ameliorates the suppression of thyroid hormone-induced granule cell neurite extension by hexabromocyclododecane (HBCD). *Neuroscience Letters* **2011**, *493* (1-2), 1-7.
261. Kalantzi, O. I.; Geens, T.; Covaci, A.; Siskos, P. A., Distribution of polybrominated diphenyl ethers (PBDEs) and other persistent organic pollutants in human serum from Greece. *Environ. Int.* **2011**, *37* (2), 349-353.
262. Rawn, D. F. K.; Sadler, A.; Quade, S. C.; Sun, W. F.; Lau, B. P. Y.; Kosarac, I.; Hayward, S.; Ryan, J. J., Brominated flame retardants in Canadian chicken egg yolks. *Food Additives & Contaminants, Part A: Chemistry, Analysis, Control, Exposure & Risk Assessment* **2011**, *28* (6), 807-815.
263. Riddell, N.; Becker, R.; Chittim, B.; Emmerling, F.; Koppen, R.; Lough, A.; McAlees, A.; McCrindle, R., Preparation and X-ray structural characterization of further stereoisomers of 1,2,5,6,9,10-hexabromocyclododecane. *Chemosphere* **2011**, *84* (7), 900-907.
264. Rosenberg, C.; Haemeilae, M.; Tornaues, J.; Saekkinen, K.; Puttonen, K.; Korpi, A.; Kiilunen, M.; Linnainmaa, M.; Hesso, A., Exposure to Flame Retardants in Electronics Recycling Sites. *Annals of Occupational Hygiene* **2011**, *55* (6), 658-665.
265. Szabo, D. T.; Diliberto, J. J.; Hakk, H.; Huwe, J. K.; Birnbaum, L. S., Toxicokinetics of the Flame Retardant Hexabromocyclododecane Alpha: Effect of Dose, Timing, Route, Repeated Exposure, and Metabolism. *Toxicological Sciences* **2011**, *121* (2), 234-244.
266. Vagula, M. C.; Kubeldis, N.; Nelatury, C. F., Environmental monitoring of brominated flame retardants. *Proceedings of SPIE* **2011**, *8029* (Sensing Technologies for Global Health, Military Medicine, and Environmental Monitoring and Biometric Technology for Human Identification VIII), 80291J/1-80291J/9.

267. Villanger, G. D.; Lydersen, C.; Kovacs, K. M.; Lie, E.; Skaare, J. U.; Jenssen, B. M., Disruptive effects of persistent organohalogen contaminants on thyroid function in white whales (*Delphinapterus leucas*) from Svalbard. *Science of the Total Environment* **2011**, *409* (13), 2511-2524.
268. Zhao, R.-S.; Hu, C.; Zhou, J.-B.; Yuan, J.-P.; Wang, S.-S.; Wang, X., Preconcentration and sensitive determination of hexabromocyclododecane diastereomers in environmental water samples using solid phase extraction with bamboo charcoal cartridge prior to rapid resolution liquid chromatography-electrospray tandem mass spectrometry. *Analytical and Bioanalytical Chemistry* **2011**, *400* (4), 1189-1195.
269. Zhao, R.-S.; Wang, X.; Zhang, L.-L.; Wang, S.-S.; Yuan, J.-P., Ionic liquid/ionic liquid dispersive liquid-liquid microextraction, a new sample enrichment procedure for the determination of hexabromocyclododecane diastereomers in environmental water samples. *Analytical Methods* **2011**, *3* (4), 831-836.
270. Georlette, P.; Finberg, I.; Reznick, G., New flame retardant systems for polypropylene. *Annual Technical Conference - Society of Plastics Engineers* **1995**, *53rd* (Vol. 3), 3536-40.
271. Plaitin, B.; Fonze, A.; Braibant, R., Competitive advantages of brominated epoxy oligomers in styrenics. *Flame Retardants '98, Proceedings of the Flame Retardants '98 Conference, 8th, London, Feb. 3-4, 1998* **1998**, 139-150.
272. Reyes, J. D.; Georlette, P., Brominated epoxy oligomer and pentabromobenzyl acrylate: new performance enhancement for new opportunities. *Tomorrow's Trends in Fire Retardant Regulations, Testing, Applications and Current Technologies, Fire Retardant Chemicals Association, [Fall Conf* **1996**, 11-27.
273. Reyes, J. D.; Georlette, P.; Finberg, I.; Reznick, G., Review of the flame retardants market for applications in polypropylene. *Recent Advances in Flame Retardancy of Polymeric Materials* **1997**, *7*, 175-185.

274. Reznick, G.; Yaakov, Y. B.; Utevkii, L.; Georlette, P.; Lopez-Cuesta, J. M., Optimization of flame retarded thermoplastics for engineering applications. *Flame Retardants '98, Proceedings of the Flame Retardants '98 Conference, 8th, London, Feb. 3-4, 1998* **1998**, 125-137.
275. Reznick, G.; Yaakov, Y. B.; Utevkii, L.; Georlette, P.; Lopez-Cuesta, J. M., Optimization of flame retarded thermoplastics for engineering applications. *Recent Advances in Flame Retardancy of Polymeric Materials* **1998**, 9, 126-143.
276. Thomas, R.; Squires, G.; Georlette, P.; Finberg, P.; Reznick, G., Benefits of complex flame retardant systems on properties of plastic compositions. *Proceedings of the Conference on Recent Advances in Flame Retardancy of Polymeric Materials* **2007**, 18, 111-118.
277. Utevski, L., Improved flame retardant systems for polypropylene. *Popular Plastics & Packaging* **1996**, 41 (2), 47-50.
278. Green, J., Phosphorus-bromine flame retardant synergy in polycarbonate/ABS blends. *Polymer Degradation and Stability* **1996**, 54 (2-3), 189-193.
279. Green, J.; Chung, J., Flame-retarding poly(butylene terephthalate) - properties, processing characteristics, and rheology. *Journal of Fire Sciences* **1990**, 8 (4), 254-65.
280. Hepp, L. R. Flame-retarded polyester molding composition with improved electrical performance. 1986-101862, 193043, 19860214., 1986.
281. Mason, J. P. Fire- and chemical-resistant thermoplastic molding compositions containing brominated polycarbonates and polyesters. 1994-285375, 1901, 19940803., 2000.
282. Mollerus Faber, R.; Van den Bogerd, J. A. Extrudable thermoplastic resin compositions for diffusive lighting with textured matte surface. 2008-159255, 2112203, 20080627., 2009.

283. Papazoglou, E.; Seibel, S. R., Modifying polycarbonate for improved processing and flame retardancy. *Fire Saf. Adv. High Perform. Plast. Prod., Pap. Jt. Meet. Soc. Plast. Eng. Fire Retard. Chem. Assoc.* **1994**, 37-51.
284. Papazoglou, E., Productivity improvements in flame retarded polycarbonate and polycarbonate blends. *Flame Retard. '94, [Proc. Conf.], 6th* **1994**, 213-23.
285. Partridge, I. K.; Maiestros, G. M., Effect of brominated bisphenol A on the cure, morphology and properties of epoxy/CTBN blends. *Plastics, Rubber and Composites Processing and Applications* **1995**, 23 (5), 325-30.
286. Seibel, S. R., Using CAE analysis to evaluate flame-retarded polycarbonates for automotive applications. *Society of Automotive Engineers, [Special Publication] SP* **1995**, SP-1099, 155-62.
287. Seibel, S. R.; Papazoglou, E., Correlating rheology, molding conditions and residual stress in flame retarded polycarbonate. *Annual Technical Conference - Society of Plastics Engineers* **1995**, 53rd (Vol. 1), 366-70.
288. Termine, E. J., Heat distortion temperature modification of rigid PVC and chlorinated PVC: a method to produce low smoke compositions. *Journal of Vinyl Technology* **1990**, 12 (4), 204-7.
289. Preparation of poly(halobenzyl acrylate) in a non-protic solvent. 1995-112326, 112326, 19950112., 2001.
290. Bar-Yaakov, Y.; Hirschsohn, Y.; Finberg, I.; Georlette, P. Flame-retarded polyethylene compositions with bromine-containing polymers as fireproofing agents. 2010-IL1082, 2011077439, 20101223., 2011.
291. Bobovitch, A.; Gutman, E.; Schenker, M.; Utevski, L.; Muskatel, M., New approach to flame retardants: thermal polymerization on fillers. *Materials Letters* **1995**, 23 (4,5,6), 317-20.

292. Dave, V., Processing, characterization, and degradation studies of flame-retarded nylon 66. *Recent Advances in Flame Retardancy of Polymeric Materials* **1995**, 6, 186-195.
293. Goldshtein, J.; Margel, S., Synthesis and characterization of new flame-retardant microspheres by dispersion polymerization of pentabromobenzyl acrylate. *European Polymer Journal* **2009**, 45 (11), 2987-2995.
294. Gutman, E.; Bobvitch, A.; Pinski, A.; Utevski, L.; Sondak, D.; Muskatel, M., Thermal analysis of the polymerization process on the surface of inorganic fillers. *Journal of Thermal Analysis* **1996**, 46 (6), 1541-1550.
295. Gutman, E. M.; Bobovitch, A. L., Mechanopolymerization of pentabromomobenzyl (mono) acrylate. *International Journal of Mechanochemistry and Mechanical Alloying* **1994**, 1 (3), 153-158.
296. Gutman, E. M.; Bobovitch, A. L., Mechanical stimulation of pentabromobenzyl acrylate polymerization on Mg(OH)₂. *European Polymer Journal* **1996**, 32 (8), 979-983.
297. Hochberg, A.; Haylock, J. C.; Mason, C. D. Flame-retardant polyamide composition. 1982-453209, 4525513, 19821227., 1985.
298. Hochberg, A.; Mason, C. D. Flame retardant amine terminated polyamide composition. 1984-113944, 147609, 19841117., 1985.
299. Lee, Y. L. Adhesive composition with functional filler for polyimide film bonding. 1993-116003, 595068, 19931004., 1994.
300. Malhotra, S. L. Coatings for ink jet transparencies. 1996-657218, 5897940, 19960603., 1999.
301. Peled, M.; Kornberg, N. Process for the preparation of poly(halobenzyl acrylate). 1996-585837, 6028156, 19960116., 2000.

302. Reznick, G.; Yaakov, Y. B.; Finberg, I.; Georlette, P.; Wilmer, R., Development of new flame retardant systems for engineering thermoplastics. *Advances in Plastics Technology, APT '01, Conference Papers, 4th, Katowice, Poland, Sept. 18-20, 2001* **2001**, 8/1-8/11.
303. Scheinert, J.; Karp, M.; Georlette, P.; Spiegelstein, M.; Reyes, J., Dioxin assessment and recycling aspects of plastics containing polybrominated flame retardants. *Organohalogen Compounds* **2000**, 47, 186-189.
304. Wilmer, R.; Borms, R.; Yaakov, Y. B.; Georlette, P., New developments for flame-retarded PBT. *ADDCON 2003, International Plastics Additives and Modifiers Conference, 9th, Vienna, Austria, Oct. 21-22, 2003* **2003**, 47-55.
305. Wiseman, D. K., New fire-retardant impact modified high performance polymers and blends. *Customer Demands Improved Total Perform. Flame Retarded Mater., [Pap. Fire Retard. Chem. Assoc. Fall Conf.]* **1993**, 99-118.
306. Yanai, S.; Cohen, Y.; Rumack, M.; Georlette, P.; Siegmann, A.; Dagan, A., Poly(pentabromobenzyl acrylate): a novel flame retardant for engineering thermoplastics. *Plastics Compounding* **1985**, 8 (7), 39-40, 42, 44.
307. Vamvuka, D.; Kakaras, E.; Kastanaki, E.; Grammelis, P., Pyrolysis characteristics and kinetics of biomass residuals mixtures with lignite. *Fuel* **2003**, 82 (15-17), 1949-1960.
308. Jeguirim, M.; Trouve, G., Pyrolysis characteristics and kinetics of *Arundo donax* using thermogravimetric analysis. *Bioresource Technology* **2009**, 100 (17), 4026-4031.
309. Flynn, J. H.; Wall, L. A., A quick, direct method for the determination of activation energy from thermogravimetric data. *Journal of Polymer Science, Part B: Polymer Letters* **1966**, 4 (5), 323-8.
310. Doyle, C. D., Estimating isothermal life from thermogravimetric data. *Journal of Applied Polymer Science* **1962**, 6 (No. 24), 639-42.

311. Kissinger, H. E., Reaction kinetics in differential thermal analysis. *Anal. Chem.* **1957**, *29*, 1702-6.
312. Zong, R.; Hu, Y.; Wang, S.; Song, L., Thermogravimetric evaluation of PC/ABS/montmorillonite nanocomposite. *Polymer Degradation and Stability* **2004**, *83* (3), 423-428.
313. Levchik, G. F.; Grigoriev, Y. V.; Balabanovich, A. I.; Levchik, S. V.; Klatt, M., Phosphorus-nitrogen containing fire retardants for poly(butylene terephthalate). *Polymer International* **2000**, *49* (10), 1095-1100.
314. Kim, J. Y.; Seo, E. S.; Kim, S. H.; Kikutani, T., Effects of annealing on structure and properties of TLCP/PEN/PET ternary blend fibers. *Macromolecular Research* **2003**, *11* (1), 62-68.
315. A. A. Doniskoi, M. A. S., *New Concepts in Polymer Science: Fire Resistant and thermally Stable Materials Derived from Chlorinated Polyethylene*. Utrecht: Boston, 2003.
316. Lum, R. M., Antimony oxide-PVC synergism: laser pyrolysis studies of the interaction mechanism. *Journal of Polymer Science, Polymer Chemistry Edition* **1977**, *15* (2), 489-97.
317. A. F. Grands, C. A. W., *Fire Retardancy of Polymeric Materials*. Marcel Dekker Publisher: New-York, 2000; p 120 - 122.
318. Gilman, J. W.; Kashiwagi, T.; Lichtenhan, J. D., Nanocomposites: a revolutionary new flame retardant approach. *SAMPE Journal* **1997**, *33* (4), 40-46.
319. Lao, S. C.; Wu, C.; Moon, T. J.; Koo, J. H.; Morgan, A.; Pilato, L.; Wissler, G., Flame-retardant polyamide 11 and 12 nanocomposites: thermal and flammability properties. *Journal of Composite Materials* **2009**, *43* (17), 1803-1818.
320. Gilman, J. W., Flammability and thermal stability studies of polymer layered-silicate (clay) nanocomposites. *Applied Clay Science* **1999**, *15* (1-2), 31-49.

321. Gilman, J. W.; Kashiwagi, T.; Brown, J. E. T.; Lomakin, S.; Giannelis, E. P.; Manias, E., Flammability studies of polymer layered silicate nanocomposites. *International SAMPE Symposium and Exhibition 1998*, 43 (Materials and Process Affordability--Keys to the Future, Book 1), 1053-1066.
322. Dave, V.; Israel, S. C., Application of direct pyrolysis chemical ionization mass spectrometry to characterize flame-retardant nylon 66. *Polymer Preprints (American Chemical Society, Division of Polymer Chemistry) 1989*, 30 (2), 203-4.
323. Dave, V.; Israel, S. C., Thermal analysis of flame-retardant nylon 66. *Polymer Preprints (American Chemical Society, Division of Polymer Chemistry) 1990*, 31 (1), 554-5.
324. Gouteux, B.; Alaei, M.; Mabury, S.; Muir, D., Oligomeric BFRS: a potential source for emerging brominated aromatic compounds. *Organohalogen Compounds 2006*, 68, 659-662.
325. Montezin, F.; Cuesta, J. M. L.; Crespy, A.; Georlette, P., Flame retardant and mechanical properties of a copolymer PP/PE containing brominated compounds/antimony trioxide blends and magnesium hydroxide or talc. *Fire and Materials 1997*, 21 (6), 245-252.
326. Sanchez, F. L.; Sanchez, A. P. Polymer composition and its manufacture for cable insulation. 2000-308237, 1092752, 20000920., 2001.
327. Siegman, A.; Yanai, S.; Dagan, A.; Cohen, Y.; Rumack, M.; Georlette, P., Poly(pentabromobenzyl acrylate), a novel flame-retardant additive for engineering thermoplastics. *Bromine Compd. Chem. Appl., [Int. Conf. Chem. Appl. Bromine Its Compd.]*, 1st 1988, 339-51.
328. Smith, B. V.; Wiseman, D. K.; Crook, E. H., Development of impact modified, flame retardant poly(butylene terephthalate) formulations. *Journal of Vinyl & Additive Technology 1995*, 1 (1), 51-4.

329. Smith, R.; Utevsikii, L.; Muskatel, M.; Finberg, L.; Scheinert, Y.; Georlette, P., The beneficial effects of brominated flame retardants in polymeric systems. *Speciality Chemicals* **1996**, *16* (2), 49-50,52.
330. Takise, O.; Saito, R. Thermoplastic polyester-based flame-retardant resin composition and thin-walled molded products. 2004-2674, 1449871, 20040206., 2004.
331. Watari, T.; Takise, O.; Tajiri, T. Insulating parts comprising polybutylene terephthalate, polyolefin, glycidyl group containing copolymer and flame retardant blend. 2005-14524, 1614716, 20050705., 2006.
332. Wiseman, D. K., Fire-retardant impact-modified nylon 6. *Plastics Compounding* **1994**, *17* (1), 51-4.
333. Helfand, E.; Tagami, Y., Theory of the interface between immiscible polymers. II. *Journal of Chemical Physics* **1972**, *56* (7), 3592-601.
334. Helfand, E.; Tagami, Y., Theory of the interface between immiscible polymers. *Journal of Polymer Science, Polymer Letters Edition* **1971**, *9* (10), 741-6.
335. Reiter, J.; Zifferer, G.; Olaj, O. F., Monte Carlo studies of the interface between two polymer melts. *Macromolecules* **1990**, *23* (1), 224-8.
336. Sperling, L. H., *Introduction to Physical Polymer Science*. John Wiley & Sons: Hoboken, New Jersey, 2006; p 557-612.
337. Xu, Y.; Hanna, M. A.; Isom, L., "Green" chemicals from renewable agricultural biomass - a mini review. *Open Agriculture Journal* **2008**, *2*, 54-61.
338. Dodds, D. R.; Gross, R. A., Chemicals from Biomass. *Science (Washington, DC, United States)* **2007**, *318* (5854), 1250-1251.
339. Meier, M. A. R.; Metzger, J. O.; Schubert, U. S., Plant oil renewable resources as green alternatives in polymer science. *Chemical Society Reviews* **2007**, *36* (11), 1788-1802.
340. Gast, L. E., *Fatty Acids*. AOCS Monograph. 7, American Oil Chemists' Society, Champaign, IL, : 1979; p 564.

341. Derksen, J. T. P.; Cuperus, F. P.; Kolster, P., Renewable resources in coatings technology: a review. *Progress in Organic Coatings* **1996**, 27 (1-4), 45-53.
342. Solomon, D. H., *The Chemistry of Organic Film Formers*. 2nd ed.; Robert E. Krieger: Malabar, Fl, 1982; p 36-37.
343. Mallegol, J.; Lemaire, J.; Gardette, J. L., Drier influence on the curing of linseed oil. *Progress in Organic Coatings* **2000**, 39 (2-4), 107-113.
344. Mallegol, J.; Gardette, J.-L.; Lemaire, J., Long-term behavior of oil-based varnishes and paints I. Spectroscopic analysis of curing drying oils. *Journal of the American Oil Chemists' Society* **1999**, 76 (8), 967-976.
345. Mallegol, J.; Gardette, J.-L.; Lemaire, J., Long-term behavior of oil-based varnishes and paints. Fate of hydroperoxides in drying oils. *Journal of the American Oil Chemists' Society* **2000**, 77 (3), 249-255.
346. Mallegol, J.; Gardette, J.-L.; Lemaire, J., Long-term behavior of oil-based varnishes and paints. Photo- and thermooxidation of cured linseed oil. *Journal of the American Oil Chemists' Society* **2000**, 77 (3), 257-263.
347. Baumann, H., Buhler, M, Fochem, H, Hirsinger, F, Zobelein, H, Falbe, J, Natural fats and oils – renewable raw materials for the chemical industry. *Angew. Chem., Int. Ed. Engl.* **1988**, 27, 41-62.
348. Liu, Z. S.; Erhan, S. Z.; Calvert, P. D., Solid freeform fabrication of epoxidized soybean oil/epoxy composites with Di-, Tri-, and polyethylene amine curing agents. *Journal of Applied Polymer Science* **2004**, 93 (1), 356-363.
349. Liu, Z. S.; Erhan, S. Z.; Xu, J.; Calvert, P. D., Development of soybean oil-based composites by solid freeform fabrication method: epoxidized soybean oil with bis or polyalkylamine curing agents system. *Journal of Applied Polymer Science* **2002**, 85 (10), 2100-2107.

350. Gerbase, A. E.; Petzhold, C. L.; Costa, A. P. O., Dynamic mechanical and thermal behavior of epoxy resins based on soybean oil. *Journal of the American Oil Chemists' Society* **2002**, *79* (8), 797-802.
351. Thames, S. F.; Yu, H., Cationic UV-cured coatings of epoxide-containing vegetable oils. *Surface and Coatings Technology* **1999**, *115* (2-3), 208-214.
352. Wan Rosli, W. D.; Kumar, R. N.; Mek Zah, S.; Hilmi, M. M., UV radiation curing of epoxidized palm oil-cycloaliphatic diepoxide system induced by cationic photoinitiators for surface coatings. *European Polymer Journal* **2003**, *39* (3), 593-600.
353. Thames, S. F.; Yu, H.; Subramanian, R., Cationic ultraviolet curable coatings from castor oil. *Journal of Applied Polymer Science* **2000**, *77* (1), 8-13.
354. Bajpai, M.; Shukla, V.; Singh, D. K.; Singh, M.; Shukla, R., A study of the film properties of pigmented UV-curable epoxidised soybean oil. *Pigment & Resin Technology* **2004**, *33* (3), 160-164.
355. Dzunuzovic, E.; Tasic, S.; Bozic, B.; Babic, D.; Dunjic, B., UV-curable hyperbranched urethane acrylate oligomers containing soybean fatty acids. *Progress in Organic Coatings* **2005**, *52* (2), 136-143.
356. Zlatanovic, A.; Lava, C.; Zhang, W.; Petrovic, Z. S., Effect of structure on properties of polyols and polyurethanes based on different vegetable oils. *Journal of Polymer Science, Part B: Polymer Physics* **2004**, *42* (5), 809-819.
357. Javni, I.; Zhang, W.; Petrovic, Z. S., Effect of different isocyanates on the properties of soy-based polyurethanes. *Journal of Applied Polymer Science* **2003**, *88* (13), 2912-2916.
358. Erhan, S. M.; Kleiman, R., Vulcanized meadowfoam oil. *Journal of the American Oil Chemists' Society* **1990**, *67* (10), 670-4.

359. Ebewele, R. O.; Iyayi, A. F.; Hymore, F. K., Synthesis and characterization of vulcanized vegetable oil from rubber seed oil. *Research Journal of Agriculture and Biological Sciences* **2010**, *6* (4), 552-556.
360. Nag, A.; Chaki, T. K.; De, K. B., Factice from oil of *Putranjiva roxburghii*. *Journal of the American Oil Chemists' Society* **1995**, *72* (3), 391-3.
361. Flory, P., *Principles of Polymer Chemistry*. Cornell University Press, Ithaca, NY: 1953; p 347-398.
362. Klaasen, R. P.; van der Leeuw, R. P. C., Fast drying cobalt-free high solids alkyd paints. *Progress in Organic Coatings* **2006**, *55* (2), 149-153.
363. Dmytryshyn, S. L.; Dalai, A. K.; Chaudhari, S. T.; Mishra, H. K.; Reaney, M. J., Synthesis and characterization of vegetable oil derived esters: evaluation for their diesel additive properties. *Bioresource Technology* **2004**, *92* (1), 55-64.
364. Miyagawa, H.; Misra, M.; Drzal, L. T.; Mohanty, A. K., Novel biobased nanocomposites from functionalized vegetable oil and organically-modified layered silicate clay. *Polymer* **2005**, *46* (2), 445-453.
365. Behera, D.; Banthia, A. K., Synthesis, characterization, and kinetics study of thermal decomposition of epoxidized soybean oil acrylate. *Journal of Applied Polymer Science* **2008**, *109* (4), 2583-2590.
366. La Scala, J.; Wool, R. P., The effect of fatty acid composition on the acrylation kinetics of epoxidized triacylglycerols. *Journal of the American Oil Chemists' Society* **2002**, *79* (1), 59-63.
367. Zou, K.; Soucek, M. D., *Macromol. Chem. Phys.* **2005**, *206* (9), 967-975.
368. Wan Rosli, W. D.; Kumar, R. N.; Mek Zah, S.; Hilmi, M. M., *Eur. Polym. J.* **2003**, *39* (3), 593-600.
369. Sasaki, H., Curing properties of cycloaliphatic epoxy derivatives. *Progress in Organic Coatings* **2007**, *58* (2-3), 227-230.

370. Gu, H.; Ren, K.; Martin, D.; Marino, T.; Neckers, D. C., Cationic UV-cured coatings containing epoxidized soybean oil initiated by new onium salts containing tetrakis(pentafluorophenyl)gallate anion. *Journal of Coatings Technology* **2002**, *74* (927), 49-52.
371. Ficek, B., Thiesen, AM., Scranton, AB., Cationic photopolymerizations of thick polymer systems: active center lifetime and mobility. *Eur. Polym. J.* **2008**, *44* 98-105.
372. Decker, C.; Moussa, K., Kinetic study of the cationic photopolymerization of epoxy monomers. *Journal of Polymer Science, Part A: Polymer Chemistry* **1990**, *28* (12), 3429-43.
373. Fouassier, J. P., *Photoinitiation, Photopolymerization and Photocuring - Fundamental and Applications*. Hanser Publishers: New York, 1995; p 102-141.
374. Crivello, J. V.; Liu, S., Photoinitiated cationic polymerization of epoxy alcohol monomers. *Journal of Polymer Science, Part A: Polymer Chemistry* **2000**, *38* (3), 389-401.
375. Crivello, J. V., Cationic polymerization - iodonium and sulfonium salt photoinitiators. *Advances in Polymer Science* **1984**, *62* (Initiators, Poly-React., Opt. Act.), 1-48.
376. Scaiano, J. C.; Nguyen, K. T.; Leigh, W. J., Diazonium salts in photochemistry. V: Photosensitized decomposition of benzenediazonium tetrafluoroborate in solutions of cationic detergents. *Journal of Photochemistry* **1984**, *24* (1), 79-86.
377. Pappas, S. P., Photoinitiation of cationic and concurrent radical-cationic polymerization. Part V. *Progress in Organic Coatings* **1985**, *13* (1), 35-64.
378. Lehmann, R. E.; Kochi, J. K., Structures and photoactivation of the charge-transfer complexes of bis(arene)iron(II) dications with ferrocene and arene donors. *Journal of the American Chemical Society* **1991**, *113* (2), 501-12.
379. Serpone, N.; Jamieson, M. A., Picosecond spectroscopy of transition metal complexes. *Coordination Chemistry Reviews* **1989**, *93* (1), 87-153.

380. Tsubakiyama, K.; Fujisaki, S.; Tabata, E.; Nakahara, S., Photosensitized polymerization of organic vinyl monomers by ferrocene. *Journal of Macromolecular Science, Chemistry* **1991**, *A28* (5-6), 557-73.
381. Gill, T. P.; Mann, K. R., Photochemistry of $[(\eta\text{-C}_5\text{H}_5)\text{Fe}(\eta\text{-p-xylyl})]\text{PF}_6$ in acetonitrile solution. Characterization and reactivity of $[(\eta\text{-C}_5\text{H}_5)\text{Fe}(\text{MeCN})_3]^+$. *Inorganic Chemistry* **1983**, *22* (14), 1986-91.
382. Maybod, H.; George, M. H., Effect of oxygen on acrylonitrile radical polymerization: application of the microwave plasma detector. *Journal of Polymer Science, Polymer Letters Edition* **1977**, *15* (11), 693-8.
383. George, M. H.; Ghosh, A., Effect of oxygen on the radical polymerization of acrylamide in ethanol and water. *Journal of Polymer Science, Polymer Chemistry Edition* **1978**, *16* (5), 981-95.
384. Decker, C.; Jenkins, A. D., Kinetic approach of oxygen inhibition in ultraviolet- and laser-induced polymerizations. *Macromolecules* **1985**, *18* (6), 1241-4.
385. Ficek, B., Thiesen, AM, Scranton, AB, Cationic photopolymerizations of thick polymer systems: active center lifetime and mobility. *European Polymer Journal* **2008**, *44*, 98-105.
386. Ito, H.; Kidokoro, N.; Ishikawa, H., Differential photocalorimetric study of cationic photopolymerization. *Journal of Photopolymer Science and Technology* **1992**, *5* (2), 235-46.
387. Uhl, F. M.; Davuluri, S. P.; Wong, S.-C.; Webster, D. C., Organically modified montmorillonite in UV curable urethane acrylate films. *Polymer* **2004**, *45* (18), 6175-6187.
388. Fouassier, J.-P., *Photoinitiation Photopolymerization and Photocuring Fundamentals and Applications*. Hanser Publishers: New York, 1995; p 145-237.

389. Meng, S.; Duran, H.; Hu, J.; Kyu, T.; Natarajan, L. V.; Tondiglia, V. P.; Sutherland, R. L.; Bunning, T. J., Influence of Photopolymerization Reaction Kinetics on Diffraction Efficiency of H-PDLC Undergoing Photopatterning Reaction in Mixtures of Acrylic Monomer/Nematic Liquid Crystals. *Macromolecules (Washington, DC, United States)* **2007**, *40* (9), 3190-3197.